Surface patterning of polymeric separation membranes and its influence on the filtration performance

By

Sajjad Maruf

B.Sc., Bangladesh University of Engineering & Technology, 2006

M.Sc., University of Colorado, 2011

A thesis submitted to the

Faculty of the Graduate School of the

University of Colorado in partial fulfillment

of the requirement for the degree of

Doctor of Philosophy

Department of Mechanical Engineering

2014

This thesis entitled:

"Surface patterning of polymeric separation membrane and its influence on the filtration performances"

written by Sajjad Maruf
has been approved for the Department of Mechanical Engineering

_____

Committee Chair: Professor Yifu Ding

_____

Professor John Pellegrino

_____

Date

The final copy of this thesis has been examined by the signatories, and we Find that both the content and the form meet acceptable presentation standards Of scholarly work in the above mentioned discipline

ABSTRACT

Sajjad Maruf

"Surface patterning of polymeric separation membranes and its influence on the filtration performance"

Thesis directed by Professor Yifu Ding

Polymeric membrane based separation technologies are crucial for addressing the global issues such as water purification. However, continuous operations of these processes are often hindered by fouling which increases mass transport resistance of the membrane to permeation and thus the energy cost, and eventually replacement of the membrane in the system. In comparison to other anti-fouling strategies, the use of controlled surface topography to mitigate fouling has not been realized mainly due to the lack of methods to create targeted topography on the porous membrane surface.

This thesis aims to develop a new methodology to create surface-patterned polymeric separation membrane to improve their anti-fouling characteristics during filtration. First, successful fabrication of sub-micron surface patterns directly on a commercial ultrafiltration (UF) membrane surface using nanoimprint lithographic (NIL) technique was demonstrated. Comprehensive filtration studies revealed that the presence of these sub-micron surface patterns mitigates not only the onset of colloidal particle deposition, but also lowers the rate of growth of cake layer after initial deposition, in comparison with un-patterned membranes. The anti-fouling effects were also observed for model protein solutions. Staged filtration experiments,

with backwash cleaning, revealed that the permeate flux of the patterned membrane after protein fouling was considerably higher than that of the pristine or un-patterned membrane.

In addition to the surface-patterning of UF membranes, successful fabrication of a surface-patterned thin film composite (TFC) membrane was shown for the first time. A two-step fabrication process was carried out by (1) nanoimprinting a polyethersulfone (PES) support using NIL, and (2) forming a thin dense film atop the PES support via interfacial polymerization (IP). Fouling experiments suggest that the surface patterns alter the hydrodynamics at the membrane-feed interface, which is effective in decreasing fouling in dead end filtration system.

In summary, this thesis represents the first ever fabrication of functional patterned polymeric separation membrane and systematic investigation of the influence of submicron surface patterns on pressure-driven liquid membrane separations. The results presented here will enable an effective non-chemical surface modification anti-fouling strategy, which can be directly added onto current commercial separation membrane manufacturing route.

ACKNOWLEDGEMNTS

For this thesis work, I would like to thank Dr. Yifu Ding for not only giving me the opportunity to join his research group but also for his hard work, advice, and patience during the mentorship which were invaluable in my academic career. His dedication and support for this research work were insurmountable and I definitely owe him a debt of gratitude for his work to support my education and career. I would also like to thank my committee members: Dr. Alan Greenberg, Dr. John Pellegrino, Dr. Wei Tan and Dr. Lauren Greenlee for their important contributions and assistance.

Many current and past members of the Nanostructured Polymer Lab have had a positive impact on my graduate career. I have had the privilege of working with two postdocs: Dae Up Ahn and David Maniglio, who were wonderful mentors and friend during their tenure. Liang Wang not only contributed to this work but also assisted and trained me using various instrument. I was very lucky to have Zhen Wang, Lewis Cox and Zheng Zhang as my lab colleagues, who each made incredible contributions to my understanding of polymer and material science. I would also like to thank Melissa Rickman and John Mersch for their contributions to this research work.

Without the support of my family, none of this would have been possible. My parents, Nurul Hossain and Rabeya Hossain, always have faith in me and it is a wonderful feeling to share this accomplishment with them. My wife, Tamzida,Khan has been a constant source of inspiration and taught me what it really means to work hard. Without her, I know that I would not have had success in graduate school. I would also like to thank my mother-in-law Anowara Bari for her support.

TABLE OF CONTENT

LIST OF TABLES

LIST OF FIGURES

CHAPTER I

INTRODUCTION

1.1 Overview of membrane technology

Separation and purification of chemical components are one of the major challenge in technological industries. Precision separation process is desirable in the food and pharmaceuticals companies to produce high quality products, to remove or recover toxic or valuable components from industrial effluent. Also, separation of unwanted constituents and organisms from drinking water is the biggest challenge in potable water industries and waste water treatment facilities. Multitude of separation techniques like distillation, precipitation, crystallization extraction, extraction etc. have been invented for this purpose [1]. In recent years, more and more of those conventional separation techniques have been replaced by a variety of processes that utilize semipermeable membranes as separation barrier.

Membranes, typically having lateral dimensions much larger than their thicknesses, provide a semi permeable barrier through which mass transport takes place under a variety of driving forces [2]. The history of membrane application goes back to the middle of eighteenth century when it was used to elucidate the barrier properties and related phenomena [3]. The first batch of commercial synthetic membranes for practical applications were manufactured in Germany during 1930's [4]. A breakthrough for industrial membrane applications was the development of asymmetric membrane by Loeb and Sourirajan in 1960's [5]. Since then, membranes

have become a major method to separate various chemical species in an energetically efficient and ecologically clean fashion. Today various membranes are used at a large scale to produce potable water from sea and brackish water, to clean industrial effluent and recover valuable chemical constituents, fractionate molecular mixtures in food and pharmaceutical companies and separate gases and vapors in petrochemical process [6-8].

Membrane separation process is typically characterized by the type of membrane used and the driving force responsible for the mass transport. Membranes have the ability to selectively allow transport of one component more readily than another, by controlling the physical and chemical properties of the membrane and permeating constituents [3, 9]. Different transport processes through membrane takes place as a result of driving force acting on individual constituents in the feed side. These driving forces along with the separation mechanism and the pore size of the membrane are listed in the table (Table 1.1).

Among various kinds of membranes, pressure-driven membrane processes are widely used because of their simplicity of operation. Pressure-driven membranes use the pressure difference between the feed side and the permeate side as a driving force to selectively permeate solvents (Table 1.1). Typically, particles and various dissolved organic and inorganic components are retained based on their size, shape and charge (Fig. 1.1). Separation efficiency of a particular constituent is given by, $R\ (\%) = 1 - \frac{C_p}{C_f}$

where C_p is the concentration at the permeate side and C_f is the concentration at the feed side.

Table 1.1: Membrane processes with driving forces and mechanisms of separation

Membrane operation	Driving force	Mechanism of
Microfiltration	Pressure	Sieve
Ultrafiltration	Pressure	Sieve
Nanofiltration	Pressure (Chemical potential)	Sieve + Diffusion
Reverse osmosis	Pressure (Chemical potential)	Diffusion
Dialysis	Concentration activity	Diffusion
Electrodialysis	Electrical potential	Ion exchange
Pervaporation	Concentration activity	Evaporation

(After Mallevialle et al [10])

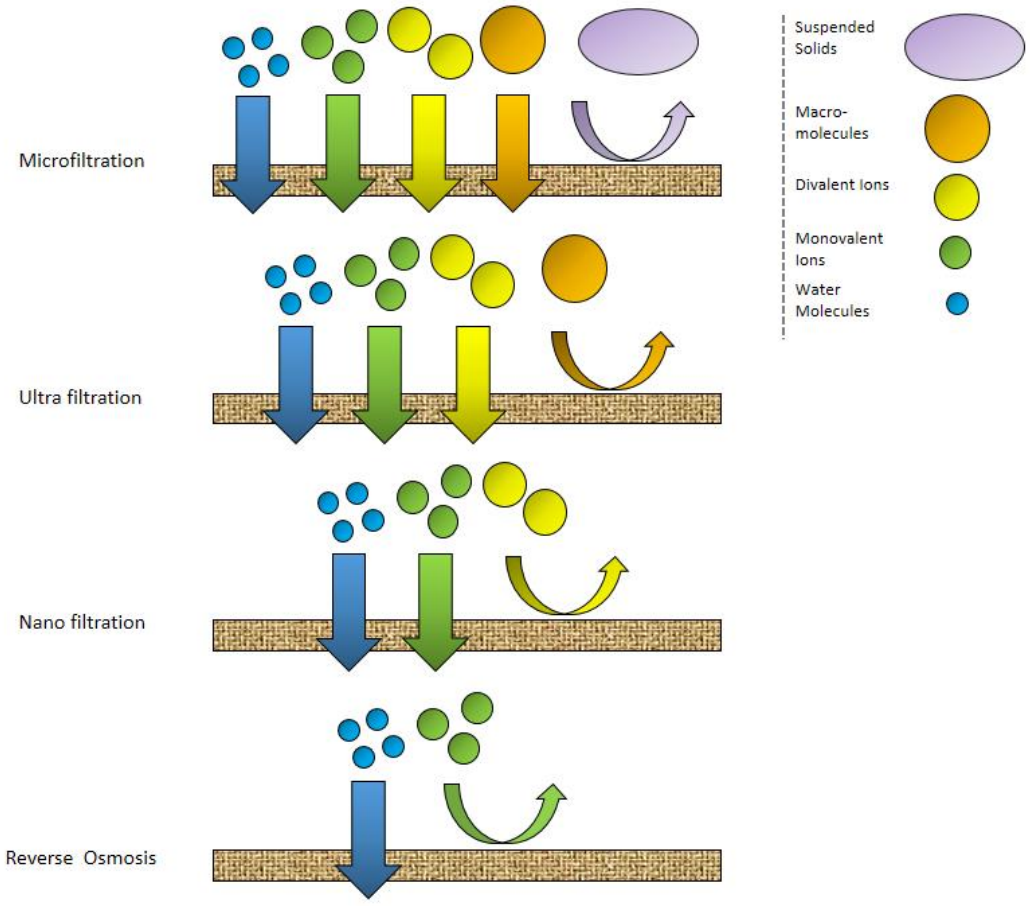

Figure 1.1: Pressure driven membrane filtration process (Drawn after Cheryan [11])

Microfiltration (MF) is a filtration process which removes impurities from a fluid by passing it through a micro-porous membrane. MF membranes typically have the largest pores (0.1 μm to 10.0 μm) among commonly used pressure driven membranes and components larger than the pore sizes are removed by sieve mechanism [12]. Typically, MF membranes are used heavily to remove solutes like suspended solids, colloids and bacteria etc. MF membrane are also used to remove particles as a pretreatment step for reverse osmosis (RO) and nanofiltration (NF) processes.

Ultrafiltration (UF) membranes have smaller pores (typically 0.1-5 nm) than MF membranes and are also capable of producing higher permeability at relatively low transmembrane pressure (TMP) [12]. During the UF process, suspended solids and/or solutes with high molecular weights are rejected at the membrane solute interface, while water and/or other low molecular weight solutes pass through as permeate. UF membranes are generally used to retain macromolecules from solution, which is often applied in the pre-treatment of desalination and waste water plant and in recovering flotation agents.

In NF membranes, pore sizes are smaller than UF membranes and typically around ~1 nm, which corresponds to the dissolved compounds with molecular weight about 300 D [13]. NF membranes are suitable for the removal of organic micro pollutants and dyes from surface water or groundwater, as well as degradation products from the effluent of biologically-treated wastewater.

RO membranes are typically composite membranes containing a thin dense barrier layer without predefined pores. In a RO process, permeation is slow and rejection mechanism follows the solution-diffusion theory [14]. Low permeability of RO process requires very high pressure (and thus energy) for operation. Water is effectively the only permeate that passes through RO membranes while all other dissolved and suspended solutes, organic and inorganic, are rejected. Rejection of the solutes is affected by the size and shape of the solutes, the ionic charge of the solutes, and the membrane characteristics.

Typical permeability of pressure-driven membranes and the corresponding pressure requirement are summarized below [1].

Microfiltration: $\Delta P \approx 0.1$ to 2 bar

Flux > 0.5 $m^3\ m^{-2}\ day^{-1}\ bar^{-1}$

Ultrafiltration: $\Delta P \approx 1$ to 5 bar

Flux ≈ 0.1 - 0.5 $m^3\ m^{-2}\ day^{-1}\ bar^{-1}$

Nanofiltration: $\Delta P \approx 5$ to 10 bar

Flux ≈ 0.05 – 0.1 $m^3\ m^{-2}\ day^{-1}\ bar^{-1}$

Reverse osmosis: $\Delta P \approx 10$ to 100 bar

Flux < 0.05 $m^3\ m^{-2}\ day^{-1}\ bar^{-1}$

All membrane processes are subject to additional resistances, beyond the membrane itself, against the permeate flux and therefore additional energy over the resistance must be supplied in the form of pressure or activity gradient in order to

keep the system performance constant. There are many factors affecting the resistances of membrane systems and they can be generally categorized into three groups, i.e.: solution chemistry, membrane properties, and operation conditions. These factors can also interact between themselves and therefore predicting the resistance of membranes can often be very complicated.

1.2 Phenomena and mechanisms of fouling in membrane processes:

Flux reduction during membrane filtration can occur for two reasons, namely, concentration polarization and fouling [15]. Concentration polarization is a natural consequence of the selective membrane based operation. The selective permeation of a feed solution leads to an accumulation of rejected components in a mass transfer boundary layer in the vicinity of the membrane surface (Fig. 1.2). The rejected constituents accumulating at the surface reduce the solvent activity and thus reduces the permeate flux. Concentration polarization is inevitable and reversible with the removal of driving force, the TMP [16].

In contrast, fouling refers to the depositions of retained particles, macromolecules, inorganic materials, and biological materials, at the membrane surface and/or inside the pores which results in a permanent reduction in the permeate flux [17, 18]. During filtration, rejected components/solutes are rejected at the membrane solution interface [19]. When the solute concentration within the boundary layer reaches a threshold value, the membrane becomes permanently fouled, developing a “cake layer” on the membrane surface, which induces additional

hydrodynamic resistance for the permeates. This cake layer can only be partially removed, often under harsh chemical conditions [20, 21], causing more energy consumption, shutdown of the productivity, and eventual replacement of the membranes [17]. Hence, much effort has been spent to mitigate the membrane fouling and prolong their lifetimes, which still remains as a grand challenge for all membrane technologies.

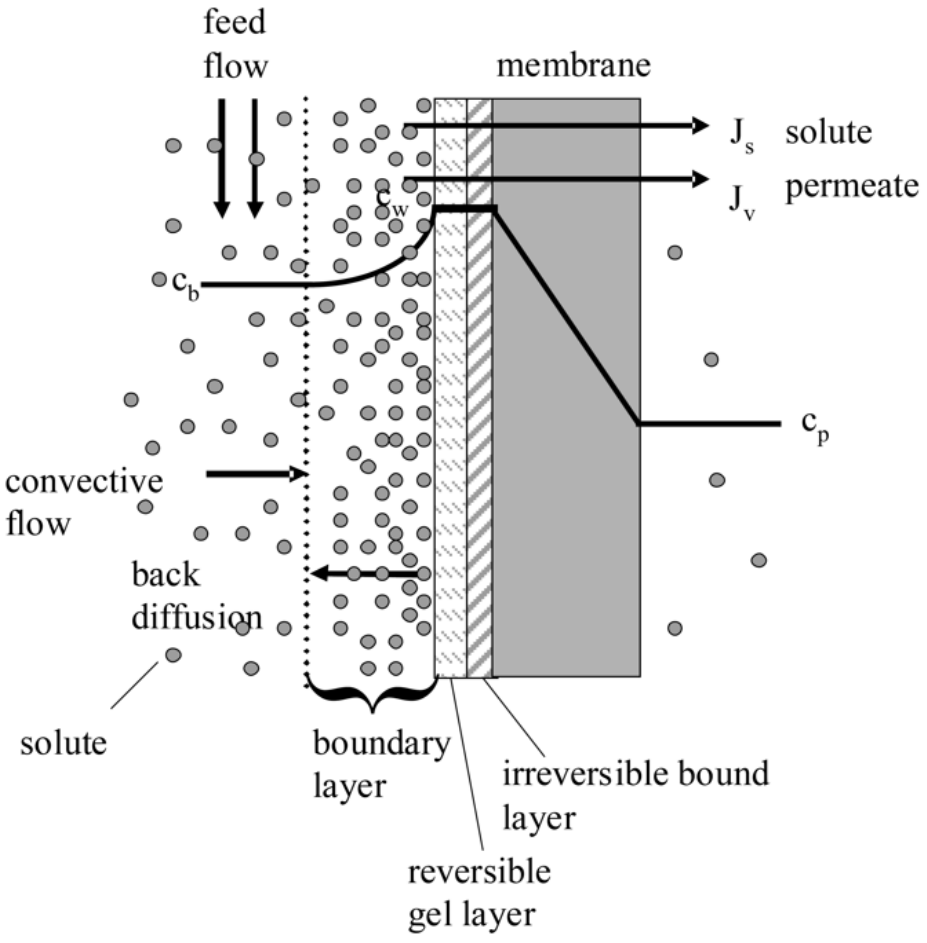

Figure 1.2: Schematic representation of concentration polarization and fouling at the membrane surface. Drawn after Goosen et al. [22]

Fouling mechanisms usually take the following forms:

- Adsorption: Adsorption is a physical and surface mechanism by which pollutants are attracted to the membrane surface and binds with the surface caused by specific interactions between the membranes and the solute or particles. Layers of particles and solutes can deposit on the membrane surface even in the absence of permeation flux, leading to an additional hydraulic resistance [16].
- Pore blockage: During filtration, pore blockage can occur by rejected components, leading to a reduction in flux due to the closure (or partial closure) of the pores. This pore blocking can be either a complete pore blocking, where each particle entirely blocks the whole pore making that particular region absolute impermeable, or the pore blocking can be standard pore blocking where particles deposit within pores and make the pore volume decreases proportionally to the volume of deposited particles [23].
- Deposition: In the deposition mechanism, rejected components grow layer by layer at the membrane surface, leading to an additional component in the hydraulic resistance. This is often referred to as a cake resistance [24]. In a deposition mechanism it is assumed that depositing components do not block the pores because of either the membrane is dense or the pores are already covered by layers of rejected components [25].

- Gel formation: Gel formation is a special kind of fouling mechanism. During filtration the level of concentration polarization becomes high enough that wall concentration is viewed as a separate component and it is typically referred as gel concentration. Although it derives from the concentration polarization, it is viewed as special fouling case as it increases the membrane resistance [26].

To understand the fouling mechanisms and properly address the fouling problem it is essential to characterize each foulant and how it effects the fouling mechanism. These foulants broadly can be divided into two categories, those that damage the surface and those that only foul the membrane surface.

- Particulates: Can be both inorganic and organic, usually in particles or colloids form. They usually physically screen the membrane surface, block the pores or thwart the membrane transport by forming cake layer [27].
- Organic foulants: Dissolved components like humic substances, oil, fulvic acid, hydrophilic and hydrophobic materials and proteins are part of this category [28]. Typically they damage the surface by adhering to the membrane surface by adsorption.
- Inorganic foulants: Various dissolved salts and scaling components belongs to this group. Dissolved components like iron, manganese, silica precipitate onto the membrane surface due to super-saturation, pH change or oxidation [29].
- Biological foulants: This category covers algae, various microorganisms like bacteria that can adhere to the membrane surface and form a permanent biofilm [30].

In simplistic terms, fouling is concerned with non-dissolved material that is either deposited on the membrane surface (or on layers that are already adhering to the membrane surface), or material deposited in the pore mouths or on the walls, or indeed a mixture of both. In order to understand the fundamentals of fouling, an insight on the transport of feed components towards the membrane surface and the physical laws that govern the transport through the membrane should be discussed. Therefore the concept of fouling and concentration polarization is introduced in this discussion that should be used later on in this dissertation.

1.2.1 Concentration polarization model

Now when a minor component is rejected at the membrane barrier (e.g., salt in RO, proteins in UF, or colloids in MF), concentration polarization occurs as a result of natural selectivity of the membrane as mentioned above. Due to the development of concentration gradient and flow conditions near the boundary layer, a back-diffusion of the solute into the bulk will occur. The degree of accumulation in this layer and its thickness can be estimated from the balance of the two factors as described below. Under steady-state conditions, the following relationships describe the relevant fluxes, as illustrated in Fig. 1.3.

From Fig. 1.3

Component 1:

$$j_{1,con} = j_1 \qquad (1)$$

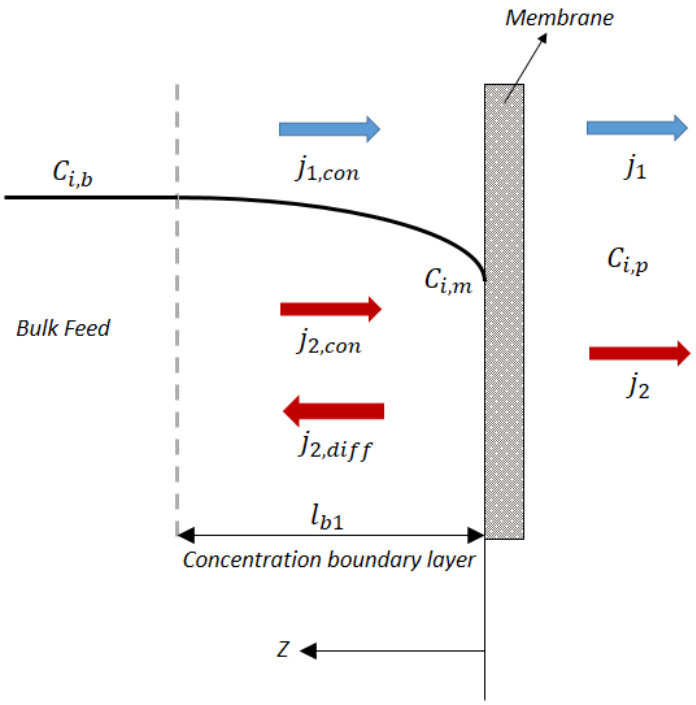

Figure 1.3: concentration polarization model.

Component 2:

$$j_{2,con} = j_{2,diff} + j_2 \tag{2}$$

By taking simplistic assumptions of steady state, Fickian diffusion, constant density and negligible concentration gradient parallel to the membrane, a mass balance on the feed side of the membrane can be obtained.

$$J.C_i = J.C_{i,p} - D_{ji}\frac{dC_i}{dZ} \tag{3}$$

Integrating the equation by applying boundary conditions

$Z = 0$ $\qquad C_i = C_{i,m}$

$Z = l_{bl}$ $\qquad C_i = C_{i,b}$

yielding,

$$j_{i,v} = \frac{D_i}{\delta_i} \ln \left[\frac{(C_{i,m} - C_{i,p})}{(C_{i,b} - C_{i,p})} \right] = k_i \ln \left[\frac{(C_{i,m} - C_{i,p})}{(C_{i,b} - C_{i,p})} \right] \quad (4)$$

where $j_{i,v}$ is the total volumetric flux, D_i is the diffusivity of solute i in water, δ_i is the thickness of the boundary layer, $C_{i,m}$ is the concentration in solution at the feed-membrane interface, $C_{i,p}$ is the permeate concentration, $C_{i,b}$ is the bulk concentration, and k_i is the mass-transfer coefficient. All C_i values refer to the concentration in solution. This "film model" analysis is based on a mass balance over an element of the boundary layer and allows the concentration at the membrane surface to be calculated from the mass-transfer coefficient.

Now for a typical system under any sort of concentration polarization, the intrinsic rejection R depends on the actual solute concentration prevailing on the membrane surface and is given by:

$$R = \frac{(C_{i,m} - C_{i,p})}{C_{i,m}} \quad (5)$$

While the observed rejection is based on the solute bulk concentrations and is given by

$$R_0 = \frac{(C_{i,b} - C_{i,p})}{C_{i,b}} \quad (6)$$

The two rejections are related by the following:

$$ln\left(\frac{1-R_0}{R_0}\right) - \ln\left(\frac{1-R}{R}\right) = \frac{J_v}{k_i} \quad (7)$$

Sutzkover et al. [31] described a simple technique for estimating $\frac{J_v}{k_i}$ in a differential RO system, such as what we used in this thesis. Their technique is based on evaluating the reduction in the permeate flux when salt solution is introduced instead of pure water. The net driving force is influenced by the changes in the osmotic pressure and assessment of the magnitude of the flux decline enables the evaluation of the membrane surface concentration. The mass transfer coefficient is given by:

$$k_i = \frac{J_{(v)salt}}{\ln\left\{\frac{\Delta P}{\pi_b - \pi_p}\cdot\left[1 - \frac{J_{(v)salt}}{J_{(v)H_2O}}\right]\right\}} \text{ or } \frac{J_{v,salt}}{k} = \ln\left\{\frac{\Delta p}{\pi_b - \pi_p}\cdot\left[1 - \frac{J_{v,salt}}{J_{v,pureH_2O}}\right]\right\} = \ln\left(\frac{1-R_o}{R_o}\cdot\frac{R}{1-R}\right) \quad (8)$$

Hence, the value of R can be simply determined from the osmotic pressures π_b and π_p of the saline feed and permeate, the observed rejections, and by measuring $J_{(v)H_2O}$, the permeate flux of the salt-free water at the same applied pressure, and $J_{v(t)}$, the permeate flux of the saline solution, all at any time t.

1.2.2 Fouling resistance model

Flux through a membrane can also be described by idealized equations. The following equation is used to describe the flux of a membrane in the absence of any fouling:

$$J_{(v)} = \frac{\Delta P - \Delta\pi_m}{\mu(R_m)} \quad (9)$$

where R_m is the empirically measured membrane resistance and the term $\Delta\pi$ is zero if the feed is a pure solvent. The inclusion of the dynamic viscosity parameter of the permeate, μ can make adjustment for any change in the feed viscosity.

Now, in the pure solvent equation, additional terms can be added to account for the hydraulic resistance caused by fouling. Regardless whether it is on the membrane surface or in the pores, foulants will affect the relationship between flux and TMP. With the presence of various kinds of fouling flux-TMP equation can be further modified by considering unifying fouling resistance. These resistances can be considered to be in series with the membrane resistance. Therefore:

$$J_{(v)} = \frac{\Delta P - \Delta \pi_m}{\mu(R_m + R_{ads} + R_{rev} + R_{irrev})} \quad (10)$$

The first of the additional hydraulic resistances, R_{ads}, is for the resistance due to surface or pore adsorption that occurs independently of permeate flux. R_{ads} can estimated by contacting the membrane with the feed in the absence of flux for a certain time and then comparing the permeation of any pure solvent flux with its pre-contact flux at a particular TMP. This enables a hydraulic resistance to be calculated and the difference between it and R_m. The other terms in eqn.10 reflect the fouling that occurs during filtration operation. This additional resistance exerted by fouling can be divided into a reversible component, R_{rev} (i.e., one that occurs during operation but is not present after switching from the feedback to pure solvent), and an irreversible component, R_{irrev}, that reflects the deposition of material that is only removable by following a strong cleaning protocols [16].

This classification allows one to distinguish different resistances (such as adsorption) that are independent of the pressure and permeate flux from fouling phenomena driven by the solvent transport through the membrane. When considering these fouling mechanisms, the strong form of critical flux, J_c, has been developed where additional resistance from adsorption is not present [24]. It has been defined as the flux at which the flux–TMP curve starts to deviate from the pure water permeation's linearity. So with the assumption that osmotic pressure is negligible

$$J > Jc \qquad J_{(v)} = \frac{\Delta P}{\mu(R_m + R_{rev} + R_{irrev})} \tag{11}$$

$$J < Jc \qquad J_{(v)} = \frac{\Delta P}{\mu(R_m)} \tag{12}$$

where at least one of R_{rev} or R_{irrev} is non-zero and where R_{ads} is considered negligible.

1.3 Antifouling strategies

Mitigation of membrane fouling still remains a grand challenge for most membrane applications. Figure 1.3 shows the number of research paper increasing exponentially each year and this highlights the importance of membrane fouling in the process industry.

Several approaches have been introduced to reduce the influence of fouling during filtration. In a broad sense they can be divided into two groups such as direct and indirect methods. Various sorts of cleaning or periodic maintenances are most frequently used direct methods to mitigate fouling for separation membranes. In the membrane industries cleaning protocols are approached in two ways; cleaning protocols developed for regular maintenance and cleaning methods developed for

recovery of performances. Well-adapted cleaning protocols can prevent the need for excessive cleaning to recover performances. These cleaning protocols can be broadly categorized in three groups: physical, chemical, and physico-chemical [32].

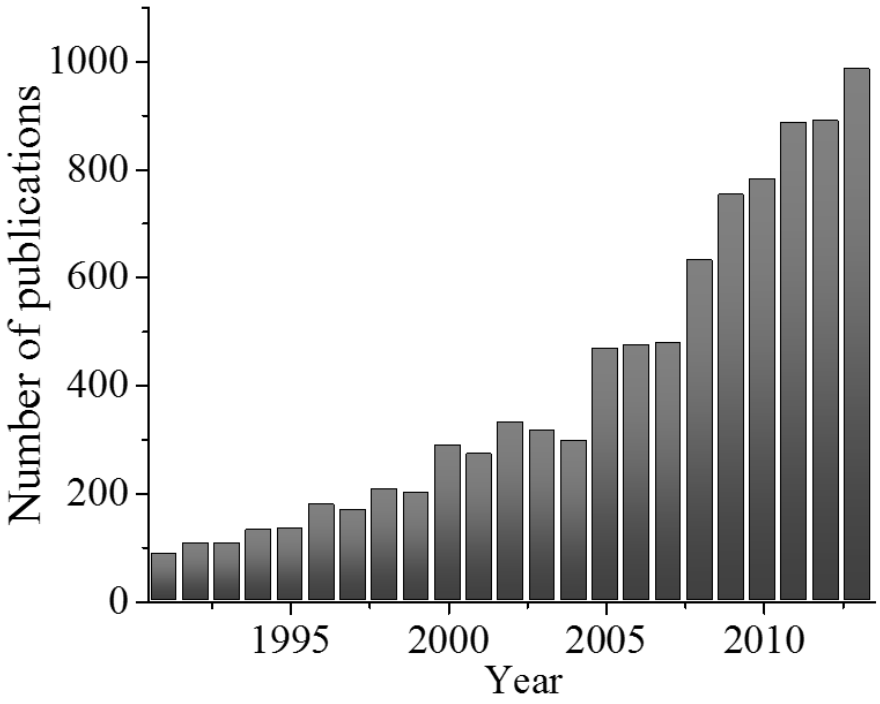

Figure 1.4: Number of publication on membrane fouling from 1991 to 2013. Plot created by searching "Membrane Fouling" in isiwebofknowledge.

Among them, physical cleaning uses mechanical force to extricate and remove foulants off the membrane surface [32]. Processes like sponge ball cleaning, forward and reverse flushing, backwashing, air flushing and CO_2 back permeation are well practiced in the membrane industries [33, 34]. Chemical cleaning process are also widely used to remove irreversible fouling from the membrane surface. In order to achieve effective cleaning, the chemical process should ideally remove the deposit and

restore membrane productivity and separation capabilities to the same level as before fouling. Identification of fouling and proper choice of cleaning agent is crucial in this type of cleaning method. Various chemical agents like caustic, oxidants, acids, chelating agents, and surfactants are commonly used in water and chemical industry [35]. However, chemical cleanings are limited to a minimum frequency as longer and repeated cleaning affect membrane lifetime [36].

Physico-chemical cleaning methods use combined physical cleaning method in juxtaposition with chemical cleaning to enhance the cleaning efficiency. This method is more often used in UF and MF filtration processes. The application of this methods usually uses forward flushing with permeate between cleanings when multiple cycles of cleaning protocols are used [32, 34]. Unfortunately, these periodic and recovery cleaning cannot keep the membrane functional for long term usage, as membrane degrades over time due to reaction with chemicals.

Fundamentally, one of the keys to fouling mitigation is controlling the interactions between the membrane and feed solution. Controlling the feed-membrane interactions have been addressed by a multitude of approaches by increasing local hydrodynamic shear stress gradients at barrier interface. These direct methods can promote mixing on the feed side, without incurring high parasitic energy losses from simply increasing flow velocities (volumetric pumping rates). Methods like turbulence promoters, use of pulsed or reversed flow, use of rotating or vibrating membranes, use of stirred cells with rotating blades near the membrane surface, and optimization of feed spacers of various types can promote this

hydrodynamic mixing and they categorized in the direct methods of reduce fouling [16] [37, 38] [39-43]. Most of these mixing enhancing processes involve highly complex system which requires an added installation cost, additional arrangements during periodic cleaning and energy cost for the mechanical promoters.

Many indirect methods have also been developed targeting modifying the membrane's surface properties (surface chemistry and/or structure) to decrease the adsorption (and possibly deposition) of species “rejected” by the membrane. This goal has been addressed by myriad researchers using novel synthetic approaches to create targeted surface chemistries [44-48] and topological structures [41, 49-51]. Among these approaches, one of the main focuses is on increasing the hydrophilicity of the membrane surface as many foulants are suspected of favoring adsorption on hydrophobic surfaces [18]. Some of the examples of these kinds of surface-modification approaches include adsorption of surfactants, coating and grafting of hydrophilic polymers, plasma treatment and the addition of hydrophilic nanoparticles onto the surface [39, 40, 42, 43, 52-54]. However, wider application of these processes has been limited by uncertainty with respect to long-term stability and scalability [18, 55].

It has been reported that the surface roughness on membrane surface can affect membrane-solute interactions [56, 57]. However, the exact relationship between membrane surface roughness and fouling remains unclear [19, 58].There have been a number of advances in creating additional targeted surface roughness into and onto membranes for a variety of applications. Among them spacerless structures have been fabricated to enhance hydrodynamic mass transfer near the

interface by embossing RO membranes [59, 60]. Coating and peeling spacer features were also created onto electrodialysis membranes [61]. Also, photolithographic and silicon micromachining methods have been used to create molds upon which membranes are cast using classical phase inversion approaches [62, 63]. It should be noted that the latter development enables a number of potential attributes, such as, surface energy modification [51] and creating microsieves for particle fractionation and high frequency backwashing beyond simply enhancing interfacial mass transfer [64, 65].

Surface patterning has proven effective for fouling reduction in non-membrane applications. A polydimethylsiloxane (PDMS) surface consisting of micron-sized arrays of riblets strongly resisted the fouling of barnacles [66]. Surface topography has also been reported to control the attachment and growth of biological cells, which are common foulants in membrane processes [67, 68]. Recently, the development of an effective anti-fouling system using patterned PDMS was reported [69]. Use of this so-called Sharklet® pattern, which mimics the topography of shark skin, reduced the settlement density of spores by ~86% as compared with a smooth PDMS surface.

These latter studies suggest the potential for a non-chemical approach to fouling control. However, few studies have been carried out that impart a pattern onto porous polymer membranes. Vogelaar et al. introduced the μ-molding technique, which utilizes the phase inversion process within a mold to fabricate porous films with micron-sized surface patterns [62, 70]. However, no performance data for these membranes were reported, possibly due to the dense skin formed at the surface that

may well limit filtration [38]. Recently though, Won et al. described the formation of polyvinylidene fluoride (PVDF) MF membranes on PDMS patterns with ~10 μm scale features [71]. They tested activated sludge dewatering at Reynolds number (*Re*) ~1100–1200 and found evidence for roughness-induced enhancement of filtration rates and resistance to microbial adhesion. Formation of permeable, structured UF hollow fibers with features on the order of 100s μm have also been reported, by Culfaz, et al., along with normal flow (aka dead-end) measurements of filtration (and NMR cake visualization) of model colloidal suspensions [72, 73]. Their studies indicated that the structured fibers influenced the position and reversibility of deposition relative to the round fibers, perhaps by a flux-self-regulation mechanism, but the effects were specific to the size distributions of the particular colloidal suspensions. Note that, most of these structures that were fabricated are in the order of microns where pressure driven membranes have to deal with foulants which has their sizes around nanometer to angstroms scale. In addition, methodology they applied require a significant change of the manufacturing process which might be very costly.

1.3. Statement of the problems

From above discussion it is evident that fouling is not only remain as a complex process but also poses as a significant challenge in the field of membrane separation technology. New methodology need to be investigated as conventional cleaning protocols and antifouling strategies cannot meet the requirement. On the other hand, limited successful antifouling strategies using surface morphology have been proposed and commercialized in non –membrane areas. Few researches also showed

interest in surface topography induced fouling mitigation areas and some fabrication methods are also invented to create targeted topography on membrane surface. However, those fabrication methods require a major alteration of the existing membrane manufacturing process and also features that were created using those methods are much larger than the typical size of most foulants. All these provide a motivation to find and implement a methodology that can create micro/nano pattern on membrane surface to mitigate various fouling.

In this thesis, we aim to develop a new methodology to create surface-patterned polymeric separation membrane and evaluate their anti-fouling characteristics during filtration. Here, the first ever fabrication of functional patterned polymeric separation membrane using nanoimprint lithography has been demonstrated and systematic investigation of the influence of submicron surface patterns on pressure-driven liquid membrane separations. The results presented here will enable an effective non-chemical surface modification anti-fouling strategy, which can be directly added onto current commercial separation membrane manufacturing route.

1.4 Organization

This thesis is organized in the following way:

This chapter, Chapter 1, gives a brief overview of the membrane process, problems and challenges and also provide an introduction to this thesis work and outlines other parts of the thesis.

Chapter 2 will detail the fabrication method, morphological evolution and its influence on membrane permeability of commercial UF membrane after imprinting with NIL.

In Chapter 3, fouling studies were carried out by comparing patterned and un-patterned membrane with model colloidal foulants.

Chapter 4 includes the study of the effects of sub-micron surface patterns on the fouling of a model protein solution (bovine serum albumin, BSA), which was investigated during active filtration and simple adsorption conditions.

Chapter 5 reports for the first time, successful fabrication of a surface-patterned thin film composite (TFC) membrane using a two-step fabrication process. Chemical, topographic, and permeation characterization was performed for the patterned TFC membranes, and their permselectivity was compared with that of a flat (un-patterned) TFC membrane prepared using the same IP procedure.

Finally, in Chapter 6, I will summarize all the thesis work and give recommendations about the future work that should be carried out.

References

1 Strathmann, H., Giorno, L. & Drioli, E. *An Introduction to Membrane Science and Technology*. (CNR-Servizio Pubblicazioni, 2006).

2 Li, X. *Mitigation of Fouling on Hollow Fiber Membrane Using Ultrasonic Tranducer* Master of Science in Engineering thesis, Purdue University Calumet, (2009)

3 Mulder, M. *Basic Principles of Membrane Technology*. (Springer, 1996).

4 Caetano, A. *Membrane Technology: Applications to Industrial Wastewater Treatment: Applications to Industrial Wastewater Treatment*. (Springer Netherlands, 1995).

5 Loeb, S. in *Synthetic Membranes:* Vol. 153 *ACS Symposium Series* 1-9 (American Chemical Society, 1981).

6 Geise, G. M. *et al.* Water purification by membranes: The role of polymer science. *Journal of Polymer Science Part B: Polymer Physics* **48**, 1685-1718, doi:10.1002/polb.22037.

7 Greenlee, L. F., Lawler, D. F., Freeman, B. D., Marrot, B. & Moulin, P. Reverse osmosis desalination: Water sources, technology, and today's challenges. *Water Research* **43**, 2317-2348, doi:http://dx.doi.org/10.1016/j.watres.2009.03.010 (2009).

8 Wessling, M., Werner, U. & Hwang, S. T. Pervaporation of aromatic C8-isomers. *Journal of Membrane Science* **57**, 257-270, doi:http://dx.doi.org/10.1016/S0376-7388(00)80682-1 (1991).

9 King, C. J. *Separation processes*. (McGraw-Hill, 1980).

10 Mallevialle, J. *et al. Water Treatment Membrane Processes*. (McGraw-Hill, 1996).

11 Cheryan, M. *Ultrafiltration and Microfiltration Handbook*. (Taylor & Francis, 1998).

12 Hubbard, A. T. *Encyclopedia of Surface and Colloid Science*. (Taylor & Francis, 2002).

13 Van Der Bruggen, B., Vandecasteele, C., Van Gestel, T., Doyen, W. & Leysen, R. A review of pressure-driven membrane processes in wastewater treatment and drinking water production. *Environmental Progress* **22**, 46-56, doi:10.1002/ep.670220116 (2003).

14 Wijmans, J. G. & Baker, R. W. The solution-diffusion model: a review. *Journal of Membrane Science* **107**, 1-21, doi:http://dx.doi.org/10.1016/0376-7388(95)00102-I (1995).

15 Jonsson, A.s. Concentration Polarization and Fouling during Ultrafiltration of Colloidal Suspensions and Hydrophobic Solutes. *Separation Science and Technology* **30**, 301-312, doi:10.1080/01496399508015840 (1995).

16 Field, R. in *Membrane Technology* 1-23 (Wiley-VCH Verlag GmbH & Co. KGaA).

17 Le-Clech, P., Chen, V. & Fane, T. A. G. Fouling in membrane bioreactors used in wastewater treatment. *J. Membr. Sci.* **284**, 17-53, doi:10.1016/j.memsci.2006.08.019 (2006).

18 Rana, D. & Matsuura, T. Surface Modifications for Antifouling Membranes. *Chemical Reviews* **110**, 2448-2471, doi:10.1021/cr800208y.

19 Elimelech, M., Xiaohua, Z., Childress, A. E. & Seungkwan, H. Role of membrane surface morphology in colloidal fouling of cellulose acetate and composite aromatic polyamide reverse osmosis membranes. *J. Membr. Sci.* **127**, 101-109 (1997).

20 Choo, K. H. & Lee, C. H. Membrane fouling mechanisms in the membrane-coupled anaerobic bioreactor. *Water Res.* **30**, 1771-1780, doi:10.1016/0043-1354(96)00053-x (1996).

21 Zhu, X. H. & Elimelech, M. Colloidal fouling of reverse osmosis membranes: Measurements and fouling mechanisms. *Environ. Sci. Technol.* **31**, 3654-3662 (1997).

22 Goosen, M. F. A. *et al.* Fouling of Reverse Osmosis and Ultrafiltration Membranes: A Critical Review. *Separation Science and Technology* **39**, 2261-2297, doi:10.1081/ss-120039343 (2005).

23 Wang, F. & University, M. S. *Combined Fouling of Pressure-driven Membranes Treating Feed Waters of Complex Composition*. (Michigan State University, 2008).

24 Bacchin, P., Aimar, P. & Field, R. W. Critical and sustainable fluxes: Theory, experiments and applications. *Journal of Membrane Science* **281**, 42-69, doi:http://dx.doi.org/10.1016/j.memsci.2006.04.014 (2006).

25 Marselina, Y., Le-Clech, P., Stuetz, R. & Chen, V. Detailed characterisation of fouling deposition and removal on a hollow fibre membrane by direct observation technique. *Desalination* **231**, 3-11, doi:http://dx.doi.org/10.1016/j.desal.2007.11.033 (2008).

26 Foley, G. *Membrane Filtration*. (Cambridge University Press).

27 Ahn, S. H. & Guo, L. J. High-Speed Roll-to-Roll Nanoimprint Lithography on Flexible Plastic Substrates. *Advanced Materials* **20**, 2044-2049, doi:10.1002/adma.200702650 (2008).

28 Wang, F. & Tarabara, V. V. Pore blocking mechanisms during early stages of membrane fouling by colloids. *Journal of Colloid and Interface Science* **328**, 464-469, doi:http://dx.doi.org/10.1016/j.jcis.2008.09.028 (2008).

29 Guo, W., Ngo, H. H. & Li, J. A mini-review on membrane fouling. *Bioresource Technology* **122**, 27-34, doi:http://dx.doi.org/10.1016/j.biortech.2012.04.089.

30 Sadr Ghayeni, S. B., Madaeni, S. S., Fane, A. G. & Schneider, R. P. Aspects of microfiltration and reverse osmosis in municipal wastewater reuse. *Desalination* **106**, 25-29, doi:http://dx.doi.org/10.1016/S0011-9164(96)00088-4 (1996).

31 Sutzkover, I., Hasson, D. & Semiat, R. Simple technique for measuring the concentration polarization level in a reverse osmosis system. *Desalination* **131**, 117-127, doi:http://dx.doi.org/10.1016/S0011-9164(00)90012-2 (2000).

32 Arnal, J. M. G. F., Beatriz; Sancho, Maria. (ed Robert Y Ning) (Intech Open science, 2011).

33 Al-Amoudi, A. & Lovitt, R. W. Fouling strategies and the cleaning system of NF membranes and factors affecting cleaning efficiency. *Journal of Membrane Science* **303**, 4-28, doi:http://dx.doi.org/10.1016/j.memsci.2007.06.002 (2007).

34 Ebrahim, S. Cleaning and regeneration of membranes in desalination and wastewater applications: State-of-the-art. *Desalination* **96**, 225-238, doi:http://dx.doi.org/10.1016/0011-9164(94)85174-3 (1994).

35 C. Liu, S. C., J. Hayes, T. Caothuy. in *AWWA 2000 Water Quality Technology Conference* (Denver, CO, 2001).

36 Kimura, K., Hane, Y., Watanabe, Y., Amy, G. & Ohkuma, N. Irreversible membrane fouling during ultrafiltration of surface water. *Water Research* **38**, 3431-3441, doi:http://dx.doi.org/10.1016/j.watres.2004.05.007 (2004).

37 Engler, J. & Wiesner, M. R. Particle fouling of a rotating membrane disk. *Water Research* **34**, 557-565, doi:http://dx.doi.org/10.1016/S0043-1354(99)00148-7 (2000).

38 Moulai-Mostefa, N., Akoum, O., Nedjihoui, M., Ding, L. & Jaffrin, M. Y. Comparison between rotating disk and vibratory membranes in the ultrafiltration of oil-in-water emulsions. *Desalination* **206**, 494-498, doi:http://dx.doi.org/10.1016/j.desal.2006.04.061 (2007).

39 Belfort, G. & Nagata, N. Fluid mechanics and cross-flow filtration: some thoughts. *Desalination* **53**, 57-79, doi:http://dx.doi.org/10.1016/0011-9164(85)85052-9 (1985).

40 Gupta, B. B., Howell, J. A., Wu, D. & Field, R. W. A helical baffle for cross-flow microfiltration. *Journal of Membrane Science* **102**, 31-42, doi:http://dx.doi.org/10.1016/0376-7388(94)00241-P (1995).

41 Ngene, I. S., Lammertink, R. G. H., Wessling, M. & Van der Meer, W. G. J. Particle deposition and biofilm formation on microstructured membranes. *Journal of Membrane Science* **364**, 43-51, doi:http://dx.doi.org/10.1016/j.memsci.2010.07.048.

42 Subramani, A., Kim, S. & Hoek, E. M. V. Pressure, flow, and concentration profiles in open and spacer-filled membrane channels. *Journal of Membrane Science* **277**, 7-17, doi:http://dx.doi.org/10.1016/j.memsci.2005.10.021 (2006).

43 van der Waal, M. J., Stevanovic, S. & Racz, I. G. Mass transfer in corrugated-plate membrane modules. II. Ultrafiltration experiments. *Journal of Membrane Science* **40**, 261-275, doi:http://dx.doi.org/10.1016/0376-7388(89)89009-X (1989).

44 Akthakul, A., Salinaro, R. F. & Mayes, A. M. Antifouling Polymer Membranes with Subnanometer Size Selectivity. *Macromolecules* **37**, 7663-7668, doi:10.1021/ma048837s (2004).

45 Asatekin, A., Kang, S., Elimelech, M. & Mayes, A. M. Anti-fouling ultrafiltration membranes containing polyacrylonitrile-graft-poly(ethylene oxide) comb copolymer additives. *Journal of Membrane Science* **298**, 136-146, doi:http://dx.doi.org/10.1016/j.memsci.2007.04.011 (2007).

46 Chapman, R. G. *et al.* Polymeric Thin Films That Resist the Adsorption of Proteins and the Adhesion of Bacteria. *Langmuir* **17**, 1225-1233, doi:10.1021/la001222d (2001).

47 McCloskey, B. D. *et al.* Influence of polydopamine deposition conditions on pure water flux and foulant adhesion resistance of reverse osmosis, ultrafiltration, and microfiltration membranes. *Polymer* **51**, 3472-3485, doi:http://dx.doi.org/10.1016/j.polymer.2010.05.008.

48 Wandera, D., Wickramasinghe, S. R. & Husson, S. M. Modification and characterization of ultrafiltration membranes for treatment of produced water. *Journal of Membrane Science* **373**, 178-188, doi:http://dx.doi.org/10.1016/j.memsci.2011.03.010.

49 Kim, M. m., Lin, N. H., Lewis, G. T. & Cohen, Y. Surface nano-structuring of reverse osmosis membranes via atmospheric pressure plasma-induced graft polymerization for reduction of mineral scaling propensity. *Journal of Membrane Science* **354**, 142-149, doi:http://dx.doi.org/10.1016/j.memsci.2010.02.053.

50 Lin, N. H., Kim, M. m., Lewis, G. T. & Cohen, Y. Polymer surface nano-structuring of reverse osmosis membranes for fouling resistance and improved flux performance. *Journal of Materials Chemistry* **20**, 4642-4652, doi:10.1039/b926918e.

51 Vogelaar, L., Lammertink, R. G. H. & Wessling, M. Superhydrophobic Surfaces Having Two-Fold Adjustable Roughness Prepared in a Single Step. *Langmuir* **22**, 3125-3130, doi:10.1021/la052701l (2006).

52 An, L. *et al.* Mechanical properties and miscibility of polyethersulfone/phenoxy blends. *Journal of Applied Polymer Science* **59**, 1843-1847, doi:10.1002/(sici)1097-4628(19960321)59:12<1843::aid-app5>3.0.co;2-q (1996).

53 Da Costa, A. R., Fane, A. G., Fell, C. J. D. & Franken, A. C. M. Optimal channel spacer design for ultrafiltration. *Journal of Membrane Science* **62**, 275-291, doi:http://dx.doi.org/10.1016/0376-7388(91)80043-6 (1991).

54 Schwinge, J., Neal, P. R., Wiley, D. E., Fletcher, D. F. & Fane, A. G. Spiral wound modules and spacers: Review and analysis. *Journal of Membrane Science* **242**, 129-153, doi:http://dx.doi.org/10.1016/j.memsci.2003.09.031 (2004).

55 Ulbricht, M. Advanced functional polymer membranes. *Polymer* **47**, 2217-2262, doi:http://dx.doi.org/10.1016/j.polymer.2006.01.084 (2006).

56 Richert, L. *et al.* Surface Nanopatterning to Control Cell Growth. *Advanced Materials* **20**, 1488-1492, doi:10.1002/adma.200701428 (2008).

57 Shirtcliffe, N. J., McHale, G., Newton, M. I., Chabrol, G. & Perry, C. C. Dual-Scale Roughness Produces Unusually Water-Repellent Surfaces. *Advanced Materials* **16**, 1929-1932, doi:10.1002/adma.200400315 (2004).

58 Yan, L., Li, Y. S., Xiang, C. B. & Xianda, S. Effect of nano-sized Al_2O_3-particle addition on PVDF ultrafiltration membrane performance. *Journal of Membrane Science* **276**, 162-167, doi:http://dx.doi.org/10.1016/j.memsci.2005.09.044 (2006).

59 Barger, M., Hoff, D., Carnahan, R. P. & Gilbert, R. A. (Google Patents, 2003).

60 Bradford, W. L., Herrington, R. E. & Clement, A. D. (Google Patents, 2007).

61 Balster, J., Stamatialis, D. F. & Wessling, M. Membrane with integrated spacer. *Journal of Membrane Science* **360**, 185-189, doi:http://dx.doi.org/10.1016/j.memsci.2010.05.011.

62 Vogelaar, L., Barsema, J. N., van Rijn, C. J. M., Nijdam, W. & Wessling, M. Phase Separation Micromolding—PSμM. *Advanced Materials* **15**, 1385-1389, doi:10.1002/adma.200304949 (2003).

63 Vogelaar, L. *et al.* Phase Separation Micromolding: A New Generic Approach for Microstructuring Various Materials. *Small* **1**, 645-655, doi:10.1002/smll.200400128 (2005).

64 Barsema, J., Nijdam, W., Van Rijn, C., Vogelaar, L. & Wessling, M. (Google Patents, 2004).

65 Brans, G., van Dinther, A., Odum, B., Schroen, C. G. P. H. & Boom, R. M. Transmission and fractionation of micro-sized particle suspensions. *Journal of*

Membrane Science **290**, 230-240, doi:http://dx.doi.org/10.1016/j.memsci.2006.12.045 (2007).

66 Petronis, A a. n., Berntsson, K., Gold, J. & Gatenholm, P. Design and microstructuring of PDMS surfaces for improved marine biofouling resistance. *Journal of Biomaterials Science, Polymer Edition* **11**, 1051-1072, doi:10.1163/156856200743571 (2000).

67 Chen, C. S., Mrksich, M., Huang, S., Whitesides, G. M. & Ingber, D. E. Geometric Control of Cell Life and Death. *Science* **276**, 1425-1428, doi:10.1126/science.276.5317.1425 (1997).

68 Ding, Y. *et al.* Thermodynamic Underpinnings of Cell Alignment on Controlled Topographies. *Advanced Materials* **23**, 421-425, doi:10.1002/adma.201001757.

69 Carman, M. L. *et al.* Engineered antifouling microtopographies-correlating wettability with cell attachment. *Biofouling* **22**, 11-21, doi:10.1080/08927010500484854 (2006).

70 Bikel, M. a., Punt, I. G. M., Lammertink, R. G. H. & Wessling, M. Micropatterned Polymer Films by Vapor-Induced Phase Separation Using Permeable Molds. *ACS Applied Materials & Interfaces* **1**, 2856-2861, doi:10.1021/am900594p (2009).

71 Won, Y. J. *et al.* Preparation and Application of Patterned Membranes for Wastewater Treatment. *Environmental Science & Technology* **46**, 11021-11027, doi:10.1021/es3020309.

72 Culfaz, P. Z., Rolevink, E., van Rijn, C., Lammertink, R. G. H. & Wessling, M. Microstructured hollow fibers for ultrafiltration. *Journal of Membrane Science* **347**, 32-41, doi:http://dx.doi.org/10.1016/j.memsci.2009.10.003.

73 Culfaz, P. Z. *et al.* Fouling Behavior of Microstructured Hollow Fiber Membranes in Dead-End Filtrations: Critical Flux Determination and NMR Imaging of Particle Deposition. *Langmuir* **27**, 1643-1652, doi:10.1021/la1037734.

CHAPTER II

FABRICATION OF SURFACE PATTERN ON UF MEMBRANE USING NANOIMPRINT LITHOGRAPHY

2.1 Introduction

Membrane technology, even after its introduction in the commercial application in early 50s, is receiving significant attention among researchers [1, 2]. With the emergence of new technologies, membrane and other related filtration processes are modified to reduce the manufacturing cost and enhance membrane performance [3, 4]. Even after improvement of membrane technologies by decades of research, commercial applications of membrane suffer a critical problem of flux decline due to membrane fouling [5, 6]. As discussed in the Chapter 1 of this dissertation, fouling is unavoidable and it is a natural product of selection based membrane operations. Many versatile approaches have been invented to address this fouling issue but broad scale application of most of these approaches is questionable due to high energy consumption, durability over long time use and scalability factors [7]. In comparison to the other methods fouling mitigation via surface patterning is quite promising as it has emerged as an important tool to mitigate fouling in many non-membrane applications [8, 9]. Discussion from Chapter 1 also revealed that fabrication of porous membrane with targeted surface topography is a challenge because of lack of effective method to create surface pattern on membrane surface.

Therefore, an effective method is needed here that can generate surface pattern on membrane with good fidelity and relatively low energy cost while providing a good permselective characteristic at the same time.

Micro/Nano-fabrication with a variety of materials has becoming increasingly assessable [10]. Generation of surface pattern using direct writing method is very popular including techniques such as focused laser beam, AFM based writing, near field scanning optical microscopy, electron beam lithography, focus ion beam lithography, inkjet writing and dip pen lithography [11]. High resolution features with minimum dimension of ~10 nm was reported to be achieved using these methods. However, in the fabrication of commercial devices, these methods are relatively very slow and very expensive for large scale application [12].

In comparison, fabrication using replication method can produce surface feature in a single step, rapidly and with high fidelity. Replication methods are also very cost effective since a master feature can be used many times, at short time scale compared to the other writing methods [13]. Among these, Nanoimprint lithography (NIL) is low cost, high throughput and high resolution replication that can be used to create features on polymeric materials/resists [14, 15]. While other replication methods during solvent casting require a significant alteration of the commercial chemical processes, NIL process can be used directly in fabricating the existing commercial membranes.

Different polymer materials like polysulfone (PS), polyethersulfone (PES), polyvinylidiene fluoride, polyacrilonitrile, cellulose acetate and polypropylene have been extensively used in ultrafiltration (UF) membranes. To choose a suitable candidate for this study one has to search for a polymer membrane that is thermoplastic, amorphous and have a broad commercial interest. PES membrane, closely related to another sulfur-containing thermoplastic polysulfone, is frequently used in microfiltration (MF) and UF processes [1, 6]. Unlike PS, PES has diphenylene sulfone repeating unit in its structure [16]. PES is preferred as a membrane over other polymers because of its wide range of temperature stability, better oxidative resistance capability (up to ~200 ppm chlorine) and wide range of pore sizes (10 Å to 0.1μm) range [17]. However, lower pressure usage to avoid fouling often confines the broader usage of PES membrane while higher hydrophobicity compared to other polymer leads to greater tendency of fouling by stronger interactions with various solutes. In this research, for the fabrication of patterned membrane, PES is chosen as a model membrane.

In this chapter, application of NIL to fabricate surface pattern directly on polyethersulfone (PES) ultrafiltration (UF) membrane was explored. NIL was carried out with flat/blank and featured Si mold systematically. Subsequently, morphological and permeance change were also studies. At first, NIL was carried with a flat mold by changing various process parameters like temperature, pressure and time and influences of these NIL process parameters on the membrane properties were analyzed. From the experiments it was revealed that effective NIL can only be carried

out at a temperature lower than the glass transition temperature (T_g) of the PES UF membrane. Effect of NIL on the membrane permeability, surface roughness, membrane thickness, porosity and surface pore size were also studied in this chapter.

2.2 Methods and Materials

2.2.1 Surface patterning of UF membrane by NIL

A commercial PES UF-type membrane (PW, GE Water and Infrastructure) with a nominal 30 kg/mol molecular mass cutoff (MWCO) was used as a model UF membrane for all the experiments described in this study. The membranes were not subjected to any pre-treatment prior to imprinting. The un-patterned, flat-sheet UF membranes were stored in dry ambient conditions, and also used without any pre-treatment. These types of UF membranes are frequently treated with glycerol solution within the pore structure to prevent drying of the membrane. Note that, here membrane samples were not cleaned prior to NIL process.

NIL process is a simple and robust technique capable of fabricating sub-10 nm features at low cost [14, 15]. A typical route for NIL processes (Fig 2.1) utilizes the thermal embossing method whereby a polymer film is squeezed into the nanoscale cavities of a rigid mold under relatively high pressure (a few MPa's) at a temperature above the T_g of the polymer. A replica is then created after mold separation at a temperature below T_g. However, it was found that imprinting at a temperature close to or higher than the T_g of the UF membrane (~184 °C) collapsed the porous structures of the UF membrane, despite excellent patterns being formed on the

membrane surface. As a result, the patterned membranes became impermeable to DI water within the pressure range normally used for UF process. Instead, when the NIL patterning of the UF membrane was carried out at a temperature below the T_g of the PES, surface patterns were successfully imprinted onto the UF membrane without much sacrificing its permeability. Eitrie 3 (Obducat, Inc.) nanoimprinter was used for imprinting for all the samples described in this study.

The molds used for nanoimprinting are standard silicon wafer having a thin native silicon oxide layer of few nanometers thick. Such silicon oxide surface is hydrophilic and water contact angle is close to 0° [16]. Two different silicon molds with different pattern features and a flat silicon mold without any features were used. The first mold (will be termed as Mold 1 from now on) had parallel lines and space gratings with a periodicity of 834 nm, groove depth of 200 nm, and a line-to-space ratio of 1:1. Second silicon mold (will be termed as Mold 2 from now on) contains parallel lines and space gratings with a periodicity of 575 nm, a line width of 210 nm and a groove depth of 180 nm. The native silicon oxide mold surface was treated with either Piranha® or Nano-strip® solution (stabilized 3:1 concentrated sulfuric acid to hydrogen peroxide solution) solution prior to the fabrication to remove organic residue.

Patterning was carried out under different imprinting conditions and mold for the PES UF membrane. At first the membranes samples were imprinted with the flat/blank mold at different temperature and pressure from 40 °C to 180 °C with pressure from 1 MPa to 4 MPa. For most of the samples imprinting was carried out

for 180s the mold was separated from the membrane samples at 40 °C. Imprinting was also carried out using above mentioned temperature and pressure range by varying imprinting time from 1 min to 7 min.

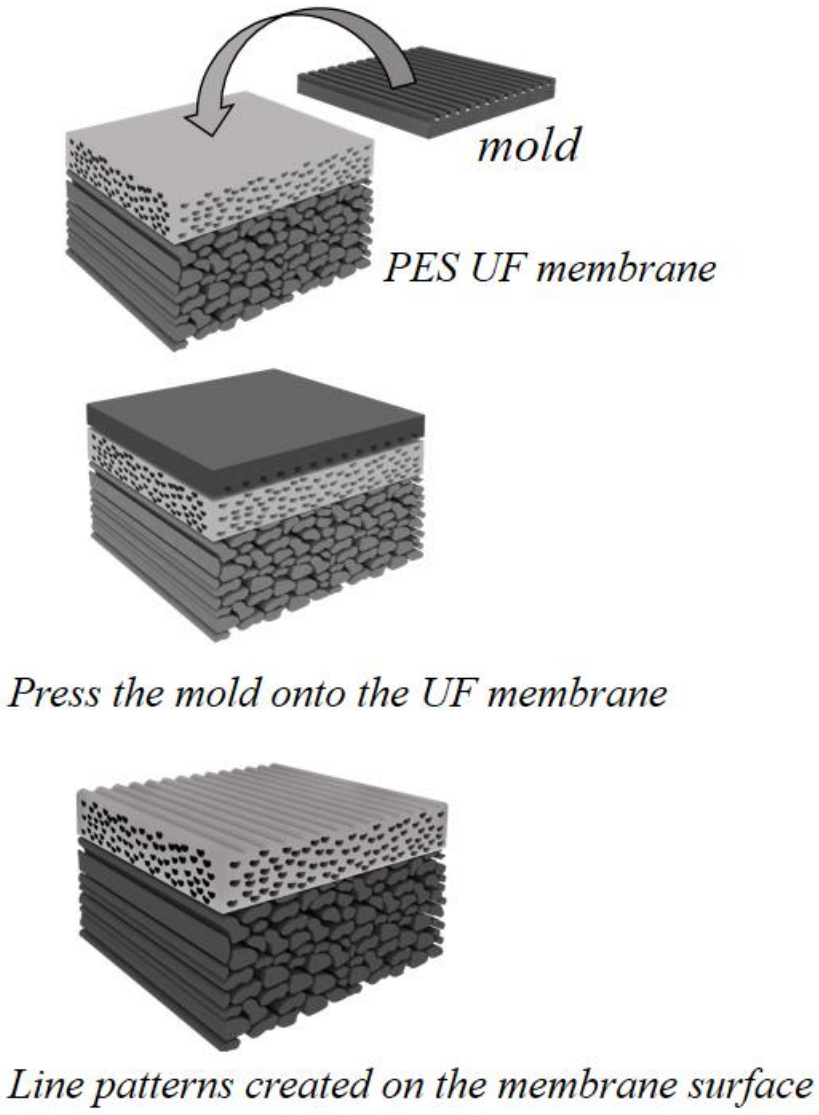

Figure 2.1: Steps used in a NIL of PES membrane. Mold with features are brought into contact with membrane surface at an elevated temperature with pressure for a certain amount of time, and demolding at temperature below the glass transition temperature of the polymer membrane.

In the second part of this work, membrane samples were imprinted with the molds having the features described previously. With the Mold 1 imprinting was carried out at 120 °C with a pressure of 4 MPa for 180 s, and the mold was separated from the membrane at 40 °C. For Mold 2, four different set of samples were imprinted varying temperature and pressure. All the imprinting for Mold 2 were carried out for 180s and the mold was separated from the membrane at 40 °C. Table 2.1 list all the samples imprinted at different NIL process condition using different molds.

Table 2.1: Acronyms of molds and patterned samples imprinted at different processing condition.

Mold 1	*Sample 1.1*	*None*	*None*	*None*	*None*
Imprinting Condition	120 °C 4 MPa	–	–	–	–
Mold 2	*Sample 2.1*	*Sample 2.2*	*Sample 2.3*	*Sample 2.4*	*Sample 2.5*
Imprinting condition	120 °C 4 MPa	140 °C 2 MPa	140 °C 4 MPa	160 °C 2 MPa	175 °C 4 MPa

2.2.2 Atomic Force Microscopy

Dimension 3100 AFM (Bruker Corporation) was used this study to examine the surface topography of un-patterned and patterned membranes. AFM measurements were performed with the tapping mode under ambient conditions using silicon cantilever probe tips (Veeco, RTESP). For patterned membranes with line-and-space grating patterns, the scan of the cantilever was kept perpendicular with the grating lines, so that faithful mapping of the surface patterns can be

obtained. For a given membrane, measurements over multiple areas were normally carried out to verify the uniformity or distribution of the patterns obtained.

2.2.3 Scanning electron microscopy (SEM)

In this study, surface topography and cross-sections of the un-patterned and patterned UF membranes were examined with a field-emission scanning electron microscope (FESEM, Zeiss, Supra 60). Membrane samples were dried in a vacuum oven prior to SEM measurements, and the membrane cross-sections were prepared using a microtome at -20 °C, and coated with a 4.5-4.7 nm gold layer.

2.2.4 Size exclusion chromatography (SEC)

MWCO values for patterned and Un-patterned membranes were determined by using size exclusion chromatography (SEC, Agilent 1100, Agilent Technologies). Filtration of a mixture of polyethylene glycols (PEGs) with varying molecular masses (100–25, 800 g/mol, Sigma Aldrich) in an aqueous solution were performed for this characterization [18]. The PEG solution was prepared at a concentration of ~1 g/L using deionized (DI) water with a resistivity 18.2 MΩ cm (a conductivity of 0.8 μS/cm). The PEG mixture solution was filtered at ~276 kPa for 1 h while permeate was collected and recorded every 10 min. The molecular mass distributions in the feed and permeate solutions were measured by the SEC with a silica column (Yarra SEC-3000 by Phenomenex). The retention coefficients for different molecular mass PEGs were determined from the permeate concentration, C_p, and bulk concentration, C_f,

as, $R_{obs}=1-C_p/C_f$. Three repetitive filtration measurements were carried out for each membrane, and the mean R_{obs} values are reported here. All the filtration experiments were conducted using cross-flow filtration setup described later in this chapter.

2.2.5 Filtration experiments with patterned UF membranes

All the filtration experiments were conducted at ~ 22 ^{o}C (the temperature of the feed), in a bench-scale cross-flow filtration module, as schematically shown in Fig. 2.2. Three membranes, fed from the same 4L reservoir with a peristaltic pump (MasterFlex), were tested in parallel simultaneously. Each membrane had a surface area of ~ 11 cm^2 and an effective filtration area of 9.7 cm^2 after being sealed in each filtration cell. Transmembrane pressure (TMP) across each membrane was maintained with a back-pressure regulator (Swagelok) and monitored with a differential pressure transducer (Omega). For each filtration experiment, the initial permeate flux were recorded and membranes were compacted with DI water, until the permeate flux from two successive measurements changed less than 2 %. Befroe and after the compaction period whole filtration set up was cleaned and DI water used for the feed was pre-filtered with 0.22 μm nitrocellulose microfiltration membrane. The compaction and the final permeate flux were also recorded. After compaction pressure was and membranes were kept sealed until morphological analysis. For a given experimental condition, statistical average of the three simultaneous filtrations is reported.

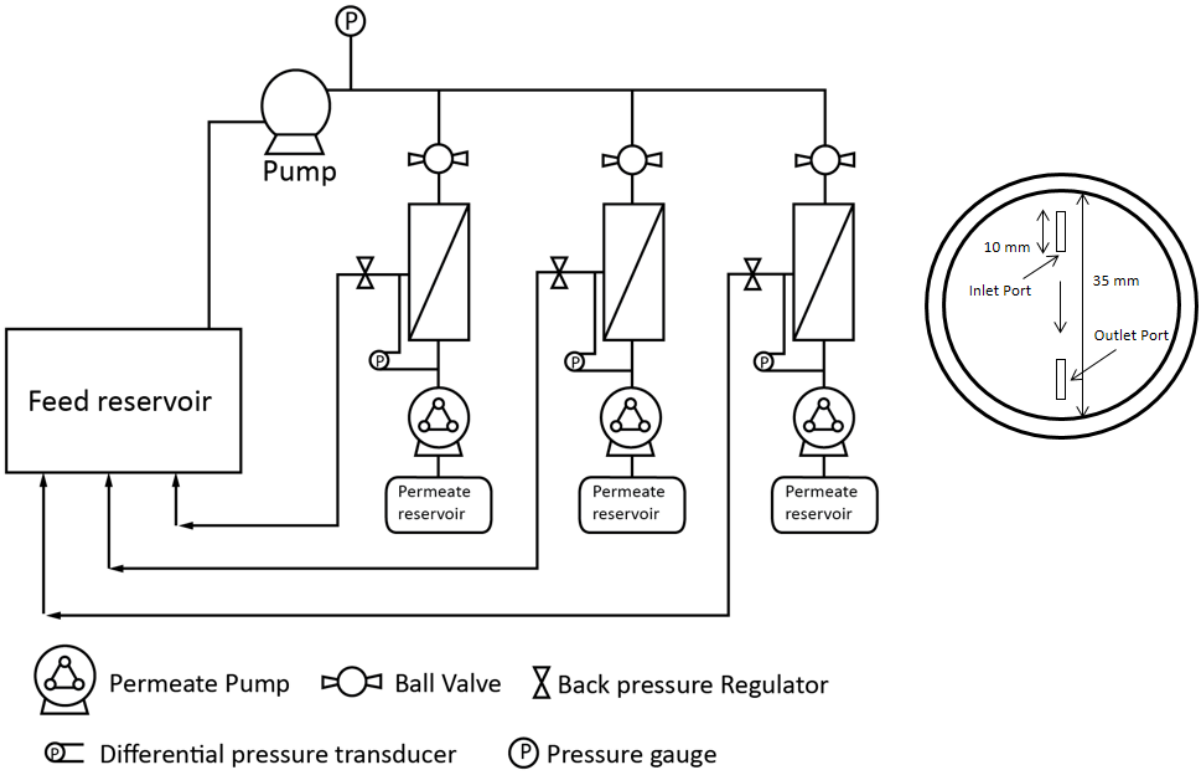

Figure 2.2. Schematic of the apparatus used for the cross-flow filtration, showing the three parallel cells (top) used simultaneously. Sketch on the right side shows the details of the cell geometry.

2.2.6 Thickness and porosity measurement of the patterned UF membranes

Thickness of the PES membranes were determined from cross-sections of the membrane sample. Cross-sections of the membrane samples were prepared by embedding the samples in a material called tissue-tek and cutting the sample at -20 ^{o}C. Five random areas were chosen to determine the membrane thickness and average value of the five measurements were reported in this study.

The porosity of the PES UF membrane was determined by the mass loss of wet membranes after drying [19]. The membrane samples was filtered at ~276 kPa for 20

min and a membrane piece with an area of 9.7 cm^2 was cut and immersed in DI water overnight at room temperature. The excess water at the membrane surface was removed by blotting with a filter paper and the thickness was determined by a digital micrometer. The weight of the wet membrane was measured before drying in a vacuum oven at 70 ^oC for 24 h. The weight of the dried membrane was measured. The overall porosity of the membrane was determined according to equation

$$\varepsilon = \frac{W_1 - W_2}{\rho A l} X\ 100 \quad (1)$$

where W_1 and W_2 are the mass of the wet and dry membranes (g), respectively, A is the membrane area (cm^2), l is the wet membrane thickness (cm) and ρ is the pure water density (0.998 gcm^{-3}).

2.3 Results and discussion

2.3.1 Surface patterning of UF by NIL below glass transition temperature

NIL is a top down approach where surface features of a master stamp are replicated into polymer surface by mechanical contact under controlled pressure, temperature and time. In typical NIL route, thermoplastic polymer thin film is transformed to a viscous liquid by heating above the T_g of the polymer indicated by region 1 in the Fig. 2.3. After reaching a certain temperature higher than T_g, the thermoplastic film is compressed between mold and substrate for a period of time, and the viscous polymer flow into the cavities of the mold. Subsequently, the mold/polymer/substrate system is cooled to a temperature below T_g of the polymer

(region 4 in Fig. 2.3) [20], with the pressure maintained. A replica is then created on the polymer surface after the mold is separated at a temperature below T_g.

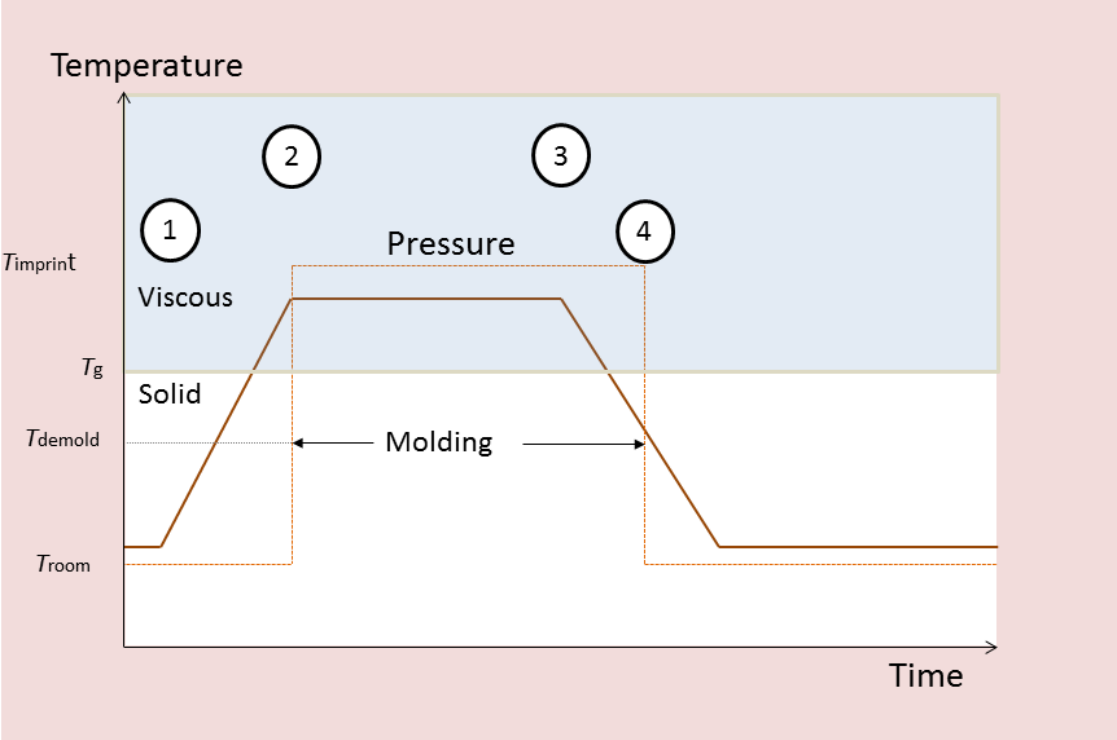

Figure 2.3: NIL process sequence: schematics of process sequence used for imprinting (temperature/pressure diagram with time dependence); (1) Heating begin, (2) Mechanical contact (emboss), (3) Cooling begin, (4) Demolding.

The T_g of the PES UF membrane were characterized by the NanoTA and from the average of five measurement, T_g was found ~184 °C, a value very close to the bulk T_g of PES [20]. Interestingly, we have found that imprinting at a temperature higher than the T_g of the UF membrane (~184 °C) completely collapsed the porous structures of the UF membrane, despite excellent patterns being formed on the membrane surface. As a result, the imprinted membranes became impermeable to DI water. In comparison, using an imprinting temperature lower than T_g of PES, the UF

membrane samples were flattened, (imprinted with flat mold) while being permeable to DI water. Although permanent deformation of a dense, glassy PES film under such a pressure is negligible [21], studies have shown that permanent deformation under moderate pressure becomes possible for porous glassy polymer films and the degree of plastic deformation increases with the porosity of the film [22]. Such enhanced plastic deformation is likely the primary deformation mechanism for the pattern created on the UF membrane.

2.3.2 DI water filtration of UF membrane imprinted with a flat wafer mold

First, we compare the DI water permeate flux for all the samples "imprinted" with a flat wafer with the un-patterned ones (PES membrane without imprinting). Figure 2.4 represents the DI water permeate flux over ~2 hours of filtration for a membrane sample imprinted with flat wafer at 160 °C and 2 MPa pressure for 180 s.

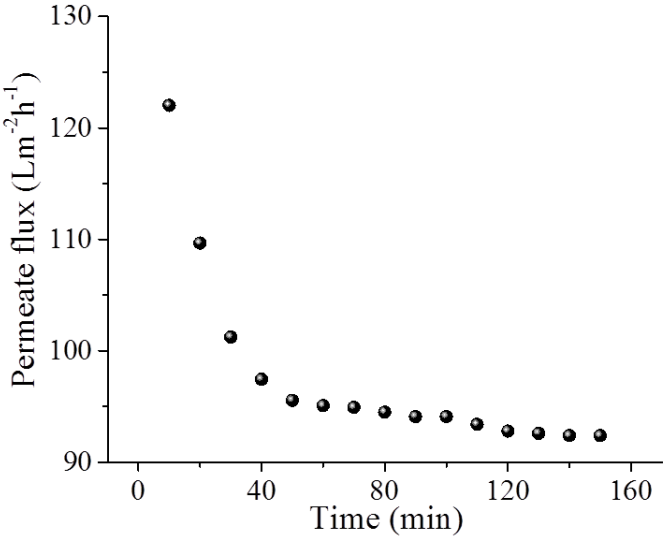

Figure 2.4: Permeate flux (TMP= 276 kPa) of DI water over filtration time for PES UF membrane imprinted with a flat wafer at 160 °C and 2 MPa pressure for 180 s.

Interestingly, even in the absence of fouling permeate flux declined over time and for this particular sample permeate flux decreased ~ 35% from the initial value. This decline of permeate flux without fouling is termed as "compaction" and it has been well documented for reverse osmosis, UF, microfiltration and other membranes used in distillation process [23-25]. Each membrane was compacted until the steady state flux was reached (flux decreasing less than 2% in 10 minutes interval). The degree of compaction for all the samples were calculated and summarized in Fig. 2.5.

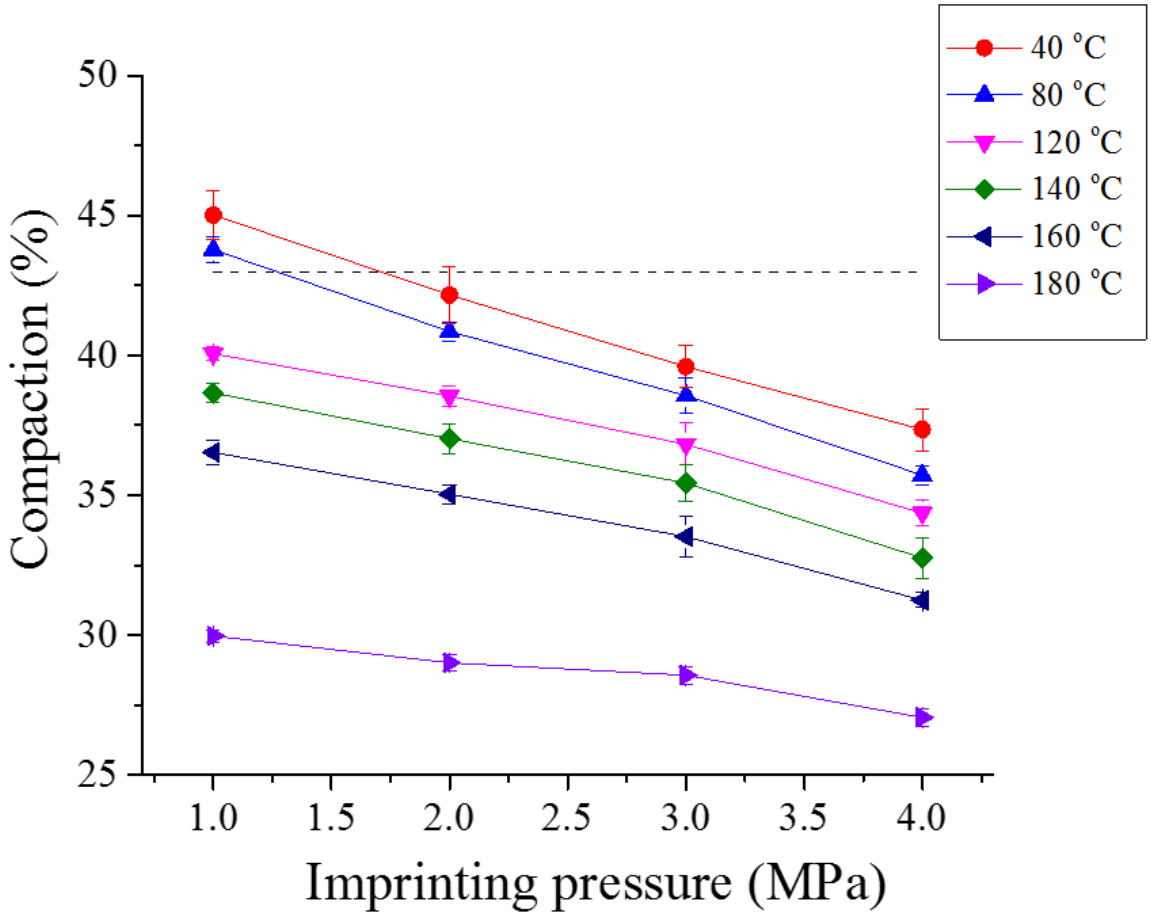

Figure 2.5: Degree of compaction of PES UF membrane as a function of imprinting pressure at different temperatures. Each data point represents the average value of three repeated experiments, and the error bars represent the corresponding standard deivation. Dotted line represents the compaction for un-patterned PES membrane.

For all the membranes, the degree of compaction decreases with pressure at a constant temperature. At lower imprinting temperature, degree of compaction decreases as much higher rate compared with the membranes imprinted at higher temperature. For that, at a constant imprinting pressure, degree of compaction also reduces with an increase in imprinting temperature.

For all the membrane samples, DI water permeate flux stabilized after ~2 hours of filtration (compaction period) and remained constant afterwards. Water permeance for all the samples imprinted with flat wafer are summarized in Fig. 2.6.

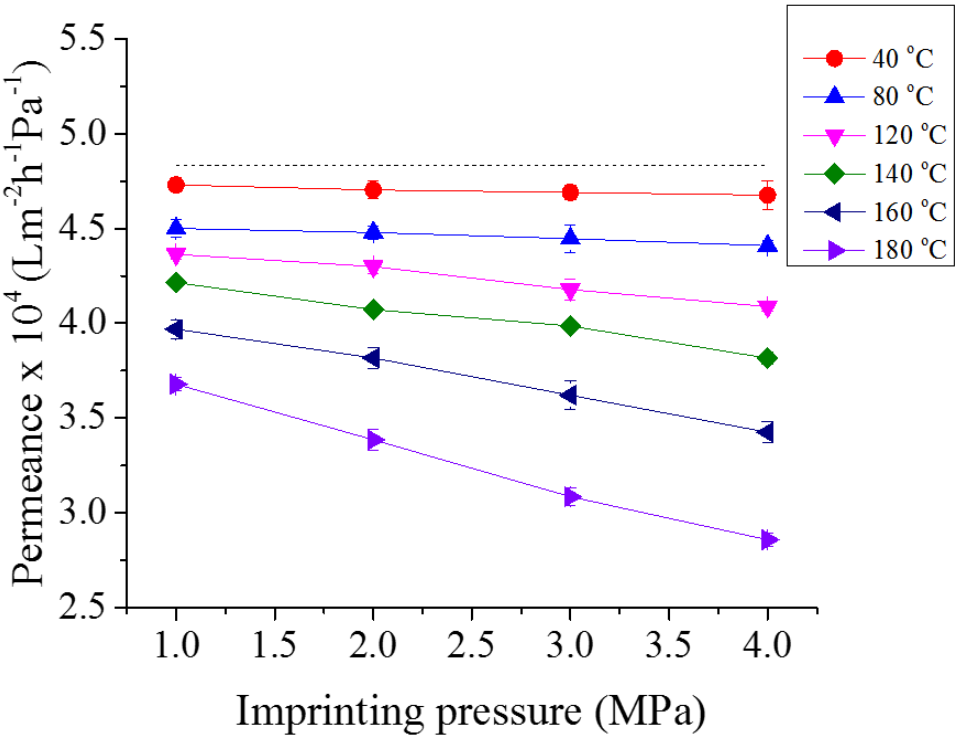

Figure 2.6: Membrane permenace after compaction of the PES UF membrane plotted as function of imprinting pressure, at different temperature. Each data point represents the average value of three repeated experiments, and the error bars present the corresponding standard deviations. Dotted line represents the membrane permenace for un-patterned (without imprinting) PES membrane.

Clearly, the NIL process reduces the membrane permeance from un-patterned membrane as indicated in Fig. 2.6. When the imprinting temperature is lower than 120 °C, membrane permeance appears to be insensitive to the imprinting pressure. However, when the imprinting temperature was higher than 120 °C, membrane permeance reduces with an increase of imprinting pressure. When imprinting temperature approached T_g of the PES membrane, water permeance decreases at much higher rate with pressure. For example, at 4 MPa membrane permeance was almost half of the permeance without any imprinting. Stabilized water permeance value from Fig. 2.6 can provide the figure-of-merit for imprinting PES UF membrane with other types of mold with features. From the figure, similar water permeance can be achieved using different combinations of NIL parameters (temperature and pressure). To further study these effects, two separate NIL protocol (120 ^{o}C- 4 MPa: 140 ^{o}C-2 MPa and 140 ^{o}C-4 MPa: 160 ^{o}C-2 MPa) that yielded the same water permeance were picked for model analysis which will be discussed later.

Note that, all the experiments discussed earlier were imprinted at different temperature and pressure using a constant imprinting time of 180 s or 3 min. The effects of imprinting time on the DI water filtration were also studied here. Figure 2.7 represents the membrane permeance plotted as a function of imprinting temperature for different imprinting time. Figure 2.7a represents when imprinted at 2 MPa and 2.7b when imprinted at 4 MPa.

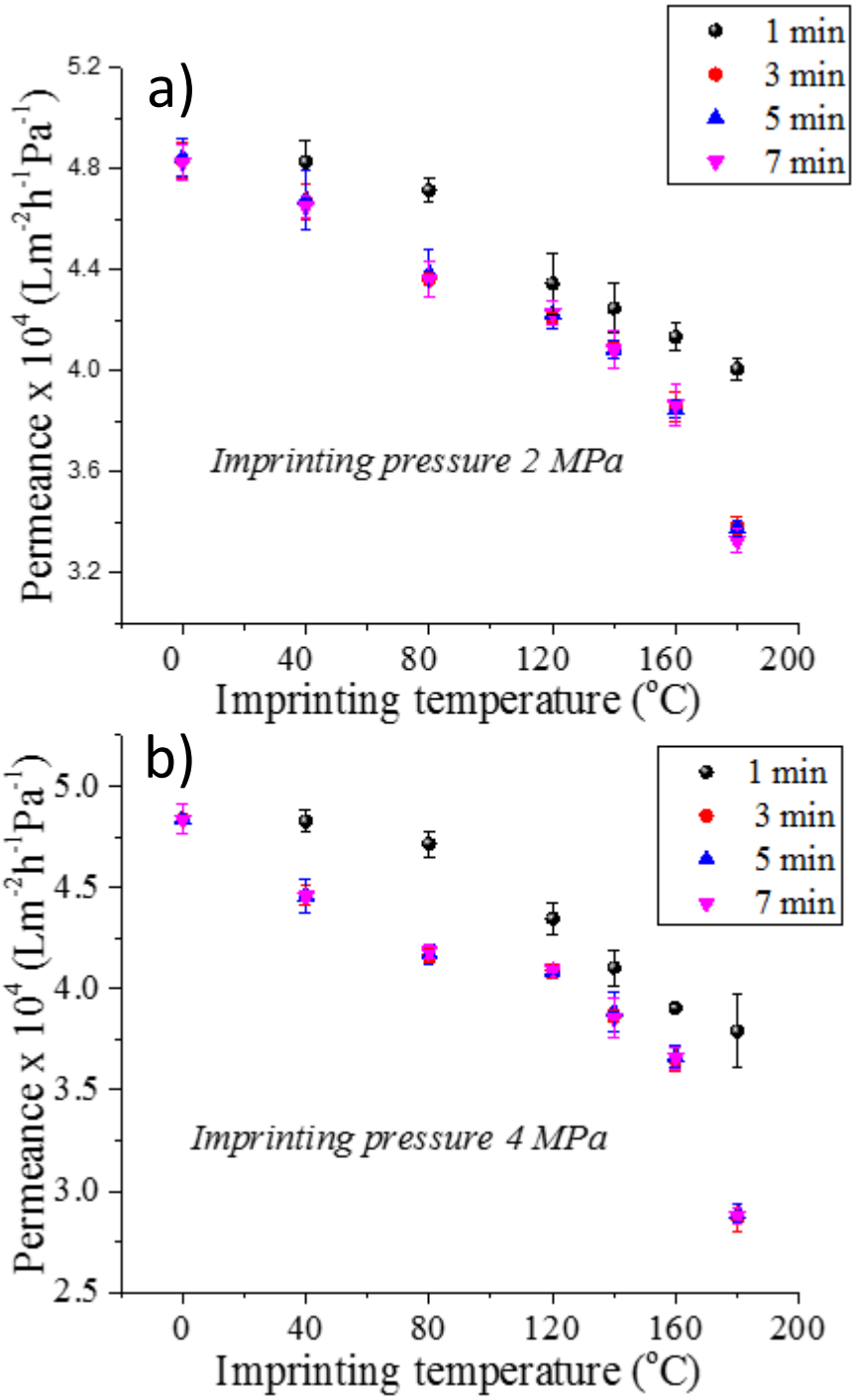

Figure 2.7: Membrane permeance plotted as function of imprinting temperature at 2 MPa (a) and 4 MPa (b) pressure using different mold contact time. Times used for the imprinting are indicated in the inset. Each data point represents average of three repeated experiment.

Consistent with previous permeance-imprinting result, membrane permeance decreases with imprinting temperature for both imprinting pressure. However, imprinting time seem to have little effect on the membrane permeance as increasing imprinting time over 3 min do not change the membrane permeance at all. These experiments suggest that the imprinting process is complete with 3 min of mechanical contact between the membrane surface and wafer mold (step 2 Fig. 2.3).

2.3.3 Surface morphology of patterned UF membrane using NIL

Figure 2.8a and 2.8b show the topographic AFM images of the un-patterned and patterned membranes. From both AFM measurements, the un-patterned membrane had a smooth surface with a root-mean-square (rms) roughness <10 nm. After the NIL process, grating patterns with an average pattern height between 100 -120 nm were created at the membrane surface (Fig. 2.8b). Clearly, the pattern height achieved is smaller than the depth of the mold (200 nm), and the cross-sections of the pattern lines do not display the sharp corners of the mold cavities.

Given that the imprinting temperature (120 °C) was less than the T_g of the PES, these pattern characteristics suggest that a large degree of viscous flow could not be achieved. Despite the minor issues regarding the fidelity of the patterning process on the UF membrane, functional surface patterns were achieved reproducibly over a 2.5 cm x 2.5 cm area suitable for filtration.

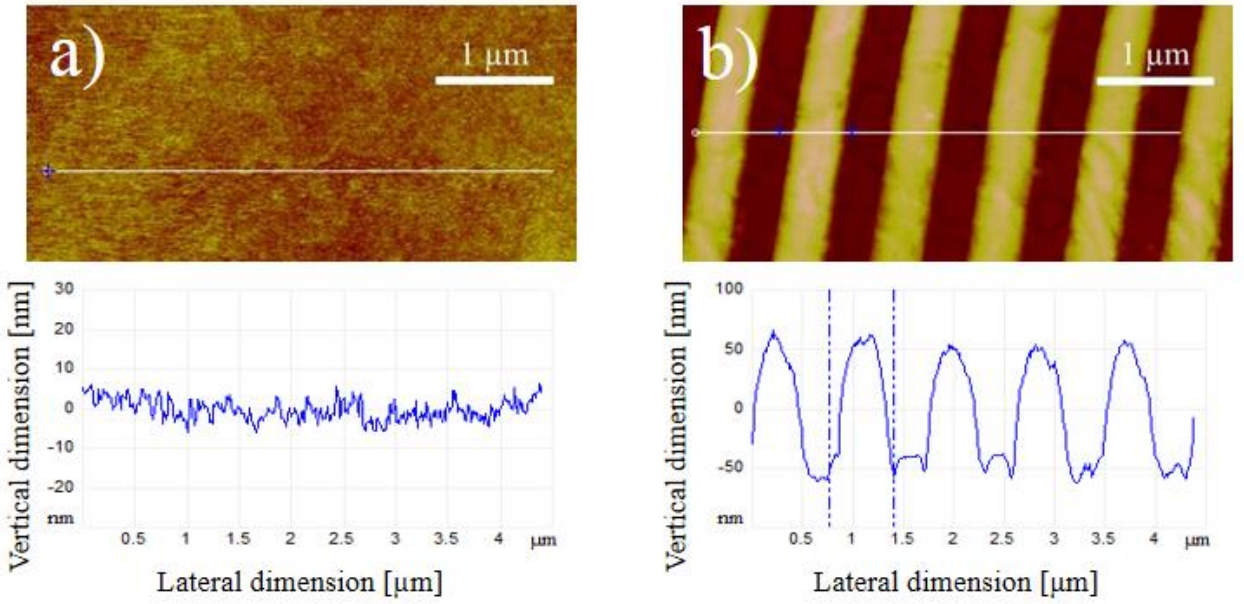

Figure 2.8: topographic AFM image of the un-patterned and patterned (sample 1.1) membranes, and the corresponding cross-sectional profiles of both membranes are shown below the AFM images. Patterned UF membrane was imprinted with Mold 1 at 120 °C at 4 MPa for 3 min.

Figure 2.9a and 2.9b show the topographic AFM images of the patterned membranes imprinted with Mold 2. After the NIL process, the membrane sample 2.1 have a grating patterns with an average pattern height between 60 -65 nm and sample 2.2 have a grating patterns with an average pattern height between 30 -35 nm at the membrane surface. Although sample 2.2 was imprinted at higher temperature but these AFM images suggest that imprinting pressure is a more effective factor in creating pattern on the membrane surface at lower temperature (less than T_g).

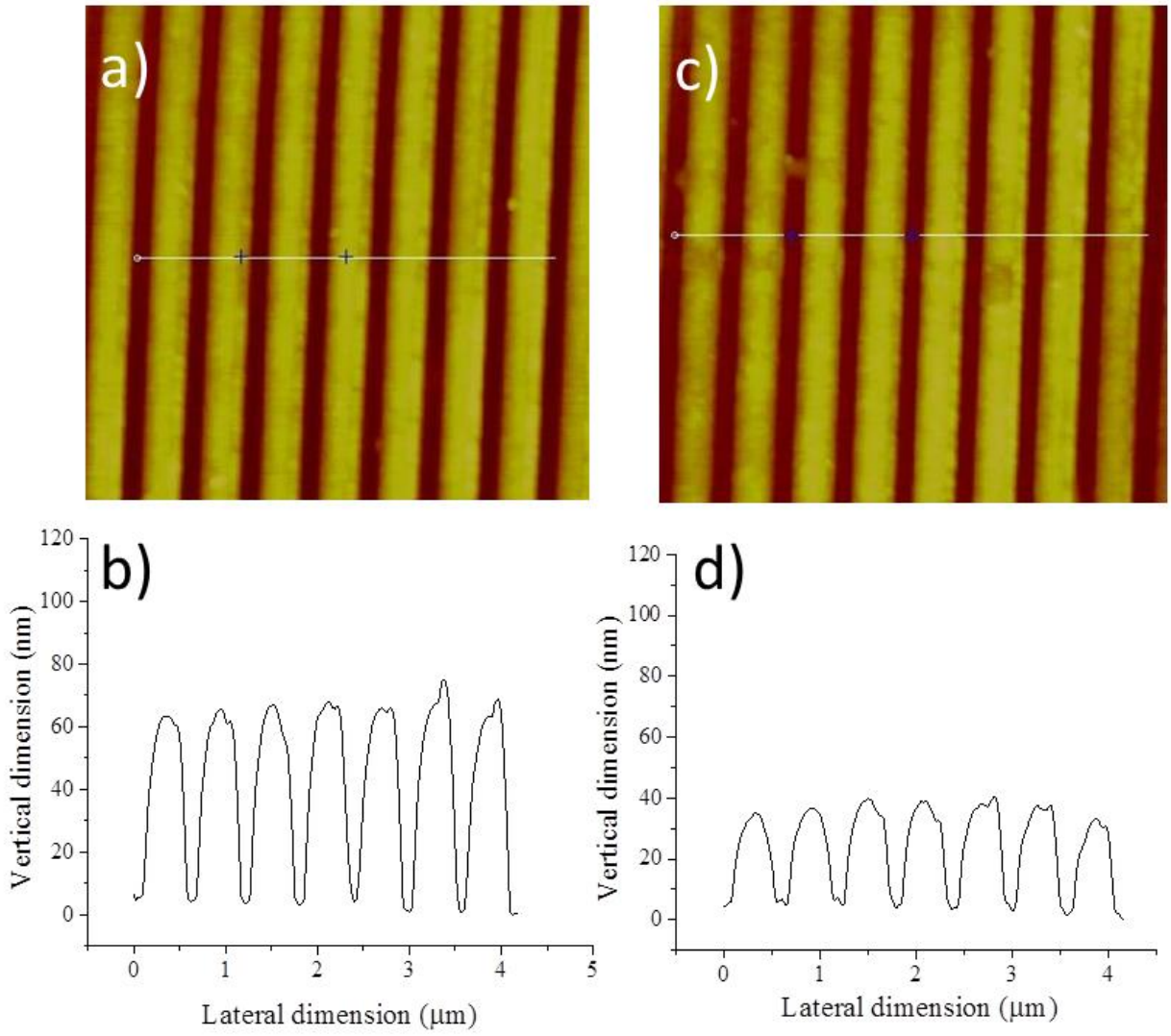

Figure 2.9: topographic AFM image of the patterned (sample 2.1 and sample 2.2) membranes, and the corresponding cross-sectional profiles of both membranes are shown below the AFM images. Patterned UF membranes were imprinted with mold 2 at (a) 120 °C at 4MPa for 3 min and (b) 140 °C at 2MPa for the same time.

Figure 2.10a and 2.10b show the topographic AFM images of the patterned membranes imprinted again with Mold 2. After the NIL process, the membrane sample 2.3 have a grating patterns with an average pattern height between 50 - 55 nm and sample 2.4 have a grating patterns with an average pattern height between

80 - 85 nm at the membrane surface. This finding is consistent with the previous morphology analysis with sample 2.1 and 2.2. Even though sample 2.4 was imprinted at higher temperature but sample 2.3 showed larger pattern height as it was imprinted at higher imprinting pressure.

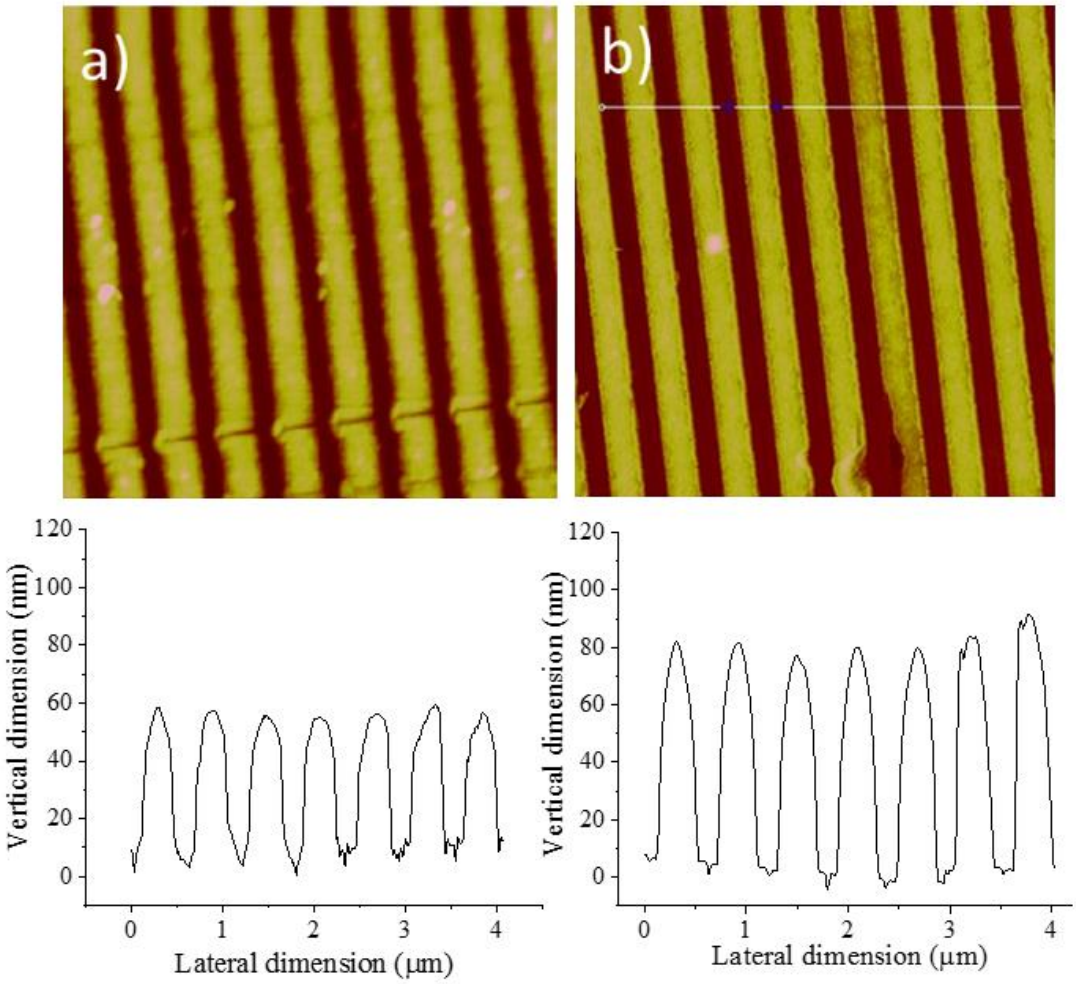

Figure 2.10: topographic AFM image of the patterned (sample 2.4 and sample 2.3) membranes, and the corresponding cross-sectional profiles of both membranes are shown below the AFM images. Patterned UF membranes were imprinted with Mold 2 at (a) 140 °C at 4 MPa for 3 min and (b) 160 °C at 2 MPa for the same time.

Figure 2.11a show the topographic AFM images of the patterned membrane imprinted at 175 °C. From the cross sectional profile, line-and-space grating patterns were created on the top surface of the UF membranes with identical pitch (575 nm). The average pattern heights (peak-to-valley) were 150 - 160 nm.

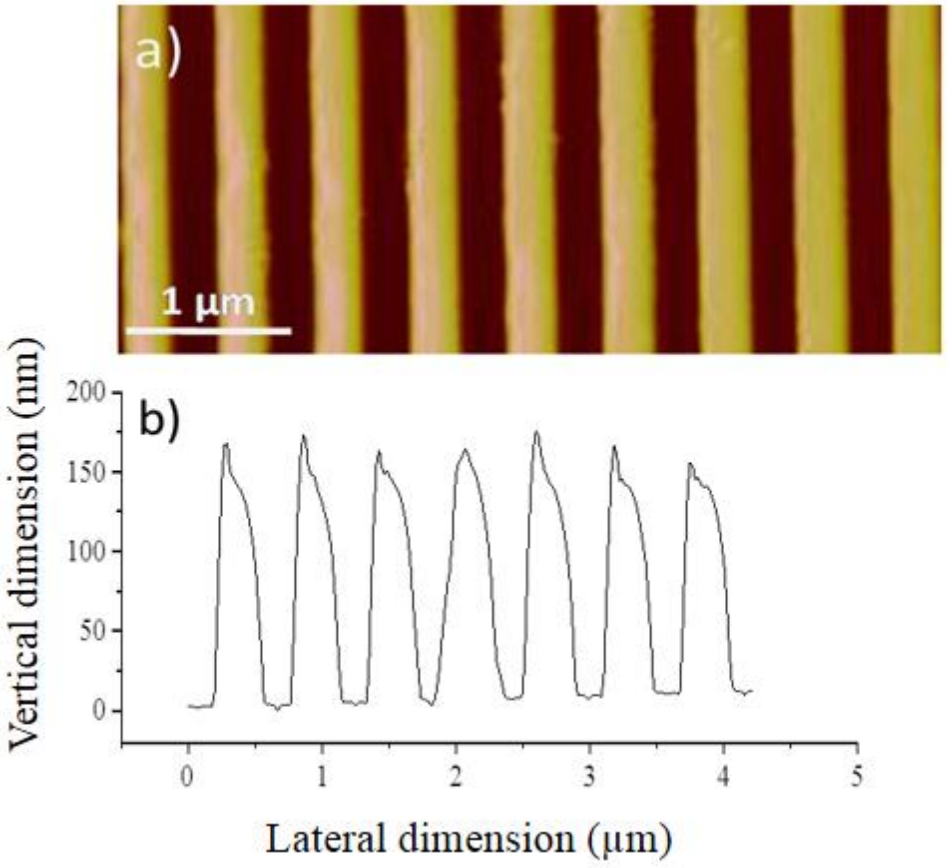

Figure 2.11: Topographic AFM image of the patterned (sample 2.5) membrane, and the corresponding cross-sectional profiles the membrane is shown below the AFM image. Patterned UF membrane was imprinted with Mold 2 at (a) 175 °C at 4 MPa for 3 min.

2.3.4 DI water filtration of patterned UF membrane

First, we compared the DI water permeate flux between the un-patterned and patterned membranes using the filtration setup as described earlier. Despite the apparent changes in the porous substructure induced by imprinting, the DI water permeate flux is comparable between un-patterned and patterned sample 1.1 membranes over a TMP range of 0 – 345 kPa. The overall water permeance was 4.81×10^{-4} $Lm^{-2}h^{-1}Pa^{-1}$ for the un-patterned membrane and 4.57×10^{-4} $Lm^{-2}h^{-1}Pa^{-1}$ for the patterned one. If the pore characteristics were identical, the larger surface area of the patterned membrane should lead to higher values of water permeate flux according to Darcy's law [26]. The observed slight reduction (2.8%) in pure water permeance of the patterned sample 1.1 membrane suggests that the benefit of increased membrane surface area is somewhat counter-balanced by a NIL-generated decreased permeance of the substructure (Fig. 2.6). Table 2.2 summarizes DI water permeance for un-patterned and different patterned membranes.

Table 2.2: DI permeance for all the patterned membranes

Membrane	*un-patterned*	1.1	2.1	2.2	2.3	2.4	2.5
RMS roughness (pattern height), nm	<10 nm	100-120	60-65	30-35	50-55	80-85	150-160
Permeance x 10^4, $Lm^{-2}h^{-1}Pa^{-1}$	4.81	4.57	4.47	4.49	3.35	3.38	2.92

Sample 2.1, 2.2, 2.3 and 2.4 were chosen to compare with the membrane permeance study done by "imprinting" the UF membrane with a flat wafer described in Session 2.3.2. Sample 2.1 (imprinted at 120 °C and 4 MPa) and sample 2.2 (imprinted at 140 °C and 2 MPa) showed the similar permeance as predicted from the permeance-NIL parameter curve in Fig. 2.6. However, average pattern height for sample 2.1 was ~ 92% higher than the sample 2.2. In a similar fashion, sample 2.3 and sample 2.4 showed similar water permeance while having significant difference in pattern height. These results suggest that NIL process can be optimized by selecting proper process temperature and pressure to achieve desired permeance of the membrane and surface patterns.

2.3.5 Influence of NIL on UF membrane structure

For membranes with a parallel array of uniform cylindrical pores, the permeability can be evaluated directly from the Hagen-Poiseuille equation as:

$$L_P = \frac{\varepsilon r_p^2}{8\mu\delta_m} \quad (3)$$

where ε is the membrane porosity (membrane pore area divided by membrane cross-sectional area), r_p is the pore radius, μ is the solution viscosity, and δ_m is the membrane thickness.

In the previous section, we have found that two different patterned membranes can show similar permeability or membrane resistance while having different surface

pattern. It is critical to understand the effect of NIL on the structure of the membranes imprinted. Fig. 2.12 presents both top-down and cross-sectional SEM images of a patterned membrane, as well as those of an un-patterned one.

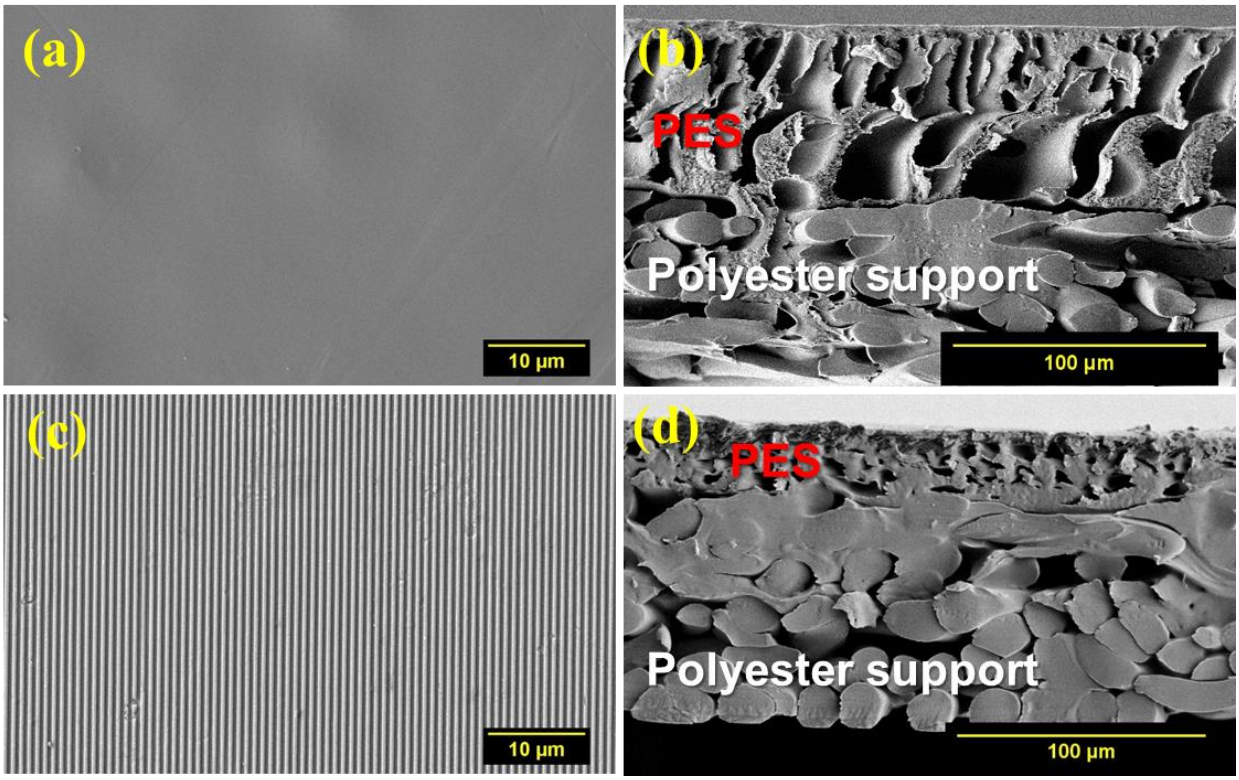

Figure 2.12: (a) and (b) are representative top surface and cross-sectional SEM images of the un-patterned membrane, respectively; (c) and (d) are representative top surface and cross-sectional SEM images of the patterned sample 1.1 membrane, respectively.

The un-patterned membrane has an asymmetric porous structure that overlies a nonwoven polyester support, as shown in Fig. 2.12b. After imprinting, the asymmetry was significantly modified (Fig. 2.12d). The relatively large micropores (micron range) below the separation layer (sub-layer) are visibly compressed in such way that the finger-like structure has disappeared. In addition, the thickness of the PES layer was found to be reduced slightly. However, it is known that the

permselectivity of the UF membrane, including both its permeance and MWCO, is largely determined by the characteristics of the barrier layer at the surface, rather than the asymmetric finger-like large-pore structures [27]. The nanometer-scale pores in the barrier layer are difficult to directly image with SEM, but can be indirectly characterized by the pure water (or buffer solution) permeance and MWCO measurements.

The MWCO is commonly used to describe the retention capabilities of a membrane and refers to the molecular mass of a solute, typically PEG, dextran or proteins, for which the membrane has retention rate greater than 90%. Fig. 2.13 shows the MWCO of both un-patterned and patterned membranes determined using PEG. The MWCO of the un-patterned membrane was determined to be ~15.4 kg/mol, which is lower than the manufacturer specification (20 kg/mol). This discrepancy has also observed by others [18], and is not uncommon due to its quantitative dependence on the specific solutes and protocols applied. More significantly, the MWCO of the patterned membrane sample 2.3 and 2.4 was found to be ~8.08 kg/mol and 9.85 11.71 kg/mol respectively (Fig. 2.13a). While MWCO of the patterned membrane sample 2.1 and 2.2 was found to be 9.48 kg/mol and 11.71 kg/mol respectively. These MWCO values also indicate that pore size at surface layer of the imprinted membrane are subjected compression due to the plastic deformation.

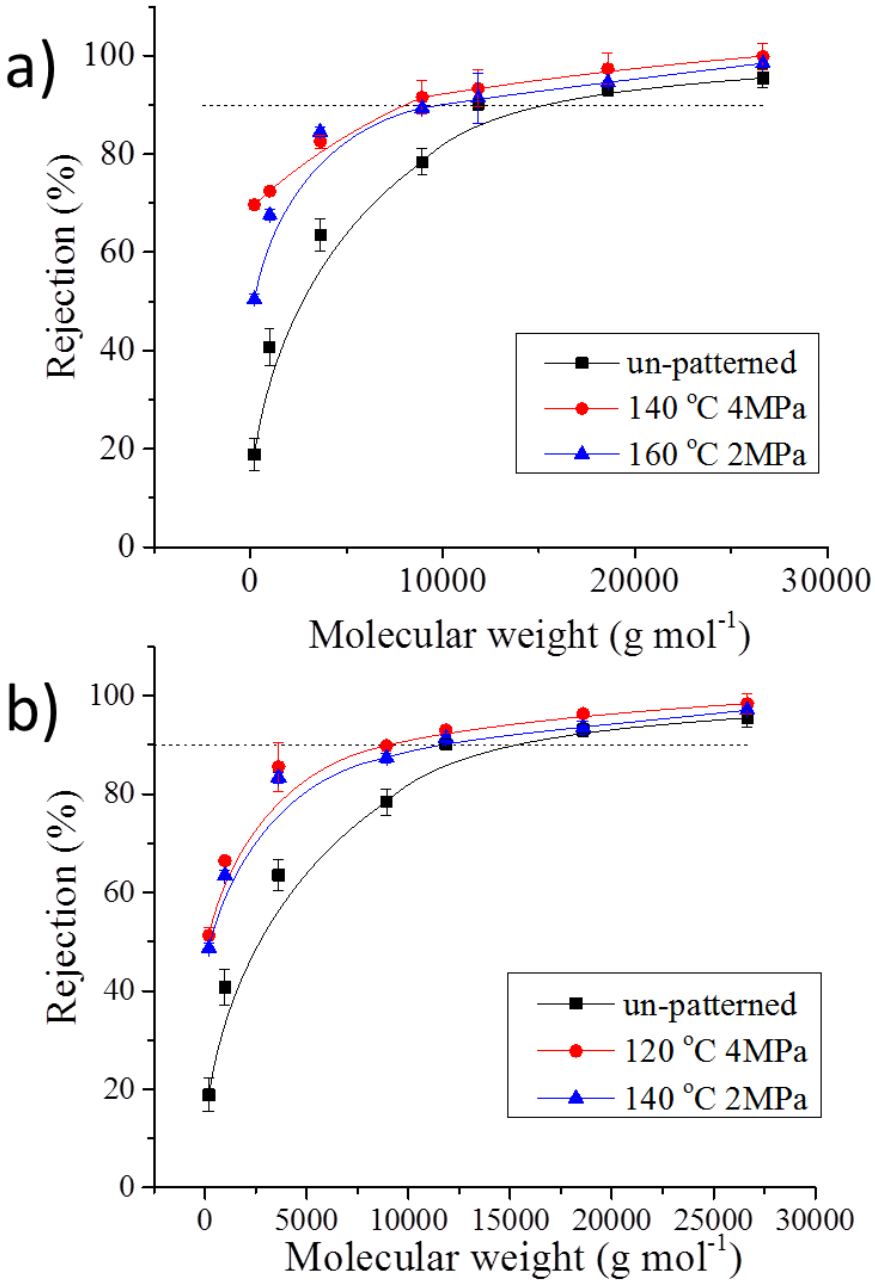

Figure 2.13: The molecular weight dependence of PEG rejection for both un-patterned (black squares) and patterned membranes a) sample 2.3 (red circles) and sample 2.4. (blue triangles) b) sample 2.1 (red circles) and sample 2.2 (blue triangles). Error bars represent the standard deviation from three replicate measurements. The solid lines are the Bezier curve fit to the experimental data, which were used to extract the MWCO.

These results indicate that the NIL process causes a notable reduction in the size and/or number of larger pores in the barrier layer. Despite showing similar permeability, MWCO for sample 2.1 was ~ 19% lower than sample 2.2. Which also suggest that higher imprinting pressure used for sample 2.1 causes more reduction in pore size that are important for the membrane's selectivity. Sample 2.3 and 2.4 also show similar trend as MWCO of the sample 2.3 (imprinted at higher pressure) was found ~ 18% lower than that of the sample 2.4.

From Fig. 2.12 it is also quite evident that, not only the asymmetric large pore structure, but also the thickness of the overall PES layer were reduced after the imprinting process. This reduction in thickness (difference in thickness between the un-patterned and a patterned membrane) is summarized for the model samples in Fig. 2.14.

Results suggest that the thickness reduction increases with imprinting temperature and imprinting pressure. However, similar to pattern height and MWCO, the thickness of the membrane appears to be influenced more by the imprinting pressure than the imprinting temperature. For membranes with similar permeability, the one imprinted with higher pressure showed larger thickness reduction even when the imprinting temperature was lower. Interestingly, Hagen - Poiseuille relationship suggests that permeability increases with decrease of membrane thickness. Lower thickness for sample 2.2 and sample 2.3 compared with sample 2.1 and 2.3 is most likely compensating the increase in the resistance resulting from the pore size reduction discussed earlier (Fig. 2.13).

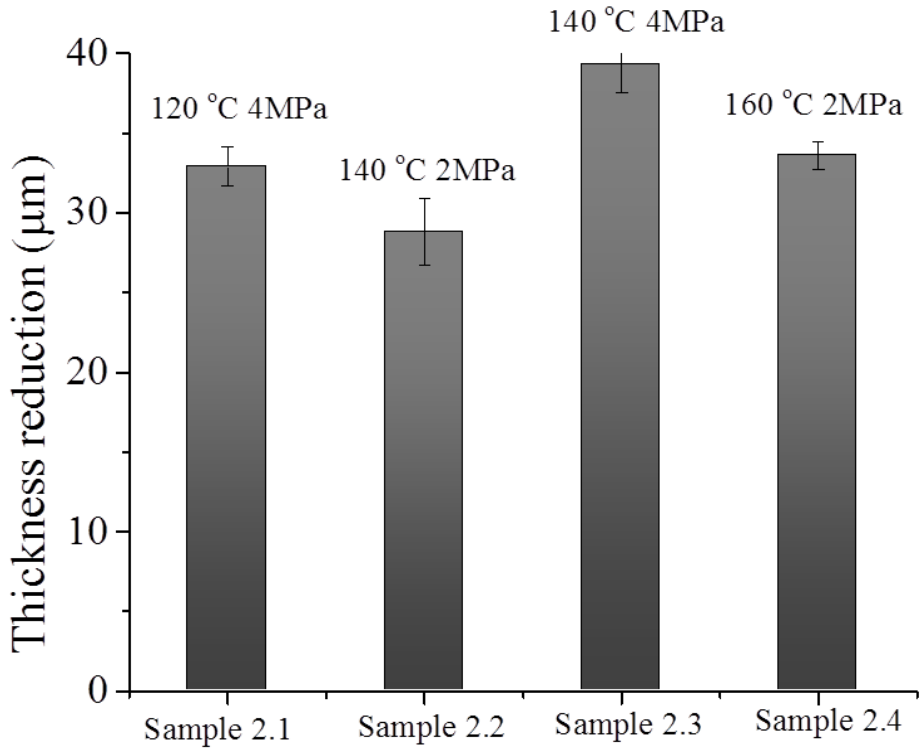

Figure 2.14: Thickness reduction for the model PES membranes imprinted with different processing parameters. Error bars represent the standard deviation from three replicate measurements.

Figure 2.12 also suggest that the overall porosity is also changing upon imprinting as larger pore structures on the bottom of the PES layer are visibly compressed compared to the un-patterned membrane. The overall porosity for the un-patterned and patterned membranes was measured by "pat and weight" method and is presented in Fig. 2.15. Each points represents average from three replicate measurements taken at different times with the same type of membrane.

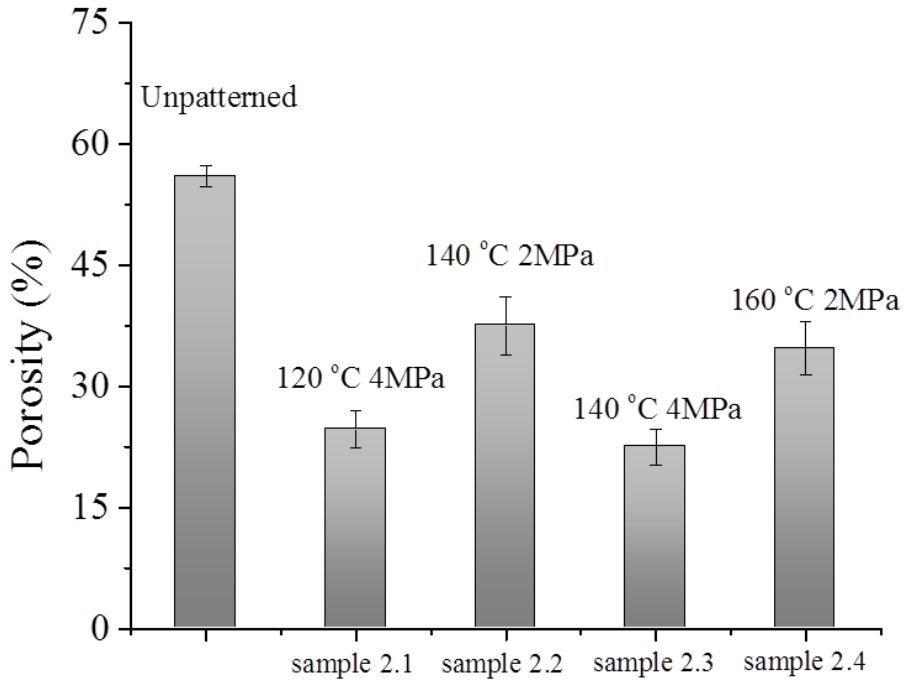

Figure 2.15: Porosity for the model PES membranes imprinted with different processing parameters. Error bars represent the standard deviation from three replicate measurements.

As expected, NIL process significantly reduces the overall porosity of the membrane. Before imprinting the un-patterned membrane had overall porosity of ~ 55%. For all patterned membranes, significant reduction in porosity is observed. Similar to the MWCO and membrane thickness, imprinting pressure appears to have a bigger influence than temperature on the porosity reduction. Note that all porosity values reported here are likely underestimate the real value, due to the increased difficulty for water to wet the smaller pores.

In this study, we first examined processing-structure-property relationship of the direct NIL patterning of PES UF membrane. It was found that by following the typical route of NIL process (using a imprinting temperature above T_g of the PES) the patterned membrane became impermeable to water under the normal pressure range for a UF process. In contrast, by imprinting at lower temperature surface patterns can be successfully imprinted onto the UF membrane surface while keeping the membrane permeable to water.

Normally, to replicate a pattern with good fidelity onto a polymer surface, it is imperative that the polymer fill the cavity of the stamp and polymer viscous flow is necessary for that. As a polymer is heated above its T_g, modulus and viscosity decrease by several orders of magnitude compared to their value at the room temperature. However, under pressure, such viscous flow would seal the small pores in the PES barrier layer and destroy the permeability of the membrane.

At $T < T_g$, 1 - 4 MPa of pressure (used in this study for imprinting the membrane) should be insufficient to make permanent deformation of dense, glassy PES. However, studies have shown that even under moderate pressure, plastic deformation of porous glassy polymer is possible and the degree of plastic deformation increases with porosity of the film [22]. This is caused by the stress concentration on the thin polymer wall between neighboring pores that can cause instability/buckling and/or viscoelastic deformation of the thin polymer walls. Such porosity-enhanced plastic deformation is believed to be the mechanism that leads to the surface pattern formation.

Viscoelastic response at room temperature has also been reported for porous polymer membranes, which causes permeate flux decline during filtration, known as "compaction" [24, 28]. In this study influence of NIL processing parameters were also studied by imprinting the PES membrane with a flat/blank mold. Even after significant compression during the NIL process, compaction was found in the flattened membrane. This can be caused by of the elastic deformation of the already-compressed membranes during pressurized filtration.

Interestingly, when variable permeance (change in permeance due to compaction) were separated from the overall membrane permeance, it seem to decrease at a higher rate at lower imprinting temperature and pressure, possibly highlighting inferior plastic deformation at those conditions. Consistently, compaction was also much lower for those samples. Measurements of steady-state water permeance after the compaction period were also summarized in this study and results indicate that temperature-pressure can be exchanged to get the same p permeance after imprinting such that imprinting with higher temperature-lower pressure can make the membrane as permeable with a membrane imprinted at lower temperature-higher pressure. Imprinting time in this case do not seem to have significant impact on imprinting of the UF membranes, as long as it is longer than 3 min.

From the AFM analysis, it is evident that, large degree of viscous flow could not be achieved as the pattern height for all the samples were smaller than the depth of the mold (200 nm for mold 1 and 180 nm for mold 2). The results also suggest that

imprinting pressure plays a significant role during imprinting as higher pattern height was achieved with higher pressure. It is likely that as large viscoelastic was not achievable for any of the samples imprinting at lower temperature ($T < T_g$), compression of the pores due to pressure was the main driving force for permanent plastic deformation. Most significantly, different pattern height was achieved with membrane having similar water permeance, which offers the guideline to pattern the membrane with desired performances.

Structural analysis of the patterned membrane shows that NIL causes a notable reduction in the membrane thickness, MWCO (pore size at the barrier layer) and overall porosity. Similar to the pattern height, imprinting pressure also seems to have more dominant role in changing the membrane structure. Pore size reductions for the sample studied were in the range of ~20-40 %. However, overall porosity reductions were in the range of ~ 33-51%. It suggests that plastic deformation was higher for the overall membrane compared to its pore size at the surface, which is consistent with the observation that plastic deformation for porous glassy polymer increases with porosity [22]. Due to asymmetric pore structure PES layers, (Fig 2.13), the overall membrane porosity increases with the depth from the membrane surface. These differences in the porosity are likely to be the reason for discrepancies in the MWCO and porosity reduction. From Hagen-Poiseuille relationship, thickness reduction increases the membrane permeance while pore size reduction and porosity reduction overcomes the effect of thickness reduction.

2.4 Conclusion

In summary, we have successfully developed a facile method to fabricate sub-micron surface pattern directly on top of a commercial membrane via NIL without adversely affecting the permeation characteristics of the membrane. Controlling NIL process parameters allows us to fabricate patterned membrane with variable pattern height, permeability and separation properties. Since the NIL process does not alter the surface chemistry of the membrane, these patterned membranes can serve as a model system to examine the effect of surface roughness on particle deposition and other types of fouling during active membrane-based filtration. This aspect will be systematically examined in the following chapters. Moreover, the fabrication method demonstrated here can potentially be scaled-up via roll-to-roll NIL and thus provides a promising manufacturing route for lithographically patterning micro- and nanoscale features onto commercial, porous separation membranes [29, 30].

References

1 Pendergast, M. M. & Hoek, E. M. V. A review of water treatment membrane nanotechnologies. Energy & Environmental Science 4, 1946-1971, doi:10.1039/c0ee00541j.

2 Qu, X., Alvarez, P. J. J. & Li, Q. Applications of nanotechnology in water and wastewater treatment. Water Research 47, 3931-3946, doi:http://dx.doi.org/10.1016/j.watres.2012.09.058.

3 Lee, K. P., Arnot, T. C. & Mattia, D. A review of reverse osmosis membrane materials for desalination-Development to date and future potential. Journal of Membrane Science 370, 1-22, doi:http://dx.doi.org/10.1016/j.memsci.2010.12.036.

4 Pinnau, I. & Freeman, B. D. in Membrane Formation and Modification Vol. 744 ACS Symposium Series 1-22 (American Chemical Society, 1999).

5 Al-Amoudi, A. & Lovitt, R. W. Fouling strategies and the cleaning system of NF membranes and factors affecting cleaning efficiency. Journal of Membrane Science 303, 4-28, doi:http://dx.doi.org/10.1016/j.memsci.2007.06.002 (2007).

6 Goosen, M. F. A. et al. Fouling of Reverse Osmosis and Ultrafiltration Membranes: A Critical Review. Separation Science and Technology 39, 2261-2297, doi:10.1081/ss-120039343 (2005).

7 Rana, D. & Matsuura, T. Surface Modifications for Antifouling Membranes. Chemical Reviews 110, 2448-2471, doi:10.1021/cr800208y.

8 Hellio, C. & Yebra, D. M. Advances in Marine Antifouling Coatings and Technologies. (Elsevier Science, 2009).

9 Schumacher, J. F. et al. Engineered antifouling microtopographies - effect of feature size, geometry, and roughness on settlement of zoospores of the green alga Ulva. Biofouling 23, 55-62, doi:10.1080/08927010601136957 (2007).

10 Geissler, M. & Xia, Y. Patterning: Principles and Some New Developments. Advanced Materials 16, 1249-1269, doi:10.1002/adma.200400835 (2004).

11 Quake, S. R. & Scherer, A. From Micro- to Nanofabrication with Soft Materials. Science 290, 1536-1540, doi:10.1126/science.290.5496.1536 (2000).

12 Moore, G. E. Cramming More Components Onto Integrated Circuits. Proceedings of the IEEE 86, 82-85, doi:10.1109/jproc.1998.658762 (1998).

13 Xia, Y. & Whitesides, G. M. Soft Lithography. Angewandte Chemie International Edition 37, 550-575, doi:10.1002/(sici)1521-3773(19980316)37:5<550::aid-anie550>3.0.co;2-g (1998).

14 Chou, S. Y., Krauss, P. R. & Renstrom, P. J. Imprint Lithography with 25-Nanometer Resolution. Science 272, 85-87, doi:10.1126/science.272.5258.85 (1996).

15 Guo, L. J. Nanoimprint Lithography: Methods and Material Requirements. Advanced Materials 19, 495-513, doi:10.1002/adma.200600882 (2007).

16 Montaudo, G., Puglisi, C., Rapisardi, R. & Samperi, F. Primary thermal degradation processes of poly(ether-sulfone) and poly(phenylene oxide) investigated by direct pyrolysis-mass spectrometry. Macromolecular Chemistry and Physics 195, 1225-1239, doi:10.1002/macp.1994.021950410 (1994).

17 Cheryan, M. Ultrafiltration and Microfiltration Handbook. (Taylor & Francis, 1998).

18 Kim, K. J. et al. A comparative study of techniques used for porous membrane characterization: pore characterization. Journal of Membrane Science 87, 35-46, doi:http://dx.doi.org/10.1016/0376-7388(93)E0044-E (1994).

19 Palacio, L., Pradanos, P., Calvo, J. I. & Hernandez, A. Porosity measurements by a gas penetration method and other techniques applied to membrane characterization. Thin Solid Films 348, 22-29, doi:http://dx.doi.org/10.1016/S0040-6090(99)00197-2 (1999).

20 Zhou, W. in Nanoimprint Lithography: An Enabling Process for Nanofabrication 111-146 (Springer Berlin Heidelberg).

21 An, L. et al. Mechanical properties and miscibility of polyethersulfone/phenoxy blends. Journal of Applied Polymer Science 59, 1843-1847, doi:10.1002/(sici)1097-4628(19960321)59:12<1843::aid-app5>3.0.co;2-q (1996).

22 Lee, J.-H., Wang, L., Kooi, S., Boyce, M. C. & Thomas, E. L. Enhanced Energy Dissipation in Periodic Epoxy Nanoframes. Nano Letters 10, 2592-2597, doi:10.1021/nl1012773.

23 Arneri, G. The effect of pressure on the bulk polymer microstructure in cellulose acetate reverse osmosis membranes. Desalination 36, 99-104, doi:http://dx.doi.org/10.1016/S0011-9164(00)88634-8 (1981).

24 Fuls, P. F., Dell, M. P. & Pearson, I. A. Non-linear flow through compressible membranes and its relation to osmotic pressure. Journal of Membrane Science 66, 37-43, doi:http://dx.doi.org/10.1016/0376-7388(92)80089-3 (1992).

25 Ohya, H. An expression method of compaction effects on reverse osmosis membranes at high pressure operation. Desalination 26, 163-174, doi:http://dx.doi.org/10.1016/S0011-9164(00)82198-0 (1978).

26 Ma, H., Bowman, C. N. & Davis, R. H. Membrane fouling reduction by backpulsing and surface modification. Journal of Membrane Science 173, 191-200, doi:http://dx.doi.org/10.1016/S0376-7388(00)00360-4 (2000).

27 Microfiltration and Ultrafiltration: Principles and Applications. (Taylor & Francis, 1996).

28 Brinkert, L., Abidine, N. & Aptel, P. On the relation between compaction and mechanical properties for ultrafiltration hollow fibers. Journal of Membrane Science 77, 123-131, doi:http://dx.doi.org/10.1016/0376-7388(93)85240-W (1993).

29 Ahn, S. H. & Guo, L. J. High-Speed Roll-to-Roll Nanoimprint Lithography on Flexible Plastic Substrates. Advanced Materials 20, 2044-2049, doi:10.1002/adma.200702650 (2008).

30 Kim, H. J. et al. Roll-to-roll manufacturing of electronics on flexible substrates using self-aligned imprint lithography (SAIL). Journal of the Society for Information Display 17, 963-970, doi:10.1889/jsid17.11.963 (2009).

CHAPTER III

INFLUENCE OF PATTERNED SURFACE ON COLLOIDAL FOULING ON ULTRAFILTRATION MEMBRANE

3.1 Introduction

Ultrafiltration (UF), a low pressure membrane filtration process, has grown exponentially during last 20 years for the production of potable water [1-3]. With their capability to remove particulates by size exclusion, UF membranes are generally used for the removal of turbidity, microorganisms like bacteria, protozoa, algae, and water born viruses [4]. In addition to that, UF process is also frequently used as pretreatment for reverse osmosis systems and final filtration stage for production of deionized water [5-7]. However, like other membrane (as discussed in Chapter 1) long term usage of UF membrane is also frequently hindered by fouling, i.e., reduction in flux or increase in transmembrane pressure (TMP) during operation due to the accumulation of materials within the pores or at the surface of the membranes [8-12]. These fouling with UF membrane causes additional energy consumption and sometime shutdown of the productivity and eventually replacement of the membrane in the system [12-16]

To address the fouling issues in UF membranes, different pretreatment and cleaning protocols have been developed in the filtration processes which can rarely avoid irreversible fouling. From the discussion of Chapter 1 it is obvious that, controlling the interactions between membrane surface and feed solutions is the key

to fouling mitigation [17, 18]. In addition, surface patterning which have been hugely successful in mitigating fouling in non-membrane areas can be a potential candidate to improve anti-fouling characteristics of UF membrane by controlling surface-feed interaction at the barrier interface.

In the previous Chapter 3 of this dissertation, an alternative methodology based on nanoimprint lithography (NIL), for creating sub-micron surface patterns on UF membranes was described. In this Chapter a direct comparison of filtration performance between un-patterned (UF membrane used as it is) and patterned membrane during filtrations of model colloidal suspensions are reported. In addition, post filtration imaging of the fouled membranes were also studied. Finally, the influence of particle size, cross-flow velocity, pattern size, and the angle between the pattern line and flow direction were systematically examined using cross-flow filtrations of colloidal suspensions on patterned.

All the filtration experiment described in this Chapter were performed under a model fouling system using colloidal silica particles and analyzed with the concept of "critical flux". Colloidal fouling in membrane systems can be a complex process where several physical and chemical phenomena can influence the overall fouling behavior [19]. Combination of hydrodynamic conditions and inter-particle interactions are attributed to such complex behavior of colloidal fouling [20]. Colloidal fouling can be investigated by studying the behavior of permeate flux during active filtration and deposition/fouling can be accurately detected by eliminating the influence of hydrodynamic and other parameters [21]. And among different colloidal

foulants, silica colloids are of particular interest as they are abundant in source waters and frequently found in fouled membrane surface [19, 21].

In recent years the concept of "critical flux" has been increasingly used as an indicator for the onset of the fouling or deposition of constituent on the membrane surface [22]. The determination of critical flux can refer the membrane filtration under "no fouling" situation, producing constant permeate flux [22, 23]. The concept of critical flux was introduced by Field et al. while working on constant flux filtration of yeast cells with microfiltration (MF) and since then it has been used as model fouling analysis for different membrane systems [24, 25]. Critical flux, J_c, is defined as the maximum permeate flux above which irreversible fouling occurs on the feed-side of the membrane surface [22]. Howell, during the an analysis of colloid fouling defined the J_c as the flux below which no colloids deposits on the membrane surface [26].

From the consideration of mass transport, the J_c can be defined more generally as the flux at which the hydrodynamic force transporting the particle towards the membrane pore is balanced by the opposing back transport forces [27]. However, it should be noted here that, diffusion is a statistical process and not all particles in a population will follow the same mechanism. Consequently, the conditions that prevent the particle from depositing on a membrane surface will not ensure that all particles will remain away from the surface [22, 24]. This implies that J_c is not a state of zero fouling; rather, J_c is a particular operating condition that separates slow fouling form rapid fouling.

Several methods have been prescribed to determine J_c of a particular filtration system. Chen et al. used hysteresis, which occurred when the flux was successively increased and decreased to detect the J_c [28]. Microscopic observations of deposited materials, providing a highly sensitive method of detecting particle deposition, have also been used to evaluate the J_c [29]. J_c was also determined by examining deviations from linearity in the plot of TMP versus the permeate flux [30, 31]. Cho and Fane found that a jump in dP/dt, which could also be used to find the J_c of the system [32]. Espinasse et al. used resistance to filtration to estimate the J_c, by plotting the normalized resistance against the permeate flux [33]. Among all the methods described in the literature, constant flux stepping and constant pressure stepping methods are two of the most common procedures [34]. In a constant pressure stepping protocol, pressure is increased from one interval to another and J_c is determined by plotting the corresponding flux as a function of TMP. At TMP below the J_c, permeate flux is independent of time, and increases linearly with increasing TMP, but above the J_c, permeate flux increases rapidly with TMP. In contrast, in a constant flux stepping protocol, flux is increased from one step to another and corresponding TMP is recorded. Likewise, above the J_c, TMP also increases rapidly over time [35, 36].

In this Chapter, J_c for patterned and un-patterned membranes were determined by both constant pressure and constant flux stepping methods. From the fouling experiments it was revealed that the presence of these sub-micron surface patterns significantly improves fouling resistance by not only deferring the onset of colloidal deposition, also lowering the rate of growth of fouling after initial deposition,

compared to the un-patterned membranes during separation experiments using colloidal suspensions. In addition, the degree of the antifouling effect increases with particle size (relative to the pattern size), cross-flow velocity, pattern size, and the angle between the pattern line and flow direction.

3.2 Methods and Materials

3.2.1. Constant pressure critical flux measurement with the un-patterned and patterned membranes

Constant pressure filtration experiments were conducted in a bench-scale module at 21°C, as schematically shown in Fig. 3.1. The module is an unconventional cross-flow system wherein the feed solution flows into the module through a small diameter tube (1/8 inch), impinges on the center of the membrane, and flows radially outward and upward (along the sides) to be collected in a larger diameter tubing (1/4 inch), which is co-annular to the feed tube, to the retentate line.

The module had an effective membrane area of 1.93 cm^2, and the nature of the flow across the surface is essentially tangential. The size of the NIL mold used for imprinting the membrane for constant pressure experiment was smaller than the sample diameter required for our filtration cell. Thus, the permeate side of all membranes were always covered by a mask to ensure that the same amount and section of the top surface area directly communicated with the lower permeate

collection channel, and that this top surface area was either entirely NIL-patterned or un-patterned.

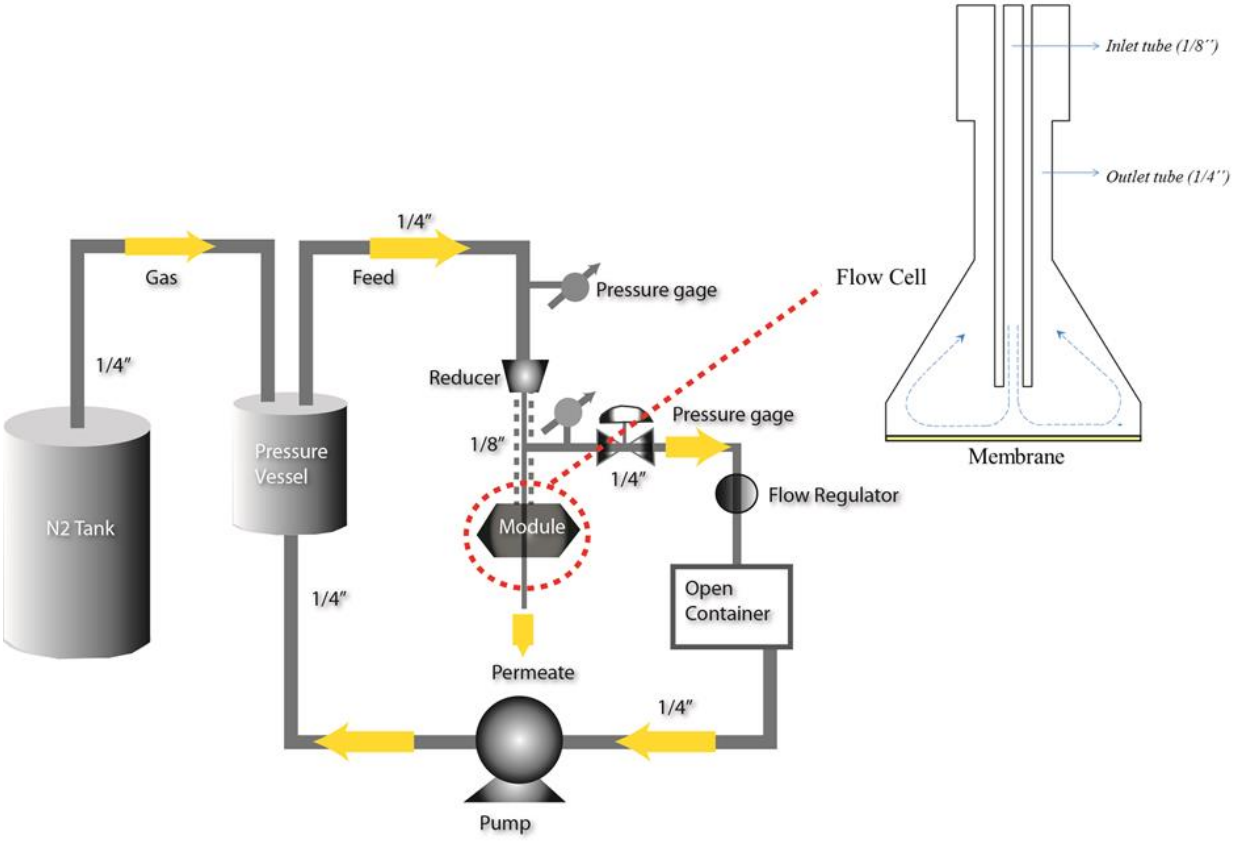

Figure 3.1: Schematic illustration of the filtration setup, and the inset shows the details of the membrane cell, with the dashed lines corresponding to the nominal flow streamline.

The feed suspension was kept in a stainless steel reservoir (1.2 L capacity) with a stirrer bar rotating at a constant rate throughout the experiments to prevent any deposition. During filtration, high-pressure nitrogen was used to supply the required TMP. The permeation mass flow-rate was obtained by weighing samples over timed-intervals using an automated electronic balance (PI-225DA, Denver Instruments).

The shear rate across the membrane surface was kept nominally constant throughout the experiment by maintaining a constant retentate volume flow-rate using flow regulators. A peristaltic pump was used to return the retentate to the feed solution at a volumetric rate of 60 cm^3/min. The overall cell volume (to the point of retentate removal) is ~3.1 cm^3, so the fluid residence time is ~3 s. The wetted surface area for the cell is ~8 cm^2, and the superficial velocity (based on an equivalent cylinder) is ~0.6 cm/s. Thus, using the equivalent hydraulic diameter and properties of water, the Reynolds number (Re) in the cell was estimated to be ~2-3 while the flow is laminar.

For each filtration experiment, deionized (DI) water was permeated at the different TMPs, and the pure water flux J_0 as well as the water permeance was calculated. For each sample, DI water was continuously filtrated for 20 min at the constant pressure, gradually increasing from 41.4 to 344.7 kPa. After this, the test suspensions were evaluated using a pressure-stepping protocol going from low to high TMP. Permeate collection was done for 5 min for the first two steps, then 3 min for the next two, and 2 min for each one thereafter. For selected values of each TMP (as discussed later), suspension filtrations were conducted for 100 min with flux calculated every two min.

The colloidal suspensions used for the feed solutions contained "AngstromSphere" (Fiber Optic Center) silica particles with diameters of 0.25, 0.5, or 1 μm. These spherical silica particles are amorphous, non-porous and contain a large quantity of silanol (Si–OH) groups to facilitate their dispersion in water. The colloid suspensions were prepared by dispersing the silica particles in DI water together with

0.5 mL (in 1.2 L) FL-70® surfactant at a concentration of 5 g/L, and were stirred vigorously over 12 h. Prior to the filtration experiments, the suspensions were sonicated for a minimum of 60 min and were allowed to cool to room temperature for 15 min. The dispersion and stability of these colloidal suspensions were examined with dynamic light scattering, confirming that little aggregation of the particles occurs during the time course of the filtration measurements shown in the Fig. 3.2. For a given feed solution, three filtration measurements were carried out on three membranes (un-patterned or patterned), and the statistical average is reported herein.

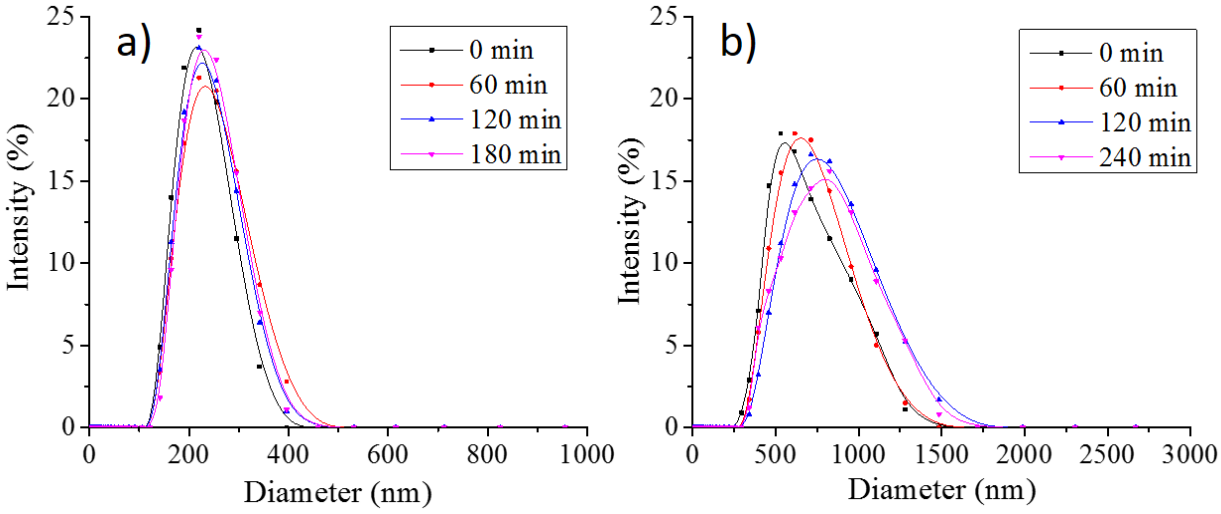

Figure 3.2: Dynamic light scattering of sample feed suspensions (a) 0.25 μm silica particles, and (b) 0.5 μm silica particles. Measurements were taken over the course of 3 h on the quiescent sample in the instrument at 25°C.

First, the filtrations of colloidal suspensions were carried out in the pressure-stepping method. In addition, time-dependent filtration experiments at constant TMP were carried out within "sub-critical flux" or "super–critical flux" zones wherein the operating pressure is below or above the pressure associated with the J_c as described later. Then, at that chosen TMP, which was different for the un-patterned and patterned membranes, the permeate flux was recorded during a 2 h of filtration.

3.2.2 Constant flux critical flux measurement with the un-patterned and patterned membranes

Colloidal suspensions containing silica particles with diameters of 0.25 or 0.5 μm from the same manufacturer described in the previous section were also conducted in a bench-scale cross-flow filtration module at ~21-22 ºC (feed temperature) measured prior to experiment, as schematically shown in Fig. 3.3. Experiments were performed in a unit that houses three separate membranes, each with a circular surface area of ~22 cm^2 and 2 mm channel height (Inset Fig 3.3).

All three membrane cells were fed from the same 4L Erlenmeyer flask used as feed reservoir with a peristaltic pump (MasterFlex). TMP was maintained with three back-pressure regulators (Swagelok) and monitored with three differential-pressure transducers (Omega) connected to a data-acquisition unit and logged in Lab View (National Instruments). The selected feed was pumped through three cross-flow cells in a parallel assembly. Membrane samples were loaded into each cell with a porous plastic backing (for mechanical support) and sealed with a rubber O-ring, yielding a membrane filtration area of 19.4 cm^2.

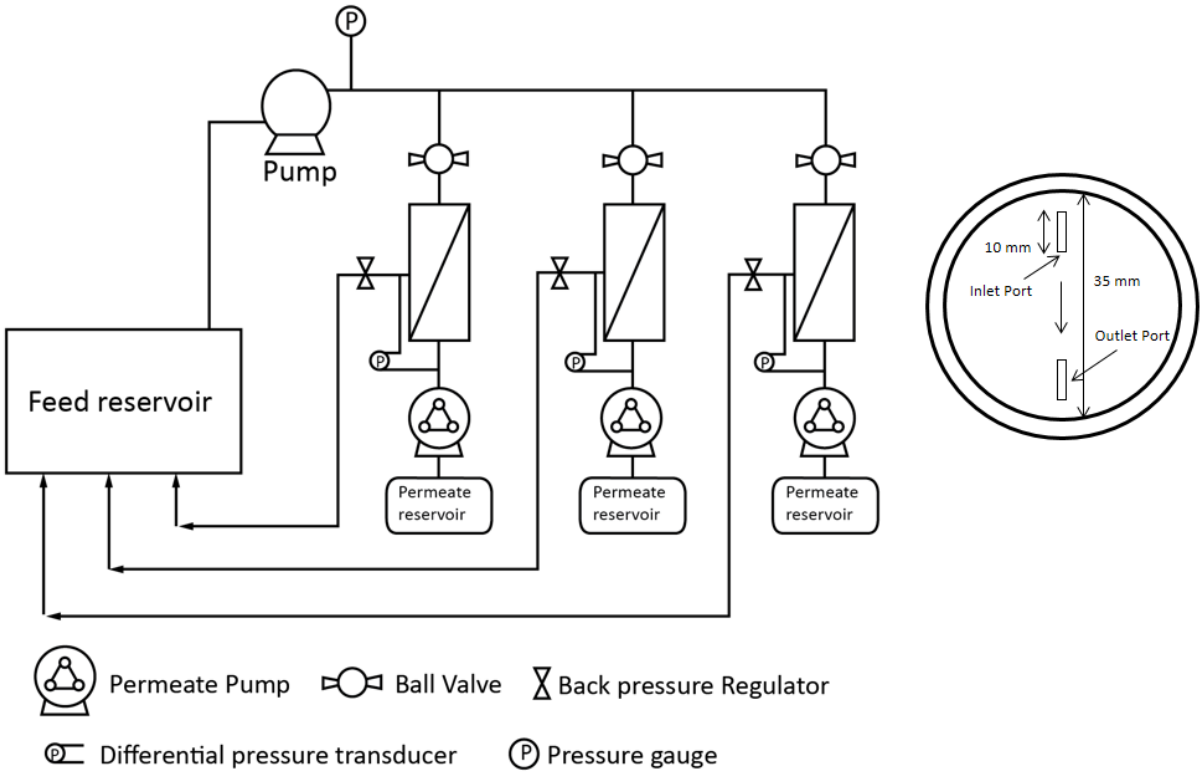

Figure 3.3. Schematic of the apparatus used for the cross-flow filtration, showing the three parallel cells (top) used simultaneously. Sketch on the right side shows the details of the cell geometry.

The permeate flux was controlled by a peristaltic pump on the permeate line leaving for each cross-flow cell. The permeate flow rates were measured by Coriolis-type flow meters positioned on the permeate lines immediately after each peristaltic pump. The peristaltic pumps, by sealing the permeate line tubing, isolated the pressure on the permeate side of the membrane from the atmosphere. The TMP could, therefore, be measured by a differential pressure transducer connected to the feed and permeate lines of each cell. The pressure difference between the feed inlet and reject outlet of a cell was small relative to the TMP measured during fouling

experiments. As the membrane fouled, the pressure on the permeate side of the membrane decreased. Because the feed pressure was fixed throughout each experiment, the TMP increased. In cases of extreme fouling (at the highest fluxes considered), the permeate pressure decreased to atmospheric pressure, resulting in a TMP equal to the gauge feed pressure. In such cases, the experiment was terminated, since a permeate line pressure less than atmospheric pressure could lead to the formation of bubbles in the permeate line, resulting in instabilities in the permeate flow rate.

For each filtration experiment, membranes were first compacted with DI water, until the permeate flux from two successive measurements changed less than 2 %. The DI water flux, an average value over 20 min filtration at a constant TMP, was determined for TMPs ranging from 68.9 to 620.5 kPa. The filtrations of colloidal suspensions were carried out using the flux-stepping procedure: permeate flux was increased in a step-wise fashion, and the corresponding TMPs at each flux step were recorded. The cross-flow velocity of the feed suspensions, $V_{cf} = Q/A_{avg}$, where Q is the volumetric flow rate of retentate and A_{avg} is the average cross-sectional area, was 0.03, 0.04426, 0.05877, 0.07352and 0.088 ms^{-1}. Reynolds number for the corresponding V_{cf} can be estimated according to, $Re = V_{cf}.dh/\nu$, where dh is the hydraulic diameter and v is the kinematic viscosity. Each flow cell housed a circular membrane with 35 mm diameter, d, in a rectangular slit. The feed enters from one side of the cell and retentate exits from the opposite side, through 10 × 3 mm slits. The channel height h = 2 mm, and the width of the channel varies along the flow path

because of the circular shape of the channel base. Based on these geometric considerations: dh is estimated as, dh = 4Vc/Sc = hd/(h+d/2), where V_c and S_c are the volume and surface area of the cell, correspondingly. The estimated Re for the different V_{cf} was ~ 120, 180, 239, 299 and 358, indicating all the cross-flow of the bulk feed during filtration were laminar.

3.2.3 Scanning electron microscopy (SEM)

In this study, surface topography of silica fouled un-patterned and patterned UF membranes, were examined with a field-emission scanning electron microscope (FESEM, Zeiss, Supra 60). Membrane samples were dried in a vacuum oven prior to SEM measurements, and the membrane cross-sections were prepared using a microtome at -20 °C, and coated with a 4.5-4.7 nm gold layer.

SEM images of membranes after colloidal filtration were obtained on different regions across the membranes. Un-patterned and patterned UF membrane samples from the 2 h experiment in the super-critical flux zone at constant pressure using the 0.5 µm silica suspension were examined for particle deposition on the membrane surface. After the filtration, samples were dried at room temperature for 24 h and then kept in a sealed petri dish at 5 ^{o}C until the microscopy. It was recognize that other drying methods reduce the possibility of artifacts due to capillary forces, but imaging artifacts on the particle deposition would be similar for both types of membranes and not significant with respect to counting the number of particles. Five images were taken from each segment and the particle coverage for each image was quantitatively assessed using ImageJ software (NIH, USA).

3.3. Result and Discussion

3.3.1. Patterned UF and un-patterned membrane

As described in the previous Chapter a commercial polyethersulfone (PES) UF-type membrane (PW, GE Water and Infrastructure) with a nominal 30 kg/mol molecular mass cutoff was used as un-patterned membrane in this study. Performances of the un-patterned membranes were compared with their patterned counterpart. Imprinting of the same commercial membrane were carried out using NIL. The detailed process of the NIL used in this thesis and morphological changes are described in Chapter 2. All together three different patterned membrane were used for the colloidal fouling study. Sample 1.1 from Chapter 2 was used for the constant pressure J_c experiment. In brief, sample 1.1 has a periodic line-and-space grating patterns (Fig. 2.8) with an average pattern height ~100–120 nm after imprinting process. Since only one type of patterned membrane was used for the constant pressure J_c experiment in this study, it will termed generally as "patterned membrane" in this Chapter and will be compared to its counterpart "un-patterned membrane".

For the constant flux J_c experiment, sample 2.1 and sample 2.5 from Chapter 2 were used as patterned membranes. In brief, sample 2.1 has a periodic line-and-space grating patterns (Fig. 2.9) with an average pattern height ~60–65 nm after and sample 2.5 has periodic line-and-space grating patterns (Fig. 2.9) with an average pattern height ~150–160 nm after the imprinting process. The impact of the pattern height on the colloidal fouling were examined with these two patterned membrane

with different height. For ease, sample 2.1 will be termed generally as “mem_L” and sample 2.5 will be termed as “mem_H” in this Chapter from now on.

3.3.2. *Constant pressure filtration of colloidal silica suspensions: critical flux and cake resistance*

First, the DI water permeate flux between the un-patterned and patterned membranes were compared using the filtration setup as described in Fig. 3.1 in the in previous section. Figure 3.4 shows the permeate (water) flux as a function of TMP for the three silica particle suspensions. In the absence of fouling, water flux for a membrane is linearly proportional to the applied TMP, which is indeed observed for both membranes (Fig. 3.4a). For both membranes, the permeate flux at low TMP increases linearly with the increase of TMP, and matches reasonably well with that of DI water. Despite the apparent changes in the porous substructure induced by imprinting, the DI water permeate flux is comparable between un-patterned and patterned membranes over a TMP range of 0–345 kPa. The overall water permeance was found 4.83×10^{-4} $Lm^{-2}h^{-1}Pa^{-1}$ for the un-patterned membrane and 4.57×10^{-4} $Lm^{-2}h^{-1}Pa^{-1}$ for the patterned one.

However, for all silica suspensions, the permeate flux for both membranes deviates from linear dependence and becomes almost independent of TMP, indicating the onset and growth of colloidal deposition (fouling). From Fig. 3.4, J_c, which is the

maximum permeate flux below which no fouling occurs, can be extracted for each membrane [37].

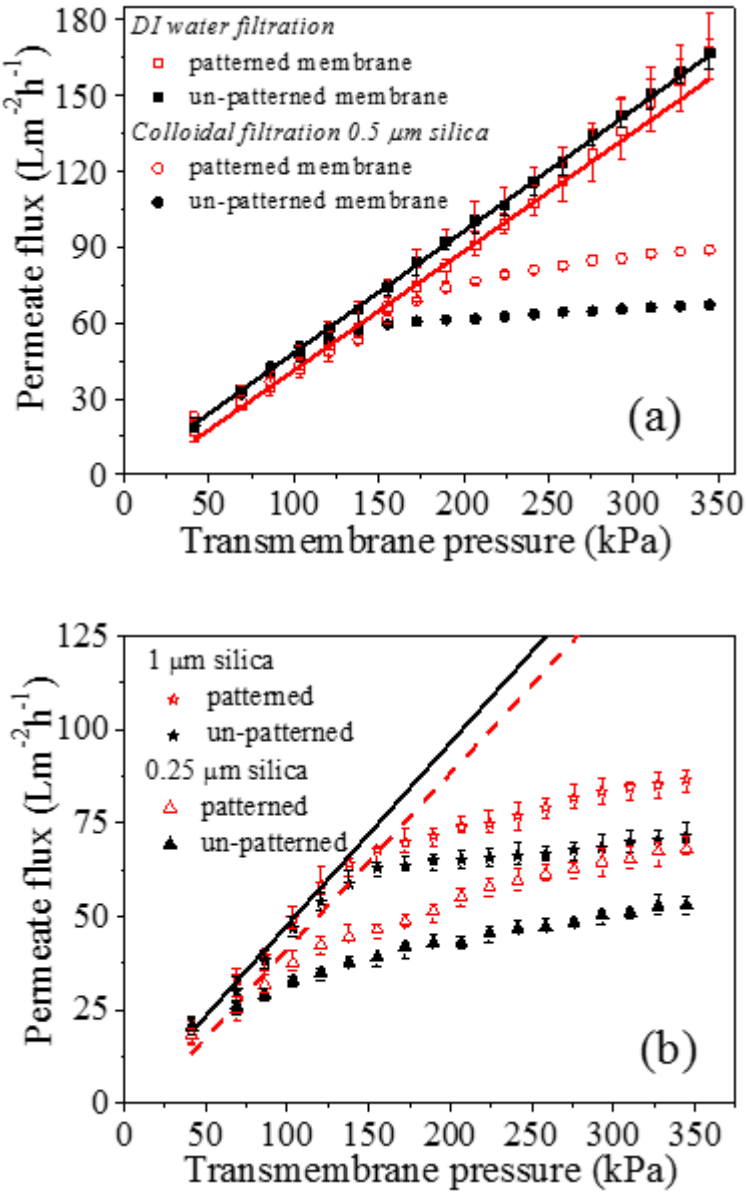

Figure 3.4: (a) Permeate (water) flux as a function of TMP for the un-patterned (filled symbols) and patterned (open symbols) membranes for pure water (squares) and a 0.5 μm aqueous silica suspension (circles). (b) Permeate flux as a function of TMP for the un-patterned (filled symbols) and patterned (open symbols) membranes for a 0.25 μm aqueous silica suspension (triangles), and a 1 μm (stars) diameter. The solid and dash lines represent the DI water filtration data shown in a).

As mentioned in the introduction, J_c was determined as the permeate flux at which deviation from linear dependence of TMP occurs and at which the value matches the clean water flux at the same TMP. Such critical flux is referred to as the "strong form" of J_c, and is commonly observed for silica, latex particles and some salt solutions where there is no strong affinity with the membrane surface [37]. Here, all of the silica suspensions on patterned or un-patterned membranes displayed strong form of J_c.

The measured values of J_c for all three silica particle suspensions are summarized in Fig. 3.5. For the un-patterned membrane, J_c increases with particle size, which is consistent with previous studies [38, 39], and is attributed to the coupling between particle diffusion and surface interactions. Brownian diffusion of particles can be neglected for diameters larger than 100 nm such that membrane-particle surface interactions dominate, which leads to higher J_c values for larger silica particles. However, for the patterned membranes, the highest value of J_c was found for the 0.5 μm silica suspension. Note that the 0.5 μm silica particle is closest in size to the width of the pattern trenches (0.415 μm). Interestingly, studies have also shown that the fouling of biological spores under quiescent conditions was minimized when the feature size approached that of the foulants [40]. The exact mechanism for such particle-size dependence is currently undetermined, but is likely to be associated with the hydrodynamic and thermodynamic effects created by the surface patterns.

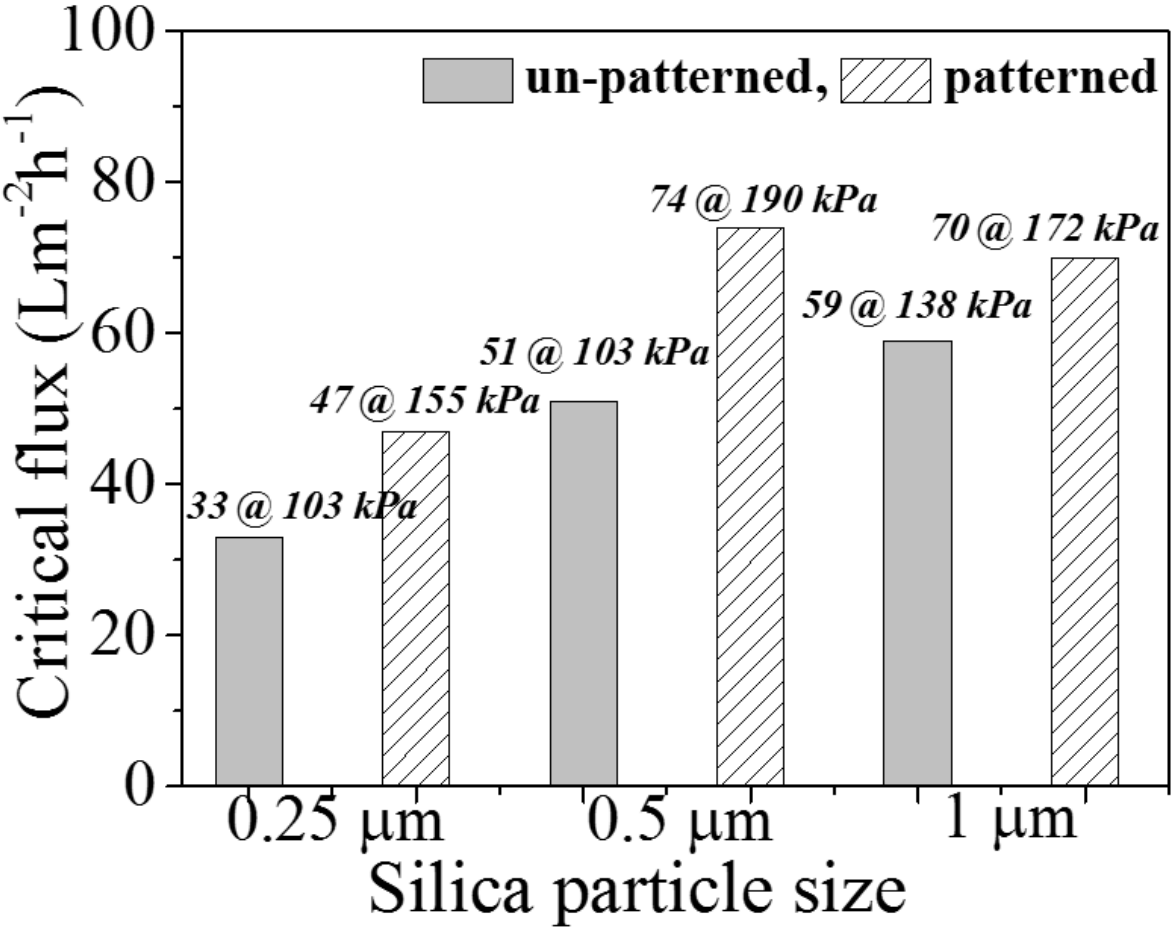

Figure 3.5: Critical flux for un-patterned (solid) and patterned (lined) membranes during the filtration of silica particle suspensions for three particle sizes, determined from the data shown in Fig. 3.4 (previous)

Most significantly, for the same-sized particles, J_c was 42%, 45%, and 17% higher for the patterned as compared with the un-patterned membranes (Fig. 3.5), indicating that the surface patterns significantly delayed the onset of colloidal fouling. To verify that the values of J_c obtained via the pressure-stepping method indeed separates the non-fouling and fouling regions, time-dependent filtration of the

0.5 μm silica particle suspensions in the "sub-critical flux" zone (below J_c) and "super-critical flux" zone (above J_c) were carried out. Fig. 3.6 shows the measured permeate flux as a function of filtration time for both un-patterned and patterned membranes at ~34.5 kPa (5 psi) above or below the respective TMP associated with J_c.

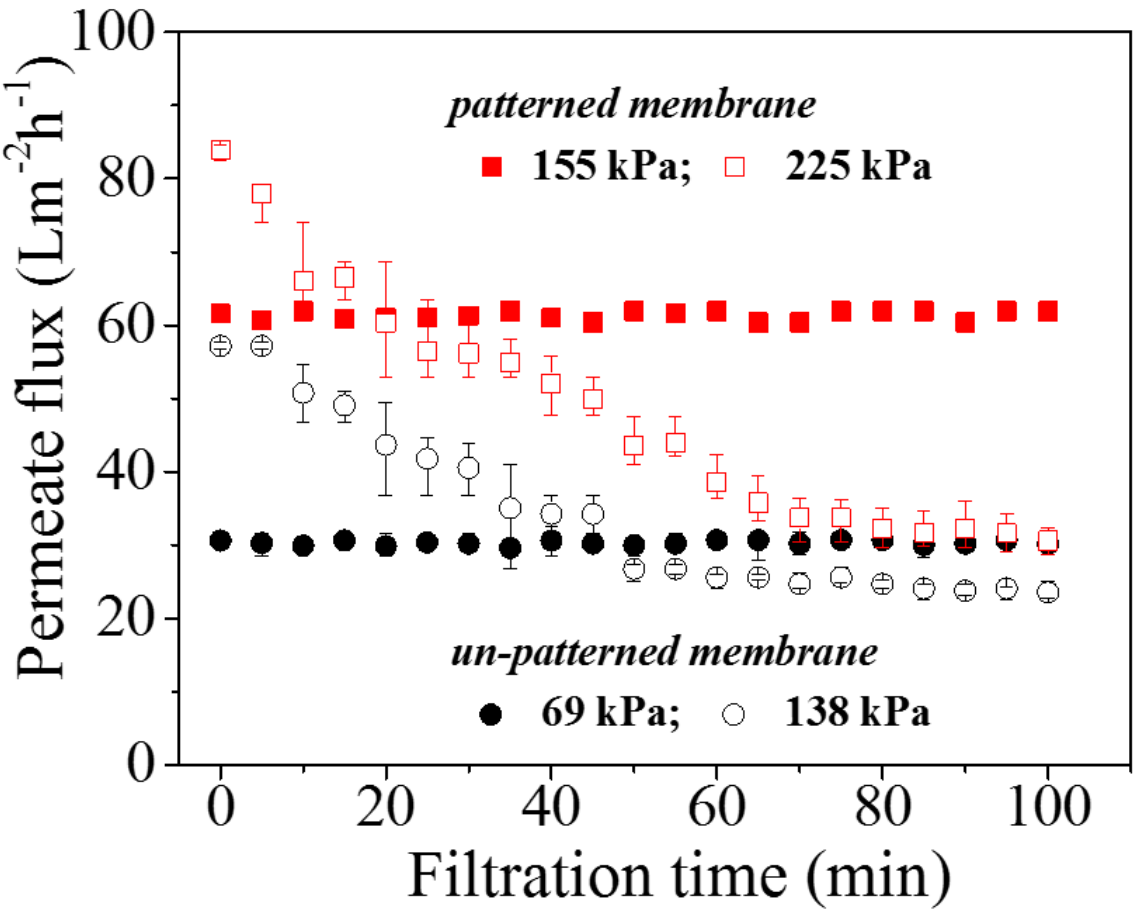

Figure 3.6: Permeate flux as a function of filtration time within the super-critical and sub-critical flux zones, 34.5 kPa above or below the TMP corresponding to the critical flux for both un-patterned and patterned membranes.

For the patterned membrane, TMP values of 155 and 225 kPa were chosen as sub- and super-critical flux points, respectively, based on a TMP at J_c of 190 kPa (Fig. 3.5). From the measurements it is evident that there is no flux reduction over 100 min of filtration, confirming that 155 kPa is indeed in the sub-critical flux zone. In contrast, the permeate flux started to decline immediately upon the start of filtration with a TMP of 225 kPa, indicating that this value is in the super-critical flux zone. Similar results were observed for the un-patterned membrane, with 69 kPa and 138 kPa in the sub- and super-critical flux zones, respectively. These time-dependent experiments confirm that the J_c obtained from analysis of the data in Fig. 3.5 indeed define the deposition and non-deposition regions of the respective membranes.

It is important to note that the onset of the deposition determined from J_c is an average value over the entire membrane, which does not require uniform surface coverage [41, 42]. Furthermore, the initially deposited particles are often loosely attached on the surface and can be removed by hydrodynamic and/or particle-particle interactions [37]. Nonetheless, it is certain that more particles arrive at the membrane surface after the permeate flux exceeds J_c and a cake layer starts to form. The rate of cake layer growth (or continuous deposition of particles) can be characterized by calculating the fouling resistance (R_f), which is the additional hydrodynamic resistance to permeation caused by the particle deposition, as estimated from the following analysis. For the permeation of pure water through a membrane, the flux (J) is given by a Darcy-type expression, $J=\Delta P/(\mu R_m)$, where ΔP is the TMP, μ is the viscosity of permeate, and R_m is the membrane resistance. The

latter is determined from the flux versus TMP measurements for pure water (Fig. 3.4). Upon colloidal fouling/deposition, an additional filtration resistance, R_f, arises, $J=\Delta P/(\mu (R_m+R_f))$. By determine the $J \sim \Delta P$ for the colloidal solution, with R_m known, R_f can be determined at each ΔP.

The R_f values of all membranes fouled with all the three silica particles are shown in Fig. 3.7. For all suspensions, the values of R_f are low and remain constant with an increase of TMP until J_c is reached. Thus, the onset of deposition could also be identified as the flux at which R_f starts to increase with TMP (Fig. 3.7), which occurred for each suspension at a higher TMP for the patterned membrane as compared with the un-patterned one. In addition, the slope of R_f versus TMP provides an estimate of the combination of the particle deposition rate and the structure of the deposited cake on the membrane surface, as illustrated in Fig. 3.7a. Specifically, the d R_f /dTMP for the patterned membrane is 33%, 41% and 29% lower than that of the un-patterned one for the 0.25, 0.5 and 1 μm particle suspensions, respectively. It should be noted that the initial jump in R_f for the patterned membrane could be due to pore-plugging of the largest (most permeable) pores in the membrane and may just be an artifact since this same characteristic was not observed with the 0.25 and 1 μm particle suspensions. Despite of this probable artifact clear rise of R_f at onset of the fouling evident for all the membrane samples.

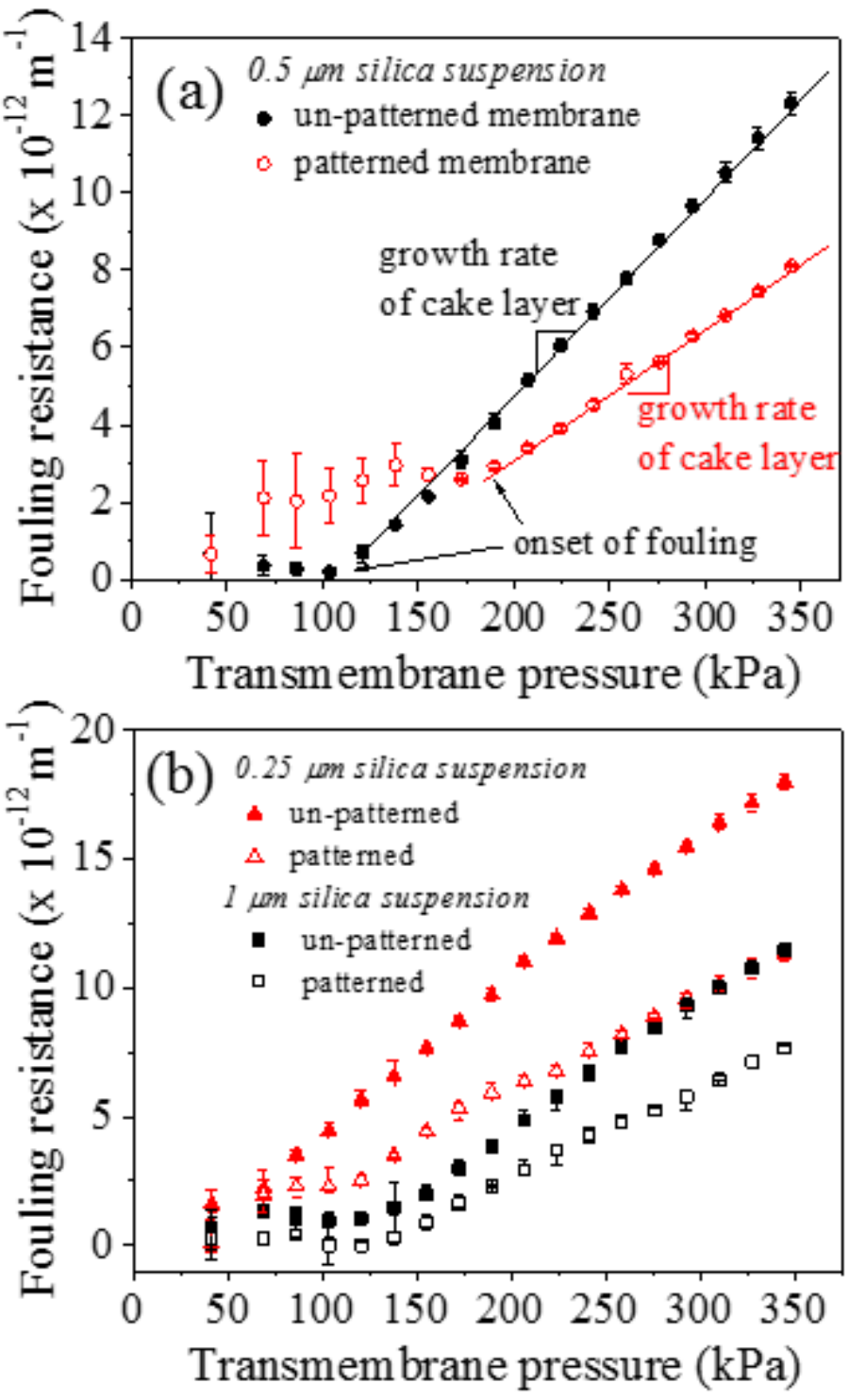

Figure 3.7: Fouling resistance as a function of TMP for the un-patterned solid symbols) and patterned (open symbols) membranes with (a) 0.5 μm, and (b) 0.25 and 1 μm silica particle suspensions, correspondingly.

3.3.3. Colloidal silica deposition on patterned membrane surface

From the measurements of J_c and R_f, surface patterns not only delay the onset of particle fouling but also decrease the continuous deposition rate. This suggests that for identical conditions the mass of particles deposited on the membrane surfaces would be significantly lower on the patterned membrane than the un-patterned one. In the following paragraphs micrographs showing the particle deposition patterns for both types of membranes is described. The membranes were prepared after 2 h of continuous filtration using the 0.5 μm silica suspension (0.5 wt%) within the super-critical flux region (TMP = 225 and 138 kPa for the patterned and un-patterned membranes, respectively).

Due to the radial-flow nature of the filtration module used the orientation angle (θ_f) between the flow and the pattern lines at the membrane surface ranges from 0 to 90°, as schematically illustrated at the top of Fig. 3.8. Such a "combinatorial" filtration setup allows for systematically examining the influence of the flow/pattern orientation on the deposition of the silica particles. The post-filtration, patterned membrane was sectioned into nine segments representing different values of θ_f. Representative SEM images at the nine segments of the post-filtration membrane surfaces, for both the un-patterned and patterned membranes are shown in Fig. 3.9 and 3.10, respectively.

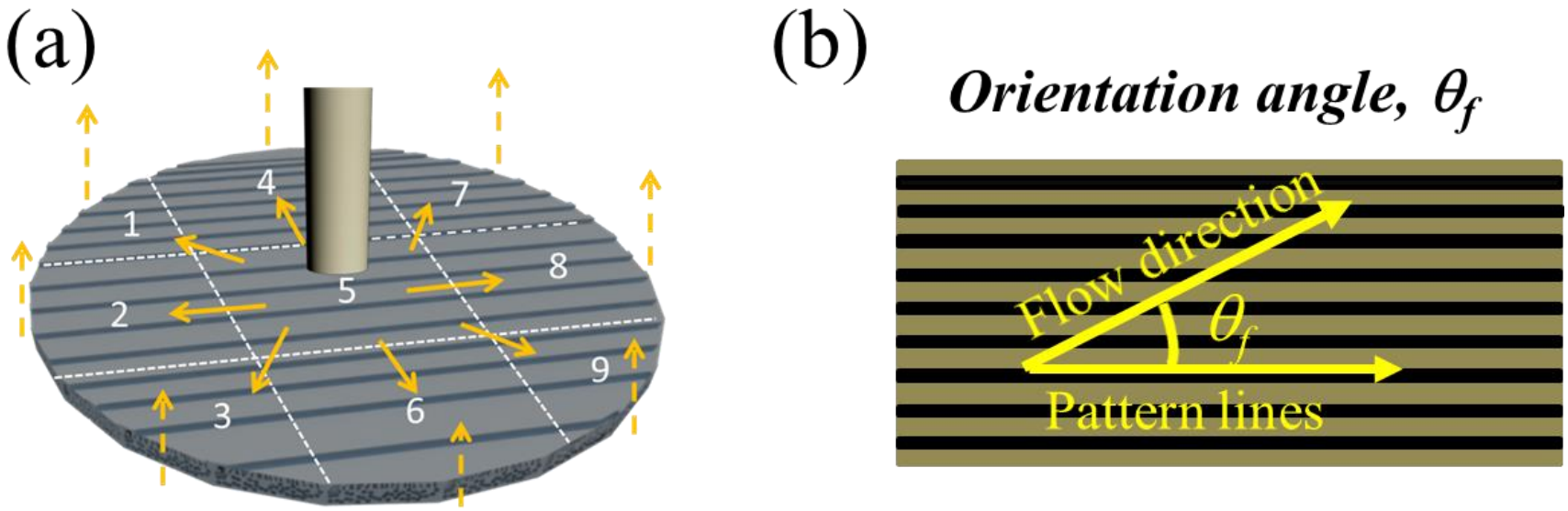

Figure 3.8: (a) Schematic illustration of the feed-solution flow pattern over the patterned membrane subsequently cut into nine different sections for SEM analysis. (b) Illustration of the orientation angle θ_f, angle between the flow direction and the pattern lines.

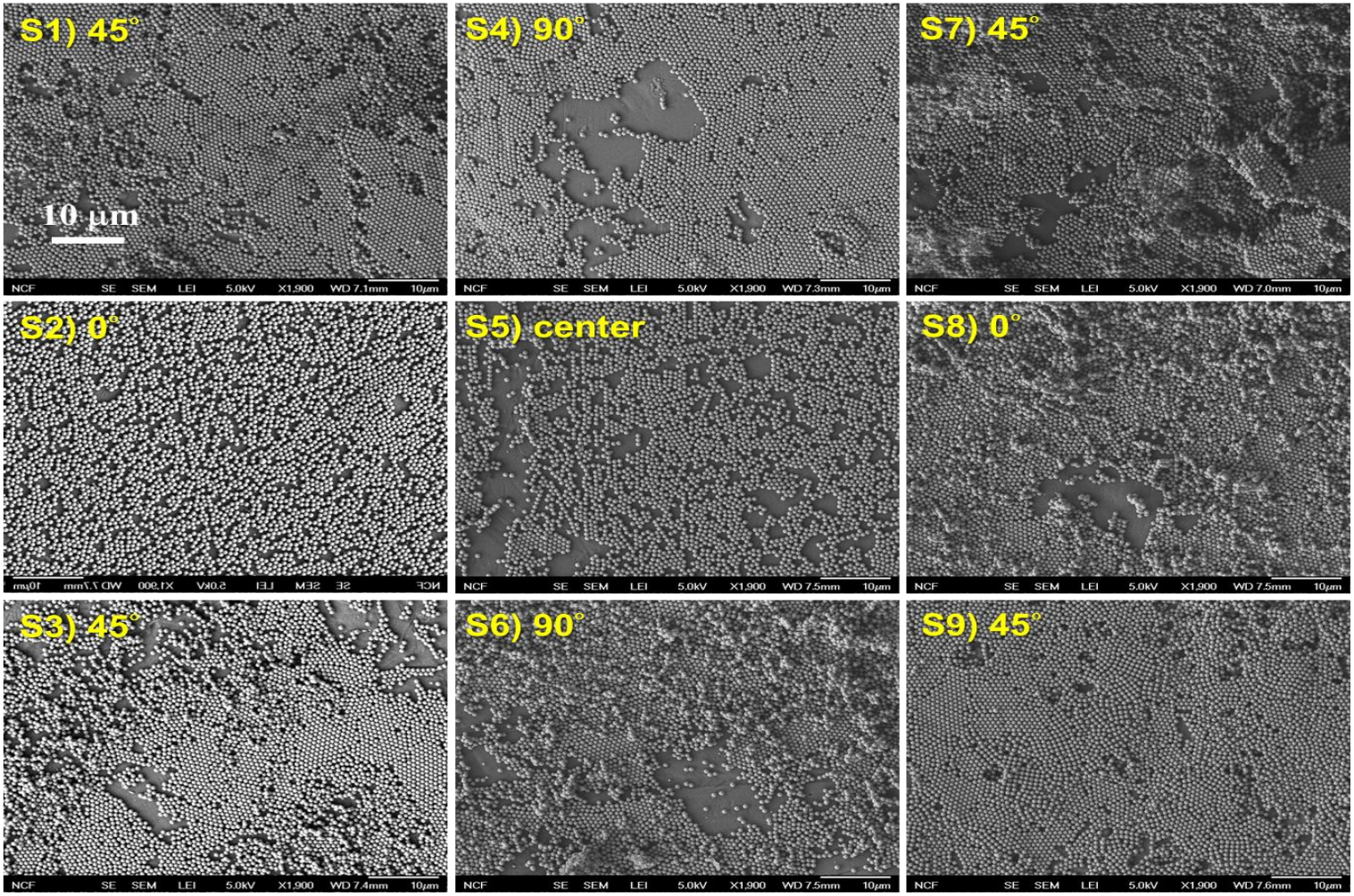

Figure 3.9: SEM images of the fouled un-patterned membranes at all nine segments of the un-patterned membrane surface. Note that there is uniform flow over these nine segments since the un-patterned membrane is flat. The nine segments were chosen as analogues to the patterned membrane and the average orientation angle was selected to compare directly with the fouled patterned membrane. The scale bar represents a length of 10 μm.

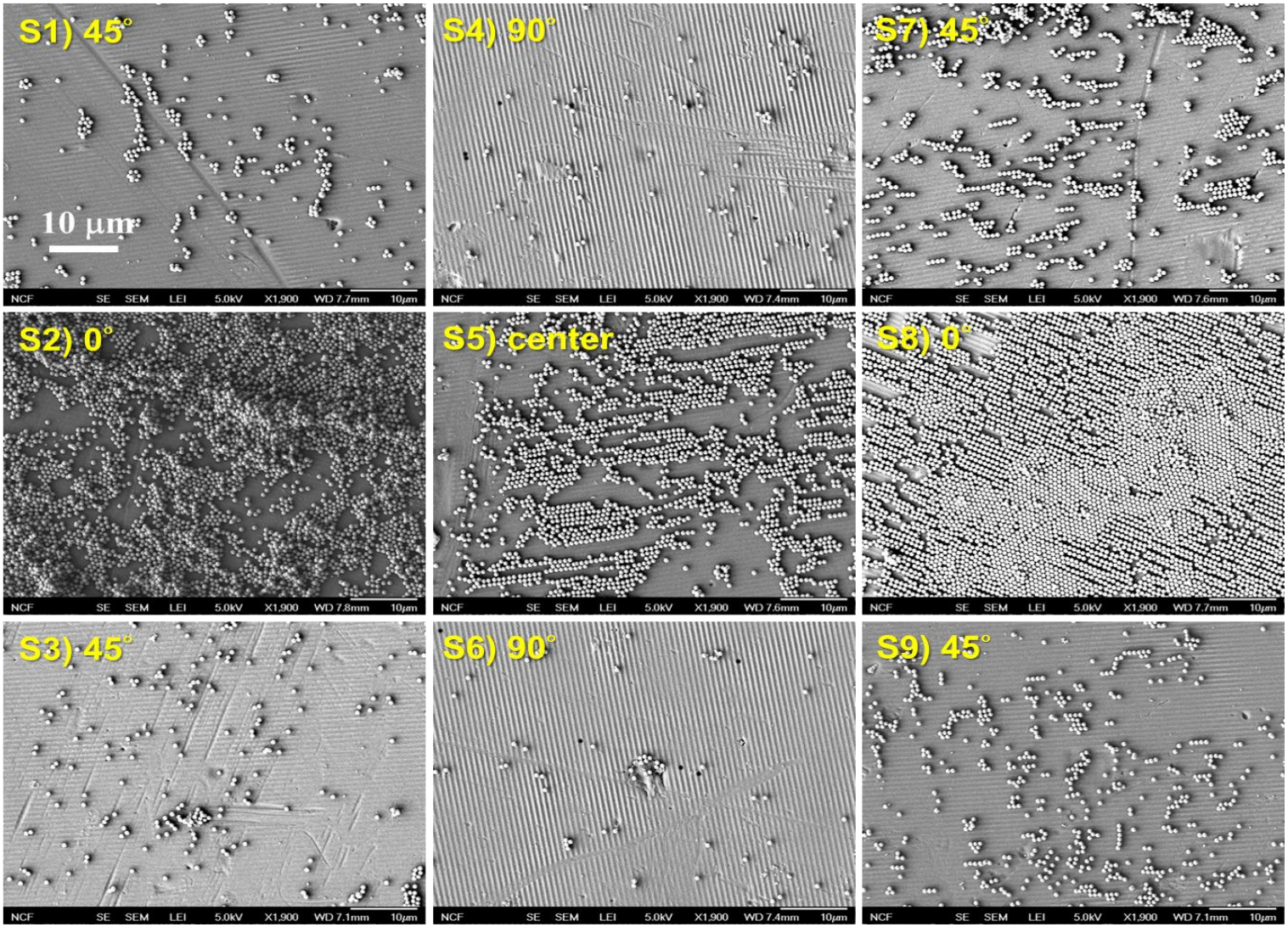

Figure 3.10: SEM images of the fouled patterned membrane at all nine segments of the fouled membrane surface; the average orientation angle of the segment is labeled on each image. The scale bar represents a length of 10 μm.

Dramatic differences in particle deposition were observed for the patterned and un-patterned membranes. The average surface coverage for the patterned membrane was 19.4 % as compared with 66.2% for the un-patterned membrane, which agrees with the observed increase of J_c, and reduced R_f, for the former. Most interestingly, particle deposition on the patterned membrane surface is highly anisotropic, depending on the value of θ_f. A very low level of surface coverage (2.2 %) occurred for regions where the θ_f = 90°, i.e. the flow was perpendicular to the orientation of the patterned lines. A monotonic increase in the surface coverage is observed with a decrease in θ_f, with the highest coverage (57.4 %) found for θ_f = 0°, i.e. the regions where the flow direction was parallel to the patterned lines (Fig. 3.10). In contrast, no such anisotropic distribution of the particle deposition is observed for the un-patterned membranes (Fig. 3.9).

3.3.4 Cross-flow filtration of colloid particles on patterned membrane surface

Above all, it was observed that the presence of sub-micron surface patterns on UF membrane surfaces significantly increases J_c during colloidal filtration, compared with the un-patterned counterpart with the same surface chemistry. Note that, a radial-flow filtration cell was adopted for the preliminary constant pressure J_c because the overall size of the patterned membrane was not large enough for cross-flow filtration measurements. Overall feed-flow direction was highly anisotropic with respect to the pattern lines on the membrane surface. Because of this reason it is challenging to systematically evaluate the hydrodynamic effect induced by the sub-

micron patterns. Patterned membrane of larger size and proper cross-flow filtration cell is needed to investigate the hydrodynamic effect.

In this latter part of this Chapter, the patterned UF membranes used (5 cm × 5 cm) were large enough for proper cross-flow filtration measurements. Again, two patterned membranes were used in this study. Among them mem_L has line and space grating patterns with an average pattern height ~60–65 and mem_H has the same type of pattern with an average pattern height ~150–160 nm.

Cross-flow filtration of silica particle suspensions over patterned UF membranes were conducted at three different configurations: the feed flow direction is parallel, diagonal, and perpendicular to that of the pattern lines (as illustrated in Fig. 3.11). Correspondingly, the angle (θ_f) between the direction of the feed flow and that of the grating lines, is 0°, 45°, and 90°. At each θ_f, silica particle suspensions with were filtrated at varying cross-flow velocity. The experiments were conducted for the un-patterned and two patterned membranes, with two different sized silica particles. After the compaction stage, the water permeance for un-patterned PES membrane was determined to be 4.81×10^{-4} $Lm^{-2}h^{-1}Pa^{-1}$. In comparison, water permeance was ~ 4.47×10^{-4} $Lm^{-2}h^{-1}Pa^{-1}$ for Mem_L, and ~ 2.92×10^{-4} $Lm^{-2}h^{-1}Pa^{-1}$ for Mem_H. The reason behind the lower permeance for Mem_H is explained in detail in Chapter 2 in this dissertation. In brief, more plastic deformation at higher imprinting temperature and pressure lowers the permeance of imprinted PES membrane.

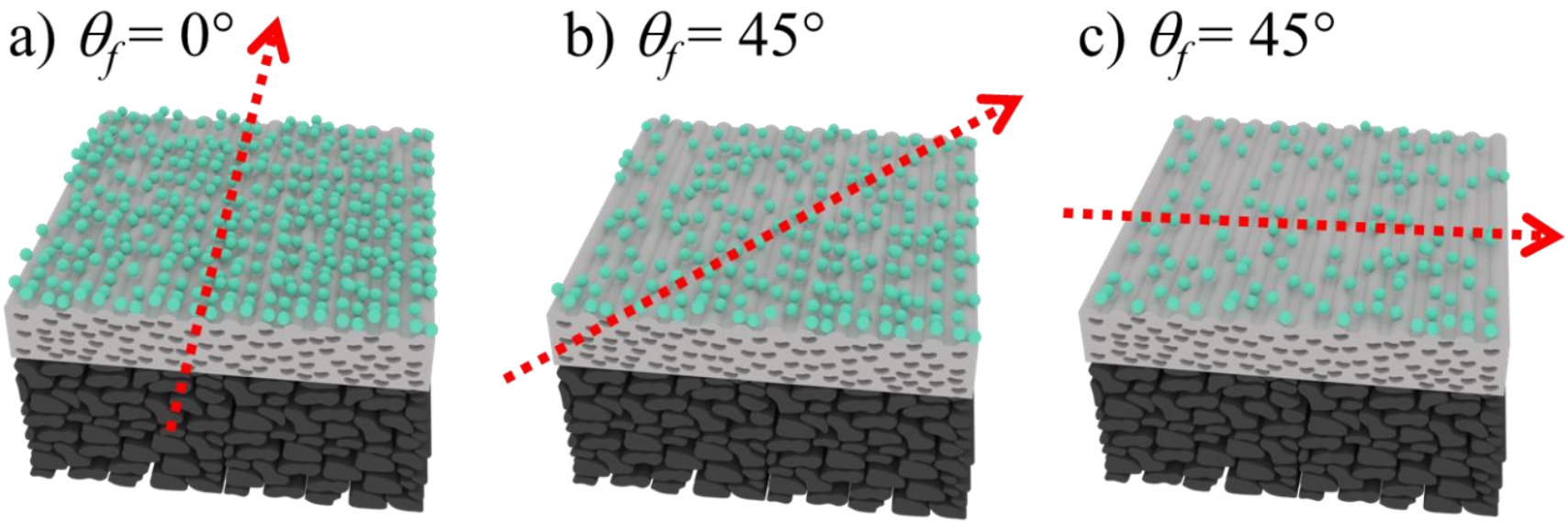

Figure 3.11: Schematics of the feed flow direction, indicated by the arrows, (a) parallel ($\theta_f = 0°$), (b) diagonal ($\theta_f = 45°$), and (c) perpendicular ($\theta_f = 90°$) to the pattern lines

Values of J_c of silica particle suspensions on different UF membranes (patterned or un-patterned) under varying hydrodynamic conditions were determined using the flux-stepping method as described earlier. Fig. 3.12a shows the representative data of the TMP as a function of permeate (water) flux, obtained from filtration of a suspension of 0.25 μm silica particle (5 g/L) through a patterned UF membrane (Mem_L) at a cross-flow velocity of 0.03 ms^{-1} (Re ~ 120) with a $\theta_f = 90°$ (Fig. 3.11c). In the region where the permeate flux was low, a linear relationship between flux and TMP was observed, a characteristic behavior expected in the absence of particle depositions. Once the permeate flux was over ~83 $Lm^{-2}h^{-1}$, TMP started to deviate from the linear dependence on the permeate flux, showing increasingly stronger dependence on the flux. The point at which the TMP-flux relationship started to deviate from the linear relationship marks the onset of colloidal deposition (fouling), and the corresponding flux is determined as J_c. From Fig. 3.12a, it is also clear that the TMP-flux relationship for the colloidal suspension matches that of DI water at flux below J_c. This type of critical flux is definitely the "strong form" of J_c, which was also observed for suspensions of silica in the J_c experiments described earlier. The theory of and definition of J_c was explained earlier in this Chapter and also in Chapter 1 in this dissertation.

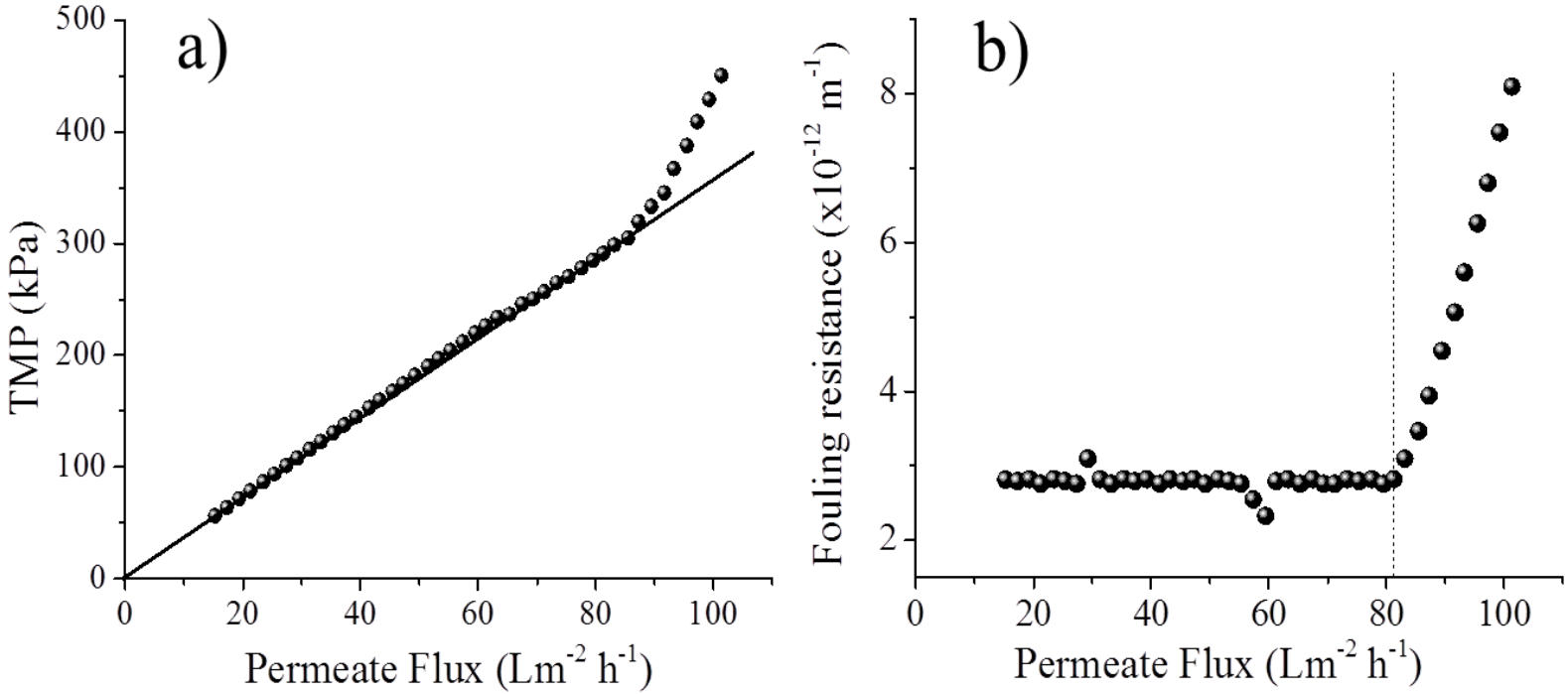

Figure 3.12: Representative data obtained from the flux-stepping measurements of Mem_L, during cross-flow filtration of colloidal suspensions: (a) TMP and (b) fouling resistance as a function of permeate flux. The conditions for the representative filtration experiment: 0.25 µm silica suspensions (5 g/L); cross-flow velocity of 0.03 ms^{-1}; and $\theta_f = 90°$. The symbols represent the experimental data for the colloidal filtration, while the solid line in a) represents the data for DI water.

The determination of J_c can determined, in a more precise fashion, by analyzing the resistance of the membranes to filtration, as explained in earlier section of 3.3.2. Fig. 3.12b plots the R_f as a function of TMP, obtained following above-described analysis, revealing that J_c can be determined as the flux at which R_f starts to sharply increase with permeate flux.

Here, all of the silica suspensions on patterned or un-patterned membranes displayed strong form of J_c, consistent with our previous measurements with radial-flow cell. Fig. 3.13 summarizes J_c measured for both un-patterned and patterned membranes at different θ_f for 0.25 and 0.5 μm silica suspensions at a cross-flow velocity of 0.03 ms^{-1}. For a given membrane, patterned or un-patterned, under identical filtration conditions, J_c of the 0.5 μm silica suspensions was larger than that of the 0.25 μm ones, which is consistent with the literature report that J_c increases with particle size when the particles are larger than 100 nm [36]. As stated earlier, for large particles, Brownian diffusion can be neglected, instead, membrane-particle surface interactions and shear-induced diffusion dominate the back-diffusion of the particles, which results in higher J_c values for larger silica particles.

For both patterned membranes, J_c increased with θ_f as the flow of the feed became more perpendicular to the pattern lines, the onset of silica particle deposition progressively delayed. For Mem_L, J_c of 0.25 (or 0.5) μm silica particles at θ_f = 90 ° was ~23 % (or 24 %) higher than the J_c measured at θ_f = 0 ° (and un-patterned membrane). In comparison, for Mem_H, J_c of 0.25 (or 0.5) μm silica particles at θf = 90 ° was ~15 % (or 24%) higher than that at θ_f = 0 °, and was ~ 30% (or 41%) than the

un-patterned membrane, correspondingly. This anisotropy of J_c on the patterned membranes is consistent with our previous SEM observations with the radial-flow cell. However, as mentioned, the J_c value at well-defined flow configuration with the filtration cell used earlier could not be quantify [43]. Note that the "pattern lines" in above mentioned membrane were practically anisotropic roughness formed by mixed matrix membrane, unlike the uniformly patterned ones in the present work.

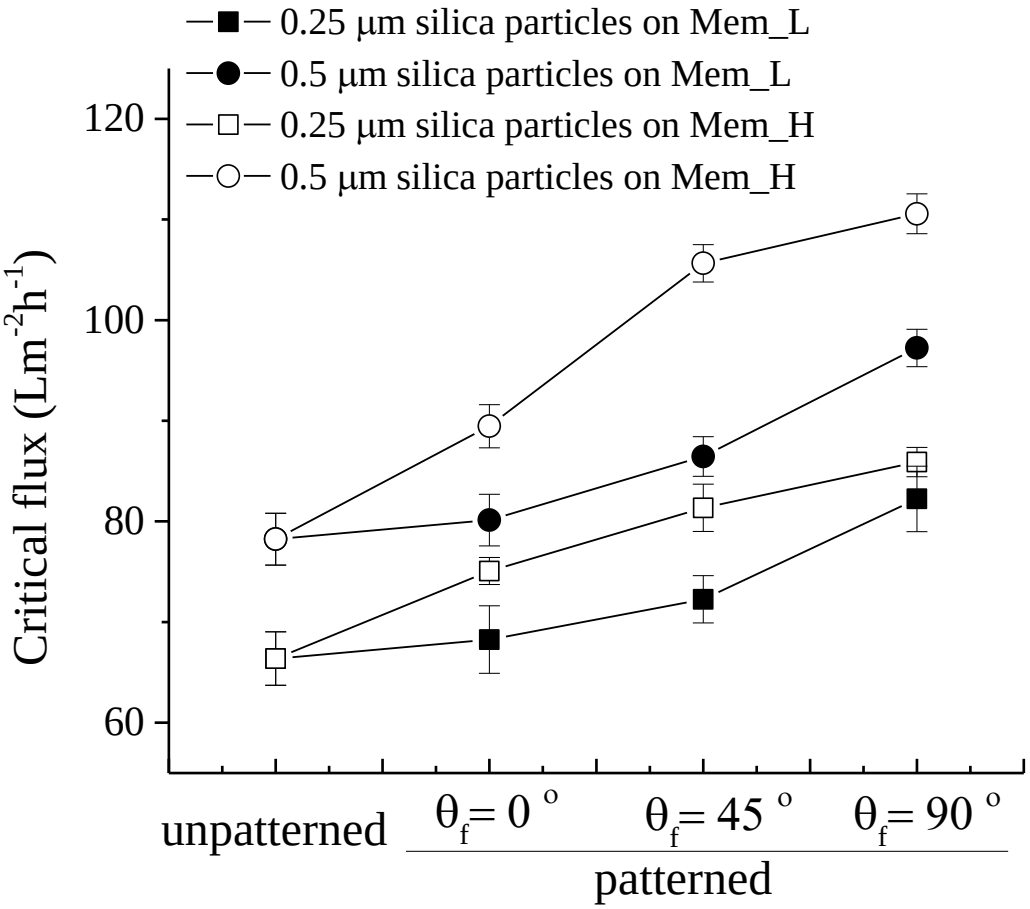

Figure 3.13: Critical flux for un-patterned and two patterned UF membranes at different flow configurations, for 0.25 μm and 0.5 μm aqueous silica suspensions (both at 5g/L). The cross-flow velocity is 0.03 ms-1. Error bar represents the standard deviation from three replicate measurements.

From Fig.3.13, at each of the three θ_f, higher values of J_c were observed for Mem_H, compared with Mem_L, despite the fact that intrinsic membrane resistance of the former was 40 % higher than the latter. It is known that the onset of deposition of particle, J_c, is the balance between the permeation drag (flux) and back-diffusion of the particles. The higher J_c on Mem_H suggests that the taller pattern could be more effective at enhancing the back-diffusion of the silica particles.

Figure 3.14 represents J_c for Mem_L as a function of V_{cf} for the 0.25 µm silica particle suspension at three different θ_f. In addition, measurement results for un-patterned membrane were included for comparison. As V_{cf} increased from 0.03 to 0.088 ms^{-1}, J_c increased ~ 81% for the un-patterned membrane, while increased ~100%, ~100%, and 92% for Mem_L at θ_f = 0°, 45°, and 90°, suggesting stronger influence of V_{cf} on the onset of particle fouling on surface-patterned membranes. Consistent with Fig. 5, J_c of Mem_L increased with the θ_f at each V_{cf}.

The dependence of J_c on V_{cf} on a planar UF or MF membrane is reasonably well understood. Higher V_{cf} of the feed leads to higher shear stress near the membrane surface that results in enhanced shear-induced diffusion of the particles [29, 43]. As the onset of particle deposition is the result of balance between the permeation drag (correspondingly J_c) and the particle diffusion, the enhanced shear-induced diffusivity will delay J_c. Under such a scenario, J_{cf} fo$_r$ a dilute particle suspension under cross-flow is given by,

$$J_c = 0.0595\,\lambda_0 \left(\frac{a^4}{L}\right)^{1/3} \ln\left(\frac{\emptyset_w}{\emptyset_b}\right) \qquad (1)$$

where λ_0 is shear rate at the membrane wall, a is the particle size and L represents length of the cross-flow path along the membrane, while ϕ_b and ϕ_w are particle volume concentrations in the bulk feed and at the membrane wall, correspondingly.

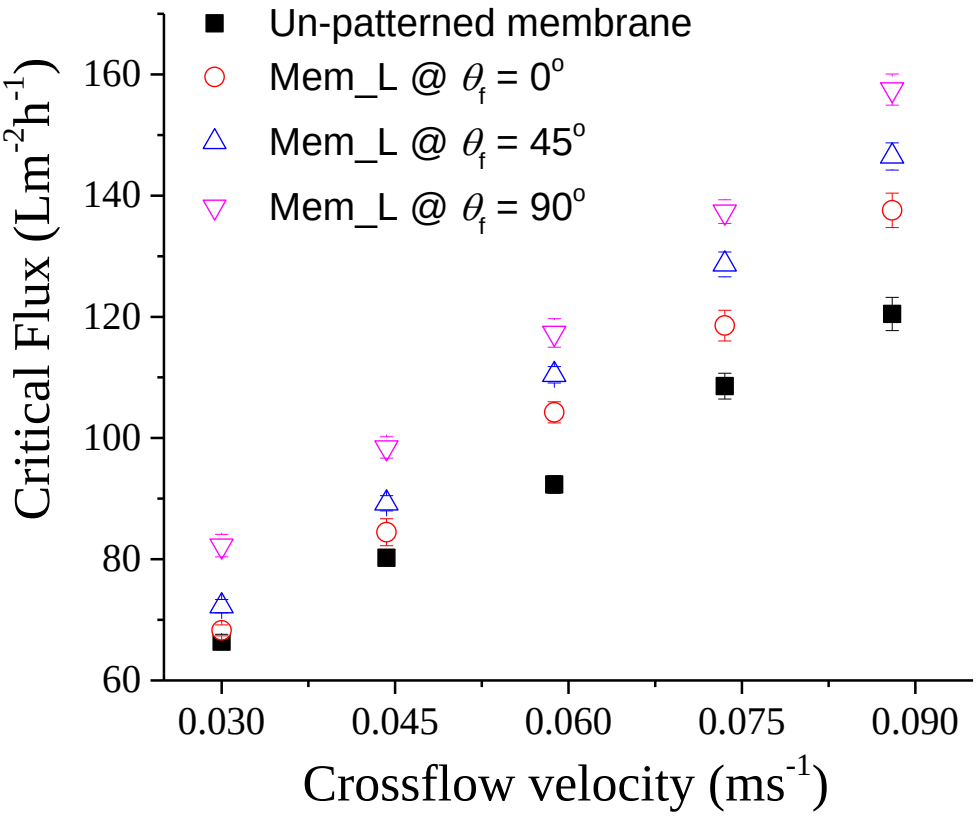

Figure 3.14: Critical flux for un-patterned and patterned (Mem_L) membranes as a function of cross-flow velocity for 0.25 µm silica particle suspensions. Error bar represent the standard deviation from three replicate measurements.

The shear rate represents the velocity gradient through a laminar hydrodynamic boundary layer and can be estimated directly from $6Q/wh^2$, in a thin rectangular channel. Clearly, shear-induced diffusivity model predict increase of J_c with the cross-flow velocity. Similar dependence of J_c on V_{cf} was also observed for the

Mem_L at different θ_f, suggesting that the shear-induced diffusion of particles indeed dictated the J_c on patterned membranes. However, at a given V_{cf}, J_c gradually increases with θ_f, indicating that additional hydrodynamic effects that further enhance the back-diffusion of the particles. Furthermore, the pattern-induced enhancement of J_c appeared to be stronger at higher V_{cf} (Fig. 3.14).

All of the above experiments show that the presence of submicron pattern can strongly increase the J_c values, i.e. delay the onset of colloidal depositions, without modifying the surface chemistry and flow behaviors of the bulk feed solution. The origin of the pattern-induced delay in particle deposition is most likely caused by the enhanced shear-induced diffusion of the particles. Under such a mechanism, the presence of the surface pattern can modify the shear stress at the membrane surface, which leads to enhanced back-diffusion of the particles during concentration polarization stage. Indeed, studies have shown that even though the overall shear stress is reduced due to the presence of micron sized pattern, but the effective/average shear stress near the membrane surface (in the vicinity of the pattern) indeed increased [44, 45]. Consequently, particles will start to deposit at larger driving force (flux), hence the critical flux increases.

The presence of surface patterns can also dramatically alter the flow profile and local streamlines in the vicinity of the patterns, and this effect has been successfully applied to promote mixing in microfluidic devices [46]. Stroock showed that at a given θ_f, the surface patterns will induce a transverse component in the flow streamline in parallel to the pattern lines [47], which becomes more dramatic with

an increase in θ_f. This explains the dramatic difference in the particle deposition with respect to the feed-flow angle with the line patterns. Note that, such an effect of transverse component would also facilitate the lateral diffusion of the particles and ultimately promote the back-diffusion of the particles. For a given surface-patterned UF membrane, with the increase of θ_f, the effective pattern features that interact with the feed solution changes. As illustrated in Fig. 3.15, the effective periodicity depends on the θ_f, as $\Gamma/\cos(\theta)$, where Γ is the periodicity of the surface pattern. Accordingly, the aspect ratio of the pattern line becomes $H\cos(\theta)/W$, where H and W are the height and width of the pattern lines. Therefore, with the increase of θ_f, the effective aspect ratio of the pattern line increases and effective periodicity decreases, i.e. the surface patterns become sharper, which might cause the shear stress near the membrane surface to increase. As stated earlier, the surface patterns will induce a transverse component in the flow streamline in parallel to the pattern lines [49], which becomes more significant with an increase in θ_f. . Note that the base channels of our cross-flow cells were circular (Fig 3.3), which cause the θ_f to deviate from the intended values (0°, 45°, and 90°). This boundary condition might be one of the reasons for the observed higher value of J_c at θ_f =0° for the patterned membranes, compared with the un-patterned one.

Besides the hydrodynamic effects, the presence of the surface patterns may also significantly alter the thermodynamic interactions between the membrane surface and the particles, and even particle-particle interactions. Hoek et al. suggested that the surface topography does change the membrane-particle

interactions in terms of the Derjaguin-Landau-Verwey-Overbeek (DLVO) interactions [48]. Additionally, the surface patterns can further influence particle-particle interactions as they settle on the membrane surface.

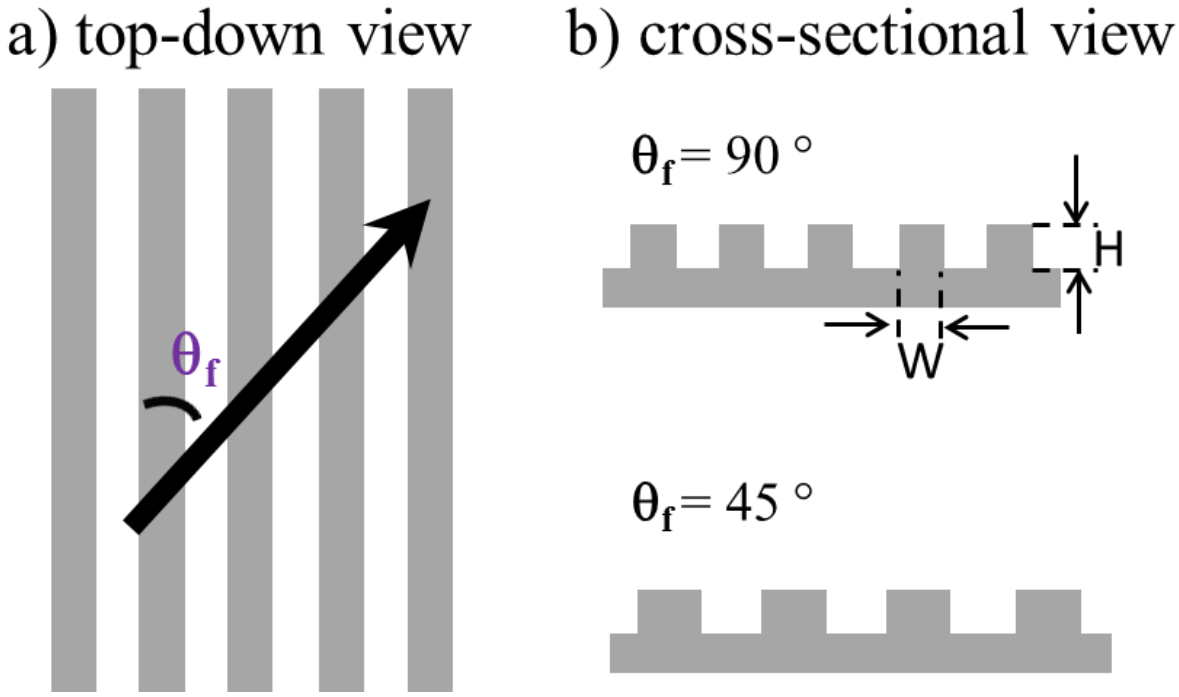

Figure 3.15: Schematic illustration of a) top-down view of feed flow over patterned surface at θ_f , and b) cross-sectional view of the effective pattern that interact with the feed, when $\theta_f = 90°$ and 45°. Notice the increase of line width at $\theta_f = 45°$, compared $\theta_f = 90°$.

From the SEM images of the un-patterned membranes, it is evident that the first layer of silica particles self-organized with hexagonal close-packing (HCP) (Fig. 3.9) reflecting a minimization of entropy. In contrast, HCP packing was not as evident on the patterned membranes. Instead, the 0.5 μm silica particles settled preferentially along the pattern trenches, and formed chain-like aggregates, with much less ordering between neighboring chains of particles (Fig. 3.10). Such a

"grapheo-epitaxial" effect may explain why the 0.415 μm pattern trenches had the least fouling of 0.5 μm silica particles (Fig 3.5). The observed fouling reduction on the patterned membranes during active filtration most likely results from the interplay between the aforementioned hydrodynamic and thermodynamic factors.

The observation that taller pattern had higher J_c is also consistent with hypothesis that sharper features could be more effective at raising the shear stress near the membrane surface. The aspect ratio of pattern lines on the Mem_H was ~2.7 times larger than that of the Mem_L. This comparison further suggests that surface patterns can be optimized for better performance of delaying particle depositions. Note that the intrinsic membrane resistance of the Mem_H is 40% higher than Mem_L, meaning that higher TMP will be needed for operating at the same permeate flux, which increases the energy cost of the operation.

3.4 Conclusions

In summary, our filtration studies revealed that the presence of these nanoscale surface patterns minimizes the deposition of colloidal particles, with both increased J_c and a lower rate of growth of total cake resistance. Such an enhancement of the J_c enables greater productivity since the sub-critical flux is higher. Microscopic analysis showed that the particle deposition was highly anisotropic on the membrane surface and that deposition decreased with the increase of orientation angle between the pattern lines and the feed-flow direction.

In the second part of the filtration study, systematic cross-flow filtration experiments of colloidal suspensions with membranes with sub-micron surface patterns was conducted. The J_c, the flux at which irreversible deposition of particle starts to occur, increases with the particle size, cross-flow velocity, angle between the flow of the feed and the lines of the patterns, and the height of the patterns. The origin of this enhanced anti-fouling behavior was attributed to the ability of sub-micron surface patterns to enhanced shear-induced lateral diffusion, by raising the average shear stress near the membrane surface and/or creating transverse flow. All these are achieved without affecting the flow of the bulk feed solutions and chemistry of the membrane.

References

1 Bacchin, P., Aimar, P. & Sanchez, V. Influence of surface interaction on transfer during colloid ultrafiltration. *Journal of Membrane Science* **115**, 49-63, doi:http://dx.doi.org/10.1016/0376-7388(95)00279-0 (1996).

2 Cho, J., Amy, G. & Pellegrino, J. Membrane filtration of natural organic matter: comparison of flux decline, NOM rejection, and foulants during filtration with three UF membranes. *Desalination* **127**, 283-298, doi:http://dx.doi.org/10.1016/S0011-9164(00)00017-5 (2000).

3 Choksuchart, P., Heran, M. & Grasmick, A. Ultrafiltration enhanced by coagulation in an immersed membrane system. *Desalination* **145**, 265-272, doi:http://dx.doi.org/10.1016/S0011-9164(02)00421-6 (2002).

4 Lin, T., Shen, B., Chen, W. & Zhang, X. Interaction mechanisms associated with organic colloid fouling of ultrafiltration membrane in a drinking water treatment system. *Desalination* **332**, 100-108, doi:http://dx.doi.org/10.1016/j.desal.2013.11.001.

5 Choi, Y. H., Kim, H. S. & Kweon, J. H. Role of hydrophobic natural organic matter flocs on the fouling in coagulation-membrane processes. *Separation and Purification Technology* **62**, 529-534, doi:http://dx.doi.org/10.1016/j.seppur.2008.03.001 (2008).

6 Goldman, G., Starosvetsky, J. & Armon, R. Inhibition of biofilm formation on UF membrane by use of specific bacteriophages. *Journal of Membrane Science* **342**, 145-152, doi:http://dx.doi.org/10.1016/j.memsci.2009.06.036 (2009).

7 Sioutopoulos, D. C., Yiantsios, S. G. & Karabelas, A. J. Relation between fouling characteristics of RO and UF membranes in experiments with colloidal organic and inorganic species. *Journal of Membrane Science* **350**, 62-82, doi:http://dx.doi.org/10.1016/j.memsci.2009.12.012.

8 Jermann, D., Pronk, W., Kagi, R., Halbeisen, M. & Boller, M. Influence of interactions between NOM and particles on UF fouling mechanisms. *Water research* **42**, 3870-3878 (2008).

9 Le-Clech, P., Chen, V. & Fane, T. A. G. Fouling in membrane bioreactors used in wastewater treatment. *Journal of Membrane Science* **284**, 17-53, doi:http://dx.doi.org/10.1016/j.memsci.2006.08.019 (2006).

10 Rana, D. & Matsuura, T. Surface Modifications for Antifouling Membranes. *Chemical Reviews* **110**, 2448-2471, doi:10.1021/cr800208y.

11 Le-Clech, P., Chen, V. & Fane, T. A. G. Fouling in membrane bioreactors used in wastewater treatment. *J. Membr. Sci.* **284**, 17-53, doi:10.1016/j.memsci.2006.08.019 (2006).

12 Potts, D. E., Ahlert, R. C. & Wang, S. S. A critical review of fouling of reverse osmosis membranes. *Desalination* **36**, 235-264 (1981).

13 Porter, M. C. Concentration Polarization with Membrane Ultrafiltration. *Industrial & Engineering Chemistry Product Research and Development* **11**, 234-&, doi:10.1021/i360043a002 (1972).

14 Song, L. F. & Elimelech, M. Theory of Concentration Polarization in Cross-flow Filtration. *J. Chem. Soc.-Faraday Trans.* **91**, 3389-3398, doi:10.1039/ft9959103389 (1995).

15 Choo, K. H. & Lee, C. H. Membrane fouling mechanisms in the membrane-coupled anaerobic bioreactor. *Water Res.* **30**, 1771-1780, doi:10.1016/0043-1354(96)00053-x (1996).

16 Zhu, X. H. & Elimelech, M. Colloidal fouling of reverse osmosis membranes: Measurements and fouling mechanisms. *Environ. Sci. Technol.* **31**, 3654-3662, doi:10.1021/es970400v (1997).

17 Belfort, G. Membrane modules: comparison of different configurations using fluid mechanics. *J. Membr. Sci.* **35**, 245-270, doi:http://dx.doi.org/10.1016/S0376-7388(00)80299-9 (1988).

18 Cleaver, J. W. & Yates, B. Mechanism of detachment of colloidal particles from a flat substrate in a turbulent flow. *J. Colloid Interface Sci.* **44**, 464-474, doi:http://dx.doi.org/10.1016/0021-9797(73)90323-8 (1973).

19 Song, L., Chen, K. L., Ong, S. L. & Ng, W. J. A new normalization method for determination of colloidal fouling potential in membrane processes. *Journal of Colloid and Interface Science* **271**, 426-433, doi:http://dx.doi.org/10.1016/j.jcis.2003.12.016 (2004).

20 Singh, G. & Song, L. Influence of sodium dodecyl sulfate on colloidal fouling potential during ultrafiltration. *Colloids and Surfaces A: Physicochemical and Engineering Aspects* **281**, 138-146, doi:http://dx.doi.org/10.1016/j.colsurfa.2006.02.036 (2006).

21 Song, L. & Singh, G. Influence of various monovalent cations and calcium ion on the colloidal fouling potential. *Journal of Colloid and Interface Science* **289**, 479-487, doi:http://dx.doi.org/10.1016/j.jcis.2005.03.072 (2005).

22 Bacchin, P., Aimar, P. & Field, R. W. Critical and sustainable fluxes: Theory, experiments and applications. *Journal of Membrane Science* **281**, 42-69, doi:http://dx.doi.org/10.1016/j.memsci.2006.04.014 (2006).

23 Goosen, M. F. A. *et al.* Fouling of Reverse Osmosis and Ultrafiltration Membranes: A Critical Review. *Separation Science and Technology* **39**, 2261-2297, doi:10.1081/ss-120039343 (2005).

24 Field, R. W., Wu, D., Howell, J. A. & Gupta, B. B. Critical flux concept for microfiltration fouling. *Journal of Membrane Science* **100**, 259-272, doi:http://dx.doi.org/10.1016/0376-7388(94)00265-Z (1995).

25 Le Clech, P., Jefferson, B., Chang, I. S. & Judd, S. J. Critical flux determination by the flux-step method in a submerged membrane bioreactor. *Journal of Membrane Science* **227**, 81-93, doi:http://dx.doi.org/10.1016/j.memsci.2003.07.021 (2003).

26 Howell, J. A. Sub-critical flux operation of microfiltration. *Journal of Membrane Science* **107**, 165-171, doi:http://dx.doi.org/10.1016/0376-7388(95)00114-R (1995).

27 Richard Bowen, W. *et al.* The effects of electrostatic interactions on the rejection of colloids by membrane pores-visualisation and quantification. *Chemical Engineering Science* **54**, 369-375, doi:http://dx.doi.org/10.1016/S0009-2509(98)00252-8 (1999).

28 Chen, V., Fane, A. G., Madaeni, S. & Wenten, I. G. Particle deposition during membrane filtration of colloids: transition between concentration polarization and cake formation. *Journal of Membrane Science* **125**, 109-122, doi:http://dx.doi.org/10.1016/S0376-7388(96)00187-1 (1997).

29 Li, H., Fane, A. G., Coster, H. G. L. & Vigneswaran, S. An assessment of depolarisation models of crossflow microfiltration by direct observation through the membrane. *Journal of Membrane Science* **172**, 135-147, doi:http://dx.doi.org/10.1016/S0376-7388(00)00334-3 (2000).

30 Chan, R., Chen, V. & Bucknall, M. P. Ultrafiltration of protein mixtures: measurement of apparent critical flux, rejection performance, and identification of protein deposition. *Desalination* **146**, 83-90, doi:http://dx.doi.org/10.1016/S0011-9164(02)00493-9 (2002).

31 Huisman, I. H., Vellenga, E., Tragardh, G. & Tragardh, C. The influence of the membrane zeta potential on the critical flux for crossflow microfiltration of particle suspensions. *Journal of Membrane Science* **156**, 153-158, doi:http://dx.doi.org/10.1016/S0376-7388(98)00328-7 (1999).

32 Cho, B. D. & Fane, A. G. Fouling transients in nominally sub-critical flux operation of a membrane bioreactor. *Journal of Membrane Science* **209**, 391-403, doi:http://dx.doi.org/10.1016/S0376-7388(02)00321-6 (2002).

33 Espinasse, B., Bacchin, P. & Aimar, P. On an experimental method to measure critical flux in ultrafiltration. *Desalination* **146**, 91-96, doi:http://dx.doi.org/10.1016/S0011-9164(02)00495-2 (2002).

34 Miller, D. J., Paul, D. R. & Freeman, B. D. A crossflow filtration system for constant permeate flux membrane fouling characterization. *Review of Scientific Instruments* **84**, -, doi:doi:http://dx.doi.org/10.1063/1.4794909.

35 Beier, S. P. & Jonsson, G. Critical flux determination by flux-stepping. *AIChE Journal* **56**, 1739-1747, doi:10.1002/aic.12099.

36 Wu, D., Howell, J. A. & Field, R. W. Critical flux measurement for model colloids. *Journal of Membrane Science* **152**, 89-98, doi:http://dx.doi.org/10.1016/S0376-7388(98)00200-2 (1999).

37 Bacchin, P., Aimar, P. & Field, R. W. Critical and sustainable fluxes: Theory, experiments and applications. *J. Membr. Sci.* **281**, 42-69, doi:10.1016/j.memsci.2006.04.014 (2006).

38 Bacchin, P., Si-Hassen, D., Starov, V., Clifton, M. J. & Aimar, P. A unifying model for concentration polarization, gel-layer formation and particle deposition in cross-flow membrane filtration of colloidal suspensions. *Chem. Eng. Sci.* **57**, 77-91, doi:10.1016/s0009-2509(01)00316-5 (2002).

39 Harmant, P. & Aimar, P. Coagulation of colloids in a boundary layer during cross-flow filtration. *Colloids and Surfaces A: Physicochemical and Engineering Aspects* **138**, 217-230 (1998).

40 Carman, M. L. *et al.* Engineered antifouling microtopographies: Â correlating wettability with cell attachment. *Biofouling* **22**, 11-21, doi:10.1080/08927010500484854 (2006).

41 Romero, C. A. & Davis, R. H. Global model of crossflow microfiltration based on hydrodynamic particle diffusion. *J. Membr. Sci.* **39**, 157-185 (1988).

42 Leonard, E. F. & Vassilieff, C. S. The Depossition of Rejected Matter in Membrane Separation Processes. *Chemical Engineering Communications* **30**, 209-217, doi:10.1080/00986448408911128 (1984).

43 Zydney, A. L. & Colton, C. K. A Cconcentration Polarization Model for the Filtrate Flux in Cross-flow Microfiltration of Particulate Suspensions. *Chemical Engineering Communications* **47**, 1-21, doi:10.1080/00986448608911751 (1986).

44 Lee, Y. K., Won, Y. J., Yoo, J. H., Ahn, K. H. & Lee, C. H. Flow analysis and fouling on the patterned membrane surface. *J. Membr. Sci.* **427**, 320-325, doi:http://dx.doi.org/10.1016/j.memsci.2012.10.010.

45 Lee, K. J. & Wu, R. M. Simulation of resistance of cross-flow microfiltration and force analysis on membrane surface. *Desalination* **233**, 239-246, doi:http://dx.doi.org/10.1016/j.desal.2007.09.048 (2008).

46 Zheo, B. & Moore, J. S. Surface-Directed Liquid Flow Inside Microchannels. *Science* **291**, 1023 (2001).

47 Stroock, A. D. & Whitesides, G. M. Controlling Flows in Microchannels with Patterned Surface Charge and Topography. *Accounts of Chemical Research* **36**, 597-604, doi:10.1021/ar0202870 (2003).

48 Hoek, E. M. V., Bhattacharjee, S. & Elimelech, M. Effect of Membrane Surface Roughness on Colloid−Membrane DLVO Interactions. *Langmuir* **19**, 4836-4847, doi:10.1021/la027083c (2003).

CHAPTER IV

INFLUENCE OF PATTERNED SURFACE ON PROTEIN FOULING OF ULTRAFILTRATION MEMBRANE

4.1 Introduction

Ultrafiltration is a separation process used in plethora of application like, wastewater treatment, reverse osmosis pre-treatment, separations in food, dairy, chemical, biochemical and pharmaceutical industries [1-3]. But continuous operation of UF membrane in those applications is challenged by membrane fouling, specially coming from the presence of macromolecules such as protein in the feed solution. As discussed earlier, fouling reduces productivity, separation effectiveness and increase the energy demand for filtration [3]. To remove protein fouling, UF membranes are often treated with harsh chemicals which also limits the membrane reusability [2]. In a typical UF plant, 30-50% of the total operating cost is spent on membrane replacement and 10-30 % spent on membrane cleaning process [4].

Like other types of foulants, proteins have a strong tendency to deposit on the barrier layer surface of the membrane, which causes a significant decrease in the membrane flux [3, 5]. Flux decline of protein feed solution can be caused by both concentration polarization and adsorption of protein onto the membrane surface [5]. Marshall et al. proposed a three separate phases for flux decline during protein

filtration. Flux declines rapidly initially due to concentration polarization followed by protein deposition. And finally reaching quasi-steady-state period of slow flux decline due to additional deposition or consolidation of the fouling layer [3]. Despite the implementation of various pretreatment and cleaning protocols, protein fouling is unavoidable and causes additional energy consumption and sometime shutdown of the filtration process and eventually replacement of the membranes in the system.

Studies on UF membranes also have revealed that protein fouling is affected by three primary categories of factors: hydrodynamic conditions (permeate flux and crossflow velocity), feed solution characteristics (solution pH, ionic composition, and foulant concentration), and membrane properties (hydrophobicity, roughness, and charge density) [6]. Extensive efforts have been directed to modifying the surface chemistry of the UF membrane to mitigate protein fouling [7-11]. However, like other methods discussed earlier most of these methods require significant alterations in the membrane manufacturing system, and their usage has been limited by the uncertainty related with their long-term stability and scalability [12].

In the previous Chapters, the use of nanoimprint lithography (NIL) to impart sub-micron surface patterns directly onto a commercial polyethersulfone (PES) UF membrane has been demonstrated. The porous nature of the amorphous barrier layer allows successful surface patterning of the membrane without adversely affecting its permeation. It was found that the presence of these patterns significantly reduced the deposition of the colloidal particles of varying sizes. Herein this Chapter, systematic results examining the influence of sub-micron surface patterns on the

deposition of protein on the membrane surface under both static adsorption and active filtration conditions are reported. In comparison to the un-patterned reference, significant reduction in protein deposition on the patterned membranes was observed, mostly due to the hydrodynamic effects associated with the surface pattern. This effect was consistently observed independent of solution pH and ionic strength.

4.2 Methods and materials

All the reagents and chemicals used in this study were of analytical grade with purity over 99%. Ultrapure water with a resistivity of 18.2 MΩ cm was used. Bovine serum albumin (BSA) with a molecular mass of ~67 kg/mol was used as a model protein foulant. BSA was received in powder form (98% purity, P5368, Sigma Aldrich) and was stored at 4 °C in the dark. BSA feed solutions were freshly prepared prior to each fouling experiment, with phosphate buffered saline (PBS) as the buffer solution. All BSA/PBS solutions used in this study were filtered with a 0.5 μm Millipore cellulose acetate MF membrane prior to the experiments to remove aggregated BSA, and were then mixed using a stirrer for a minimum of 120 min.

A commercial PES UF membrane was used as a model UF membrane in this study. Details about the membrane can be found in the Chapter 2. This UF membrane has intrinsic root mean square (rms) roughness of ~10 nm and performances of this membrane will be compared to a surface patterned membrane fabricated using NIL from the same UF membrane (described in detail in Chapter 2). Sample 1.1 from Chapter 2 was used as a model patterned membrane for study. In brief, after the

imprinting with NIL periodic line-and-space grating patterns (Fig. 2.8) with an average pattern height ~100–120 nm were present in the patterned UF membrane. Since only one type of patterned membrane was used in this study, it will termed generally as "patterned membrane" in this Chapter and will be compared to its counterpart "un-patterned membrane". All filtration experiments were conducted in a radial flow type bench-scale module described in Chapter 3.2.1 (schematically shown in Fig. 3.1).

For a given membrane, both un-patterned and patterned, the constant-volume multistage filtration experiment can be divided into six steps as schematically shown in Fig. 4.1. The membrane was (1) initially compacted with DI water at a TMP ~207 kPa and then (2) at a TMP ~276 kPa. Filtration to stabilize compaction was performed over the time period needed to collect 15 mL/cm^2 of permeate volume. Compaction was considered complete if the differential flux from two successive measurements during this filtration, changed less than 2%. All of the following filtrations (steps 3-6) were carried out at a TMP ~276 kPa: (3) PBS was filtered, and the permeate volume was recorded every 10 min until the collection of 15 mL/cm^2 permeate, in order to determine the flux. Note that the PBS solution is completely permeable through the UF membrane; (4) a BSA/PBS solution, with a BSA concentration 1 g/L, was used as the feed and filtered for collection of 10.4 mL/cm^2 of permeate. During this stage, permeate flow was recorded every 6 min in closed vials to measure the flux and permselectivity. The ionic strength of the feed solution was adjusted by using reagent-grade sodium chloride, and the pH was

balanced by using hydrochloric acid and sodium hydroxide; (5) the BSA/PBS feed was replaced with the PBS solution, and the TMP gradient was resumed for 60 min to determine the steady-state flux for the fouled membrane; and (6) the whole filtration system was cleaned by flushing DI water without any TMP gradient. Lastly, the steady-state flux for the DI water-cleaned membrane was again determined by filtration with the PBS solution. The membrane samples after the filtration was inspected via FE-SEM using the method described in Chapter 3.2.3 and BSA deposited on the fouled membranes were characterized using a desorption method.

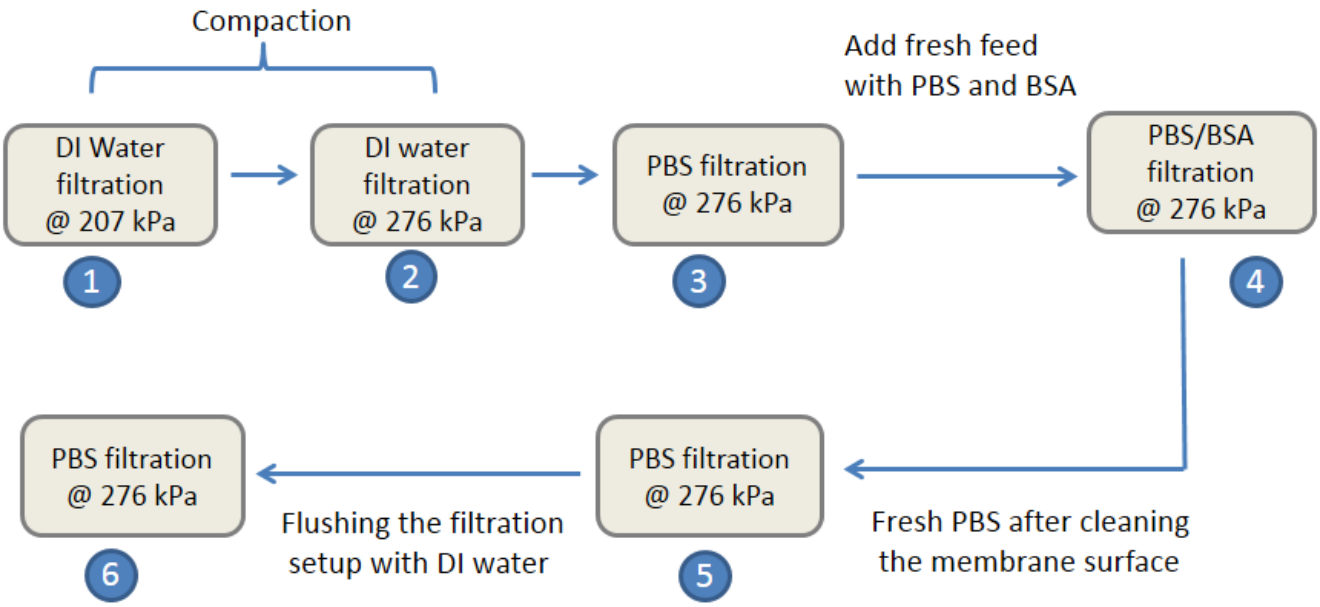

Figure 4.1: Flowchart for the different stages of the filtrations used to characterize the un-patterned and patterned membranes.

Amount of protein (BSA) deposit on the membrane surface were characterized using UV-vis spectroscopy. BSA were eluted from the membrane surface suing a

desorption method [12, 13]. Coupons with an area of 0.8 cm^2 were cut from the fouled membranes and sonicated in an ice bath within a PBS solution for 1 h. The concentrations of the BSA desorbed from the fouled membrane into the PBS solution were measured via UV–vis spectroscopy (8452A diode array spectrophotometer, Hewlett Packard) using a predetermined absorption-concentration calibration curve for the BSA–PBS solution.

Adsorption isotherms of BSA were determined for un-patterned and patterned membranes under both stirred and non-stirred conditions without TMP, i.e. under non-filtration conditions. A given membrane sample (1.93 cm^2 external surface area, identical to that used in active filtration) was attached to a glass slide with the barrier layer side in contact with the BSA/PBS solution. An overhead stirring shaft was used to maintain constant stirring during the isothermal experiment under stirred condition. BSA/PBS solutions with varying concentration but constant pH (7.4) were used. After 2 h exposure in a given solution, the membrane sample was taken out and rinsed with DI water to remove the loosely attached BSA on the membrane surface. Total adsorption of BSA on the membrane surface was then determined using the desorption method described above [13]. Note that complete BSA adsorption on UF membranes can take variable amounts of time, but 1 h has been observed in some cases [14, 15]. Specifically, commercial cellulose acetate and polysulfone membranes (Denmark Sugar Corporation) were used with a 1.5% BSA concentration by Matthiasson et al. in their experiment [14]. In addition, Ko et al. used polycarbonate Nuclepore PC015 and regenerated cellulose Amixon YM membranes in their

experiment with a BSA concentration of 0.5%. 2 h adsorption duration was chosen as it is comparable to the fouling duration during active filtration in step 4 of the multi-staged filtration shown in Fig. 4.1. Here, all of the sorption experiments were carried out with a stir bar (8 cm in length) at 834 rpm.

4.3 Results and discussion

4.3.1 Protein fouling on patterned and un-patterned membrane

As shown in Fig. 4.1, multistage filtration of different feed solutions while collecting a constant volume of permeate has been utilized to compare the difference in fouling characteristics between the un-patterned and the patterned membranes [16, 17]. In particular, aqueous PBS solution permeance before and after the BSA/PBS filtration were compared to quantify the influence of any deposited BSA layer on the permeance of the fouled membrane. Fig. 4.2 plots the permeate flux against permeate volume for different feed solutions following the exact filtration protocols in Fig. 4.1. The use of permeate volume instead of filtration time is more effective when comparing fouling between different types of membranes because it normalizes with respect to the total solute presented to the membrane [18]. Also, it gives one the opportunity to directly compare permenace before and after fouling to comprehend the permanent effect fouling have on the membrane permeability. Note that, during this flux comparative study the exact solutions were used for both patterned and un-patterned membranes.

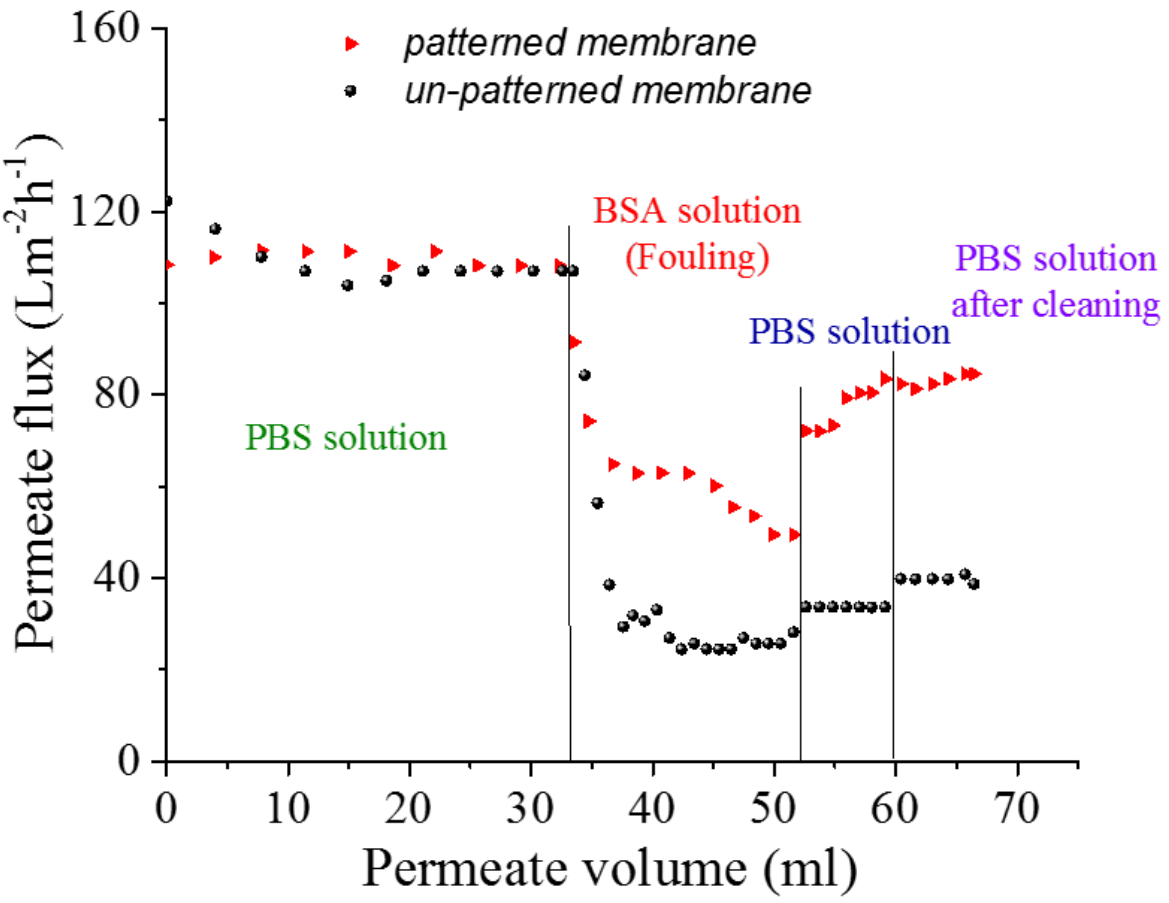

Figure 4.2: Permeate (PBS) flux (TMP=276 kPa) versus permeate volume for both un-patterned (circles) and patterned (triangles) membranes during filtration stages 3–6 as specified in Fig. 4.1

Both the membranes were compacted with DI water at a TMP ~207 kPa and then (2) at a TMP ~276 kPa as shown in Fig. 4.3. Filtration to stabilize compaction was performed over the time period needed to collect 15 mL/cm^2 of permeate volume. After the compaction the overall water permeance was found 4.87×10^{-4} Lm^{-2}h^{-1}Pa^{-1} for the un-patterned membrane and 4.73×10^{-4} Lm^{-2}h^{-1}Pa^{-1} for the patterned membrane.

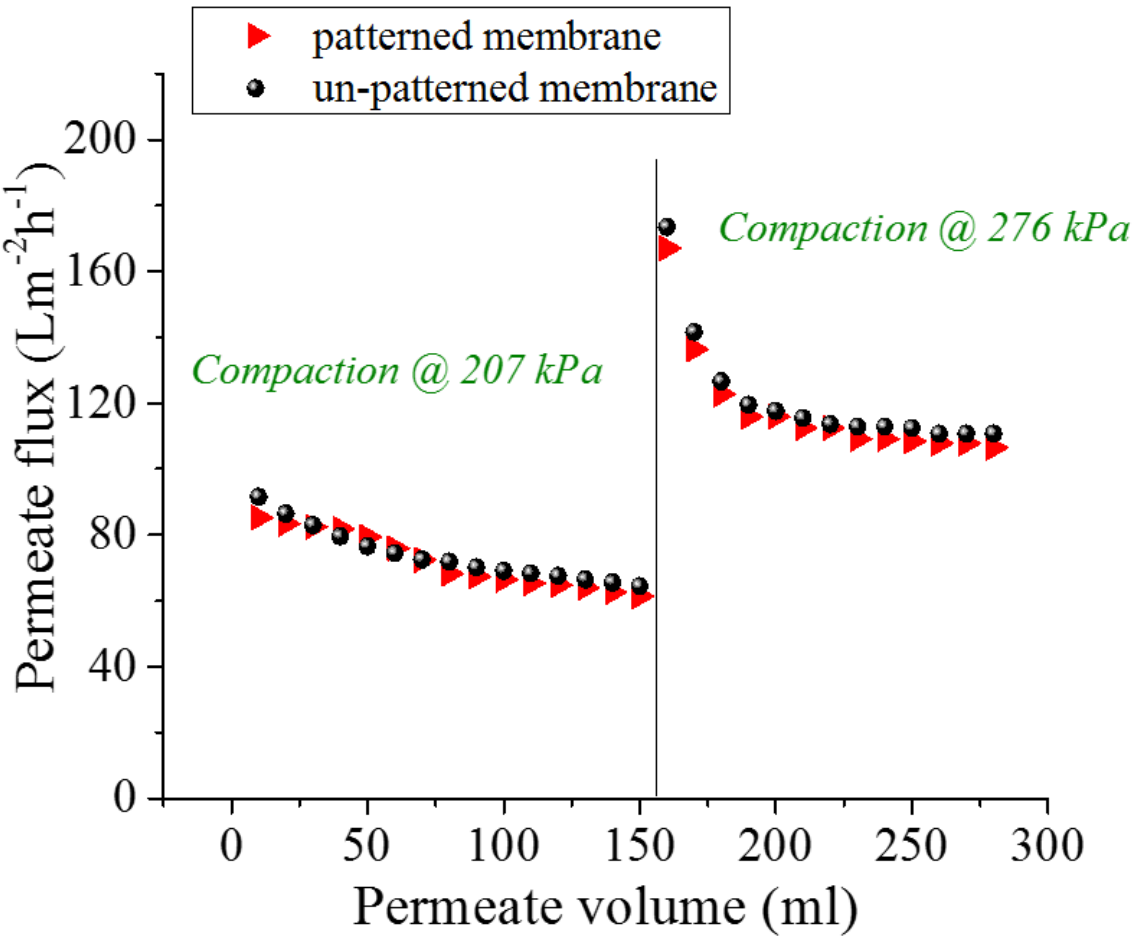

Figure 4.3: Permeate (DI water) flux (TMP=276 kPa) versus permeate volume for both un-patterned (circles) and patterned (triangles) membranes during compaction stages 1–1 as specified in Fig. 4.1.

After the membranes were compaction with DI water filtration PBS solution was used as the feed solution. As shown in Fig. 4.4, the un-patterned membrane still showed a slight compaction indicated by the flux reduction, while the patterned membrane did not display such behavior. This is consistent with a previous observation mentioned in Chapter 2 that the mechanical compression of the UF membrane prior to the filtration indeed reduced the compaction effect during filtration.

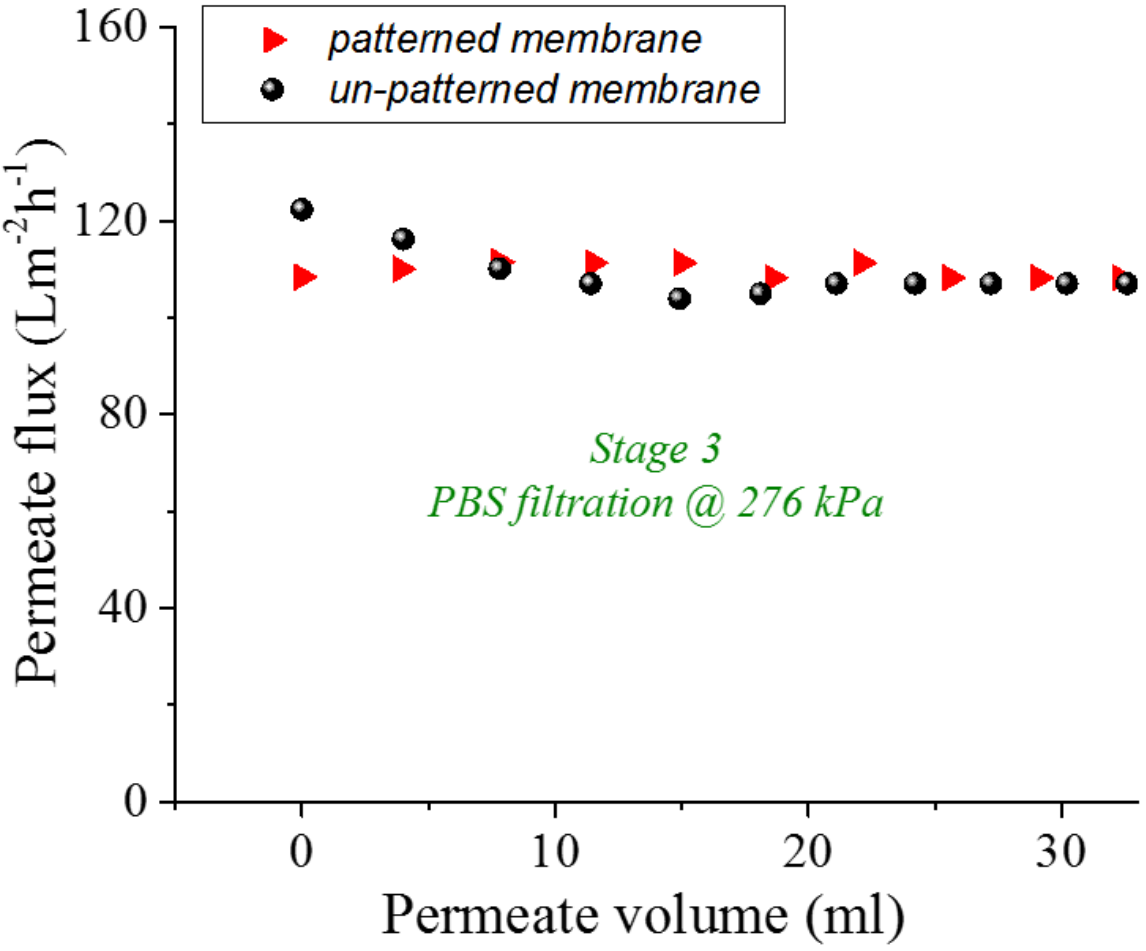

Figure 4.4: Permeate (PBS) flux (TMP=276 kPa) versus permeate volume for both un-patterned (circles) and patterned (triangles) membranes during PBS filtration stage 3 as specified in Fig. 4.1.

Following the PBS solution filtration, a BSA/PBS solution was used as the feed solution (step 4). For both membranes, the permeate flux (PBS) declined rapidly upon the start of the filtration (immediately due to the increased osmotic pressure, followed by concentration polarization and any adsorption effects) and gradually reaches a psuedo-steady-state flux (Fig. 4.5), which indicates the increase of permeation resistance due to BSA concentration polarization and fouling [19, 20].

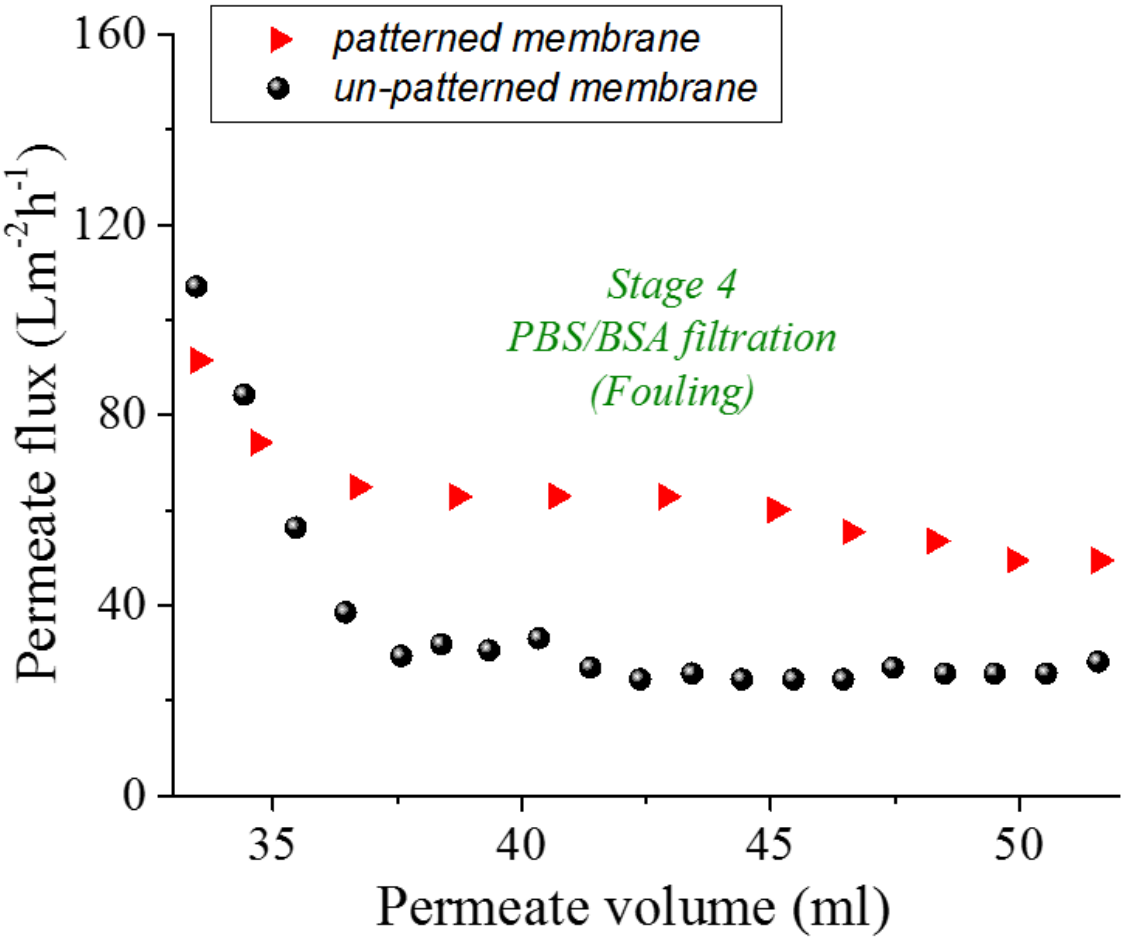

Figure 4.5: Permeate (PBS) flux (TMP=276 kPa) versus permeate volume for both un-patterned (circles) and patterned (triangles) membranes during BSA fouling stage 3 as specified in Fig. 4.1.

After the BSA/PBS filtration, the feed was replaced with the PBS solution, to characterize permeability of the as-fouled membranes (step 5 in Fig. 4.1). Here, the PBS flux was steady for the un-patterned membrane as it had been subjected to compaction and fouling as shown in Fig 4.6. In comparison, a slight increase in the PBS flux was observed for the as-fouled patterned membranes, which suggests that some loosely attached BSA was removed during this filtration step. Finally, filtration

using PBS solutions was carried out after moderate cleaning of the whole filtration system with DI water (step 6 in Fig. 4.1). PBS flux increased by ~14% for the un-patterned membrane, but remained relatively constant for the patterned membrane, in comparison with PBS flux prior to cleaning (Fig. 4.6). The kinetics of the flux decline in step 4 (filtration of BSA in PBS) suggests lower concentration polarization for the patterned membrane and a concomitantly lower rate of (strongly attached) protein adsorption versus the un-patterned one.

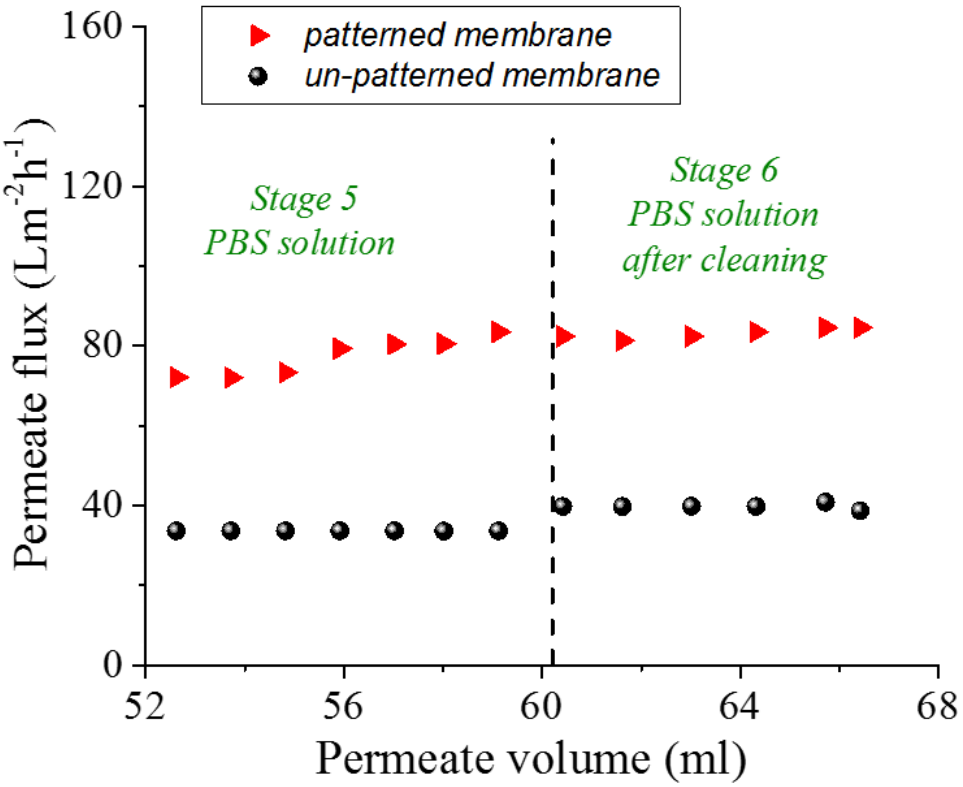

Figure 4.6: Permeate (PBS) flux (TMP=276 kPa) versus permeate volume for both un-patterned (circles) and patterned (triangles) membranes during BSA fouling stage 3 as specified in Fig. 4.1.

Fig. 4.7 summarizes the average values of the permeate flux at different stages of the filtration experiments discussed above. The error bars represent the standard deviation obtained from three replicate experiments. The PBS permeance was 4.1×10^{-4} $Lm^{-2}h^{-1}Pa^{-1}$ for the un-patterned membrane and 3.97×10^{-4} $Lm^{-2}h^{-1}Pa^{-1}$ for the patterned membrane, i.e. both membranes showed similar PBS permeance, which is consistent with DI water permeance values discussed previously.

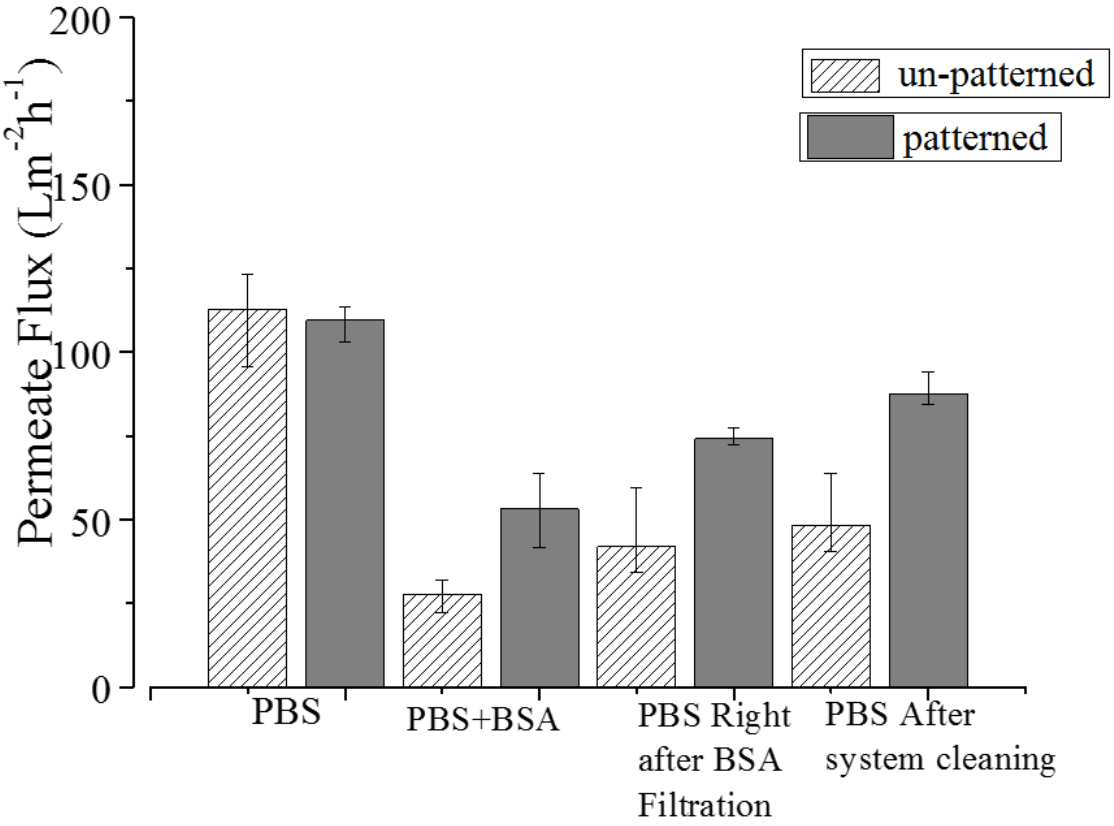

Figure 4.7: Average PBS fluxes for the un-patterned (shaded bars) and patterned (gray bars) membranes, for the different filtration stages shown in (a). The error bars represent the standard deviations from three replicate measurements. The BSA/PBS solution had a concentration of 1.0 g/L, pH=7.4, and an ionic strength of 0.13 M.

In addition, during BSA/PBS filtration, the fouling was evidently more extensive for the un-patterned membrane than for the patterned one, causing a ~75% versus 51% flux reduction, respectively. The protein partitioning that leads to the flux reduction arises from concentration polarization, loose attachment and irreversible deposition (both in and onto) the membrane surface [21]. After system cleaning, i.e. a DI water flush, the concentration polarization and loosely attached BSA can be removed resulting in partial flux recovery [21, 22].

Often, the overall fouling resistance of the membrane can be characterized using a flux recovery ratio (FRR) that represents the ratio between the PBS permeance after the system flushing and that before the fouling [23]. Specifically, the FRR of the un-patterned and patterned membranes was ~43% and ~88%, respectively, showing that the presence of the surface patterns significantly reduced the irreversible BSA deposition. In summary, the average permeate fluxes for the patterned membrane were ~91%, ~75%, and ~82% higher than the un-patterned one during filtration of BSA/PBS, after BSA fouling, and after system flushing, respectively.

After the filtration experiments, both un-patterned and patterned membrane samples were characterized using FE-SEM. Representative SEM images of the un-patterned membrane sample (Fig. 4.8b) showed patchy and denser depositions of BSA on the membrane surface, in comparison to the more sporadic distribution of BSA on the patterned membrane surface (Fig. 4.8d). The SEM images (Fig. 4.8a and c) of both membranes without fouling were also shown as references.

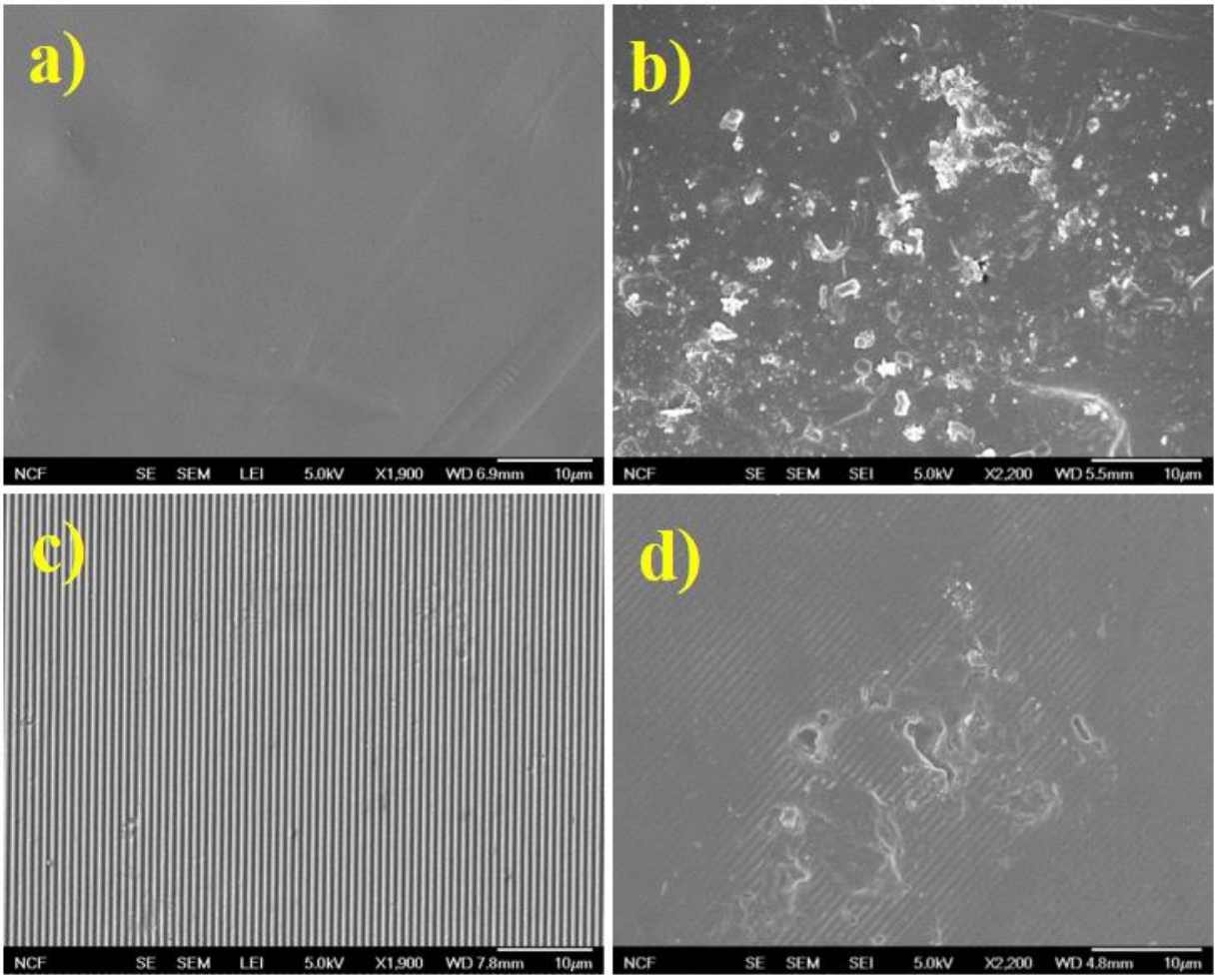

Figure 4.8: (a) and (c) are representative SEM images of the un-patterned and patterned membranes before the filtration, and (b) and (d) are representative SEM images of the fouled un-patterned and patterned membranes after staged filtrations, respectively.

To obtain a more statistically significant measure of the deposited BSA on both membranes, UV–vis measurements of the desorbed BSA (into a PBS buffer) was carried out. Fig. 4.9 shows the representative UV–vis absorption versus wavelength for the BSA desorbed from the un-patterned and patterned membranes after the above-described multistage filtrations. Clearly, more BSA was collected from the fouled, un-patterned membrane than from the patterned one. By using the

absorption–concentration calibration for the BSA/PBS solution, the areal averages of BSA coverage on the un-patterned and patterned membranes were measured to be 24.1±2.2 mg/m^2 and 16.9±3.4 mg/m^2, from three replicated measurements. These levels are consistent with, although lower than, those measured by others during dynamic adsorption (active filtration) [24]. Note that BSA fouling normally includes both pore blocking and physical deposition on the surface, and the desorption protocol used in this experiment would only release loosely-attached BSA.

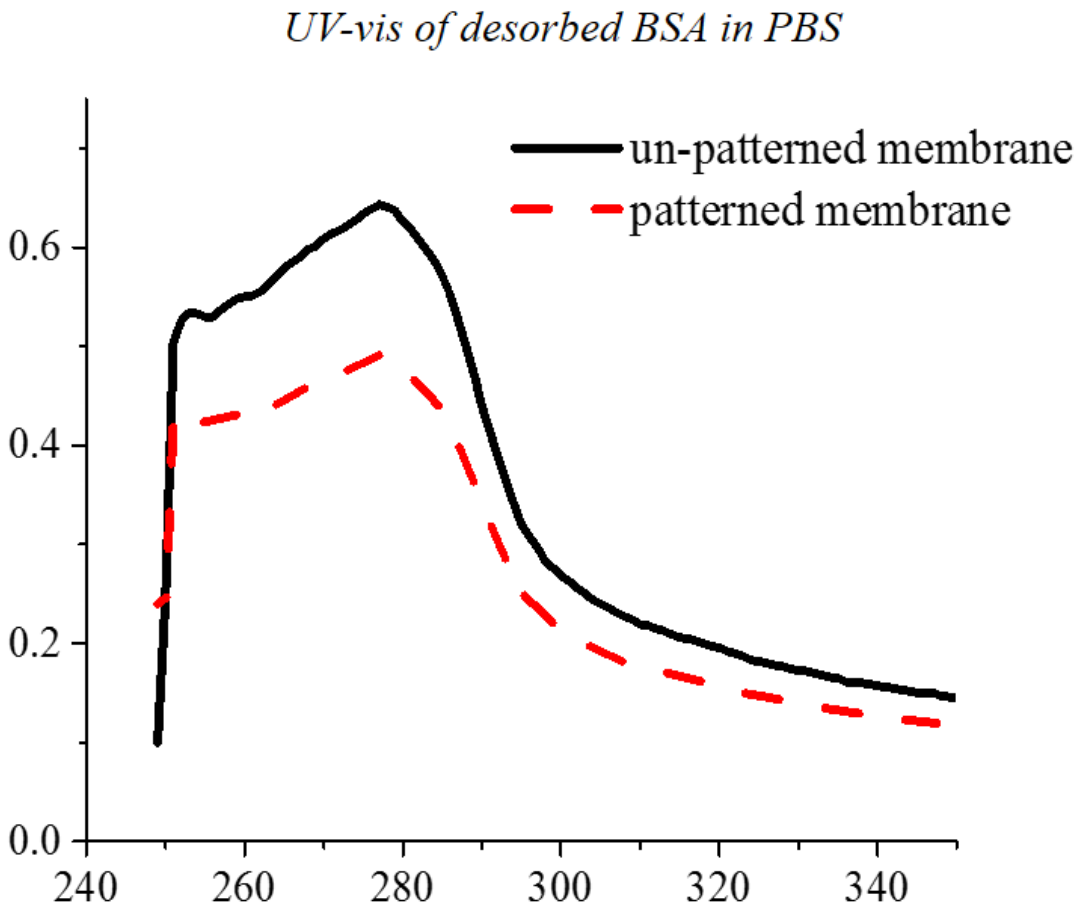

Figure 4.9: Representative UV–vis adsorption curves for BSA desorbed from the fouled un-patterned (solid line) and patterned (dashed line) membranes.

4.3.2 Effect of pH and ionic strength on flux recovery after protein fouling

It is well-known that the degree of protein–membrane interaction is dependent on the feed solution chemistry including pH and ionic strength, which affects both the rate and extent of BSA fouling [3, 6, 19, 25, 26]. Filtration of BSA/PBS solutions with varying pH values and ionic strengths on both un-patterned and patterned membranes were carried out following the same protocols shown in Fig. 4.1. Fig. 4.10 shows the FRR of PBS permeate as a function of pH values of the BSA/PBS solutions with two different ionic strengths for both membranes. These results illustrate that under all solution conditions the patterned membrane follows the same trends as the un-patterned one, but with less irreversible flux reduction (i.e., higher flux recovery).

Changes in pH and ionic strength will influence the electrostatic nature (and therefore electrokinetic interactions) of both the BSA and the PES membrane. In general, the apparent negative charge density of the PES membrane will increase and become asymptotic with respect to pH and ionic strength due to anion adsorption subject to the ultimate charge screening effect from higher electrolyte concentration [27]. The BSA undergoes charge and conformational changes with both pH and ionic strength that will affect its interactions with the membrane and itself, thus leading to the observed fouling influences observed during these filtration experiments [3, 19, 26].

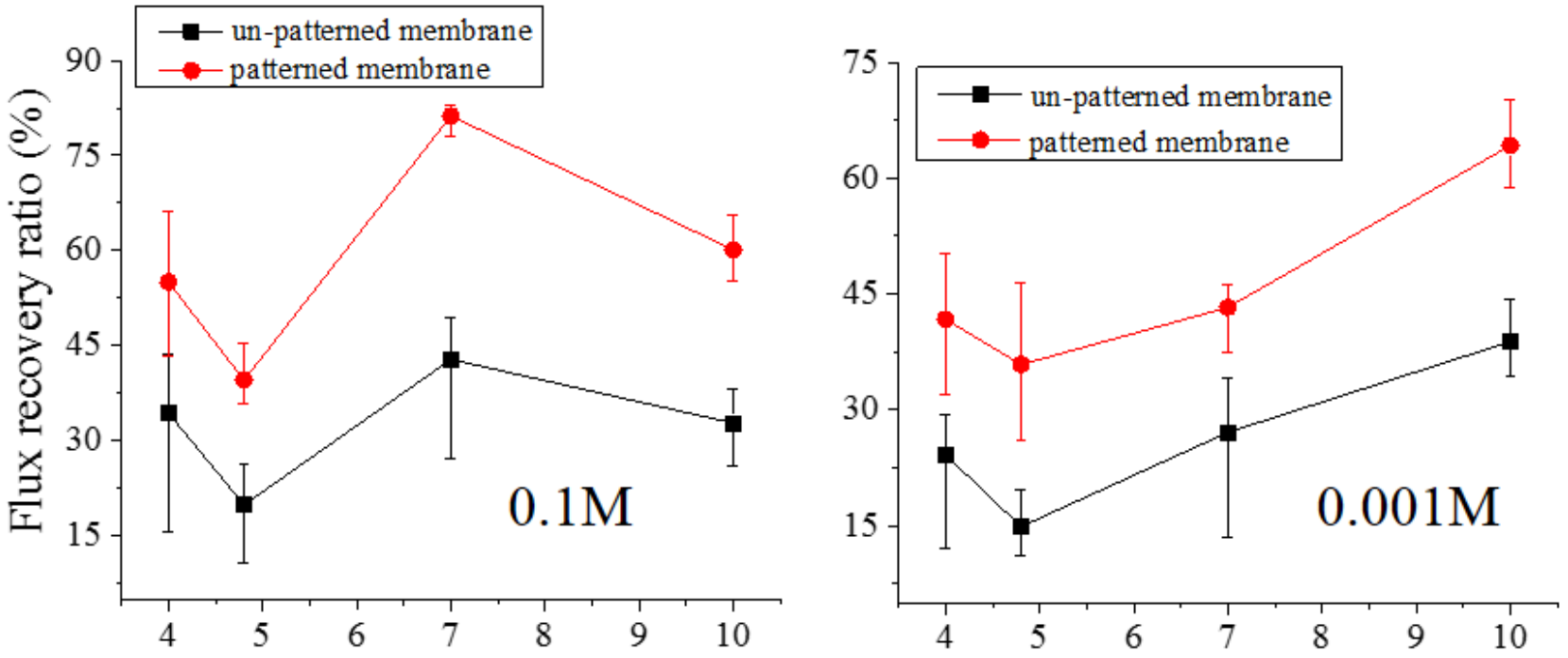

Figure 4.10: PBS flux recovery ratio of the un-patterned and patterned PES membranes as a function of the pH values of the BSA/PBS feed solutions at an ionic strength of (a) 0.1 M and (b) 0.001 M. The error bars represent standard deviations from three replicate measurements.

Irrespective of the ionic strength of the feed solution, both membranes displayed the lowest FRR (or most severe BSA fouling) for the BSA/PBS solution with pH=4.8, which is the isoelectric point (IEP) of BSA [28, 29]. The net charge of BSA at the IEP is zero, and there is much less electrostatic repulsion to hinder BSA deposition onto both the bare membrane and already-adsorbed BSA, which results in a more tightly packed layer [14, 30-32]. In comparison, at pH values higher or lower than its IEP, the BSA molecules have a net charge, and the electrostatic repulsions between them would result in a less tightly packed layer at the membrane surface [33].

With increased ionic strength, the electrostatic repulsion among the charged BSA molecules as well as the electrostatic repulsion (pH>IEP) or attraction (pH<IEP) between the BSA and membrane surfaces would be shielded [33-35]. Overall these effects would be expected to lead to more fouling of BSA, and a lower FRR, with an increase of ionic strength, which is somewhat different than what was observed. The increased FRR at higher ionic strength could reflect greater amount of loosely attached BSA aggregation (and more easily flushed away) foulant layers. The exact mechanisms by which pH and ionic strength affect protein deposition is unclear and will be studied in future experiments. Despite this uncertainty it is of considerable importance that the patterned membranes showed significantly higher FRR than their un-patterned counterparts, and both exhibited the same trends for the range of pH and ionic strengths examined.

In summary, it appears that the lower degree of fouling with the patterned membranes is consistently observed and not related in major fashion to specific interactions between membrane–BSA and BSA–BSA. Indeed, protein fouling during filtration is a complex phenomenon where permeation drag, tangential flow over the membrane surface, and specific solute–surface interactions are critical [6, 36].

4.3.3 Static protein adsorption on un-patterned and patterned membranes

To decouple the permeation drag from the other factors, adsorption of BSA on the membrane surface was measured under non-filtration conditions, i.e., stirring in a beaker at 830 rpm for 2 h. The patterned membrane has an almost constant offset of 5 mg/m^2 less than the un-patterned one for all of the different BSA (in PBS) concentrations (Fig. 4.11). The flow field generated by the stirring is largely tangential with respect to the membrane surface, and the associated shear stress at the surface helps to reduce BSA adsorption and aggregates under some circumstances [67][37]. Fig. 4.11 suggests that the presence of the surface pattern can induce higher shear stress in the vicinity of the membrane surface, at least locally, during active stirring. Indeed, a recent study by Lee et al. found that, during active filtration, the shear stress at the top of the pattern lines on the membrane surface tends to be higher, which limits the deposition of solutes in the feed solution [38]. From their shear stress model analysis they have also emphasized on the importance of using patterned membrane surface in mitigating fouling.

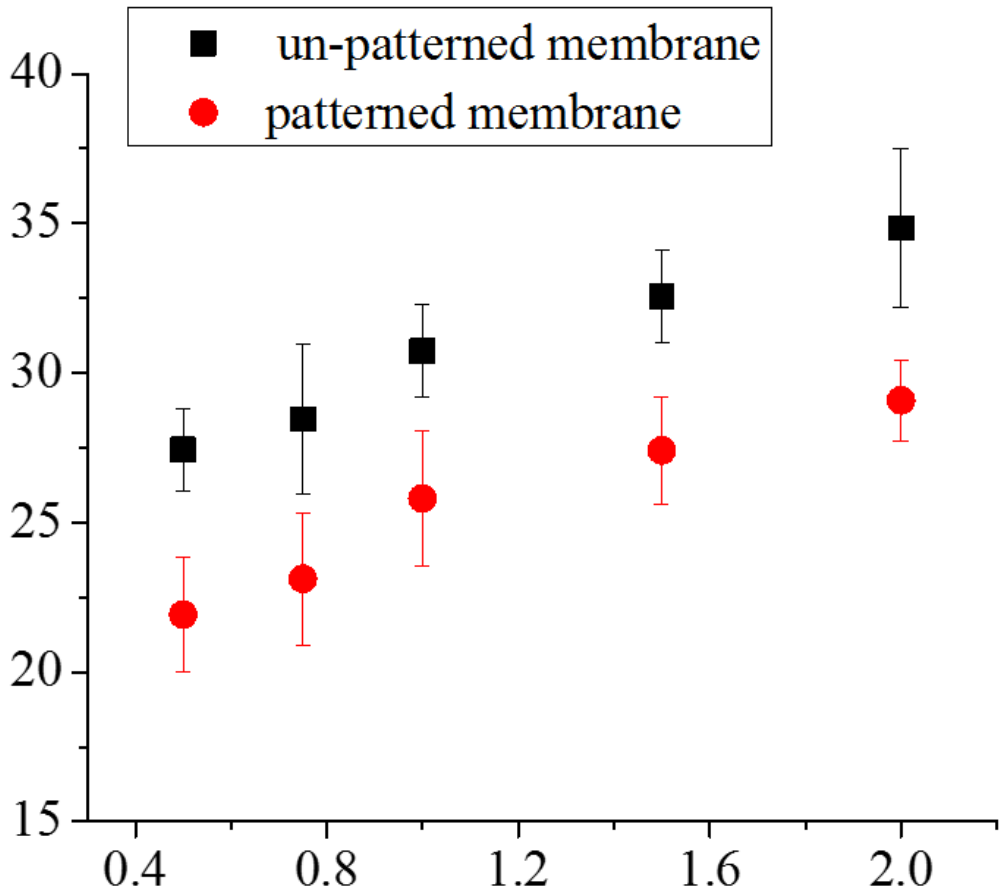

Figure 4.11: BSA adsorption isotherms for the un-patterned (squares) and patterned PES membranes (circles). The pH and ionic strength of all of the BSA/PBS solutions were 7.4 and 0.13 M, respectively. The error bars are the standard deviation from three replicate measurements.

The effect whereby surface patterns influence the flow profile and local streamlines in the vicinity of the patterns has been successfully applied to promote mixing in microfluidic devices [39, 40]. McDonough et al. showed that turbulent momentum transport created by surface roughness can indeed reduce the concentration polarization at a membrane surface during filtration [41]. Recent work by Lee et al. suggests the presence of a vortex within the micron-sized pattern valleys

as well as high shear stress localized on top of the pattern lines [38]. Both factors caused appreciable reduction in microbial fouling even with the modest crossflow.

Therefore, it is likely that the presence of the nano-patterned submicron patterns can induce similar localized turbulence and/or shear stresses, which give rise to the observed reduction of BSA fouling during filtration. Our results suggest that lower concentration polarization decreases the rate of fouling, but it is unclear how this effect is influenced by the specific features of the surface pattern, in terms of the pitch, line-to-space ratio, and shape of the line. Regardless, the presence of submicron surface patterns indeed showed significant reduction in the fouling of both colloids [37] and the BSA reported in this paper.

4.4. Conclusion

In this second study, systematic filtration protocols and measurement of adsorption of BSA solutions revealed that the presence of surface patterns significantly reduced the protein adsorption (fouling), when compared with the flat and smooth un-patterned membrane. The enhanced antifouling characteristic is most likely caused by the hydrodynamic interactions between the patterned surface and the feed solution. Such an effect was found to be persistent regardless of the pH and ionic strength of the feed solutions that were tested

References

1 Baker, R. *Membrane Technology and Applications*. (Wiley, 2004).

2 Goosen, M. F. A. *et al.* Fouling of Reverse Osmosis and Ultrafiltration Membranes: A Critical Review. *Separation Science and Technology* **39**, 2261-2297, doi:10.1081/ss-120039343 (2005).

3 Marshall, A. D., Munro, P. A. & Tragardh, G. The effect of protein fouling in microfiltration and ultrafiltration on permeate flux, protein retention and selectivity: A literature review. *Desalination* **91**, 65-108, doi:http://dx.doi.org/10.1016/0011-9164(93)80047-Q (1993).

4 Noble, R. D. & Stern, S. A. *Membrane Separations Technology: Principles and Applications*. (Elsevier Science, 1995).

5 Boyd, R. F. & Zydney, A. L. Analysis of protein fouling during ultrafiltration using a two-layer membrane model. *Biotechnology and Bioengineering* **59**, 451-460, doi:10.1002/(sici)1097-0290(19980820)59:4<451::aid-bit8>3.0.co;2-f (1998).

6 Belfort, G., Davis, R. H. & Zydney, A. L. The behavior of suspensions and macromolecular solutions in crossflow microfiltration. *Journal of Membrane Science* **96**, 1-58, doi:http://dx.doi.org/10.1016/0376-7388(94)00119-7 (1994).

7 An, L. *et al.* Mechanical properties and miscibility of polyethersulfone/phenoxy blends. *Journal of Applied Polymer Science* **59**, 1843-1847, doi:10.1002/(sici)1097-4628(19960321)59:12<1843::aid-app5>3.0.co;2-q (1996).

8 Kim, I. C. & Lee, K.-H. Dyeing process wastewater treatment using fouling resistant nanofiltration and reverse osmosis membranes. *Desalination* **192**, 246-251, doi:http://dx.doi.org/10.1016/j.desal.2005.05.030 (2006).

9 Luo, M. L., Zhao, J. Q., Tang, W. & Pu, C. S. Hydrophilic modification of poly(ether sulfone) ultrafiltration membrane surface by self-assembly of TiO2 nanoparticles. *Applied Surface Science* **249**, 76-84, doi:http://dx.doi.org/10.1016/j.apsusc.2004.11.054 (2005).

10 Reddy, A. V. R., Mohan, D. J., Bhattacharya, A., Shah, V. J. & Ghosh, P. K. Surface modification of ultrafiltration membranes by preadsorption of a negatively charged polymer: I. Permeation of water soluble polymers and inorganic salt solutions and fouling resistance properties. *Journal of Membrane Science* **214**, 211-221, doi:http://dx.doi.org/10.1016/S0376-7388(02)00547-1 (2003).

11 Wang, P., Tan, K. L., Kang, E. T. & Neoh, K. G. Synthesis, characterization and anti-fouling properties of poly(ethylene glycol) grafted poly(vinylidene fluoride) copolymer membranes. *Journal of Materials Chemistry* **11**, 783-789, doi:10.1039/b007310p (2001).

12 Rana, D. & Matsuura, T. Surface Modifications for Antifouling Membranes. *Chemical Reviews* **110**, 2448-2471, doi:10.1021/cr800208y.

13 Kujundzic, E., Greenberg, A. R., Fong, R. & Hernandez, M. Monitoring Protein Fouling on Polymeric Membranes Using Ultrasonic Frequency-Domain Reflectometry. *Membranes* **1**, 195-216.

14 Matthiasson, E. The role of macromolecular adsorption in fouling of ultrafiltration membranes. *Journal of Membrane Science* **16**, 23-36, doi:http://dx.doi.org/10.1016/S0376-7388(00)81297-1 (1983).

15 Muthukumaran, S. *et al.* The use of ultrasonic cleaning for ultrafiltration membranes in the dairy industry. *Separation and Purification Technology* **39**, 99-107, doi:http://dx.doi.org/10.1016/j.seppur.2003.12.013 (2004).

16 Chiang, Y. C., Chang, Y., Higuchi, A., Chen, W. Y. & Ruaan, R.-C. Sulfobetaine-grafted poly(vinylidene fluoride) ultrafiltration membranes exhibit excellent antifouling property. *Journal of Membrane Science* **339**, 151-159, doi:http://dx.doi.org/10.1016/j.memsci.2009.04.044 (2009).

17 Nabe, A., Staude, E. & Belfort, G. Surface modification of polysulfone ultrafiltration membranes and fouling by BSA solutions. *Journal of Membrane Science* **133**, 57-72, doi:http://dx.doi.org/10.1016/S0376-7388(97)00073-2 (1997).

18 Seidel, A. & Elimelech, M. Coupling between chemical and physical interactions in natural organic matter (NOM) fouling of nanofiltration membranes: implications for fouling control. *Journal of Membrane Science* **203**, 245-255, doi:http://dx.doi.org/10.1016/S0376-7388(02)00013-3 (2002).

19 Jones, K. L. & O'Melia, C. R. Protein and humic acid adsorption onto hydrophilic membrane surfaces: effects of pH and ionic strength. *Journal of Membrane Science* **165**, 31-46, doi:http://dx.doi.org/10.1016/S0376-7388(99)00218-5 (2000).

20 van den Berg, G. B. & Smolders, C. A. Flux decline in ultrafiltration processes. *Desalination* **77**, 101-133, doi:http://dx.doi.org/10.1016/0011-9164(90)85023-4 (1990).

21 Ko, M. K. & Pellegrino, J. J. Determination of osmotic pressure and fouling resistance and their effects of performance of ultrafiltration membranes. *Journal of Membrane Science* **74**, 141-157, doi:http://dx.doi.org/10.1016/0376-7388(92)87079-D (1992).

22 Chang, Y. *et al.* Surface grafting control of PEGylated poly(vinylidene fluoride) antifouling membrane via surface-initiated radical graft copolymerization. *Journal of Membrane Science* **345**, 160-169, doi:http://dx.doi.org/10.1016/j.memsci.2009.08.039 (2009).

23 Celik, E., Liu, L. & Choi, H. Protein fouling behavior of carbon nanotube/polyethersulfone composite membranes during water filtration. *Water Research* **45**, 5287-5294, doi:http://dx.doi.org/10.1016/j.watres.2011.07.036.

24 Ko, M. K., Pellegrino, J. J., Nassimbene, R. & Marko, P. Characterization of the adsorption-fouling layer using globular proteins on ultrafiltration membranes. *Journal of Membrane Science* **76**, 101-120, doi:http://dx.doi.org/10.1016/0376-7388(93)85210-N (1993).

25 Burns, D. B. & Zydney, A. L. Effect of solution pH on protein transport through ultrafiltration membranes. *Biotechnology and Bioengineering* **64**, 27-37, doi:10.1002/(sici)1097-0290(19990705)64:1<27::aid-bit3>3.0.co;2-e (1999).

26 Mockel, D., Staude, E. & Guiver, M. D. Static protein adsorption, ultrafiltration behavior and cleanability of hydrophilized polysulfone membranes. *Journal of Membrane Science* **158**, 63-75, doi:http://dx.doi.org/10.1016/S0376-7388(99)00028-9 (1999).

27 Ariza, M. J. & Benavente, J. Streaming potential along the surface of polysulfone membranes: a comparative study between two different experimental systems and determination of electrokinetic and adsorption parameters. *Journal of Membrane Science* **190**, 119-132, doi:http://dx.doi.org/10.1016/S0376-7388(01)00430-6 (2001).

28 Brown, L., Narsimhan, G. & Wankat, P. C. Foam fractionation of globular proteins. *Biotechnology and Bioengineering* **36**, 947-959, doi:10.1002/bit.260360910 (1990).

29 Wallevik, K. Spontaneous in vivo isomerization of bovine serum albumin as a determinant of its normal catabolism. *The Journal of Clinical Investigation* **57**, 398-407, doi:10.1172/jci108291 (1976).

30 Aimar, P., baklouti, S. & sanchez, V. Membrane-solute interactions: influence on pure solvent transfer during ultrafiltration. *Journal of Membrane Science* **29**, 207-224, doi:http://dx.doi.org/10.1016/S0376-7388(00)82470-9 (1986).

31 Suki, A., Fane, A. G. & Fell, C. J. D. Flux decline in protein ultrafiltration. *Journal of Membrane Science* **21**, 269-283, doi:http://dx.doi.org/10.1016/S0376-7388(00)80218-5 (1984).

32 Swaminathan, T., Chaudhuri, M. & Sirkar, K. K. Effect of pH on solvent flux during stirred ultrafiltration of proteins. *Biotechnology and Bioengineering* **23**, 1873-1880, doi:10.1002/bit.260230813 (1981).

33 Bloomfield, V. The Structure of Bovine Serum Albumin at Low pH*. *Biochemistry* **5**, 684-689, doi:10.1021/bi00866a039 (1966).

34 Ang, W. S. & Elimelech, M. Protein (BSA) fouling of reverse osmosis membranes: Implications for wastewater reclamation. *Journal of Membrane Science* **296**, 83-92, doi:http://dx.doi.org/10.1016/j.memsci.2007.03.018 (2007).

35 Jones, K. L. & O'Melia, C. R. Ultrafiltration of protein and humic substances: effect of solution chemistry on fouling and flux decline. *Journal of Membrane Science* **193**, 163-173, doi:http://dx.doi.org/10.1016/S0376-7388(01)00492-6 (2001).

36 Zhang, Z., Dalgleish, D. G. & Goff, H. D. Effect of pH and ionic strength on competitive protein adsorption to air/water interfaces in aqueous foams made with mixed milk proteins. *Colloids and Surfaces B: Biointerfaces* **34**, 113-121, doi:http://dx.doi.org/10.1016/j.colsurfb.2003.11.009 (2004).

37 Santos, O., Nylander, T., Paulsson, M. & Tragardth, C. Whey protein adsorption onto steel surface - effect of temperature, flow rate, residence time and aggregation. *Journal of Food Engineering* **74**, 468-483, doi:http://dx.doi.org/10.1016/j.jfoodeng.2005.03.037 (2006).

38 Lee, Y. K., Won, Y. J., Yoo, J. H., Ahn, K. H. & Lee, C. H. Flow analysis and fouling on the patterned membrane surface. *Journal of Membrane Science* **427**, 320-325, doi:http://dx.doi.org/10.1016/j.memsci.2012.10.010.

39 Stroock, A. D. *et al.* Chaotic Mixer for Microchannels. *Science* **295**, 647-651, doi:10.1126/science.1066238 (2002).

40 Stroock, A. D. & Whitesides, G. M. Controlling Flows in Microchannels with Patterned Surface Charge and Topography. *Accounts of Chemical Research* **36**, 597-604, doi:10.1021/ar0202870 (2003).

41 Mc Donogh, R. M., Bauser, H., Stroh, N. & Grauschopf, U. Experimental in situ measurement of concentration polarisation during ultra- and micro-filtration of bovine serum albumin and Dextran Blue solutions. *Journal of Membrane Science* **104**, 51-63, doi:http://dx.doi.org/10.1016/0376-7388(95)00011-Z (1995).

CHAPTER V

SURFACE PATTERNED THIN FILM COMPOSTIE MEMBRANE

5.1 Introduction

TFC membranes have experienced remarkable development since the concept of interfacial polymerization (IP) was introduced [1]. Cadotte and co-workers developed the first TFC membrane that has since become the most widely used membrane for a multitude of reverse osmosis (RO) and nanofiltration (NF) applications [2]. Today, 80% of the total desalination installations in the world are depends upon thin film composite (TFC) membranes [3, 4]. TFC membranes have become the industry standard over the last several decades because of continuing research and development efforts that improved their selectivity and permeability together with excellent mechanical strength and fouling resistance by modifying both the barrier layer and the porous support [2, 5-7].

Among different types of TFC membranes, the use of a crosslinked aromatic polyamide thin film as a barrier layer is the most widely used in RO and NF processes [8-11]. A typical TFC polyamide membrane utilize an ultrathin (~200 nm) polyamide barrier layer (PBL), which provides the permeability and selectivity (i.e., permselectivity) of the membrane. This PBL on TFC membranes is typically formed over the porous supports via in- situ IP of a poly-functional amine and an acid chloride at the organic solvent/water interface [12-16]. For the fabrication of TFC, often

ultrafiltration membranes based on polysulfone (PS), polyethersulfone (PES) and polyvinylidene fluoride (PVDF) are used as the porous support because of its toughness and manufacturing compatibility (Fig. 5.1) [17-19].

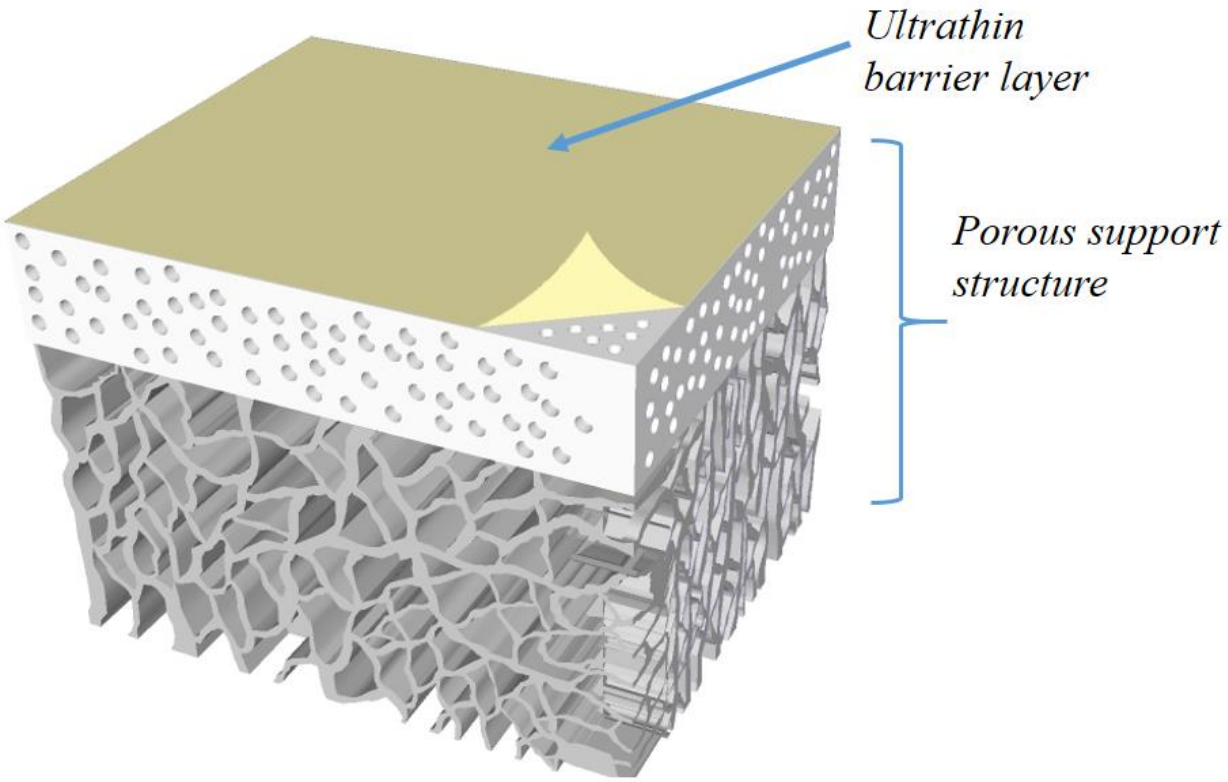

Figure 5.1: Schematic illustration of a TFC membrane highlighting the different layers of the composite film; (Top) typical chemical structure of the cross-linked aromatic polyamide barrier layer.

Like other liquid-filtration membranes, TFC membranes are subject to fouling and concentration polarization, which reduce the performances of the membrane during filtration [20, 21]. To address this fouling issue, much research continues to be carried out over decades. Among these research various chemical treatments, adsorption of surfactants, low-temperature plasma treatments, irradiation methods

and addition of hydrophilic particles on the membrane surface have attracted lot of interest [12, 22-24]. Nonetheless, broader and large scale usage of these mitigation techniques are limited because of the doubt over their durability and scalability.

In the previous Chapters, the use of nanoimprint lithography (NIL) to impart sub-micron surface patterns directly onto a commercial PES ultrafiltration (UF) membrane without sacrificing its permselectivity have been demonstrated. The presence of these patterns significantly reduced deposition of both colloidal particles and protein during filtration. Now, inspired from the previous conclusions, it is a logical judgment to also investigate the possibility of fabrication of surface patterned TFC membrane and probe their capability for fouling mitigation. However, the use of controlled surface topography to mitigate fouling or concentration polarization in TFC membranes has been scarce mainly due to the lack of methods to create targeted surface topography on the membrane surface. The nature of the IP process, i.e. fast reaction at the organic/water interface, presents a major obstacle for tailoring the structures and properties of the polyamide barrier layers [25, 26].

So far very few reports have featured surface topography/roughness on TFC membrane surface and their effect on fouling mitigation. Elimelech et al. suggested that surface roughness leads to higher fouling rate by comparing rougher TFC polyamide membrane to relatively smooth cellulose acetate RO counterparts [27]. From a modeling analysis Ramon et al. concluded that surface roughness for TFC can amplify or dampens adsorption or scaling initiation sites [28].

In this Chapter, the first time fabrication of a functional TFC membrane with well-controlled surface patterns are reported. The two-step fabrication process consisted of forming a dense polyamide barrier layer via IP atop a nanoimprinted UF support membrane. Systematic characterization of the patterned TFC membrane was carried out, and the results show that this approach can indeed create reliable TFC membranes with separation performance comparable with current commercial TFC RO/NF membranes. The comparison between the patterned and un-patterned TFC membrane indicates that surface patterns can be an effective approach to mitigate concentration polarization, scaling and protein fouling.

This Chapter also report filtration results from a collaborative work led by Melissa Rickman using the same patterned TFC membrane. In that study, filtration tests were performed in a cross-flow filtration cell, allowing for better characterization of the boundary layer compared to the stirred cell used previously. The glycerol/NaCl/water fractionation properties are evaluated using the solution-diffusion model, and the fouling properties are evaluated based on permeance decline, permeance recovery, and post-mortem characterization.

5.2 Methods and Materials

Patterned thin film composite (TFC) membranes were fabricated via a two-step process that consisted of (1) nanoimprinting the PES support, and (2) forming a thin dense film atop the PES support via interfacial polymerization (IP). The PES UF membrane after the imprinting process described in the last session were cleaned

with and stored in de-ionized (DI) water in the dark until forming the polyamide layer. Un-patterned TFC membranes that served as a reference were fabricated using the same IP process on the PES UF membranes.

Figure 5.2 describes the two step process used to fabricate pattern TFC membrane. Both patterned and un-patterned UF membranes were taped to a glass plate with the skin layer facing upwards, and placed in an aqueous amine monomer solution as shown in Fig. 5.2.

The aqueous amine solution was prepared by adding 2 g of triethylamine (TEA, 99.5 %, Sigma Aldrich), and 4 g of (+) 10-camphor sulfonic acid (CSA, 99.0 %, Sigma Aldrich), to ~ 80 mL of DI water under vigorous stirring. CSA improves the absorption of the amine solution in the support membrane, while TEA accelerates the MPD-TMC reaction [7]. After complete dissolution of the TEA–CSA mixture, DI water was added to reach a total solution of 100 mL. Next, 2 g of 1, 3-phenylenediamine (MPD, Sigma Aldrich) was added to the TEA–CSA solution. The entire UF membrane was then immersed in the aqueous MPD–TEA–CSA solution for 8 s, and the excess solution on the membrane surfaces was removed with an air blower. Subsequently, the amine-soaked UF membrane was immersed in a hexane solution (Fisher scientific) containing 0.1 % (w/v) trimesoyl chloride (TMC, 99 %, Sigma-Aldrich) for 8 s. The resulting membrane was withdrawn from the hexane solution, cured at 70°C for 10 min, and washed thoroughly with DI water. Here, the protocols for the polyamide thin film formation were based on the formulation used by Ghosh et al. with the exception of a much shorter IP exposure time [7, 8]. Finally,

the as-prepared TFC membranes, with or without surface patterns, were stored in DI water at 5 °C in the dark.

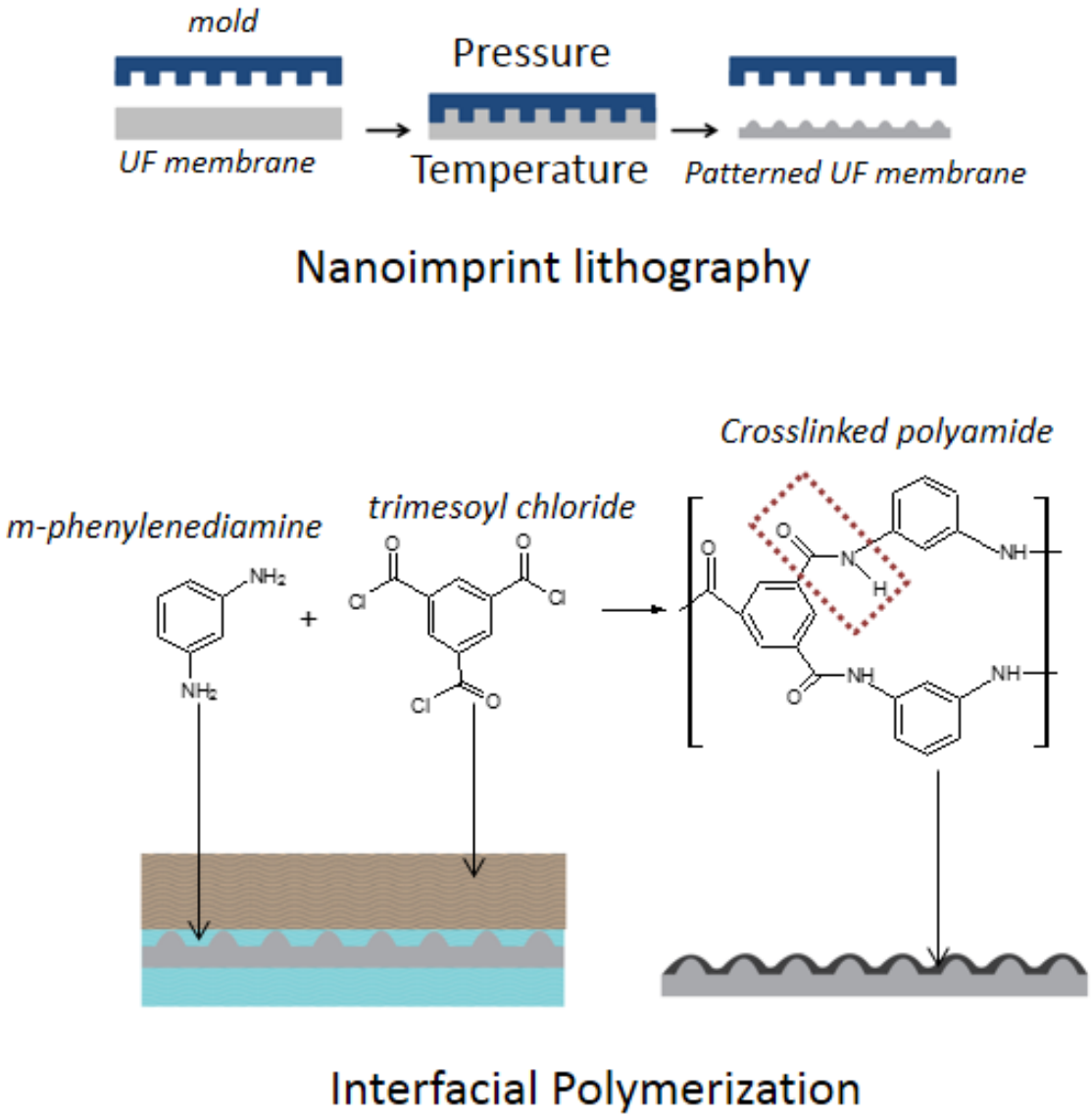

Figure 5.2: A schematic representation of the two step process used to fabricate the patterned TFC membranes. After NIL step, the monomers m-phenylenediamine and trimesoyl chloride react to form a highly cross-linked polyamide layer atop the patterned PES UF membrane used as a support.

All of the filtration experiments with the TFC membranes were conducted in a Sterlitech HP4750 high-pressure stainless steel stirred cell (Sterlitech, WA) (Fig 2.4) using a constant-pressure, stirred/unstirred, dead-end (normal flow) filtration configuration. The cell has an inner diameter of 3.2 cm and an effective membrane area of 8.48 cm^2, and uses high-pressure nitrogen to supply the required pressure. The permeation mass flow-rate was obtained by weighing samples over timed intervals using an automated electronic balance (PI-225DA, Denver Instrument). All of the filtration experiments were carried out at room temperature (~ 25 °C).

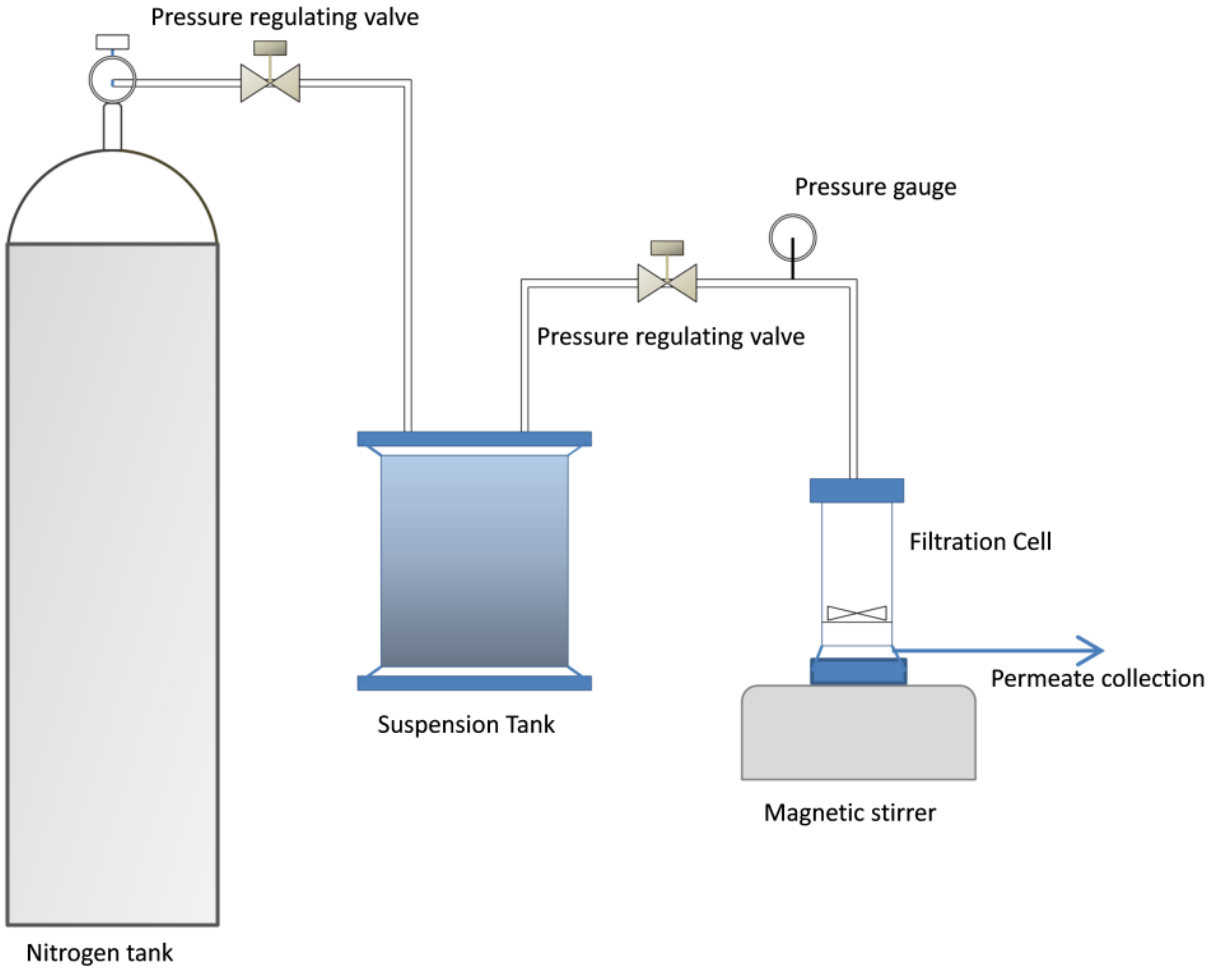

Figure 5.3: Schematic of the dead-end filtration set up.

The entire experimental protocol utilized the following steps. For a given membrane, DI water filtration was carried out at three operating pressures, 1.38, 2.07 and 2.76 MPa, for 2 h, following a 2.5 to 3 h membrane compaction at each pressure. Permeate flux approached steady state after the compaction period, and compaction for the membranes (estimated by the change in membrane resistance relative to the initial, uncompacted state) typically ranged from 28-33 %. After the completion of the pressure stepping, DI water filtration was conducted at 2.76 MPa for 12 h. Subsequently, the pressure was released completely, and the DI water feed was replaced with a 1000 mg/L aqueous NaCl (Mallinckrodt, St. Louis, MO) solution. Filtration of the salt solution was carried out at a pressure of 2.76 MPa over 3 h, and the collected permeate was weighed and the conductivity was measured every 10 min. The conductivity was measured with an Ultrameter 6P (Myron L, Carlsbad, CA), and the concentrations were calculated from the calibration curve prepared for the instrument. For each membrane sample, NaCl filtration was performed twice for both stirred and unstirred conditions. After the NaCl filtration, the pressure was released, and whole filtration system along with the membrane sample was rinsed in DI water, and the NaCl solution was replaced by a 1000 mg/L $CaCl_2$ aqueous solution. Filtration of the $CaCl_2$ solution was carried out using the same protocol as that for the NaCl solution, at both stirred and unstirred conditions.

After the $CaCl_2$ filtration the pressure was again released, and the whole filtration system along with the membrane sample was cleaned using DI water.

Finally, the solution was replaced by a 1000 mg/L CaSO4 (gypsum) solution for a scaling experiment, which was performed using an operating pressure of 2.76 MPa over 24 h under the stirred condition only. After each filtration experiment, the membranes sample was collected and rinsed with DI water to remove loosely attached gypsum crystals from the membrane surface and kept in a refrigerator at 5 °C in a sealed container for SEM inspection. SEM images of the scaled membranes were taken at different and representative regions across the membrane samples. The SEM samples were prepared by drying the scaled membranes at room temperature for 24 h and then resealing them in a petri dish at 5 °C until the SEM imaging. Prior to SEM imaging, both patterned and un-patterned membranes were coated with ~4 nm of gold.

For the cross-flow filtration, each set of membranes was tested in triplicate. Experiments were conducted using a similar type of 3-cell cross-flow filtration module apparatus described in Chapter 2.2.5. Briefly, three membranes, each with a surface area of 9.6 cm^2, are contained in a single membrane module. A pump (Hydra-Cell, D/G-03 Series) is used to pressurize the solution from a single, 4 L feed, and is split into three streams upstream of the module, such that the three replicates are obtained simultaneously from the same feed solution fed in parallel. The imprinted membranes were installed such that the grooves were orthogonal to the cross-flow. Membranes were conditioned with DI water at 25°C and a transmembrane pressure (TMP) of either 1.2 or 2.4 MPa. Cross-flow was provided at a rate of 0.26 m/s (Re ~ 103). Permeance was measured using a balance and timer, and is reported herein as

the permeate flux per unit TMP (L/m^2/h/MPa, or LMH/MPa). Membrane conditioning was continued for up to 13 days, until the pure water permeance (PWP) decreased less than 3% over the previous 24 h period. Next, the feed was replaced with a solution of 0.14 M NaCl and 0.014 M glycerol in water, and the pressure was again increased to its initial value. The solution permeance was measured for 5 h to ensure its stability, and then samples were taken from the feed and permeate for later analysis. Next, a model protein foulant, BSA, was added to the feed at a concentration of 0.1 g/L, and the solution permeance was measured periodically. Samples were again taken from the feed and permeate after 2 h. The permeance decline during BSA filtration was measured for 2 h for the membranes tested at 1.2 MPa, and for 26 h for the membranes tested at 2.4 MPa. Finally, the pressure regulators were opened; the system was flushed three times with 4 L DI water (12 L total) at the same crossflow velocity as used in the filtration studies; the pressure regulators were reset to the initial pressure; and then the final pure water permeance was measured.

Samples were later analyzed for their glycerol and NaCl concentrations using high-pressure liquid chromatography (HPLC) with refractive index detection (Agilent 1100 Series). 50 µL samples were injected into a hydrogen column (Phenomenex Rezex RHA), which was maintained at 60°C. The mobile phase was degassed DI water with a flow rate of 0.6 mL/min. Concentrations were calculated using calibration curves, ensuring that measurements were taken within the linear response range between concentration and refractive index.

Transport was modeled using the solution-diffusion model [29]. Corrections for the concentration polarization boundary layer were made using a Sherwood correlation for laminar flow in a horizontal slit [30], consistent with the geometry of our membrane module [31]. The primary transport metric used herein is the separation factor, $\alpha_{i/j}$, and is calculated as the ratio between solution-diffusion permeance coefficients, P, for penetrants i and j, i.e., $\alpha_{i/j} = P_i/P_j$. The penetrants include water (w), NaCl (electrolyte, e), and the glycerol (reduced carbon, r). If $\alpha_{i/j} < 1$, then penetrant i is less permeable than penetrant j, given the same activity driving force; if $\alpha_{i/j} > 1$, then the converse is true. The filtration protocol is summarized in table 5.1.

Table 5.1: Summary of filtration protocol that was performed for three patterned and three un-patterned TFC membranes at 1.2 and 2.4 MPa.

Feed composition	**Transport metrics**
DI water	initial PWP until compaction criterion met (<3% change per day)
0.14 M NaCl, 0.014 M glycerol, water	solution-diffusion permeance coefficients (P_i), overall solution permeance (LMH/MPa)
1 g/L BSA, 0.14 M NaCl, 0.014 M glycerol, water	solution-diffusion permeance coefficients (P_i), overall solution permeance (LMH/MPa)
DI water	final PWP

After the cross-flow filtration, A post-mortem biochemical assay was used to characterize the protein associated with the membrane after permeation experiments [32]. After removing the membranes from the test cell, the membrane sample was

sectioned into a ~7 cm^2 coupon. Next, the mass of each membrane coupon was measured using a high-resolution microbalance (Model ME235S, Sartorius, Gottingen, Germany). Water-soluble proteins were then eluted from the membrane coupons and their concentration measured using the following procedure: 1) the membrane coupon was aseptically placed in a 50 mL clean plastic test tube; 2) 15 mL of ultrapure sterile water was added, and the resulting solution was sonicated on ice for 1 h; 3) the eluent was analyzed for protein content using a bicinchoninic acid kit and a BSA standard calibrator (Pierce, Rockford, IL); and 4) a spectrophotometer (model DR/2010, Hach, Loveland, CO) was used to measure the sample's absorbance at 562 nm. The lower detection limit of this protein assay under the conditions it was used is 12 µg/cm2. The mass of the membrane coupon was again measured, and the percent increase in mass of the protein-fouled membranes compared to the sonicated membranes was calculated. Finally, the sonication protocol was repeated a second time to determine whether most of the protein on the membrane surface that could easily be removed via sonication was removed during the first iteration of the sonication protocol.

5.3 Results and discussion

5.3.1 Characterization of surface-patterned TFC membranes for dead-end filtration

The FTIR spectra of the surfaces of the imprinted PES UF substrate with (patterned TFC membrane) and without (support only) the IP dense layer are compared in Figure 5.4. Note that, the IR spectrum of an un-patterned TFC

membrane is not included in the figure since it was identical to that of the patterned TFC membrane.

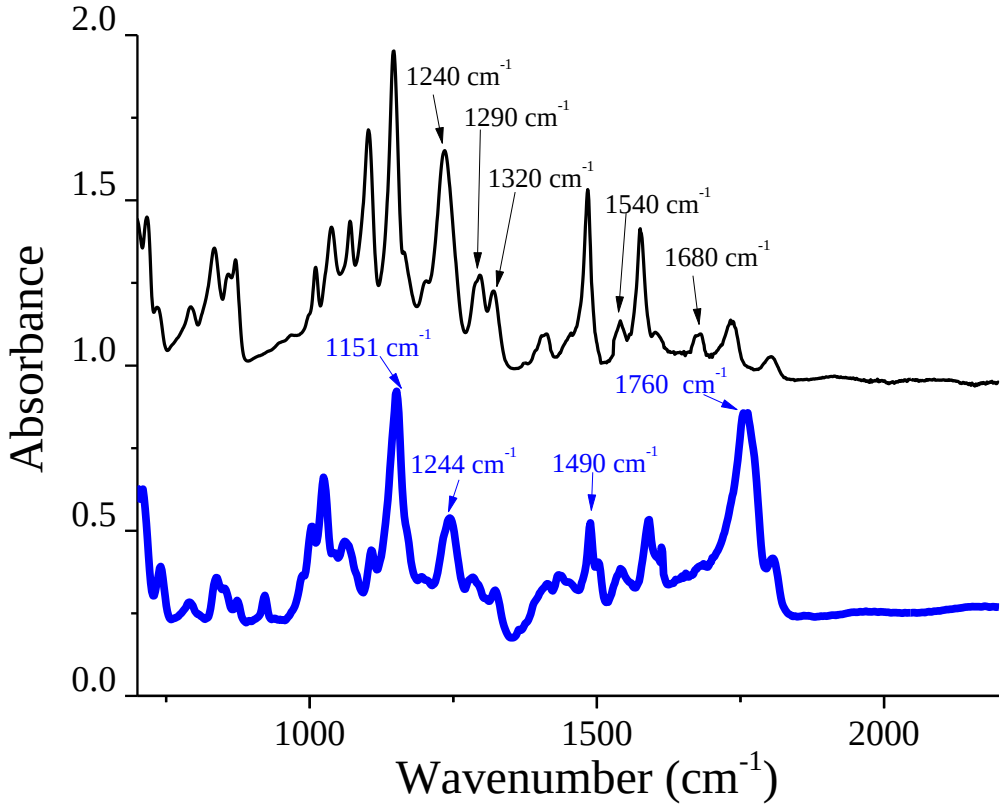

Figure 5.4: Comparison of representative FTIR-ATR spectra for a patterned TFC membrane (thin solid line) and a patterned PES UF support membrane (thick solid line). Representative spectra of un-patterned TFC membranes are identical to that of the patterned TFC membrane in the figure.

For the patterned PES UF membrane, the strong absorption band at 1760 cm^{-1} represents C=O stretching. The sharp absorption peaks at 1151, 1244, and 1490 cm^{-1} were ascribed to the symmetrical stretching vibration of the SO_2 group, C–O–C vibrations, and C–S vibration, respectively [33, 34]. All of these characteristic peaks are consistent with the chemical structure of PES. Because the calculated

penetration depth of the ATR-FTIR spectroscopy was about 1- 5 μm in the wavelength region of interest, the IR spectrum of the TFC membrane surface shown in Fig. 5.4 is necessarily a combination of the polyamide barrier layer and the underlying PES support. The vibrational signatures associated with the polyamide layer include the new peaks around 1240, 1290 and 1320 cm^{-1} corresponding to stretching of aromatic amines I, II and III, respectively, as well as those at ~1540 and 1680 cm^{-1} representing stretching of amides I and II, respectively [34, 35]. These spectra confirm the formation of polyamide barrier layers on both the patterned and un-patterned UF membrane used as a support for the IP process described in section 2.2 (Chapter 2).

Figure 5.5 summarizes the morphological characterization of the patterned and un-patterned PES UF support membrane and the corresponding TFC membranes. A detailed characterization of the imprinted UF membranes was reported in Chapter 2. The un-patterned UF membrane (Fig. 5.5a) has a smooth surface with an RMS roughness of less than 10 nm as determined from the AFM surface profile shown in Fig. 5.5c). After the imprinting process, periodic line-and-space grating patterns (Fig. 5.5d and 5.5e) with an average pattern height ~100-120 nm were present (Fig. 5.5f).

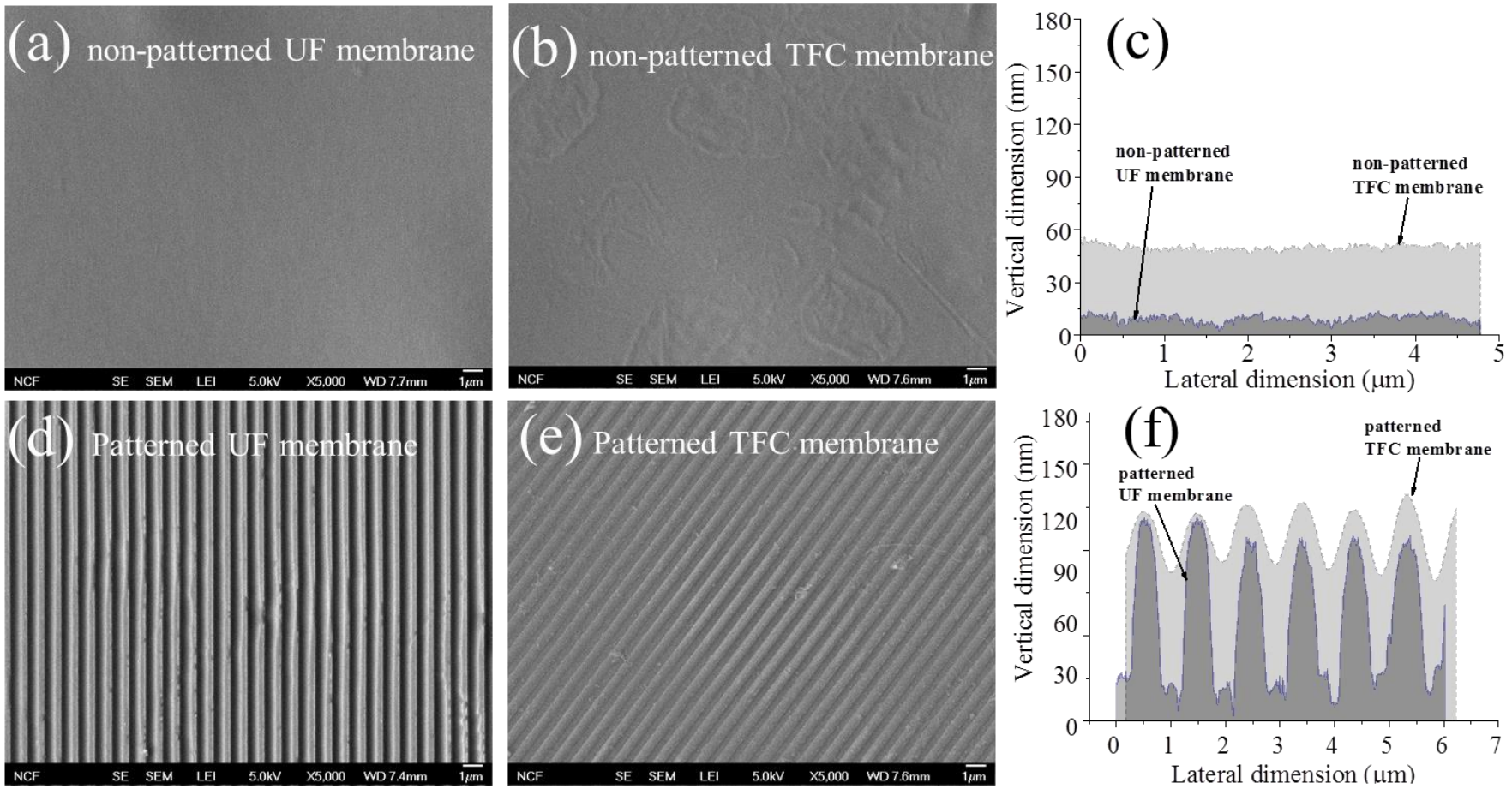

Figure 5.5: Morphological characterization of the patterned and un-patterned TFC membranes and UF support membranes. Representative top-surface SEM images of (a) the un-patterned PES UF support membrane, (b) un-patterned TFC membrane, (d) patterned UF membrane support, and (e) patterned TFC membrane. Images (c) and (f) are representative cross-sectional profiles for un-patterned and patterned TFC membranes obtained from AFM scans. Note that the overlay of the TFC layer on the patterned UF membrane shown in panel (f) is a schematic representation rather than an actual profile, as it is challenging to isolate the barrier layer in this system.

In addition, the imprinting process apparently increases the density of the porous PES support as inferred by a decrease in the MWCO of the membrane from 15.4 to 9.20 kg/mol. However, the DI water flux was quite similar for the un-patterned and patterned UF membranes most likely due to the increased actual (versus projected) surface area after imprinting. An IP process was used to form a polyamide layer on both un-patterned and patterned UF membranes. In Fig. 5.5b the surface of the un-patterned TFC membrane appeared very smooth, which was confirmed from the AFM measurement which showed an RMS roughness of ~ 14 nm (Fig. 5.5c). This surface topography is notably different from the much rougher, "ridge-and-valley" structure of the typical aromatic crosslinked polyamide films described in the literature [36]. However, TFC membranes with relatively smooth crosslinked polyamide barrier layers have also been reported [36, 37]. It has been shown that the ridge-and-valley structure develops from the growth of the stiff aromatic polyamide chains perpendicularly to the organic solvent/water interface, and becomes significant only when the overall barrier layer grows above a certain thickness [38]. Here, the thickness of the polyamide film on the un-patterned TFC membrane was determined as only ~ 40 nm, as determined via an AFM scan on the isolated barrier layer on a Si wafer (Fig. 5.5c) using previously described techniques [39]. This relatively low value of barrier layer thickness might be caused by a combination of air blowing during the soaking of the MPD solution and the short reaction time (8 s) used for the IP process. Indeed, reaction time during IP is a known

factor affecting the thickness of the polyamide layer, and a shorter reaction time would be expected to yield a thinner polyamide film [17, 26].

Fig. 5.5e shows the top surface morphology of the patterned TFC membrane. From AFM measurements (Fig. 5.5f), the patterned surfaces on the ridge and valley were even smoother than that of the un-patterned TFC membrane at the same local length scale. According to Pacecho, et al. [36], a denser porous substrate used for the IP process produces a smoother polyamide layer. As noted previously, the patterned UF membrane was indeed denser than the un-patterned UF membrane, as determined from both cross-sectional SEM and MWCO measurements in Chapter 2. In fact the starting PW UF membrane may be even denser that the UF substrates commonly used in commercial TFC fabrication. Note that the thickness of the barrier layer on the ridge and valley of the pattern are as yet unresolved. Thus, the overlay of the TFC layer on the patterned UF membrane shown in Fig, 5.5f is a schematic representation rather than an actual profile, which is provided only for enhanced perspective of the fabrication process. The isolation of the patterned barrier layer was unsuccessful due to film rupture, most likely at the thinnest region on the ridge of the patterned support. However, it is important to emphasize that TFC membranes with periodic surface patterns on the surface were indeed fabricated successfully, and their filtration characteristics are discussed in the following section.

5.3.2. DI water filtration of un-patterned and patterned TFC membranes

First, the DI water permeate flux of un-patterned and patterned TFC membranes were compared using the dead-end filtration setup (Fig. 5.3). This arrangement was used instead of conventional cross-flow filtration because of the limited size of our current patterned UF membrane supports. As shown in Fig. 5.6, water flux for both membranes increased linearly with the applied pressure, which is expected for membranes in the absence of fouling. Note that at each pressure membranes were compacted until the flux reached a steady-state value. The flux data reported in Fig. 5.6 are mean values over two hours of filtration at the steady-state condition. At higher pressure, slight deviation from the linear flux-pressure relationship was observed for both membranes, which is attributed to increased membrane compaction under higher pressure [40]. Overall, the water permeate flux for the patterned and un-patterned TFC membranes was similar, with a slightly higher flux observed for patterned membranes at higher pressures. The patterned TFC membrane may be somewhat more compaction-resistant, particularly in the relatively high pressure region, possibly because of the densification of the UF membrane support during the NIL process. The details of the evolution of compaction of patterned UF membrane are described in Chapter 2 of this dissertation. It was fouled that UF membrane become more compaction resistance upon imprinting.

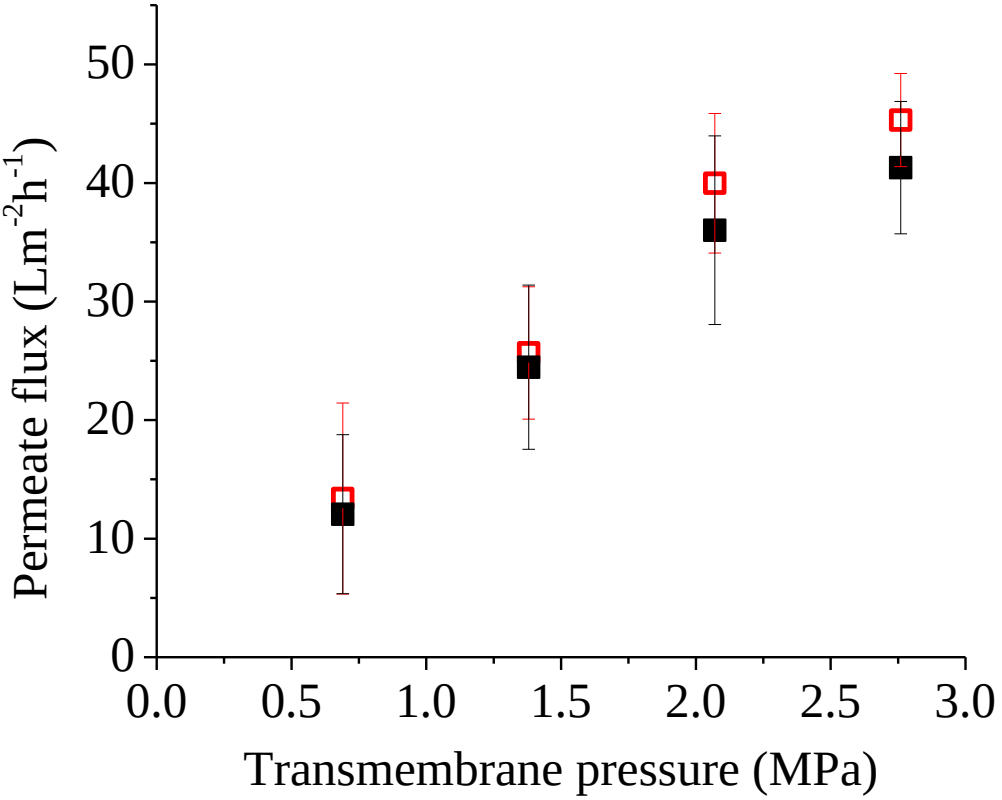

Figure 5.6: DI water permeate flux as a function of TMP for the un-patterned (solid symbols) and patterned TFC membranes (empty symbols).

Subsequently, the permeate flux of the un-patterned and patterned membranes were determined at 2.75 MPa over 8 h of filtration and compared with that of several commercial RO and NF membranes using the same filtration conditions. The permeate fluxes after compaction are summarized in Fig. 5.7. Each points represents average value of three replicate measurement.

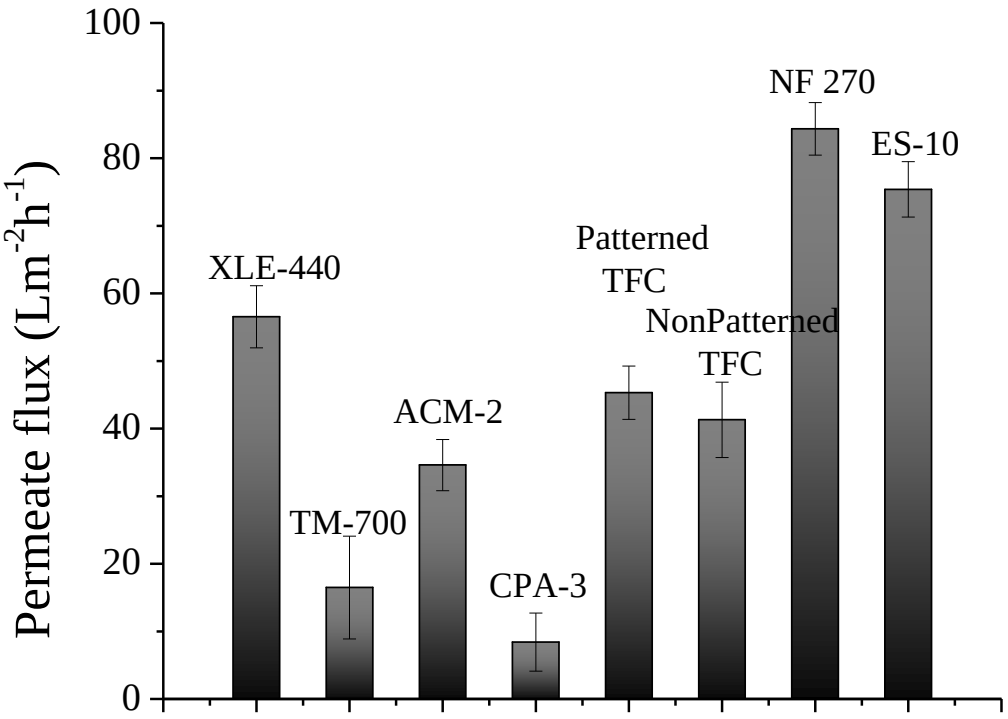

Figure 5.7: Comparison of DI water permeate flux values of the un-patterned and patterned TFC membranes with those of several commercial NF and RO membranes.

The four commercial TFC RO membranes, XLE-440 (DOW Filmtec), CPA 3 (Hydranautics), ACM 2 (Trisep), and TM-700 (Toray), share the same tri-layer configuration as the TFC membranes fabricated in this study. Although the exact chemistry of the polyamide layer likely differs for the different commercial membranes, they are all based on the MPD-TMC IP process (Fig. 5.2) [41]. The two NF membranes, NF 270 (Hydranautics) and ES-10 (Nitto Denko), also have similar aromatic polyamide structures, but typically have much higher water permeate flux

and lower ion rejection (particularly for monovalent ions) than the RO membranes [42]. TFC RO membranes are used primarily for water desalination, while NF membranes are used for the removal of mineral scale, biological matter, colloidal particles and insoluble organic constituents from water feedstreams [43].

As shown in Fig. 5.7, both patterned and un-patterned TFC membranes showed higher PWP flux as compared to most of the RO membranes (except XLE-440) and lower flux than the two NF membranes. Since the water permeate flux of a TFC membrane depends on the properties of the barrier layer (chemistry, crosslinking density, thickness, roughness) as well as those of the substrate [4, 17, 44], further interpretation of the differences in Fig. 5.7 is beyond the scope of this study. However, the data represented in Fig. 5.7 confirm that the IP procedure that was employed for the un-patterned and patterned UF substrates achieved water permeate flux values that compare favorably with those of typical RO and NF membranes that use similar barrier layer chemistry.

5.3.3 NaCl and $CaCl_2$ Filtration of un-patterned and patterned TFC membrane

Figure 5.8 presents the permeation results for both patterned and un-patterned TFC membranes during filtration over 3 h of the NaCl solution. Initial observed salt rejection for all of the samples was ~ 91 % with relatively variability (Fig. 5.8b). Initial permeate was collected after 25 min of filtration to allow the system to stabilize.

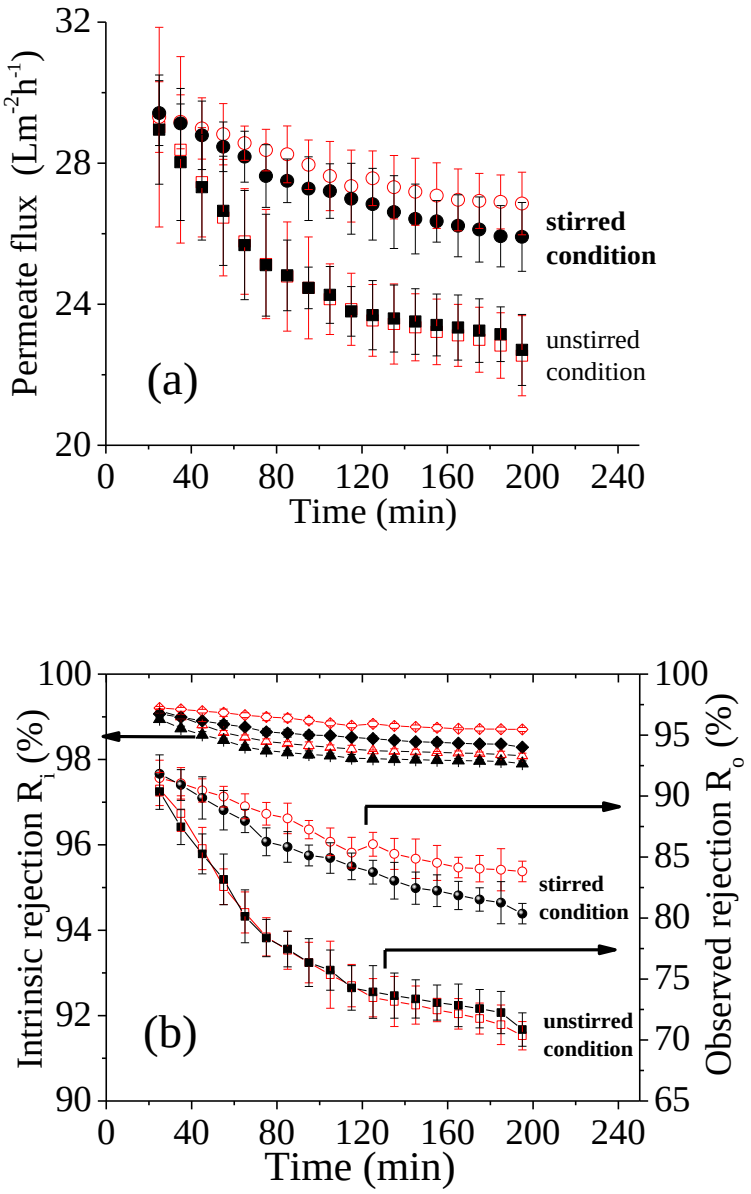

Figure 5.8: Filtration results for the un-patterned and patterned TFC membranes with an aqueous 1 g/L NaCl solution (pH = 7.1, TMP = 2.75 MPa and T = 25 ± 0.5 °C). (a) Permeate flux and b) rejection. In (b) the intrinsic rejection is presented for un-patterned (filled symbols) and patterned (open symbols) membranes at unstirred (triangle) and stirred (diamond) conditions; the observed rejection is shown for the on-patterned (filled symbols) and patterned (open symbols) TFC membranes at the unstirred (squares) and stirred (circles) condition.

The observed salt rejection, R_o, was calculated from the bulk concentration of salt in the permeate (C_p) and feed (C_f) solutions, according to R_o (%) = (1- C_p/ C_f). In any RO/NF filtration system the observed salt rejection does not represent the true membrane separation capability due to concentration polarization. Intrinsic salt rejection, R_i = (1- C_p/ C_m), based on the boundary layer solute concentration (C_m) is normally higher than R_o because C_m is higher than C_f [45-47]. C_m can be determined from a mass balance over the boundary layer (described in Chapter 1) according to

$$j_{i,v} = \frac{D_i}{\delta_i} \ln \left[\frac{(c_{i,m} - c_{i,p})}{(c_{i,b} - c_{i,p})} \right] = k_i \ln \left[\frac{(c_{i,m} - c_{i,p})}{(c_{i,b} - c_{i,p})} \right] \quad (1)$$

where $j_{i,v}$ is the total volumetric flux, D_i is the diffusivity of solute i in water, δi is the thickness of the boundary layer, $c_{i,m}$ is the concentration in solution at the feed-membrane interface, $c_{i,p}$ is the permeate concentration, $c_{i,b}$ is the bulk concentration, and k_i is the mass-transfer coefficient [48]. The mass-transfer coefficient was estimated using the osmotic pressure model described by Sutzkover et al. [49], which assumes no composition dependence for water permeance through the membrane. Further information regarding calculation of the mass-transfer coefficient and boundary layer concentration is available in the supporting information. Accordingly, the R_i for the membrane samples were in the range of 98-99 % over the period of the filtration time.

Since the UF support membrane had an observed rejection of ~7 % for NaCl with a permeate flux of ~ 621 L·m^{-2}·h^{-1}, the high NaCl rejection (and correspondingly low flux) for both TFC membranes verifies the successful formation of dense and

continuous polyamide barrier layers. In comparison, MPD/TMC-based TFC RO membranes have been reported to have a NaCl rejection between 65-99 % [50-57], while commercial membranes can attain over 99.5 % rejection [58]. The variability in these rejection values is caused by the barrier layer properties, operating conditions, and additional membrane modifications [59, 60]. In addition, polyamide-based TFC NF membranes have a reported NaCl rejection range between 60-80 % [61, 62]. Thus, the TFC membranes prepared for this study had a NaCl selectivity less than that of commercial RO membranes, and higher than typical NF membranes. These values are consistent with the lower DI water flux comparisons presented in Fig. 5.7 such that the patterned and un-patterned TFC membranes, can be regarded as "tight NF" or "loose RO" membranes.

For each membrane, permeate flux (Fig. 5.8a) and observed salt rejection (Fig. 5.8b) gradually decreased with filtration time while the intrinsic salt rejection remained essentially constant. Specifically, the initial flux for each membrane for was ~29 $L \cdot m^{-2} \cdot h^{-1}$. For the unstirred condition the flux decreased over time by ~21% for the un-patterned membrane and ~22% for the patterned one. With stirring, flux reduction was ~12% and ~8% for the un-patterned and patterned membrane, respectively. Similar to the permeate flux, the observed salt rejection decreased ~22% for both un-patterned and patterned membranes in the unstirred unstirred condition, and for the stirred condition ~13% and ~9 % for the un-patterned and patterned membranes, respectively. These time-dependent reductions in permeate flux and

observed solute rejection are due to both the increased feed salinity due to water removal, and the concentration polarization at the membrane-solution interface [46].

The practical water (A) and salt permeances (B) [65] for the salt filtration were calculated using the relationships $A = J_w/(\Delta P - \Delta\pi)$ and $B = C_p J_w/(C_m - C_p)$. Results, which are detailed in the supporting information, indicated that the water permeance decreased significantly while the salt permeance remained relatively constant over the filtration period. Concentration buildup at the membrane barrier layer increases the osmotic pressure, which in turn decreases the water permeance by reducing the effective TMP [49]. For unstirred filtration conditions concentration polarization is more severe because the boundary layer, over which diffusion returns the solute to the bulk solution, is larger [64, 65]. Back diffusion is enhanced by advection due to stirring (the boundary layer moves closer to the membrane surface), which leads to less concentration polarization. This explanation is consistent with the effects shown in Fig. 5.8.

Although the flux and salt rejections appear quite similar for the un-patterned and patterned TFC membranes for the unstirred condition, there are small but important differences when stirring was applied. Here, the flux and salt rejection for the un-patterned membranes evidenced a more pronounced decrease over the 3 h filtration period as compared to their patterned counterparts. This behavior strongly suggests that the presence of the surface patterns on the TFC membrane changes the mass transfer in the vicinity of the membrane surface, i.e., enhances back diffusion to the bulk. The presence of the surface patterns is likely to modify the flow profile

and local streamlines of the feed solution in the proximity of the patterns, producing localized turbulence and/or large shear stresses [66]. Note that the secondary flows depend on the Reynolds number (Re) of the tangential flow over the membrane, and can be much more extensive at higher Re values.

Filtration experiments were also performed with a model divalent salt, $CaCl^2$, using the same protocols. Initial salt rejection for all of the samples was ~97 % with somewhat higher variability than that with NaCl due to the larger size of the cation (Ca^{2+}) [67-69]. Permeate flux for $CaCl^2$ filtration was lower than that for NaCl due to higher osmotic pressure and greater concentration polarization from the interaction between the negatively charged TFC membrane and the divalent Ca^{2+} salt [70, 71]. As was the case for NaCl (Fig. 5.8), both permeate flux (Fig. 5.9a) and observed salt rejections (Fig. 5.9b) for all of the samples decreased from the onset of the experiment while intrinsic salt rejection remained relatively constant. Under unstirred conditions, the flux decreased by ~26% and ~28% for the un-patterned and the patterned TFC membranes, respectively. The salt rejection evidenced similar decreases of ~26% for the un-patterned membranes and ~29% for the patterned membranes. With stirring, the un-patterned and patterned membranes had flux decreases of ~13% and ~9% and salt rejection declines of 13% and ~10%, respectively. Hence, results from filtration of both monovalent and divalent salt solutions are consistent and imply that the better performance of the patterned membranes is due to reduced concentration polarization arising from surface-pattern-induced hydrodynamic effects.

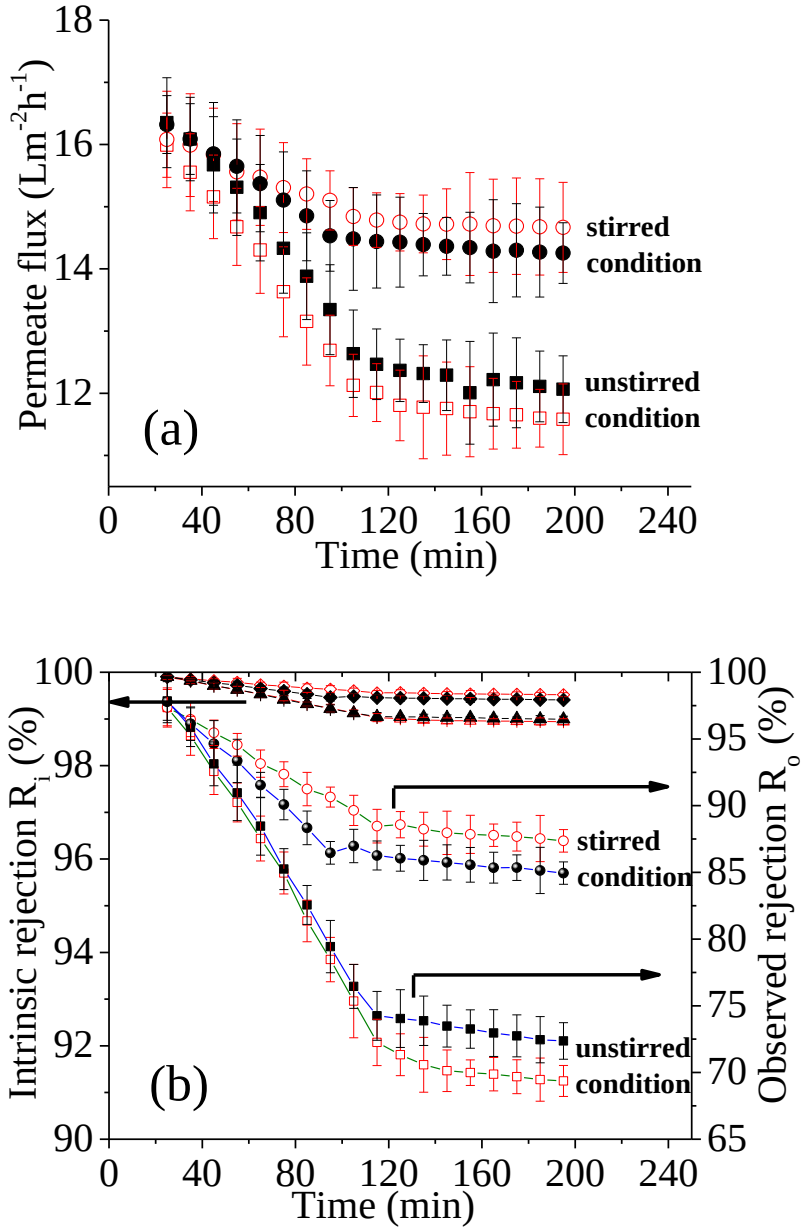

Figure 5.9: Filtration results for the un-patterned and patterned TFC membranes with an aqueous 1 g/L $CaCl_2$ solution (pH = 7.2, TMP = 2.75 MPa and T = 25 ± 0.5 °C). (a) Permeate flux and (b) rejection. In (b) the intrinsic rejection is presented for un-patterned (filled symbols) and patterned (open symbols) membranes at unstirred (triangle) and stirred (diamond) conditions; the observed rejection is shown for the un-patterned (filled symbols) and patterned (open symbols) TFC membranes at the unstirred (squares) and stirred (circles) condition.

Scaling experiments with a 1 g/L $CaSO_4$ (gypsum) solution were performed on both un-patterned and patterned TFC membranes using dead-end filtration system but only with stirring. As shown in Fig. 5.10a, the initial permeate flux of both membranes was ~25 $L \cdot m^{-2} \cdot h^{-1}$, and subsequently decreased in two distinct stages. After 6-7 h of filtration, the flux decreased ~ 9.7% and ~ 6.7% for the un-patterned and patterned TFC membranes, respectively, which is primarily due to the increasing osmotic pressure of the feed and the associated concentration polarization effect as observed in Figs. 5.8 and 5.9. Subsequently, a steeper flux decline was observed for each membrane type whereby after 24 h the initial values of flux had declined by~ 47% and ~ 40% of for the un-patterned and patterned membranes, respectively. The second stage of flux decline is attributed to the scaling of gypsum on the membrane surfaces [72, 73]. From Fig. 5.10a, it appears that the onset of scaling on the patterned TFC membrane (~ 6 h) was somewhat more rapid than for the un-patterned membrane (~ 7.5 h). This induction time indicates the point at which $CaSO_4$ reached its solubility limit in the feed solution such that precipitation on the membrane surface is initiated. Continued precipitation initiates scaling which leads to a marked decline in the permeate flux as less surface area is accessible for the permeate [74, 75]. Because of the higher permeate flux of the patterned membrane during the initial stage, oversaturation of the $CaSO_4$ was likely reached sooner.

5.3.4 Scaling with $CaSO_4$ solutions

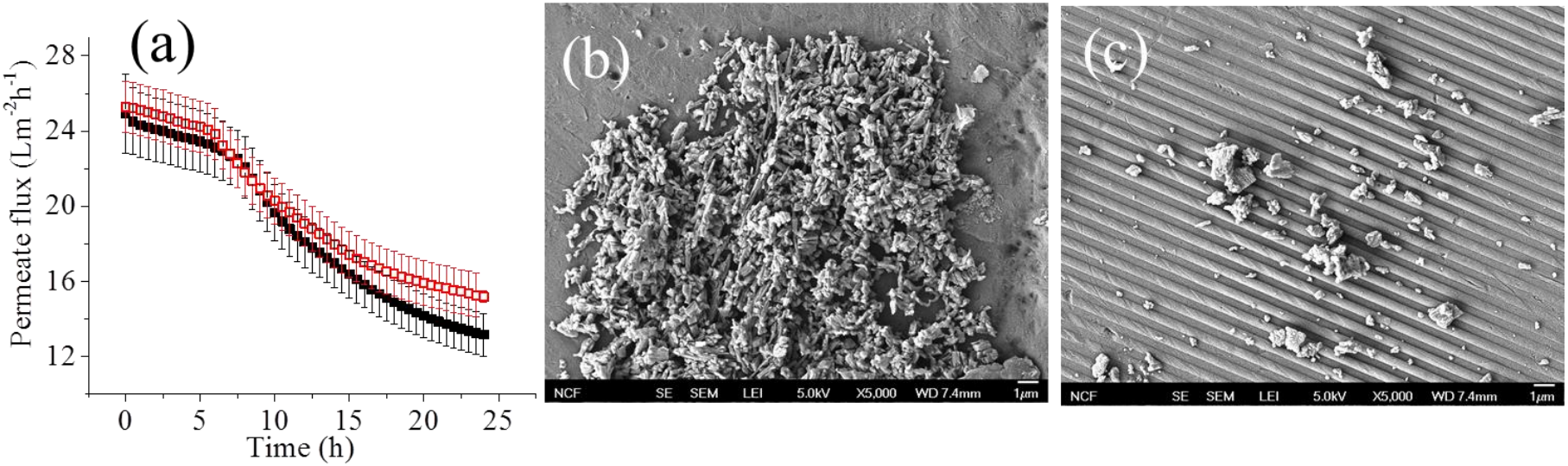

Figure 5.10. (a) Permeate flux as function of filtration time for the stirred condition for un-patterned (solid squares) and patterned (empty squares) TFC membranes in an aqueous 1 g/L $CaSO_4$ solution (pH = 7.4, TMP = 2.75 MPa and T = 25 ± 0.5 °C) . Representative SEM images of the un-patterned (b) and patterned (c) TFC membrane surface after 24 h of $CaSO_4$ filtration.

Fig. 5.10b and 5.10c present representative SEM images of gypsum on the un-patterned and patterned TFC membranes after the 24 h filtration period. Note that crystallization of the $CaSO_4$ during filtration can occur via both homogeneous nucleation in the bulk feed solution and heterogeneous nucleation on the membrane surface. The latter mechanism often produces distinctive plate-like crystal forms [76]. The morphology of the gypsum crystals (Fig. 5.10b and 5.10c) was bulk-like on both membranes with very few needle-like (and no clear plate-like) crystallites in Fig. 5.10b, which suggests that the scaling was dominated by bulk crystallization of the gypsum [77, 78]. Despite the shorter induction time for scaling on the patterned membrane, the flux decline due to scaling is appreciably lower than for the un-patterned membrane (Fig. 5.10a). This might be attributed to the sparser distribution of the gypsum crystals on the patterned membrane surface, presumably due to the aforementioned pattern-induced hydrodynamic effect.

5.3.5 Characterization of surface-patterned TFC membranes for cross-flow filtration

AFM profiles and SEM images of the un-patterned TFC, patterned UF, and patterned TFC surfaces are shown in Fig. 5.11. The un-patterned TFC membranes have random surface roughness on the order of 10 nm. The patterned UF substrate has a regular, patterned surface with ~60 nm groove depth, while the groove depth of the polyamide thin-film, which was fabricated on top of the patterned UF substrate, has a reduced groove depth of ~30 nm. Thus, the interfacial polymerization fills in some of the surface pattern of the UF membrane, but still results in a regularly-

patterned surface with larger protrusions compared to the random roughness on the un-patterned TFC membrane.

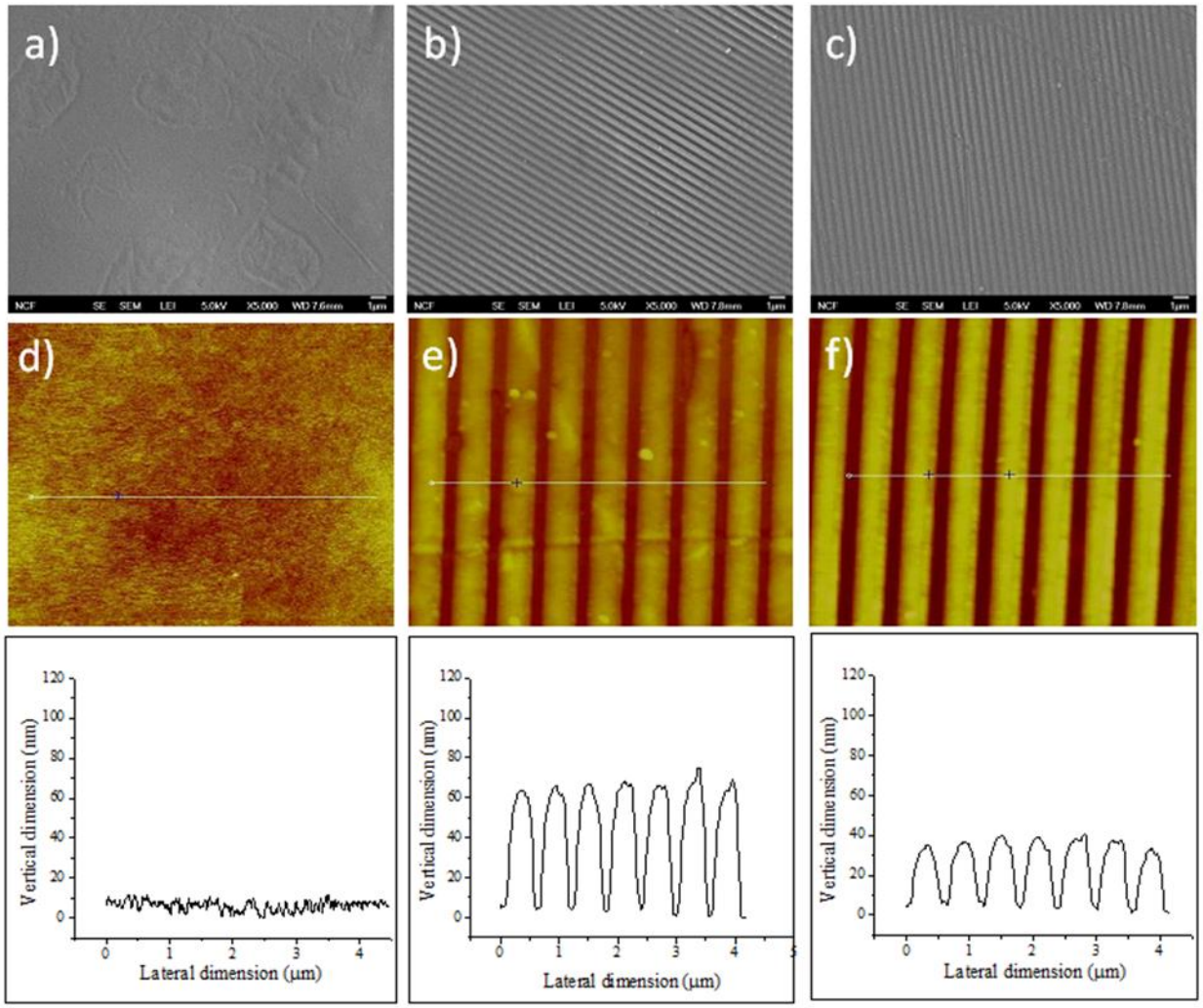

Figure 5.11: Morphological characterization of the un-patterned TFC, patterned UF and Patterned TFC membranes. Representative top-surface SEM images of (a) un-patterned membrane, (b) patterned UF support membrane, (c) patterned TFC membrane. Images (d), (e) and (f) are representative topographic AFM image of un-patterned UF, patterned UF and patterned TFC membranes obtained from AFM scans. The corresponding cross-sectional profiles of both patterned membranes are shown below the AFM images.

5.3.6 Cross-flow filtration of un-patterned and patterned TFC membrane

Prior to filtration experiments, all membranes were first compacted with DI water at a TMP of either 1.2 or 2.4 MPa. Figure 5.12 shows an example of the permeance measured for each of three patterned TFC membrane replicates during the initial conditioning period at 2.4 MPa. During this time, the PWP of all membranes decreases, likely due to the compaction of the UF support membrane (Chapter 3). Note that the variance between replicates is rather large. This finding is not surprising given the non-automated, lab-scale techniques that were employed to fabricate the membranes. Despite their different initial permeances, each membrane displayed similar trends in permeance decline during compaction.

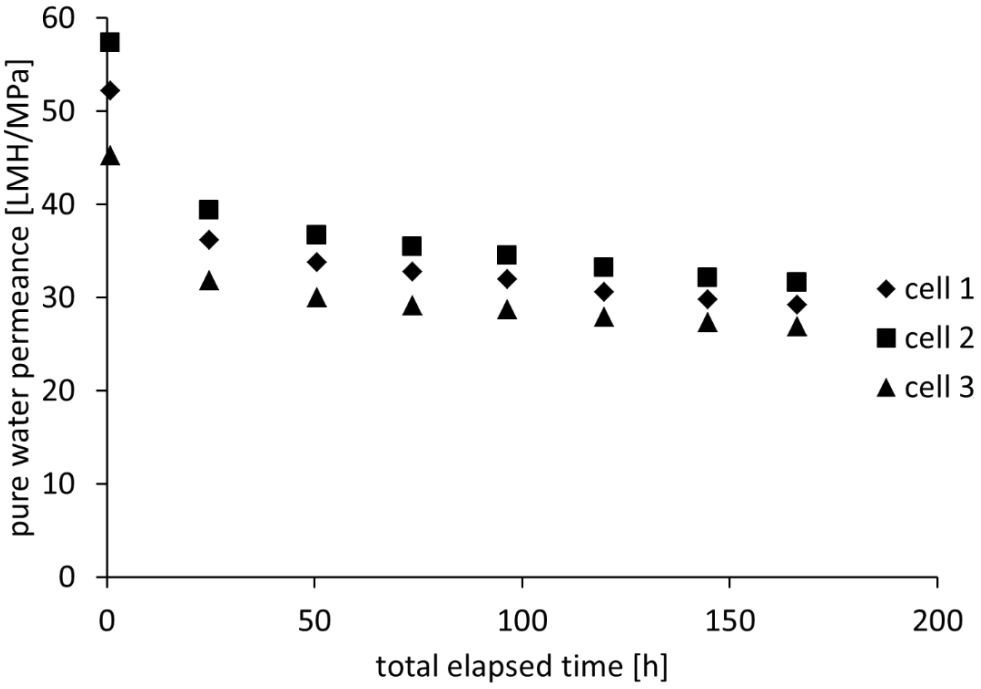

Figure 5.12: Permeance decline during initial conditioning of three patterned TFC membrane replicates at 2.4 MPa.

In an attempt to present the data with minimal clutter, Fig. 5.13 shows the mean values from the triplicate measurements, and 90% confidence intervals are included only for the final marker on each series.

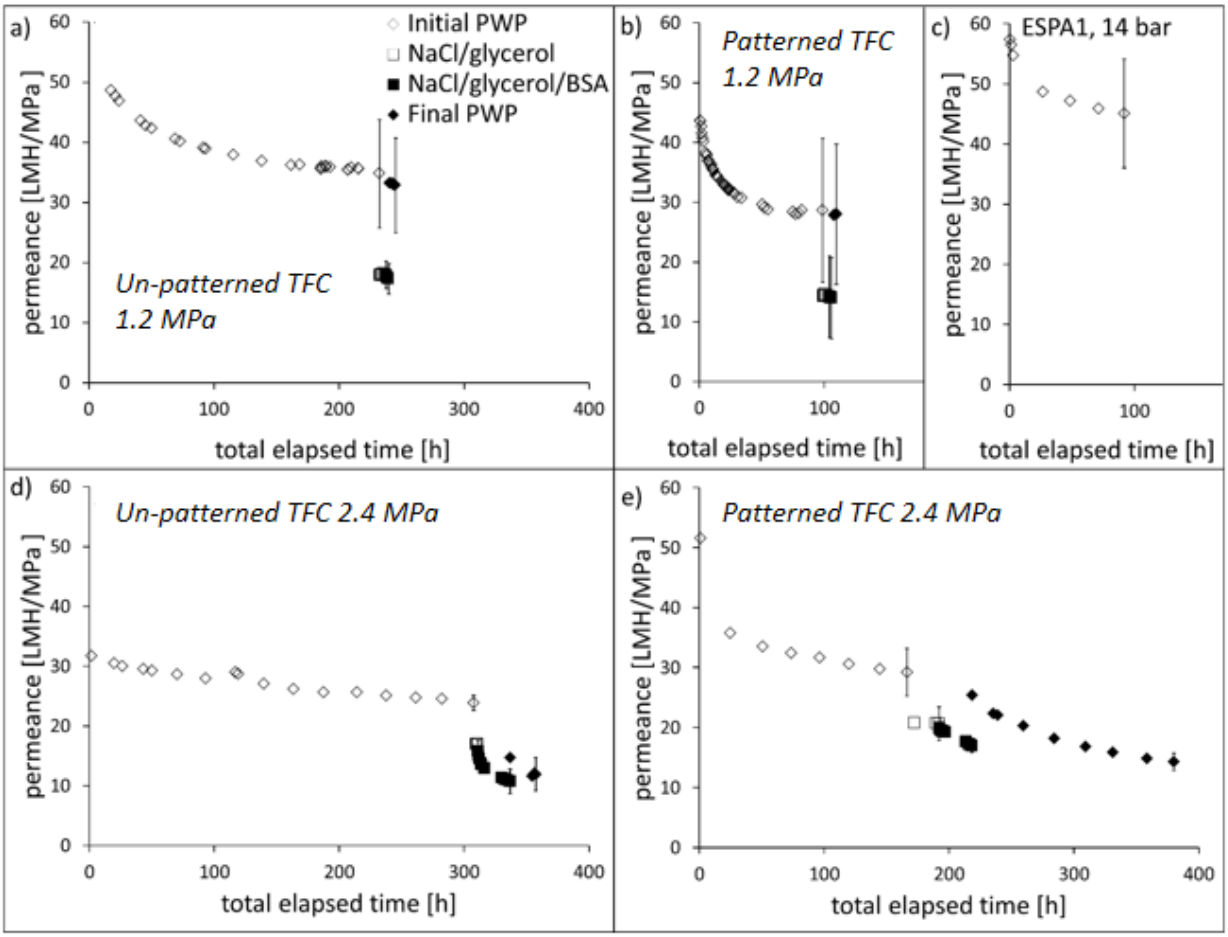

Figure 5.13: Pressure-normalized volumetric flux during un-patterned TFC and patterned TFC experiments at 1.2 and 2.4 MPa. Initial pure water permeance of ESPA1 (a commercial membrane) is also included to compare compaction behavior. Confidence bars are 90% confidence intervals for three membrane replicates. Only confidence intervals for the last marker in each series to reduce clutter was included.

During this time, the PWP of all membranes decreases, likely due to substrate deformation (open diamond markers in Fig. 5.13). Although the patterned TFC membrane permeance at 1.2 MPa stabilizes after ~3 days, the permeance of the

patterned TFC at higher pressure and the un-patterned TFC at both higher and lower pressures continues to decrease monotonically over longer times. This behavior is also consistent with a commercial PA membrane (ESPA1, Hydranautics, Fig. 5.13c). To accommodate the polymer deformation that occurs over long timescales, a criterion was set such that there be less than 3% decrease in PWP over the previous 24 h period for a membrane to be considered "stable." The patterned TFC membrane may stabilize more quickly than the un-patterned TFC membrane at 1.2 MPa because the substrate has essentially been pre-compacted during the nanoimprinting process, which applies a pressure of 4.0 MPa to the mold at elevated temperature (120° C).

In general, increased PWP conditioning time and pressure reduces the variance between replicates (for example, compare the uncertainties in Fig. 5.13a vs 5.13d, and Fig. 5.13b vs 5.13e). This finding can be rationalized by reduced variance in the substrate structure as the pores collapse and the substrate becomes more compact. The un-patterned TFC membranes in Fig. 5.13d are the same as those in Fig. 5.13a. The un-patterned membranes were initially tested at the lower pressure, and since the membrane permeance did not change significantly during the low-pressure experiment, the membranes were used again for the high-pressure filtration experiment. Subsequent conditioning at the higher pressure further reduced the permeance of these un-patterned TFC membranes, indicating that the substrate deforms more when it is supporting a greater mechanical force. Note that the permeance of the un-patterned TFC membranes at 2.4 MPa increased 2-5% at ~115 h. This increase corresponds to a power outage that turned off the pump, and hence

reduced the pressure, and shows that the substrate deformation that occurs during membrane conditioning is at least partially recoverable. In short, these results remind us that the reported PWP for a polymer membrane is highly sensitive to that membrane's history. Moreover, these baseline measurements for the rate of change in membrane permeance are necessary when interpreting subsequent fouling behavior.

After the stabilization of the PWP, the membranes' fractionation properties were measured for solutions containing water, NaCl, and glycerol, with and without BSA. The NaCl and glycerol true rejections (i.e., using the calculated concentration at the liquid side of the feed-membrane interface, rather than the bulk concentration) for each membrane/pressure combination are given in Table 5.2. Due to the high glycerol and NaCl retention, it was assumed that BSA was mostly retained. A one-way analysis of variance (ANOVA) reveals that none of the species' permeance coefficients varies significantly ($p = 0.34$, 0.16, and 0.52 for glycerol, NaCl, and water, respectively) for solutions with BSA versus those without it. Thus it was concluded that, only minimal further mixture non-idealities were introduced by the addition of the BSA.

Table 5.2: NaCl and glycerol rejections for un-patterned and patterned TFC membranes, with and without BSA, at 1.2 and 2.4 MPa. The ± values are 90% confidence intervals for three membrane replicates.

		R_{NaCl} [%]		$R_{glycerol}$ [%]	
		no BSA	+ BSA	no BSA	+ BSA
1.2 MPa	Un-patterned TFC	86 ± 8	87 ± 7	88 ± 4	89 ± 3
	Patterned TFC	90 ± 4	90 ± 4	92 ± 5	94 ± 4
2.4 MPa	Un-patterned TFC	95 ± 2	95 ± 1	95 ± 1	96 ± 2
	Patterned TFC	95 ± 1	96 ± 1	95 ± 2	96 ± 2

Figure 5.14 shows the separation factors between water, glycerol, and NaCl for the patterned and un-patterned TFC membranes, together with other classes of commercial polymeric membranes [14]. Within the uncertainties of our experiments, imprinting the substrate does not substantially change the separation properties of the composite material. The variance within a batch of the un-patterned TFC and patterned TFC membranes is similar to that from a section of a roll of commercially-available FA-PA membrane (ESPA 1). The un-patterned TFC and patterned membranes fall within a similar but distinct region compared to commercial FA-PA membranes that were also tested. Specifically, the water/glycerol separation factors are similar for both sets of membranes, but the membranes that were fabricated are more permeable to NaCl vs glycerol, whereas the converse is true for the commercial membranes. Material variations between TFC, and that formed in commercial membranes, is the likely rationale for this $\alpha_{e/r}$ difference, but further elucidation of the dense layer transport is beyond the scope of the current study. The variance

between batches of the patterned TFC membranes is on the order of the variance within any given batch of membranes.

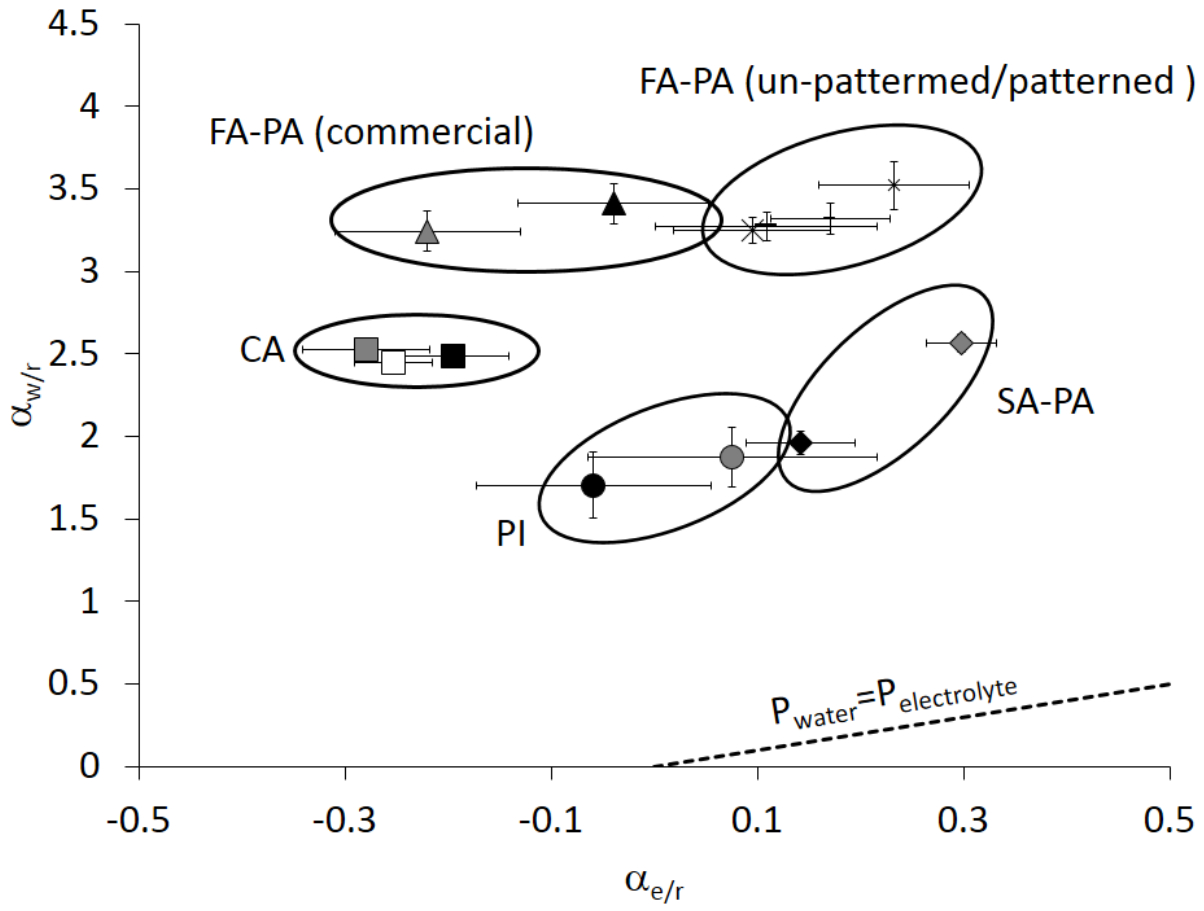

Figure 5.14: Separation factors between water (w), glycerol (r), and NaCl (e) for a variety of polymer material classes. Confidence bars are 90% confidence intervals for three membrane replicates. Adapted from [31]. CA (cellulose acetate), PI (polyimide), SA-PA (semi-aromatic polyamide), FA-PA (fully-aromatic polyamide)

After the permeance was measured for several hours to ensure its stability, a model protein foulant, BSA, was added to the feed, and the permeance continued to be monitored for evidence of possible flux decline. Due to the variance between the permeance of membranes in a single batch, in order to provide more clarity for the

average response the water permeance coefficient after BSA addition is normalized to the water permeance coefficient for the solution, prior to BSA addition. After 2 h, the permeance of all membranes tested at the lower pressure reduces minimally, to 95-97% of its value before BSA addition for the un-patterned TFC membranes, and 97-98% for the patterned TFC membranes (Fig. 5.15).

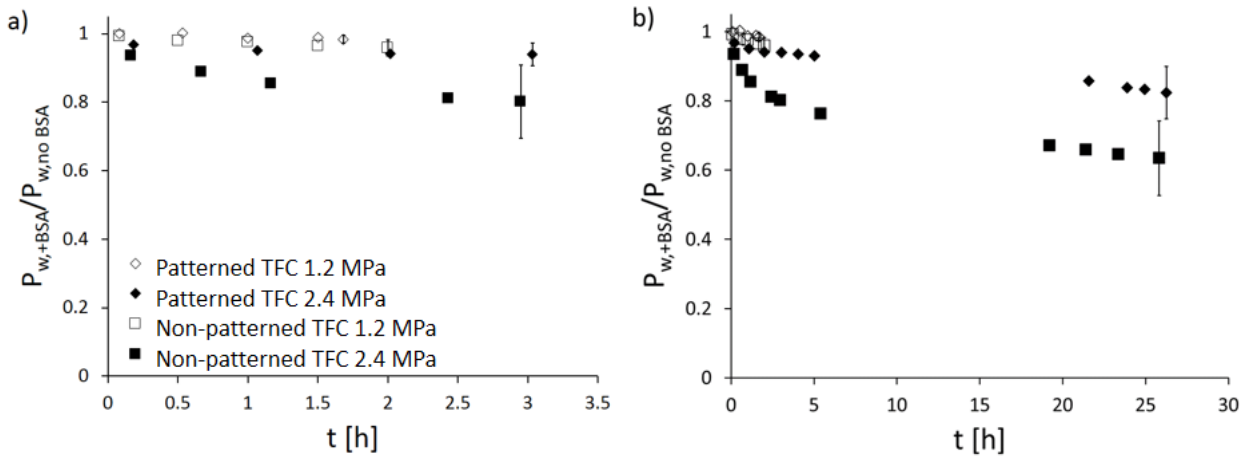

Figure 5.15: Water permeance coefficient during BSA fouling ($P_{w,+BSA}$) normalized to water permeance coefficient prior to BSA addition ($P_{w,no\ BSA}$), as a function of time after BSA addition (t), for patterned and un-patterned TFC membranes at 1.2 and 2.4 MPa (open and filled symbols, respectively). Confidence bars are 90% confidence intervals for three membrane replicates. The LHS plot (a) shows an expanded scale for short times.

This low permeance decline is likely due to operation below the critical flux for BSA. A value of $J_v/k_i < 1$, where J_v is the volumetric flux and k_i is the mass transfer coefficient, indicates the flux is sub-critical. In other words, the rate of mass transfer of the solute back to the bulk is greater than (or equal to) its rate of convection toward the membrane, and deposition on the membrane is not expected

[79]. For the experiments at 1.2 MPa, operation is likely near the critical flux for BSA deposition, such that the slight decrease in water permeance is primarily from BSA adsorption. Note that, osmotic composition effects were already included in the activity coefficients. The slightly greater permeance reduction for the un-patterned TFCmembranes could be due to the higher initial permeance of that batch of membranes, leading to a higher value of J_v/k_i. In other words, any possible effects of the different architectures are convoluted with their different initial permeances.

Table 5.3: Volumetric flux divided by the calculated mass transfer coefficient (J_v/k_i) for NaCl, glycerol, and BSA in un-patterned and patterned TFC membranes at 1.2 and 2.4 Mpa. The ± values are 90% confidence intervals for three membrane replicates.

J_v/k_i		NaCl	glycerol	BSA
1.2 MPa	Un-patterned TFC	0.2 ± 0.0	0.2 ± 0.0	1.3 ± 0.2
	Patterned TFC	0.1 ± 0.1	0.2 ± 0.1	1.1 ± 0.5
2.4 MPa	Un-patterned TFC	0.3 ± 0.0	0.4 ± 0.0	2.4 ± 0.1
	Patterned TFC	0.3 ± 0.0	0.5 ± 0.1	2.9 ± 0.4

At the higher pressure, a greater initial decline in the normalized water permeance is observed for both membranes (Fig. 5.15). However, despite the higher initial permeance of the patterned TFC membranes, and thus higher J_v/k_i, the decrease in permeance is significantly less for the patterned TFC than for the un-patterned membranes (p = 0.018 for a paired two sample t-test). The un-patterned

TFC membranes experience a rapid drop in permeance over the first few hours of operation, which then stabilizes to a more modest rate of permeance decline, similar to that of the patterned membranes. This initial drop in permeance is likely associated with BSA deposition. As BSA is deposited, the permeance decreases until the flux is again sub-critical and adsorption (and possibly compaction of the fouling layer) dominates. The greater permeance decline for the un-patterned membranes suggests that the patterned TFC membranes have improved hydrodynamics at the membrane-liquid interface, providing better disruption of the boundary layer and allowing for a higher critical flux. Permeance decline is still extant for the patterned TFC membranes under these conditions, but there is a significant delay in its onset, such that $P_{w+BSA}/P_{w,no\ BSA}$ = 0.82 was reached in ~2.5 h for the un-patterned TFC membranes versus 26 h for the patterned membranes, despite the higher initial solution permeance for the latter (see Fig. 5.13).

After each permeation experiment with BSA solutions, the system was flushed with DI water (in simple cross-flow with no applied pressure) and then the permeances of pure water were again measured ("Final PWP" in Fig. 5.13). Table summarizes the percentage of the initial PWP that was recovered after filtration, relative to the fouled membrane:

$$\text{permeance recovery} = \frac{\left(PWP_{cleaned} - PWP_{fouled}\right)}{\left(PWP_{initial} - PWP_{fouled}\right)} \times 100\%$$

Table 5.4: Summary of permeance recoveries after BSA filtration and post-mortem characterizations. The ± values are 90% confidence intervals for three membrane replicates. The mass change compares the mass of the fouled membrane to the mass of the same membrane after sonication, and the protein concentration is that measured in the sonication supernatant.

		permeance recovery [%]	mass change [%]	protein concentration [µg/cm^2]
1.2 MPa	Un-patterned TFC	89 ± 2	n/a	n/a
	Patterned TFC	96 ± 1	0.1 ± 0.1	98 ± 2
2.4 MPA	Un-patterned TFC	30 ± 8	0.7 ± 0.6	111 ± 1
	Patterned TFC	69 ± 9	0.3 ± 0.1	104 ± 10

Not surprisingly, the un-patterned and patterned TFC membranes that were operated at the lower pressure, and experienced little permeance decline, recovered much of their initial permeance. The permeance recovery was slightly higher for the patterned TFC membrane, but these membranes were also slightly less permeable than the un-patterned TFC, and so they may have experienced a little less of the already low BSA deposition. The estimated J_v/k_{BSA} of the un-patterned was 1.3 versus 1.1 for the patterned TFC at the 1.2 MPa condition (see Table).

The membranes operated at 2.4 MPa recovered much less of their initial permeance. Nonetheless, the patterned membranes have ~twice the permeance recovery compared to the un-patterned TFC membranes, consistent with their improved permeance during BSA filtration. After continuing the pure water

permeation for 17 h, there is a surprising ~20% and 12% drop in permeance for the un-patterned and patterned TFC membranes, respectively. The PWP of the patterned TFC membranes was continued to measure for 7 days. During this time, the permeance declined rapidly before reaching a more stable value of 4% decrease per day. The drop in permeance takes place at a much faster rate than what was expected if it was simply caused by compaction of the membrane itself, for which the permeance decline criterion of < 3%/day was already set before starting the experimental protocol.

The long-term decline in the permeance of fouled patterned TFC membranes at 2.4 MPa appears to be caused by compaction of the deposited protein layer. The post-mortem protein analysis (Table) confirms that BSA is present on the membranes after the final PWP. This protein was likely adsorbed to the membrane surface such that it was not washed away during the post-filtration flushing or PWP. Note that the protein concentration represents only the protein that was removed by our sonication protocol. After the first sonication, this protocol was repeated, and the amount of protein that could be removed during the second sonication was 16 $\mu g/cm^2$ for each set of membranes. For reference, this value is only slightly higher than the lower detection limit of the bioassay under the conditions used (12 $\mu g/cm^2$). Thus, it appears that most of the protein that could be easily removed using sonication is removed in the first hour of sonication.

Post-mortem analysis in Table 6.4 shows that the membranes with reduced permeance recovery also had more material removed during sonication and a higher

protein concentration in the sonication supernatant, at 85% confidence. In other words, the more "fouled" membranes may also accumulate more material. This protein concentration only represents the adsorbed protein that could not be removed by the shear from crossflow in the membrane module, yet could be removed by our sonication protocol. This analysis provides support for the hypothesis that a compact protein layer is present on the surface of the membrane, and is also consistent with recent work on BSA membrane fouling, in which the authors reported the formation of a compressible protein layer [80]. These results also suggest the protein layer on the patterned TFC membranes has a more open structure, such that it was more easily removed by the simple cross- flow in our protocol. Meanwhile, the protein layer on the un-patterned membrane could have a more compact structure, which requires more vigorous methods (i.e., sonication) for its removal.

5.4 Conclusion

In this study, first time fabrication of a submicron-patterned TFC membrane via interfacial polymerization on a nanoimprinted UF membrane used as a support was demonstrated. Thin crosslinked aromatic polyamide barrier layer films were successfully formed on the patterned membrane, as confirmed by FTIR spectroscopy and electrolyte versus water permselectivity determined from filtration experiments. The patterned TFC membrane exhibited water permeance and salt rejection comparable to that of commercial TFC RO membranes. Compared with their un-patterned counterparts, the patterned TFC membranes demonstrated higher flux

and rejection values when convection was present as a result of stirring. Scaling experiments revealed that gypsum distribution on the surface of the patterned membranes was more widely scattered in comparison to that on the un-patterned membranes. Overall, these results suggest that the surface patterns induced hydrodynamic secondary flows at the membrane-feed interface which were effective in lessening concentration polarization as well as in reducing scaling.

During the cross-flow filtration, below the critical flux, the difference between un-patterned and patterned TFC is not significant. Also, No differences in the glycerol/NaCl/water fractionation properties of the un-patterned and patterned TFC could be distinguished. However, above the critical flux, the patterned membranes have less permeance decline and greater permeance recovery compared to their un-patterned counterparts. Notably, at the higher pressure and at the conditions investigated, the patterned TFC membranes can operate for ten times longer than the un-patterned membranes. Results suggest that, although protein accumulates on both un-patterned and patterned NF membranes, its rate of deposition may be slowed on the patterned TFC membrane due to improved local hydrodynamics caused by the regular surface patterning. These features and the local shear environment may also result in a less dense protein layer, which is easier to remove with the shear provided during cross-flow filtration compared to the protein layer on the un-patterned surface.

References

1 Morgan, P. W. *Condensation polymers: by interfacial and solution methods*. (Interscience Publishers, 1965).

2 Petersen, R. J. Composite reverse osmosis and nanofiltration membranes. *Journal of Membrane Science* **83**, 81-150, doi:http://dx.doi.org/10.1016/0376-7388(93)80014-O (1993).

3 Glater, J., Zachariah, M. R., McCray, S. B. & McCutchan, J. W. Reverse osmosis membrane sensitivity to ozone and halogen disinfectants. *Desalination* **48**, 1-16, doi:http://dx.doi.org/10.1016/0011-9164(83)80001-0 (1983).

4 Greenlee, L. F., Lawler, D. F., Freeman, B. D., Marrot, B. & Moulin, P. Reverse osmosis desalination: Water sources, technology, and today's challenges. *Water Research* **43**, 2317-2348, doi:http://dx.doi.org/10.1016/j.watres.2009.03.010 (2009).

5 Hilal, N., Al-Zoubi, H., Darwish, N. A., Mohamma, A. W. & Abu Arabi, M. A comprehensive review of nanofiltration membranes:Treatment, pretreatment, modelling, and atomic force microscopy. *Desalination* **170**, 281-308, doi:http://dx.doi.org/10.1016/j.desal.2004.01.007 (2004).

6 Lau, W. J., Ismail, A. F., Misdan, N. & Kassim, M. A. A recent progress in thin film composite membrane: A review. *Desalination* **287**, 190-199, doi:http://dx.doi.org/10.1016/j.desal.2011.04.004.

7 Luo, M.-L., Zhao, J.-Q., Tang, W. & Pu, C.-S. Hydrophilic modification of poly(ether sulfone) ultrafiltration membrane surface by self-assembly of TiO2 nanoparticles. *Applied Surface Science* **249**, 76-84, doi:http://dx.doi.org/10.1016/j.apsusc.2004.11.054 (2005).

8 Baker, R. *Membrane Technology and Applications*. (Wiley, 2004).

9 Fritzmann, C., LÃ¶wenberg, J., Wintgens, T. & Melin, T. State-of-the-art of reverse osmosis desalination. *Desalination* **216**, 1-76, doi:http://dx.doi.org/10.1016/j.desal.2006.12.009 (2007).

10 Lee, K. P., Arnot, T. C. & Mattia, D. A review of reverse osmosis membrane materials for desalinationâ€"Development to date and future potential. *Journal of Membrane Science* **370**, 1-22, doi:http://dx.doi.org/10.1016/j.memsci.2010.12.036.

11 Peng, W. & Escobar, I. C. Rejection Efficiency of Water Quality Parameters by Reverse Osmosis and Nanofiltration Membranes. *Environmental Science & Technology* **37**, 4435-4441, doi:10.1021/es034202h (2003).

12 Belfer, S., Purinson, Y., Fainshtein, R., Radchenko, Y. & Kedem, O. Surface modification of commercial composite polyamide reverse osmosis membranes. *Journal*

of Membrane Science **139**, 175-181, doi:http://dx.doi.org/10.1016/S0376-7388(97)00248-2 (1998).

13 Cadotte, J. E., King, R. S., Majerle, R. J. & Petersen, R. J. Interfacial Synthesis in the Preparation of Reverse Osmosis Membranes. *Journal of Macromolecular Science: Part A - Chemistry* **15**, 727-755, doi:10.1080/00222338108056764 (1981).

14 Mukherjee, D., Kulkarni, A. & Gill, W. N. Flux enhancement of reverse osmosis membranes by chemical surface modification. *Journal of Membrane Science* **97**, 231-249, doi:http://dx.doi.org/10.1016/0376-7388(94)00165-U (1994).

15 Roh, I. J., Park, S. Y., Kim, J. J. & Kim, C. K. Effects of the polyamide molecular structure on the performance of reverse osmosis membranes. *Journal of Polymer Science Part B: Polymer Physics* **36**, 1821-1830, doi:10.1002/(sici)1099-0488(199808)36:11<1821::aid-polb3>3.0.co;2-t (1998).

16 Song, Y., Sun, P., Henry, L. L. & Sun, B. Mechanisms of structure and performance controlled thin film composite membrane formation via interfacial polymerization process. *Journal of Membrane Science* **251**, 67-79, doi:http://dx.doi.org/10.1016/j.memsci.2004.10.042 (2005).

17 Ghosh, A. K. & Hoek, E. M. V. Impacts of support membrane structure and chemistry on polyamide-polysulfone interfacial composite membranes. *Journal of Membrane Science* **336**, 140-148, doi:10.1016/j.memsci.2009.03.024 (2009).

18 Kim, H. I. & Kim, S. S. Plasma treatment of polypropylene and polysulfone supports for thin film composite reverse osmosis membrane. *Journal of Membrane Science* **286**, 193-201, doi:http://dx.doi.org/10.1016/j.memsci.2006.09.037 (2006).

19 Singh, P. S. *et al.* Probing the structural variations of thin film composite RO membranes obtained by coating polyamide over polysulfone membranes of different pore dimensions. *Journal of Membrane Science* **278**, 19-25, doi:http://dx.doi.org/10.1016/j.memsci.2005.10.039 (2006).

20 Vrouwenvelder, J. S. & van der Kooij, D. Diagnosis, prediction and prevention of biofouling of NF and RO membranes. *Desalination* **139**, 65-71, doi:10.1016/s0011-9164(01)00295-8 (2001).

21 Xu, P., Drewes, J. E., Kim, T. U., Bellona, C. & Amy, G. Effect of membrane fouling on transport of organic contaminants in NF/RO membrane applications. *Journal of Membrane Science* **279**, 165-175, doi:10.1016/j.memsci.2005.12.001 (2006).

22 Mukherjee, D., Kulkarni, A. & Gill, W. N. Chemical treatment for improved performance of reverse osmosis membranes. *Desalination* **104**, 239-249, doi:http://dx.doi.org/10.1016/0011-9164(96)00047-1 (1996).

23 Rana, D. & Matsuura, T. Surface Modifications for Antifouling Membranes. *Chem. Rev.* **110**, 2448-2471, doi:10.1021/cr800208y.

24 Yang, H.-L., Lin, J. C.-T. & Huang, C. Application of nanosilver surface modification to RO membrane and spacer for mitigating biofouling in seawater desalination. *Water Research* **43**, 3777-3786, doi:http://dx.doi.org/10.1016/j.watres.2009.06.002 (2009).

25 Freger, V. Nanoscale Heterogeneity of Polyamide Membranes Formed by Interfacial Polymerization. *Langmuir* **19**, 4791-4797, doi:10.1021/la020920q (2003).

26 Freger, V. Kinetics of film formation by interfacial polycondensation. *Langmuir* **21**, 1884-1894, doi:10.1021/la048085v (2005).

27 Elimelech, M., Zhu, X., Childress, A. E. & Hong, S. Role of membrane surface morphology in colloidal fouling of cellulose acetate and composite aromatic polyamide reverse osmosis membranes. *Journal of Membrane Science* **127**, 101-109 (1997).

28 Ramon, G. Z. & Hoek, E. M. V. Transport through composite membranes, part 2: Impacts of roughness on permeability and fouling. *Journal of Membrane Science* **425-426**, 141-148 (2013).

29 Wijmans, J. G. The solution-diffusion model: a review. *Journal of Membrane Science* **107**, 1-21 (1995).

30 Cussler, E. L. *Diffusion: Mass Transfer in Fluid Systems, 2nd Ed.*, (Cambridge University Press, 1997).

31 Rickman, M., Davis, R. H. & Pellegrino, J. Fractionation of organic fuel precursors from electrolytes with membranes. *Industrial & Engineering Chemistry Research* **52**, 10530-10539, doi:10.1021/ie4008908 (2013).

32 Kujundzic, E. *et al.* Biofouling potential of industrial fermentation broth components during microfiltration. *Journal of Membrane Science* **349**, 44-55 (2010).

33 Belfer, S., Fainchtain, R., Purinson, Y. & Kedem, O. Surface characterization by FTIR-ATR spectroscopy of polyethersulfone membranes-unmodified, modified and protein fouled. *Journal of Membrane Science* **172**, 113-124, doi:http://dx.doi.org/10.1016/S0376-7388(00)00316-1 (2000).

34 Coates, J. Interpretation of Infrared Spectra, A Practical Approach. *Encyclopedia of Analytical Chemistry*.

35 Silverstein, R. M. & Webster, F. X. *Spectrometric identification of organic compounds*. (Wiley, 1998).

36 Pacheco, F. A., Pinnau, I., Reinhard, M. & Leckie, J. O. Characterization of isolated polyamide thin films of RO and NF membranes using novel TEM techniques. *Journal of Membrane Science* **358**, 51-59, doi:http://dx.doi.org/10.1016/j.memsci.2010.04.032.

37 Song, Y., Liu, F. & Sun, B. Preparation, characterization, and application of thin film composite nanofiltration membranes. *Journal of Applied Polymer Science* **95**, 1251-1261, doi:10.1002/app.21338 (2005).

38 Enkelmann, V. & Wegner, G. Mechanism of interfacial polycondensation and the direct synthesis of stable polyamide membranes. *Die Makromolekulare Chemie* **177**, 3177-3189, doi:10.1002/macp.1976.021771106 (1976).

39 Maruf, S. H., Ahn, D. U., Greenberg, A. R. & Ding, Y. Glass transition behaviors of interfacially polymerized polyamide barrier layers on thin film composite membranes via nano-thermal analysis. *Polymer* **52**, 2643-2649, doi:http://dx.doi.org/10.1016/j.polymer.2011.04.022.

40 Rautenbach, R., Linn, T. & Eilers, L. Treatment of severely contaminated waste water by a combination of RO, high-pressure RO and NF-potential and limits of the process. *Journal of Membrane Science* **174**, 231-241, doi:http://dx.doi.org/10.1016/S0376-7388(00)00388-4 (2000).

41 Kim, T. U. & Boulder, U. o. C. a. *Transport of Organic Micropollutants Through Nanofiltration (NF) and Reverse Osmosis (RO) Membranes: Mechanisms, Modeling, and Applications*. (University of Colorado at Boulder, 2006).

42 Freger, V. Swelling and Morphology of the Skin Layer of Polyamide Composite Membranes:- An Atomic Force Microscopy Study. *Environmental Science & Technology* **38**, 3168-3175, doi:10.1021/es034815u (2004).

43 Lin, Y. Effects of Physicochemical Properties of Nanofiltration Membranes on the Rejection of Small Organic DBP Precursors. *Journal of Environmental Engineering* **139**, 127-136, doi:doi:10.1061/(ASCE)EE.1943-7870.0000623.

44 Pendergast, M. M. & Hoek, E. M. V. A review of water treatment membrane nanotechnologies. *Energy & Environmental Science* **4**, 1946-1971, doi:10.1039/c0ee00541j.

45 Hoek, E. M. V. & Elimelech, M. Cake-Enhanced Concentration Polarization:â€‰ A New Fouling Mechanism for Salt-Rejecting Membranes. *Environmental Science & Technology* **37**, 5581-5588, doi:10.1021/es0262636 (2003).

46 Sablani, S. S., Goosen, M. F. A., Al-Belushi, R. & Wilf, M. Concentration polarization in ultrafiltration and reverse osmosis: a critical review. *Desalination* **141**, 269-289, doi:http://dx.doi.org/10.1016/S0011-9164(01)85005-0 (2001).

47 Voros, N. G., Maroulis, Z. B. & Marinos-Kouris, D. Salt and water permeability in reverse osmosis membranes. *Desalination* **104**, 141-154, doi:http://dx.doi.org/10.1016/0011-9164(96)00037-9 (1996).

48 Murthy, Z. V. P. & Gupta, S. K. Estimation of mass transfer coefficient using a combined nonlinear membrane transport and film theory model. *Desalination* **109**, 39-49, doi:http://dx.doi.org/10.1016/S0011-9164(97)00051-9 (1997).

49 Sutzkover, I., Hasson, D. & Semiat, R. Simple technique for measuring the concentration polarization level in a reverse osmosis system. *Desalination* **131**, 117-127, doi:http://dx.doi.org/10.1016/S0011-9164(00)90012-2 (2000).

50 Ghosh, A. K., Jeong, B.-H., Huang, X. & Hoek, E. M. V. Impacts of reaction and curing conditions on polyamide composite reverse osmosis membrane properties. *Journal of Membrane Science* **311**, 34-45, doi:http://dx.doi.org/10.1016/j.memsci.2007.11.038 (2008).

51 Hirose, M., Ito, H. & Kamiyama, Y. Effect of skin layer surface structures on the flux behaviour of RO membranes. *Journal of Membrane Science* **121**, 209-215, doi:http://dx.doi.org/10.1016/S0376-7388(96)00181-0 (1996).

52 Kong, C., Kanezashi, M., Yamomoto, T., Shintani, T. & Tsuru, T. Controlled synthesis of high performance polyamide membrane with thin dense layer for water desalination. *Journal of Membrane Science* **362**, 76-80, doi:http://dx.doi.org/10.1016/j.memsci.2010.06.022.

53 Prakash Rao, A., Joshi, S. V., Trivedi, J. J., Devmurari, C. V. & Shah, V. J. Structure-performance correlation of polyamide thin film composite membranes: effect of coating conditions on film formation. *Journal of Membrane Science* **211**, 13-24, doi:http://dx.doi.org/10.1016/S0376-7388(02)00305-8 (2003).

54 Wei, X., Wang, Z., Chen, J., Wang, J. & Wang, S. A novel method of surface modification on thin-film-composite reverse osmosis membrane by grafting hydantoin derivative. *Journal of Membrane Science* **346**, 152-162, doi:http://dx.doi.org/10.1016/j.memsci.2009.09.032.

55 Jegal, J., Min, S. G. & Lee, K.-H. Factors affecting the interfacial polymerization of polyamide active layers for the formation of polyamide composite membranes. *Journal of Applied Polymer Science* **86**, 2781-2787, doi:10.1002/app.11257 (2002).

56 Lu, X., Bian, X. & Shi, L. Preparation and characterization of NF composite membrane. *Journal of Membrane Science* **210**, 3-11, doi:http://dx.doi.org/10.1016/S0376-7388(02)00120-5 (2002).

57 Rahimpour, A., Jahanshahi, M., Peyravi, M. & Khalili, S. Interlaboratory studies of highly permeable thin-film composite polyamide nanofiltration membrane. *Polymers for Advanced Technologies* **23**, 884-893, doi:10.1002/pat.1984.

58 Kim, T. U., Drewes, J. E., Summers, R. S. & Amy, G. L. Solute transport model for trace organic neutral and charged compounds through nanofiltration and reverse osmosis membranes. *Water Research* **41**, 3977-3988, doi:10.1016/j.watres.2007.05.055 (2007).

59 Kim, S. H., Kwak, S.-Y. & Suzuki, T. Positron Annihilation Spectroscopic Evidence to Demonstrate the Flux-Enhancement Mechanism in Morphology-Controlled Thin-Film-Composite (TFC) Membrane. *Environmental Science & Technology* **39**, 1764-1770, doi:10.1021/es049453k (2005).

60 Xie, W. *et al.* Polyamide interfacial composite membranes prepared from m-phenylene diamine, trimesoyl chloride and a new disulfonated diamine. *Journal of Membrane Science* **403-404**, 152-161, doi:http://dx.doi.org/10.1016/j.memsci.2012.02.038.

61 Hagmeyer, G. & Gimbel, R. Modelling the rejection of nanofiltration membranes using zeta potential measurements. *Separation and Purification Technology* **15**, 19-30 (1999).

62 Skluzacek, J. M., Tejedor, M. I. & Anderson, M. A. NaCl rejection by an inorganic nanofiltration membrane in relation to its central pore potential. *Journal of Membrane Science* **289**, 32-39, doi:http://dx.doi.org/10.1016/j.memsci.2006.11.034 (2007).

63 Wijmans, J. G. The role of permeant molar volume in the solution-diffusion model transport equations. *Journal of Membrane Science* **237**, 39-50, doi:http://dx.doi.org/10.1016/j.memsci.2004.02.028 (2004).

64 van den Berg, G. B. & Smolders, C. A. Flux decline in ultrafiltration processes. *Desalination* **77**, 101-133, doi:http://dx.doi.org/10.1016/0011-9164(90)85023-4 (1990).

65 Bowen, W. R. & Jenner, F. Theoretical descriptions of membrane filtration of colloids and fine particles: An assessment and review. *Advances in Colloid and Interface Science* **56**, 141-200, doi:http://dx.doi.org/10.1016/0001-8686(94)00232-2 (1995).

66 Lee, Y. K., Won, Y.-J., Yoo, J. H., Ahn, K. H. & Lee, C.-H. Flow analysis and fouling on the patterned membrane surface. *J. Membr. Sci.* **427**, 320-325, doi:http://dx.doi.org/10.1016/j.memsci.2012.10.010.

67 Merkel, T. C. *et al.* Ultrapermeable, Reverse-Selective Nanocomposite Membranes. *Science* **296**, 519-522, doi:10.1126/science.1069580 (2002).

68 Tu, K. L., Nghiem, L. D. & Chivas, A. R. Coupling effects of feed solution pH and ionic strength on the rejection of boron by NF/RO membranes. *Chemical Engineering Journal* **168**, 700-706, doi:http://dx.doi.org/10.1016/j.cej.2011.01.101.

69 Kim, D. Y. *et al.* Modeling of solute transport in multi-component solution for reverse osmosis membranes. *Desalination and Water Treatment* **15**, 20-28, doi:10.5004/dwt.2010.1662.

70 Bason, S. & Freger, V. Phenomenological analysis of transport of mono- and divalent ions in nanofiltration. *Journal of Membrane Science* **360**, 389-396, doi:http://dx.doi.org/10.1016/j.memsci.2010.05.037.

71 Goosen, M. F. A. *et al.* Fouling of Reverse Osmosis and Ultrafiltration Membranes: A Critical Review. *Separation Science and Technology* **39**, 2261-2297, doi:10.1081/ss-120039343 (2005).

72 Hasson, D., Drak, A. & Semiat, R. Inception of CaSO4 scaling on RO membranes at various water recovery levels. *Desalination* **139**, 73-81, doi:http://dx.doi.org/10.1016/S0011-9164(01)00296-X (2001).

73 Lee, S., Kim, J. & Lee, C.-H. Analysis of CaSO4 scale formation mechanism in various nanofiltration modules. *Journal of Membrane Science* **163**, 63-74, doi:http://dx.doi.org/10.1016/S0376-7388(99)00156-8 (1999).

74 Gilron, J. & Hasson, D. Calcium sulphate fouling of reverse osmosis membranes: Flux decline mechanism. *Chemical Engineering Science* **42**, 2351-2360, doi:http://dx.doi.org/10.1016/0009-2509(87)80109-4 (1987).

75 Pervov, A. G. Scale formation prognosis and cleaning procedure schedules in reverse osmosis systems operation. *Desalination* **83**, 77-118, doi:http://dx.doi.org/10.1016/0011-9164(91)85087-B (1991).

76 Antony, A. *et al.* Scale formation and control in high pressure membrane water treatment systems: A review. *Journal of Membrane Science* **383**, 1-16, doi:http://dx.doi.org/10.1016/j.memsci.2011.08.054.

77 Amjad, Z. Applications of antiscalants to control calcium sulfate scaling in reverse osmosis systems. *Desalination* **54**, 263-276, doi:http://dx.doi.org/10.1016/0011-9164(85)80022-9 (1985).

78 Shih, W.-Y., Rahardianto, A., Lee, R.-W. & Cohen, Y. Morphometric characterization of calcium sulfate dihydrate (gypsum) scale on reverse osmosis membranes. *Journal of Membrane Science* **252**, 253-263, doi:http://dx.doi.org/10.1016/j.memsci.2004.12.023 (2005).

79 Bacchin, P., Aimar, P. & Field, R. W. Critical and sustainable fluxes: Theory, experiments and applications. *Journal of Membrane Science* **281**, 42-69 (2006).

80 Wang, Y. N. & Tang, C. T. Protein fouling of nanofiltration, reverse osmosis, and ultrafiltration membranes-The role of hydrodynamic conditions, solution chemistry, and membrane properties. *Journal of Membrane Science* **376**, 275-282 (2011).

CHAPTER VII

CONCLUSIONS AND FUTURE RESEARCH

7.1 Thesis Summary

This thesis aims to develop an effective methodology to create surface patterned polymeric separation membrane to improve their anti-fouling characteristics during filtration. By using nanoimprinting lithography (NIL) submicron surface pattern was directly fabricated onto the surface of a commercial ultrafiltration (UF) membrane, as discussed in Chapter 2 of this dissertation. The effect of NIL process on the surface morphology, pore structure and permeability was studied by varying imprinting process parameters. The study from this thesis revealed that an unconventional low temperature ($T < T_g$) NIL is effective in generating a submicron surface pattern on a commercial polyethersulfone (PES) membrane without impeding much of its transport properties.

Since the NIL process does not alter the surface chemistry of the membrane, these patterned membranes can serve as a model system to examine the effect of surface roughness on particle deposition and other types of fouling during active membrane-based filtration. Our filtration studies with colloidal suspensions revealed that the presence of nanoscale surface patterns minimized the deposition of colloidal particles, with both increased critical flux and a lower rate of growth of total cake

resistance after deposition. Such an enhancement of the critical flux enables the UF membrane to operate under conditions (pressure) that provide greater productivity without the presence of any fouling since the sub-critical flux is higher compared to un-patterned counterpart. Microscopic analysis indicated that the particle deposition was highly anisotropic on the membrane surface and that deposition decreased with the increase of orientation angle between the pattern lines and the feed-flow direction.

Systematic cross-flow filtrations of colloidal suspensions on UF membranes with patterned surfaces also revealed that critical flux increases with particle size, cross-flow velocity, the angle between the feed flow and the pattern lines, and the pattern height. All together these experimental findings with colloidal particles consistently suggest that surface patterning is an effective approach to possibly enhance shear-induced lateral diffusion, which ultimately delays the colloidal particle deposition.

After the colloidal fouling study on patterned UF membrane, influence of surface pattern on PES UF membrane surface on protein fouling was studied by comparing performances of patterned PES UF with their un-patterned counterpart. Systematic filtration protocols and measurement of adsorption of protein solutions revealed that the presence of surface patterns significantly reduced the protein adsorption (fouling), when compared with the un-patterned flat membrane. The enhanced antifouling characteristic is most likely caused by the hydrodynamic interactions between the imprinted surface and the feed solution. Such an effect was

found to be persistent regardless of the pH and ionic strength of the feed solutions that were tested.

Later in this thesis, first time fabrication of a submicron-patterned thin film composite (TFC) membrane via interfacial polymerization on a nanoimprinted UF membrane without adversely affecting permselective properties were reported. Thin crosslinked aromatic polyamide barrier layer films atop a patterned support membrane was achieved, which was further characterized by FTIR spectroscopy and filtration experiments. The patterned TFC membrane exhibited water permeance and salt rejection comparable to that of commercial TFC RO membranes. Compared with their un-patterned counterparts, the patterned TFC membranes demonstrated higher flux and rejection values when convection was present as a result of stirring. Scaling experiments revealed that gypsum distribution on the surface of the patterned membranes was more widely scattered in comparison to that on the non-patterned membranes. Cross-flow experiment of a complex protein/electrolyte/organic mixture indicated that patterned TFC membrane can run 10 times longer in super-critical flux operation than un-patterned TFC membrane. Furthermore, the patterned membranes has the ability to recover more of their initial pure water permeance after the fouling permeation experiments, compared to the non-patterned ones.

7.2 Contributions

Overall study from this thesis work suggest that the presence of surface patterns on membrane surface were effective in mitigating fouling for all the cases

that are studied in this thesis. As discussed earlier in detail, Surface pattern induced hydrodynamic secondary flows along with higher shear stress at the membrane-feed interface probably produce larger back-diffusion mass transport of the foulants and eventually delays/reduce the fouling deposition. This thesis provides a facile fabrication methodology of generating surface pattern with UF and TFC (used in RO and NF) membranes. A systematic study on NIL process, membrane permeability and morphological evolution were presented which future investigator can use as a fabrication guide for NIL generated surface patterned separation membrane.

In general this thesis represents the first report describing the influence of submicron surface patterns on pressure-driven, liquid-based membrane separations. The results presented here provide a compelling rationale for systematic investigation of the exact mechanisms underlying the observed enhancement in fouling mitigation. Moreover, the fabrication method demonstrated here can be scaled-up via roll-to-roll NIL, and thus provides a promising manufacturing route for surface patterning as an effective alternative to chemical modification for fouling mitigation for liquid-based separation membranes.

7.3 Future research recommendations

The methodology introduced in this dissertation provides a natural guide to future research. NIL provides a new domain of generating surface pattern directly on polymeric separation membrane using an unconventional low temperature route. While prescribed methodology in this dissertation provides a guide line for fouling mitigation strategy, deeper level of study and understanding can still give solution to

some open questions and provide the pathway for future directions. The remainder of this section will lay out some of these immediately accessible avenues for future research.

7.3.1 NIL with different polymeric membranes.

Different types of polymeric membrane can be used for the study of surface patterning with NIL with a condition of the membrane being amorphous. Amorphous polymers like polysulfone, atactic polypropylene, polyethylene, polyvinyl chloride, and polycarbonates are frequently used in UF and MF applications. These polymeric membranes can also be used as model systems for optimization and study the potential synergistic effect of surface topography and surface chemistry on fouling mitigation. However, to choose a polymer membrane, one should be careful about glass transition temperature (T_g) and melting temperature (T_m) of the polymer. It was evident from these study that low temperature NIL is effective path for surface patterning of membrane. T_g of the chosen polymer should be higher than the operating capabilities of traditional NIL to avoid imprinting in rubbery zone.

7.3.2 Morphological evolution UF membrane upon imprinting

More rigorous and systematic analysis of the structural evolution upon NIL on various membrane materials can shed light on the mechanism involved in the patterning of porous materials. For example, porosity of the imprinted membrane measured in this study could not provide the exclusive porosity information of only the PES layer which is more responsible for the mass transport. In addition, pore size

distributions are regarded as an important parameter, which were not measured in this study to correctly determine membrane mass transport and permselectivity. Note that, the porosity measurement and pore size (MWCO) measurements were performed in this dissertation for comparative analysis of the changes that happen in the patterned UF membrane after imprinting, not for an accurate quantitative analysis. Pore tortuosity of the asymmetric pores after imprinting can also be studied to draw the exact picture of evolution of the membrane structure upon imprinting.

Another direction for research can be the model study of imprinting UF membranes of different pore sizes. It was reported in this dissertation that pore size of the membrane decreases upon imprinting which also result in the loss of permeability of the membrane. However, one can imprint a membrane with larger pore size at higher temperature and pressure to achieve good pattern height as well as high permeability of solvent.

7.3.3 Fabricating patterned membrane with complex nanostructures.

This dissertation provided the groundwork for surface patterning of commercial membrane using NIL and only much simplistic line and groove patterns were fabricated and studied. However, complex micro and nanostructures have been reported to be more effective in mitigating biological foulants. In addition, by fabrication of a complex structure hydrodynamic conditions may also be changed significantly.

7.3.4 Influence of surface pattern on interfacial polymerization of cross-linked polyamide membranes

Interfacial polymerization is very fast and complex process. Various parameters like reaction time, monomer concentration and support membrane plays an important role in this polymerization process. In this dissertation, the influence of these parameters were not studied systematically. It was observed that with higher reaction time results in a much thicker layer of polyamide film which completely smoothed out the patterns on the support membrane. However, by choosing patterned UF support membrane of different morphology one can determine the role of reaction time when interfacial reaction occurs in patterned surface.

In the interfacial polymerization of polyamide films, polyfunctional amide diffuses through organic phase and newly formed polyamide phase for additional reaction. However, how patterned/denser membrane can influence this diffusion mechanism and eventually the interfacial polymerization are yet to be studied. Also the thickness of the polyamide film formed over the patterned UF membrane could not be measured in this dissertation. From the schematic overlay of the AFM images of patterned UF and TFC membranes, it is likely that the polyamide film has different thickness in ridge and valleys of the UF membrane which can also provide the local hot spot for higher mass transport and thus onset of fouling.

BIBLIOGRPAHY

1. Ahn, S. H. & Guo, L. J. High-Speed Roll-to-Roll Nanoimprint Lithography on Flexible Plastic Substrates. *Advanced Materials* **20**, 2044-2049, doi:10.1002/adma.200702650 (2008).

2. Aimar, P., baklouti, S. & sanchez, V. Membrane-solute interactions: influence on pure solvent transfer during ultrafiltration. *Journal of Membrane Science* **29**, 207-224, doi:http://dx.doi.org/10.1016/S0376-7388(00)82470-9 (1986).

3. Akthakul, A., Salinaro, R. F. & Mayes, A. M. Antifouling Polymer Membranes with Subnanometer Size Selectivity. *Macromolecules* **37**, 7663-7668, doi:10.1021/ma048837s (2004).

4. Al-Amoudi, A. & Lovitt, R. W. Fouling strategies and the cleaning system of NF membranes and factors affecting cleaning efficiency. *Journal of Membrane Science* **303**, 4-28, doi:http://dx.doi.org/10.1016/j.memsci.2007.06.002 (2007).

5. Amjad, Z. Applications of antiscalants to control calcium sulfate scaling in reverse osmosis systems. *Desalination* **54**, 263-276, doi:http://dx.doi.org/10.1016/0011-9164(85)80022-9 (1985).

6. An, L. *et al.* Mechanical properties and miscibility of polyethersulfone/phenoxy blends. *Journal of Applied Polymer Science* **59**, 1843-1847, doi:10.1002/(sici)1097-4628(19960321)59:12<1843::aid-app5>3.0.co;2-q (1996).

7. Ang, W. S. & Elimelech, M. Protein (BSA) fouling of reverse osmosis membranes: Implications for wastewater reclamation. *Journal of Membrane Science* **296**, 83-92, doi:http://dx.doi.org/10.1016/j.memsci.2007.03.018 (2007).

8. Antony, A. *et al.* Scale formation and control in high pressure membrane water treatment systems: A review. *Journal of Membrane Science* **383**, 1-16, doi:http://dx.doi.org/10.1016/j.memsci.2011.08.054.

9. Ariza, M. J. & Benavente, J. Streaming potential along the surface of polysulfone membranes: a comparative study between two different experimental systems and determination of electrokinetic and adsorption parameters. *Journal of Membrane Science* **190**, 119-132, doi:http://dx.doi.org/10.1016/S0376-7388(01)00430-6 (2001).

10. Arnal, J. M. G. F., Beatriz; Sancho, Maria. (ed Robert Y Ning) (Intech Open science, 2011).

11. Arneri, G. The effect of pressure on the bulk polymer microstructure in cellulose acetate reverse osmosis membranes. Desalination 36, 99-104, doi:http://dx.doi.org/10.1016/S0011-9164(00)88634-8 (1981).

12. Asatekin, A., Kang, S., Elimelech, M. & Mayes, A. M. Anti-fouling ultrafiltration membranes containing polyacrylonitrile-graft-poly(ethylene oxide) comb copolymer additives. *Journal of Membrane Science* **298**, 136-146, doi:http://dx.doi.org/10.1016/j.memsci.2007.04.011 (2007).

13. Bacchin, P., Aimar, P. & Field, R. W. Critical and sustainable fluxes: Theory, experiments and applications. *Journal of Membrane Science* **281**, 42-69 (2006).

14. Bacchin, P., Aimar, P. & Sanchez, V. Influence of surface interaction on transfer during colloid ultrafiltration. *Journal of Membrane Science* **115**, 49-63, doi:http://dx.doi.org/10.1016/0376-7388(95)00279-0 (1996).

15. Bacchin, P., Si-Hassen, D., Starov, V., Clifton, M. J. & Aimar, P. A unifying model for concentration polarization, gel-layer formation and particle deposition in cross-flow membrane filtration of colloidal suspensions. *Chem. Eng. Sci.* **57**, 77-91, doi:10.1016/s0009-2509(01)00316-5 (2002).

16. Baker, R. *Membrane Technology and Applications*. (Wiley, 2004).

17. Balster, J., Stamatialis, D. F. & Wessling, M. Membrane with integrated spacer. *Journal of Membrane Science* **360**, 185-189, doi:http://dx.doi.org/10.1016/j.memsci.2010.05.011.

18. Barger, M., Hoff, D., Carnahan, R. P. & Gilbert, R. A. (Google Patents, 2003).

19. Barsema, J., Nijdam, W., Van Rijn, C., Vogelaar, L. & Wessling, M. (Google Patents, 2004).

20. Bason, S. & Freger, V. Phenomenological analysis of transport of mono- and divalent ions in nanofiltration. *Journal of Membrane Science* **360**, 389-396, doi:http://dx.doi.org/10.1016/j.memsci.2010.05.037.

21. Beier, S. P. & Jonsson, G. Critical flux determination by flux-stepping. *AIChE Journal* **56**, 1739-1747, doi:10.1002/aic.12099.

22. Belfer, S., Fainchtain, R., Purinson, Y. & Kedem, O. Surface characterization by FTIR-ATR spectroscopy of polyethersulfone membranes-unmodified, modified and protein fouled. *Journal of Membrane Science* **172**, 113-124, doi:http://dx.doi.org/10.1016/S0376-7388(00)00316-1 (2000).

23. Belfer, S., Purinson, Y., Fainshtein, R., Radchenko, Y. & Kedem, O. Surface modification of commercial composite polyamide reverse osmosis membranes. *Journal of Membrane Science* **139**, 175-181, doi:http://dx.doi.org/10.1016/S0376-7388(97)00248-2 (1998).

24. Belfort, G. & Nagata, N. Fluid mechanics and cross-flow filtration: some thoughts. *Desalination* **53**, 57-79, doi:http://dx.doi.org/10.1016/0011-9164(85)85052-9 (1985).

25. Belfort, G. Membrane modules: comparison of different configurations using fluid mechanics. *J. Membr. Sci.* **35**, 245-270, doi:http://dx.doi.org/10.1016/S0376-7388(00)80299-9 (1988).
26. Belfort, G., Davis, R. H. & Zydney, A. L. The behavior of suspensions and macromolecular solutions in crossflow microfiltration. *Journal of Membrane Science* **96**, 1-58, doi:http://dx.doi.org/10.1016/0376-7388(94)00119-7 (1994).

27. Bikel, M. a., Punt, I. G. M., Lammertink, R. G. H. & Wessling, M. Micropatterned Polymer Films by Vapor-Induced Phase Separation Using Permeable Molds. *ACS Applied Materials & Interfaces* **1**, 2856-2861, doi:10.1021/am900594p (2009).

28. Bloomfield, V. The Structure of Bovine Serum Albumin at Low pH*. *Biochemistry* **5**, 684-689, doi:10.1021/bi00866a039 (1966).

29. Bowen, W. R. & Jenner, F. Theoretical descriptions of membrane filtration of colloids and fine particles: An assessment and review. *Advances in Colloid and Interface Science* **56**, 141-200, doi:http://dx.doi.org/10.1016/0001-8686(94)00232-2 (1995).

30. Boyd, R. F. & Zydney, A. L. Analysis of protein fouling during ultrafiltration using a two-layer membrane model. *Biotechnology and Bioengineering* **59**, 451-460, doi:10.1002/(sici)1097-0290(19980820)59:4<451::aid-bit8>3.0.co;2-f (1998).

31. Bradford, W. L., Herrington, R. E. & Clement, A. D. (Google Patents, 2007).

32. Brans, G., van Dinther, A., Odum, B., Schroen, C. G. P. H. & Boom, R. M. Transmission and fractionation of micro-sized particle suspensions. *Journal of Membrane Science* **290**, 230-240, doi:http://dx.doi.org/10.1016/j.memsci.2006.12.045 (2007).

33. Brinkert, L., Abidine, N. & Aptel, P. On the relation between compaction and mechanical properties for ultrafiltration hollow fibers. Journal of Membrane Science 77, 123-131, doi:http://dx.doi.org/10.1016/0376-7388(93)85240-W (1993).

34. Brown, L., Narsimhan, G. & Wankat, P. C. Foam fractionation of globular proteins. *Biotechnology and Bioengineering* **36**, 947-959, doi:10.1002/bit.260360910 (1990).

35. Burns, D. B. & Zydney, A. L. Effect of solution pH on protein transport through ultrafiltration membranes. *Biotechnology and Bioengineering* **64**, 27-37, doi:10.1002/(sici)1097-0290(19990705)64:1<27::aid-bit3>3.0.co;2-e (1999).

36. C. Liu, S. C., J. Hayes, T. Caothuy. in *AWWA 2000 Water Quality Technology Conference* (Denver, CO, 2001).

37. Cadotte, J. E., King, R. S., Majerle, R. J. & Petersen, R. J. Interfacial Synthesis in the Preparation of Reverse Osmosis Membranes. *Journal of Macromolecular Science: Part A - Chemistry* **15**, 727-755, doi:10.1080/00222338108056764 (1981).

38. Caetano, A. *Membrane Technology: Applications to Industrial Wastewater Treatment: Applications to Industrial Wastewater Treatment*. (Springer Netherlands, 1995).

39. Carman, M. L. *et al.* Engineered antifouling microtopographies-correlating wettability with cell attachment. *Biofouling* **22**, 11-21, doi:10.1080/08927010500484854 (2006).

40. Celik, E., Liu, L. & Choi, H. Protein fouling behavior of carbon nanotube/polyethersulfone composite membranes during water filtration. *Water Research* **45**, 5287-5294, doi:http://dx.doi.org/10.1016/j.watres.2011.07.036.

41. Chan, R., Chen, V. & Bucknall, M. P. Ultrafiltration of protein mixtures: measurement of apparent critical flux, rejection performance, and identification of protein deposition. *Desalination* **146**, 83-90, doi:http://dx.doi.org/10.1016/S0011-9164(02)00493-9 (2002).

42. Chang, Y. *et al.* Surface grafting control of PEGylated poly(vinylidene fluoride) antifouling membrane via surface-initiated radical graft copolymerization. *Journal of Membrane Science* **345**, 160-169, doi:http://dx.doi.org/10.1016/j.memsci.2009.08.039 (2009).

43. Chapman, R. G. *et al.* Polymeric Thin Films That Resist the Adsorption of Proteins and the Adhesion of Bacteria. *Langmuir* **17**, 1225-1233, doi:10.1021/la001222d (2001).

44. Chen, C. S., Mrksich, M., Huang, S., Whitesides, G. M. & Ingber, D. E. Geometric Control of Cell Life and Death. *Science* **276**, 1425-1428, doi:10.1126/science.276.5317.1425 (1997).

45. Chen, V., Fane, A. G., Madaeni, S. & Wenten, I. G. Particle deposition during membrane filtration of colloids: transition between concentration polarization and cake formation. *Journal of Membrane Science* **125**, 109-122, doi:http://dx.doi.org/10.1016/S0376-7388(96)00187-1 (1997).

46. Cheryan, M. *Ultrafiltration and Microfiltration Handbook*. (Taylor & Francis, 1998).

47. Chiang, Y. C., Chang, Y., Higuchi, A., Chen, W. Y. & Ruaan, R.-C. Sulfobetaine-grafted poly(vinylidene fluoride) ultrafiltration membranes exhibit excellent antifouling property. *Journal of Membrane Science* **339**, 151-159, doi:http://dx.doi.org/10.1016/j.memsci.2009.04.044 (2009).

48. Cho, B. D. & Fane, A. G. Fouling transients in nominally sub-critical flux operation of a membrane bioreactor. *Journal of Membrane Science* **209**, 391-403, doi:http://dx.doi.org/10.1016/S0376-7388(02)00321-6 (2002).

49. Cho, J., Amy, G. & Pellegrino, J. Membrane filtration of natural organic matter: comparison of flux decline, NOM rejection, and foulants during filtration with three UF membranes. *Desalination* **127**, 283-298, doi:http://dx.doi.org/10.1016/S0011-9164(00)00017-5 (2000).
50. Choi, Y. H., Kim, H. S. & Kweon, J. H. Role of hydrophobic natural organic matter flocs on the fouling in coagulation-membrane processes. *Separation and Purification Technology* **62**, 529-534, doi:http://dx.doi.org/10.1016/j.seppur.2008.03.001 (2008).

51. Choksuchart, P., Heran, M. & Grasmick, A. Ultrafiltration enhanced by coagulation in an immersed membrane system. *Desalination* **145**, 265-272, doi:http://dx.doi.org/10.1016/S0011-9164(02)00421-6 (2002).

52. Choo, K. H. & Lee, C. H. Membrane fouling mechanisms in the membrane-coupled anaerobic bioreactor. *Water Res.* **30**, 1771-1780, doi:10.1016/0043-1354(96)00053-x (1996).

53. Chou, S. Y., Krauss, P. R. & Renstrom, P. J. Imprint Lithography with 25-Nanometer Resolution. Science 272, 85-87, doi:10.1126/science.272.5258.85 (1996).

54. Cleaver, J. W. & Yates, B. Mechanism of detachment of colloidal particles from a flat substrate in a turbulent flow. *J. Colloid Interface Sci.* **44**, 464-474, doi:http://dx.doi.org/10.1016/0021-9797(73)90323-8 (1973).

55. Coates, J. Interpretation of Infrared Spectra, A Practical Approach. *Encyclopedia of Analytical Chemistry*.

56. Culfaz, P. Z. et al. Fouling Behavior of Microstructured Hollow Fiber Membranes in Dead-End Filtrations: Critical Flux Determination and NMR Imaging of Particle Deposition. Langmuir 27, 1643-1652, doi:10.1021/la1037734.

57. Culfaz, P. Z., Rolevink, E., van Rijn, C., Lammertink, R. G. H. & Wessling, M. Microstructured hollow fibers for ultrafiltration. *Journal of Membrane Science* **347**, 32-41, doi:http://dx.doi.org/10.1016/j.memsci.2009.10.003.

58. Cussler, E. L. *Diffusion: Mass Transfer in Fluid Systems, 2nd Ed.*, (Cambridge University Press, 1997).

59. Da Costa, A. R., Fane, A. G., Fell, C. J. D. & Franken, A. C. M. Optimal channel spacer design for ultrafiltration. *Journal of Membrane Science* **62**, 275-291, doi:http://dx.doi.org/10.1016/0376-7388(91)80043-6 (1991).

60. Ding, Y. *et al.* Thermodynamic Underpinnings of Cell Alignment on Controlled Topographies. *Advanced Materials* **23**, 421-425, doi:10.1002/adma.201001757.

61. Ebrahim, S. Cleaning and regeneration of membranes in desalination and wastewater applications: State-of-the-art. *Desalination* **96**, 225-238, doi:http://dx.doi.org/10.1016/0011-9164(94)85174-3 (1994).

62. Elimelech, M., Xiaohua, Z., Childress, A. E. & Seungkwan, H. Role of membrane surface morphology in colloidal fouling of cellulose acetate and composite aromatic polyamide reverse osmosis membranes. *J. Membr. Sci.* **127**, 101-109 (1997).

63. Elimelech, M., Zhu, X., Childress, A. E. & Hong, S. Role of membrane surface morphology in colloidal fouling of cellulose acetate and composite aromatic polyamide reverse osmosis membranes. *Journal of Membrane Science* **127**, 101-109 (1997).

64. Engler, J. & Wiesner, M. R. Particle fouling of a rotating membrane disk. *Water Research* **34**, 557-565, doi:http://dx.doi.org/10.1016/S0043-1354(99)00148-7 (2000).

65. Enkelmann, V. & Wegner, G. Mechanism of interfacial polycondensation and the direct synthesis of stable polyamide membranes. *Die Makromolekulare Chemie* **177**, 3177-3189, doi:10.1002/macp.1976.021771106 (1976).

66. Espinasse, B., Bacchin, P. & Aimar, P. On an experimental method to measure critical flux in ultrafiltration. *Desalination* **146**, 91-96, doi:http://dx.doi.org/10.1016/S0011-9164(02)00495-2 (2002).

67. Field, R. in *Membrane Technology* 1-23 (Wiley-VCH Verlag GmbH & Co. KGaA).

68. Field, R. W., Wu, D., Howell, J. A. & Gupta, B. B. Critical flux concept for microfiltration fouling. *Journal of Membrane Science* **100**, 259-272, doi:http://dx.doi.org/10.1016/0376-7388(94)00265-Z (1995).

69. Foley, G. *Membrane Filtration*. (Cambridge University Press).

70. Freger, V. Kinetics of film formation by interfacial polycondensation. *Langmuir* **21**, 1884-1894, doi:10.1021/la048085v (2005).

71. Freger, V. Nanoscale Heterogeneity of Polyamide Membranes Formed by Interfacial Polymerization. *Langmuir* **19**, 4791-4797, doi:10.1021/la020920q (2003).

72. Freger, V. Swelling and Morphology of the Skin Layer of Polyamide Composite Membranes:- An Atomic Force Microscopy Study. *Environmental Science & Technology* **38**, 3168-3175, doi:10.1021/es034815u (2004).

73. Fritzmann, C., Lowenberg, J., Wintgens, T. & Melin, T. State-of-the-art of reverse osmosis desalination. *Desalination* **216**, 1-76, doi:http://dx.doi.org/10.1016/j.desal.2006.12.009 (2007).

74. Fuls, P. F., Dell, M. P. & Pearson, I. A. Non-linear flow through compressible membranes and its relation to osmotic pressure. Journal of Membrane Science 66, 37-43, doi:http://dx.doi.org/10.1016/0376-7388(92)80089-3 (1992).

75. Geise, G. M. *et al.* Water purification by membranes: The role of polymer science. *Journal of Polymer Science Part B: Polymer Physics* **48**, 1685-1718, doi:10.1002/polb.22037.

76. Geissler, M. & Xia, Y. Patterning: Principles and Some New Developments. Advanced Materials 16, 1249-1269, doi:10.1002/adma.200400835 (2004).

77. Ghosh, A. K. & Hoek, E. M. V. Impacts of support membrane structure and chemistry on polyamide-polysulfone interfacial composite membranes. *Journal of Membrane Science* **336**, 140-148, doi:10.1016/j.memsci.2009.03.024 (2009).

78. Ghosh, A. K., Jeong, B.-H., Huang, X. & Hoek, E. M. V. Impacts of reaction and curing conditions on polyamide composite reverse osmosis membrane properties. *Journal of Membrane Science* **311**, 34-45, doi:http://dx.doi.org/10.1016/j.memsci.2007.11.038 (2008).

79. Gilron, J. & Hasson, D. Calcium sulphate fouling of reverse osmosis membranes: Flux decline mechanism. *Chemical Engineering Science* **42**, 2351-2360, doi:http://dx.doi.org/10.1016/0009-2509(87)80109-4 (1987).

80. Glater, J., Zachariah, M. R., McCray, S. B. & McCutchan, J. W. Reverse osmosis membrane sensitivity to ozone and halogen disinfectants. *Desalination* **48**, 1-16, doi:http://dx.doi.org/10.1016/0011-9164(83)80001-0 (1983).

81. Goldman, G., Starosvetsky, J. & Armon, R. Inhibition of biofilm formation on UF membrane by use of specific bacteriophages. *Journal of Membrane Science* **342**, 145-152, doi:http://dx.doi.org/10.1016/j.memsci.2009.06.036 (2009).

82. Goosen, M. F. A. *et al.* Fouling of Reverse Osmosis and Ultrafiltration Membranes: A Critical Review. *Separation Science and Technology* **39**, 2261-2297, doi:10.1081/ss-120039343 (2005).

83. Greenlee, L. F., Lawler, D. F., Freeman, B. D., Marrot, B. & Moulin, P. Reverse osmosis desalination: Water sources, technology, and today's challenges. *Water Research* **43**, 2317-2348, doi:http://dx.doi.org/10.1016/j.watres.2009.03.010 (2009).

84. Guo, L. J. Nanoimprint Lithography: Methods and Material Requirements. Advanced Materials 19, 495-513, doi:10.1002/adma.200600882 (2007).

85. Guo, W., Ngo, H. H. & Li, J. A mini-review on membrane fouling. *Bioresource Technology* **122**, 27-34, doi:http://dx.doi.org/10.1016/j.biortech.2012.04.089.

86. Gupta, B. B., Howell, J. A., Wu, D. & Field, R. W. A helical baffle for cross-flow microfiltration. *Journal of Membrane Science* **102**, 31-42, doi:http://dx.doi.org/10.1016/0376-7388(94)00241-P (1995).

87. Hagmeyer, G. & Gimbel, R. Modelling the rejection of nanofiltration membranes using zeta potential measurements. *Separation and Purification Technology* **15**, 19-30 (1999).

88. Harmant, P. & Aimar, P. Coagulation of colloids in a boundary layer during cross-flow filtration. *Colloids and Surfaces A: Physicochemical and Engineering Aspects* **138**, 217-230 (1998).

89. Hasson, D., Drak, A. & Semiat, R. Inception of CaSO4 scaling on RO membranes at various water recovery levels. *Desalination* **139**, 73-81, doi:http://dx.doi.org/10.1016/S0011-9164(01)00296-X (2001).

90. Hellio, C. & Yebra, D. M. Advances in Marine Antifouling Coatings and Technologies. (Elsevier Science, 2009).

91. Hilal, N., Al-Zoubi, H., Darwish, N. A., Mohamma, A. W. & Abu Arabi, M. A comprehensive review of nanofiltration membranes:Treatment, pretreatment, modelling, and atomic force microscopy. *Desalination* **170**, 281-308, doi:http://dx.doi.org/10.1016/j.desal.2004.01.007 (2004).

92. Hirose, M., Ito, H. & Kamiyama, Y. Effect of skin layer surface structures on the flux behaviour of RO membranes. *Journal of Membrane Science* **121**, 209-215, doi:http://dx.doi.org/10.1016/S0376-7388(96)00181-0 (1996).

93. Hoek, E. M. V. & Elimelech, M. Cake-Enhanced Concentration Polarization:â€‰ A New Fouling Mechanism for Salt-Rejecting Membranes. *Environmental Science & Technology* **37**, 5581-5588, doi:10.1021/es0262636 (2003).

94. Hoek, E. M. V., Bhattacharjee, S. & Elimelech, M. Effect of Membrane Surface Roughness on Colloid−Membrane DLVO Interactions. *Langmuir* **19**, 4836-4847, doi:10.1021/la027083c (2003).

95. Howell, J. A. Sub-critical flux operation of microfiltration. *Journal of Membrane Science* **107**, 165-171, doi:http://dx.doi.org/10.1016/0376-7388(95)00114-R (1995).

96. Hubbard, A. T. *Encyclopedia of Surface and Colloid Science*. (Taylor & Francis, 2002).

97. Huisman, I. H., Vellenga, E., Tragardh, G. & Tragardh, C. The influence of the membrane zeta potential on the critical flux for crossflow microfiltration of particle suspensions. *Journal of Membrane Science* **156**, 153-158, doi:http://dx.doi.org/10.1016/S0376-7388(98)00328-7 (1999).

98. Jegal, J., Min, S. G. & Lee, K. H. Factors affecting the interfacial polymerization of polyamide active layers for the formation of polyamide composite membranes. *Journal of Applied Polymer Science* **86**, 2781-2787, doi:10.1002/app.11257 (2002).

99. Jermann, D., Pronk, W., Kagi, R., Halbeisen, M. & Boller, M. Influence of interactions between NOM and particles on UF fouling mechanisms. *Water research* **42**, 3870-3878 (2008).

100. Jones, K. L. & O'Melia, C. R. Protein and humic acid adsorption onto hydrophilic membrane surfaces: effects of pH and ionic strength. *Journal of Membrane Science* **165**, 31-46, doi:http://dx.doi.org/10.1016/S0376-7388(99)00218-5 (2000).

101. Jones, K. L. & O'Melia, C. R. Ultrafiltration of protein and humic substances: effect of solution chemistry on fouling and flux decline. *Journal of Membrane Science* **193**, 163-173, doi:http://dx.doi.org/10.1016/S0376-7388(01)00492-6 (2001).

102. Jonsson, A.s. Concentration Polarization and Fouling during Ultrafiltration of Colloidal Suspensions and Hydrophobic Solutes. *Separation Science and Technology* **30**, 301-312, doi:10.1080/01496399508015840 (1995).

103. Kim, D. Y. *et al.* Modeling of solute transport in multi-component solution for reverse osmosis membranes. *Desalination and Water Treatment* **15**, 20-28, doi:10.5004/dwt.2010.1662.

104. Kim, H. I. & Kim, S. S. Plasma treatment of polypropylene and polysulfone supports for thin film composite reverse osmosis membrane. *Journal of Membrane Science* **286**, 193-201, doi:http://dx.doi.org/10.1016/j.memsci.2006.09.037 (2006).

105. Kim, H. J. et al. Roll-to-roll manufacturing of electronics on flexible substrates using self-aligned imprint lithography (SAIL). Journal of the Society for Information Display 17, 963-970, doi:10.1889/jsid17.11.963 (2009).

106. Kim, I. C. & Lee, K.-H. Dyeing process wastewater treatment using fouling resistant nanofiltration and reverse osmosis membranes. *Desalination* **192**, 246-251, doi:http://dx.doi.org/10.1016/j.desal.2005.05.030 (2006).

107. Kim, K. J. et al. A comparative study of techniques used for porous membrane characterization: pore characterization. Journal of Membrane Science 87, 35-46, doi:http://dx.doi.org/10.1016/0376-7388(93)E0044-E (1994).

108. Kim, M. m., Lin, N. H., Lewis, G. T. & Cohen, Y. Surface nano-structuring of reverse osmosis membranes via atmospheric pressure plasma-induced graft polymerization for reduction of mineral scaling propensity. *Journal of Membrane Science* **354**, 142-149, doi:http://dx.doi.org/10.1016/j.memsci.2010.02.053.

109. Kim, S. H., Kwak, S. Y. & Suzuki, T. Positron Annihilation Spectroscopic Evidence to Demonstrate the Flux-Enhancement Mechanism in Morphology-Controlled Thin-Film-Composite (TFC) Membrane. *Environmental Science & Technology* **39**, 1764-1770, doi:10.1021/es049453k (2005).

110. Kim, T. U. & Boulder, U. o. C. a. *Transport of Organic Micropollutants Through Nanofiltration (NF) and Reverse Osmosis (RO) Membranes: Mechanisms, Modeling, and Applications*. (University of Colorado at Boulder, 2006).

111. Kim, T. U., Drewes, J. E., Summers, R. S. & Amy, G. L. Solute transport model for trace organic neutral and charged compounds through nanofiltration and reverse osmosis membranes. *Water Research* **41**, 3977-3988, doi:10.1016/j.watres.2007.05.055 (2007).

112. Kimura, K., Hane, Y., Watanabe, Y., Amy, G. & Ohkuma, N. Irreversible membrane fouling during ultrafiltration of surface water. *Water Research* **38**, 3431-3441, doi:http://dx.doi.org/10.1016/j.watres.2004.05.007 (2004).

113. King, C. J. *Separation processes*. (McGraw-Hill, 1980).

114. Ko, M. K. & Pellegrino, J. J. Determination of osmotic pressure and fouling resistance and their effects of performance of ultrafiltration membranes. *Journal of Membrane Science* **74**, 141-157, doi:http://dx.doi.org/10.1016/0376-7388(92)87079-D (1992).

115. Ko, M. K., Pellegrino, J. J., Nassimbene, R. & Marko, P. Characterization of the adsorption-fouling layer using globular proteins on ultrafiltration membranes.

Journal of Membrane Science **76**, 101-120, doi:http://dx.doi.org/10.1016/0376-7388(93)85210-N (1993).

116. Kong, C., Kanezashi, M., Yamomoto, T., Shintani, T. & Tsuru, T. Controlled synthesis of high performance polyamide membrane with thin dense layer for water desalination. *Journal of Membrane Science* **362**, 76-80, doi:http://dx.doi.org/10.1016/j.memsci.2010.06.022.
117. Kujundzic, E. *et al.* Biofouling potential of industrial fermentation broth components during microfiltration. *Journal of Membrane Science* **349**, 44-55 (2010).

118. Kujundzic, E., Greenberg, A. R., Fong, R. & Hernandez, M. Monitoring Protein Fouling on Polymeric Membranes Using Ultrasonic Frequency-Domain Reflectometry. *Membranes* **1**, 195-216.

119. Lau, W. J., Ismail, A. F., Misdan, N. & Kassim, M. A. A recent progress in thin film composite membrane: A review. *Desalination* **287**, 190-199, doi:http://dx.doi.org/10.1016/j.desal.2011.04.004.

120. Le Clech, P., Jefferson, B., Chang, I. S. & Judd, S. J. Critical flux determination by the flux-step method in a submerged membrane bioreactor. *Journal of Membrane Science* **227**, 81-93, doi:http://dx.doi.org/10.1016/j.memsci.2003.07.021 (2003).

121. Le-Clech, P., Chen, V. & Fane, T. A. G. Fouling in membrane bioreactors used in wastewater treatment. *Journal of Membrane Science* **284**, 17-53, doi:http://dx.doi.org/10.1016/j.memsci.2006.08.019 (2006).

122. Lee, J. H., Wang, L., Kooi, S., Boyce, M. C. & Thomas, E. L. Enhanced Energy Dissipation in Periodic Epoxy Nanoframes. Nano Letters 10, 2592-2597, doi:10.1021/nl1012773.

123. Lee, K. J. & Wu, R. M. Simulation of resistance of cross-flow microfiltration and force analysis on membrane surface. *Desalination* **233**, 239-246, doi:http://dx.doi.org/10.1016/j.desal.2007.09.048 (2008).

124. Lee, K. P., Arnot, T. C. & Mattia, D. A review of reverse osmosis membrane materials for desalination - Development to date and future potential. *Journal of Membrane Science* **370**, 1-22, doi:http://dx.doi.org/10.1016/j.memsci.2010.12.036.

125. Lee, S., Kim, J. & Lee, C. H. Analysis of CaSO4 scale formation mechanism in various nanofiltration modules. *Journal of Membrane Science* **163**, 63-74, doi:http://dx.doi.org/10.1016/S0376-7388(99)00156-8 (1999).

126. Lee, Y. K., Won, Y. J., Yoo, J. H., Ahn, K. H. & Lee, C. H. Flow analysis and fouling on the patterned membrane surface. *Journal of Membrane Science* **427**, 320-325, doi:http://dx.doi.org/10.1016/j.memsci.2012.10.010.

127. Leonard, E. F. & Vassilieff, C. S. The Depossition of Rejected Matter in Membrane Separation Processes. *Chemical Engineering Communications* **30**, 209-217, doi:10.1080/00986448408911128 (1984).

128. Li, H., Fane, A. G., Coster, H. G. L. & Vigneswaran, S. An assessment of depolarisation models of crossflow microfiltration by direct observation through the membrane. *Journal of Membrane Science* **172**, 135-147, doi:http://dx.doi.org/10.1016/S0376-7388(00)00334-3 (2000).

129. Li, X. *Mitigation of Fouling on Hollow Fiber Membrane Using Ultrasonic Tranducer* Master of Science in Engineering thesis, Purdue University Calumet, (2009)

130. Lin, N. H., Kim, M. m., Lewis, G. T. & Cohen, Y. Polymer surface nano-structuring of reverse osmosis membranes for fouling resistance and improved flux performance. *Journal of Materials Chemistry* **20**, 4642-4652, doi:10.1039/b926918e.

131. Lin, T., Shen, B., Chen, W. & Zhang, X. Interaction mechanisms associated with organic colloid fouling of ultrafiltration membrane in a drinking water treatment system. *Desalination* **332**, 100-108, doi:http://dx.doi.org/10.1016/j.desal.2013.11.001.

132. Lin, Y. Effects of Physicochemical Properties of Nanofiltration Membranes on the Rejection of Small Organic DBP Precursors. *Journal of Environmental Engineering* **139**, 127-136, doi:doi:10.1061/(ASCE)EE.1943-7870.0000623.

133. Loeb, S. in *Synthetic Membranes:* Vol. 153 *ACS Symposium Series* 1-9 (American Chemical Society, 1981).

134. Lu, X., Bian, X. & Shi, L. Preparation and characterization of NF composite membrane. *Journal of Membrane Science* **210**, 3-11, doi:http://dx.doi.org/10.1016/S0376-7388(02)00120-5 (2002).

135. Luo, M. L., Zhao, J. Q., Tang, W. & Pu, C. S. Hydrophilic modification of poly(ether sulfone) ultrafiltration membrane surface by self-assembly of TiO2 nanoparticles. *Applied Surface Science* **249**, 76-84, doi:http://dx.doi.org/10.1016/j.apsusc.2004.11.054 (2005).

136. Luo, M.-L., Zhao, J. Q., Tang, W. & Pu, C. S. Hydrophilic modification of poly(ether sulfone) ultrafiltration membrane surface by self-assembly of TiO2 nanoparticles. *Applied Surface Science* **249**, 76-84, doi:http://dx.doi.org/10.1016/j.apsusc.2004.11.054 (2005).

137. Ma, H., Bowman, C. N. & Davis, R. H. Membrane fouling reduction by backpulsing and surface modification. Journal of Membrane Science 173, 191-200, doi:http://dx.doi.org/10.1016/S0376-7388(00)00360-4 (2000).

138. Mallevialle, J. *et al. Water Treatment Membrane Processes.* (McGraw-Hill, 1996).

139. Marselina, Y., Le-Clech, P., Stuetz, R. & Chen, V. Detailed characterisation of fouling deposition and removal on a hollow fibre membrane by direct observation

technique. *Desalination* **231**, 3-11, doi:http://dx.doi.org/10.1016/j.desal.2007.11.033 (2008).

140. Marshall, A. D., Munro, P. A. & Tragardh, G. The effect of protein fouling in microfiltration and ultrafiltration on permeate flux, protein retention and selectivity: A literature review. *Desalination* **91**, 65-108, doi:http://dx.doi.org/10.1016/0011-9164(93)80047-Q (1993).
141. Maruf, S. H., Ahn, D. U., Greenberg, A. R. & Ding, Y. Glass transition behaviors of interfacially polymerized polyamide barrier layers on thin film composite membranes via nano-thermal analysis. *Polymer* **52**, 2643-2649, doi:http://dx.doi.org/10.1016/j.polymer.2011.04.022.

142. Matthiasson, E. The role of macromolecular adsorption in fouling of ultrafiltration membranes. *Journal of Membrane Science* **16**, 23-36, doi:http://dx.doi.org/10.1016/S0376-7388(00)81297-1 (1983).

143. Mc Donogh, R. M., Bauser, H., Stroh, N. & Grauschopf, U. Experimental in situ measurement of concentration polarisation during ultra- and micro-filtration of bovine serum albumin and Dextran Blue solutions. *Journal of Membrane Science* **104**, 51-63, doi:http://dx.doi.org/10.1016/0376-7388(95)00011-Z (1995).

144. McCloskey, B. D. *et al.* Influence of polydopamine deposition conditions on pure water flux and foulant adhesion resistance of reverse osmosis, ultrafiltration, and microfiltration membranes. *Polymer* **51**, 3472-3485, doi:http://dx.doi.org/10.1016/j.polymer.2010.05.008.

145. Merkel, T. C. *et al.* Ultrapermeable, Reverse-Selective Nanocomposite Membranes. *Science* **296**, 519-522, doi:10.1126/science.1069580 (2002).

146. Microfiltration and Ultrafiltration: Principles and Applications. (Taylor & Francis, 1996).

147. Miller, D. J., Paul, D. R. & Freeman, B. D. A crossflow filtration system for constant permeate flux membrane fouling characterization. *Review of Scientific Instruments* **84**, -, doi:doi:http://dx.doi.org/10.1063/1.4794909.

148. Mockel, D., Staude, E. & Guiver, M. D. Static protein adsorption, ultrafiltration behavior and cleanability of hydrophilized polysulfone membranes. *Journal of Membrane Science* **158**, 63-75, doi:http://dx.doi.org/10.1016/S0376-7388(99)00028-9 (1999).

149. Montaudo, G., Puglisi, C., Rapisardi, R. & Samperi, F. Primary thermal degradation processes of poly(ether-sulfone) and poly(phenylene oxide) investigated by direct pyrolysis-mass spectrometry. Macromolecular Chemistry and Physics 195, 1225-1239, doi:10.1002/macp.1994.021950410 (1994).
150. Moore, G. E. Cramming More Components Onto Integrated Circuits. Proceedings of the IEEE 86, 82-85, doi:10.1109/jproc.1998.658762 (1998).

151. Morgan, P. W. *Condensation polymers: by interfacial and solution methods*. (Interscience Publishers, 1965).

152. Moulai-Mostefa, N., Akoum, O., Nedjihoui, M., Ding, L. & Jaffrin, M. Y. Comparison between rotating disk and vibratory membranes in the ultrafiltration of oil-in-water emulsions. *Desalination* **206**, 494-498, doi:http://dx.doi.org/10.1016/j.desal.2006.04.061 (2007).

153. Mukherjee, D., Kulkarni, A. & Gill, W. N. Chemical treatment for improved performance of reverse osmosis membranes. *Desalination* **104**, 239-249, doi:http://dx.doi.org/10.1016/0011-9164(96)00047-1 (1996).

154. Mukherjee, D., Kulkarni, A. & Gill, W. N. Flux enhancement of reverse osmosis membranes by chemical surface modification. *Journal of Membrane Science* **97**, 231-249, doi:http://dx.doi.org/10.1016/0376-7388(94)00165-U (1994).

155. Mulder, M. *Basic Principles of Membrane Technology*. (Springer, 1996).

156. Murthy, Z. V. P. & Gupta, S. K. Estimation of mass transfer coefficient using a combined nonlinear membrane transport and film theory model. *Desalination* **109**, 39-49, doi:http://dx.doi.org/10.1016/S0011-9164(97)00051-9 (1997).

157. Muthukumaran, S. *et al.* The use of ultrasonic cleaning for ultrafiltration membranes in the dairy industry. *Separation and Purification Technology* **39**, 99-107, doi:http://dx.doi.org/10.1016/j.seppur.2003.12.013 (2004).

158. Nabe, A., Staude, E. & Belfort, G. Surface modification of polysulfone ultrafiltration membranes and fouling by BSA solutions. *Journal of Membrane Science* **133**, 57-72, doi:http://dx.doi.org/10.1016/S0376-7388(97)00073-2 (1997).

159. Ngene, I. S., Lammertink, R. G. H., Wessling, M. & Van der Meer, W. G. J. Particle deposition and biofilm formation on microstructured membranes. *Journal of Membrane Science* **364**, 43-51, doi:http://dx.doi.org/10.1016/j.memsci.2010.07.048.

160. Noble, R. D. & Stern, S. A. *Membrane Separations Technology: Principles and Applications*. (Elsevier Science, 1995).

161. Ohya, H. An expression method of compaction effects on reverse osmosis membranes at high pressure operation. Desalination 26, 163-174, doi:http://dx.doi.org/10.1016/S0011-9164(00)82198-0 (1978).

162. Pacheco, F. A., Pinnau, I., Reinhard, M. & Leckie, J. O. Characterization of isolated polyamide thin films of RO and NF membranes using novel TEM techniques. *Journal of Membrane Science* **358**, 51-59, doi:http://dx.doi.org/10.1016/j.memsci.2010.04.032.

163. Palacio, L., Pradanos, P., Calvo, J. I. & Hernandez, A. Porosity measurements by a gas penetration method and other techniques applied to membrane characterization. Thin Solid Films 348, 22-29, doi:http://dx.doi.org/10.1016/S0040-6090(99)00197-2 (1999).

164. Pendergast, M. M. & Hoek, E. M. V. A review of water treatment membrane nanotechnologies. *Energy & Environmental Science* **4**, 1946-1971, doi:10.1039/c0ee00541j.

165. Peng, W. & Escobar, I. C. Rejection Efficiency of Water Quality Parameters by Reverse Osmosis and Nanofiltration Membranes. *Environmental Science & Technology* **37**, 4435-4441, doi:10.1021/es034202h (2003).

166. Pervov, A. G. Scale formation prognosis and cleaning procedure schedules in reverse osmosis systems operation. *Desalination* **83**, 77-118, doi:http://dx.doi.org/10.1016/0011-9164(91)85087-B (1991).

167. Petersen, R. J. Composite reverse osmosis and nanofiltration membranes. *Journal of Membrane Science* **83**, 81-150, doi:http://dx.doi.org/10.1016/0376-7388(93)80014-O (1993).

168. Petronis, A a. n., Berntsson, K., Gold, J. & Gatenholm, P. Design and microstructuring of PDMS surfaces for improved marine biofouling resistance. *Journal of Biomaterials Science, Polymer Edition* **11**, 1051-1072, doi:10.1163/156856200743571 (2000).

169. Pinnau, I. & Freeman, B. D. in Membrane Formation and Modification Vol. 744 ACS Symposium Series 1-22 (American Chemical Society, 1999).

170. Porter, M. C. Concentration Polarization with Membrane Ultrafiltration. *Industrial & Engineering Chemistry Product Research and Development* **11**, 234-&, doi:10.1021/i360043a002 (1972).

171. Potts, D. E., Ahlert, R. C. & Wang, S. S. A critical review of fouling of reverse osmosis membranes. *Desalination* **36**, 235-264 (1981).

172. Prakash Rao, A., Joshi, S. V., Trivedi, J. J., Devmurari, C. V. & Shah, V. J. Structure-performance correlation of polyamide thin film composite membranes: effect of coating conditions on film formation. *Journal of Membrane Science* **211**, 13-24, doi:http://dx.doi.org/10.1016/S0376-7388(02)00305-8 (2003).

173. Qu, X., Alvarez, P. J. J. & Li, Q. Applications of nanotechnology in water and wastewater treatment. Water Research 47, 3931-3946, doi:http://dx.doi.org/10.1016/j.watres.2012.09.058.

174. Quake, S. R. & Scherer, A. From Micro- to Nanofabrication with Soft Materials. Science 290, 1536-1540, doi:10.1126/science.290.5496.1536 (2000).

175. Rahimpour, A., Jahanshahi, M., Peyravi, M. & Khalili, S. Interlaboratory studies of highly permeable thin-film composite polyamide nanofiltration membrane. *Polymers for Advanced Technologies* **23**, 884-893, doi:10.1002/pat.1984.

176. Ramon, G. Z. & Hoek, E. M. V. Transport through composite membranes, part 2: Impacts of roughness on permeability and fouling. *Journal of Membrane Science* **425-426**, 141-148 (2013).

177. Rana, D. & Matsuura, T. Surface Modifications for Antifouling Membranes. *Chemical Reviews* **110**, 2448-2471, doi:10.1021/cr800208y.

178. Rautenbach, R., Linn, T. & Eilers, L. Treatment of severely contaminated waste water by a combination of RO, high-pressure RO and NF-potential and limits of the process. *Journal of Membrane Science* **174**, 231-241, doi:http://dx.doi.org/10.1016/S0376-7388(00)00388-4 (2000).

179. Reddy, A. V. R., Mohan, D. J., Bhattacharya, A., Shah, V. J. & Ghosh, P. K. Surface modification of ultrafiltration membranes by preadsorption of a negatively charged polymer: I. Permeation of water soluble polymers and inorganic salt solutions and fouling resistance properties. *Journal of Membrane Science* **214**, 211-221, doi:http://dx.doi.org/10.1016/S0376-7388(02)00547-1 (2003).

180. Richard Bowen, W. *et al.* The effects of electrostatic interactions on the rejection of colloids by membrane pores-visualisation and quantification. *Chemical Engineering Science* **54**, 369-375, doi:http://dx.doi.org/10.1016/S0009-2509(98)00252-8 (1999).

181. Richert, L. *et al.* Surface Nanopatterning to Control Cell Growth. *Advanced Materials* **20**, 1488-1492, doi:10.1002/adma.200701428 (2008).

182. Rickman, M., Davis, R. H. & Pellegrino, J. Fractionation of organic fuel precursors from electrolytes with membranes. *Industrial & Engineering Chemistry Research* **52**, 10530-10539, doi:10.1021/ie4008908 (2013).

183. Roh, I. J., Park, S. Y., Kim, J. J. & Kim, C. K. Effects of the polyamide molecular structure on the performance of reverse osmosis membranes. *Journal of Polymer Science Part B: Polymer Physics* **36**, 1821-1830, doi:10.1002/(sici)1099-0488(199808)36:11<1821::aid-polb3>3.0.co;2-t (1998).

184. Romero, C. A. & Davis, R. H. Global model of crossflow microfiltration based on hydrodynamic particle diffusion. *J. Membr. Sci.* **39**, 157-185 (1988).

185. Sablani, S. S., Goosen, M. F. A., Al-Belushi, R. & Wilf, M. Concentration polarization in ultrafiltration and reverse osmosis: a critical review. *Desalination* **141**, 269-289, doi:http://dx.doi.org/10.1016/S0011-9164(01)85005-0 (2001).

186. Sadr Ghayeni, S. B., Madaeni, S. S., Fane, A. G. & Schneider, R. P. Aspects of microfiltration and reverse osmosis in municipal wastewater reuse. *Desalination* **106**, 25-29, doi:http://dx.doi.org/10.1016/S0011-9164(96)00088-4 (1996).

187. Santos, O., Nylander, T., Paulsson, M. & Tragardth, C. Whey protein adsorption onto steel surface - effect of temperature, flow rate, residence time and aggregation. *Journal of Food Engineering* **74**, 468-483, doi:http://dx.doi.org/10.1016/j.jfoodeng.2005.03.037 (2006).

188. Schumacher, J. F. et al. Engineered antifouling microtopographies - effect of feature size, geometry, and roughness on settlement of zoospores of the green alga Ulva. Biofouling 23, 55-62, doi:10.1080/08927010601136957 (2007).

189. Schwinge, J., Neal, P. R., Wiley, D. E., Fletcher, D. F. & Fane, A. G. Spiral wound modules and spacers: Review and analysis. *Journal of Membrane Science* **242**, 129-153, doi:http://dx.doi.org/10.1016/j.memsci.2003.09.031 (2004).

190. Seidel, A. & Elimelech, M. Coupling between chemical and physical interactions in natural organic matter (NOM) fouling of nanofiltration membranes: implications for fouling control. *Journal of Membrane Science* **203**, 245-255, doi:http://dx.doi.org/10.1016/S0376-7388(02)00013-3 (2002).

191. Shih, W. Y., Rahardianto, A., Lee, R. W. & Cohen, Y. Morphometric characterization of calcium sulfate dihydrate (gypsum) scale on reverse osmosis membranes. *Journal of Membrane Science* **252**, 253-263, doi:http://dx.doi.org/10.1016/j.memsci.2004.12.023 (2005).

192. Shirtcliffe, N. J., McHale, G., Newton, M. I., Chabrol, G. & Perry, C. C. Dual-Scale Roughness Produces Unusually Water-Repellent Surfaces. *Advanced Materials* **16**, 1929-1932, doi:10.1002/adma.200400315 (2004).

193. Silverstein, R. M. & Webster, F. X. *Spectrometric identification of organic compounds*. (Wiley, 1998).

194. Singh, G. & Song, L. Influence of sodium dodecyl sulfate on colloidal fouling potential during ultrafiltration. *Colloids and Surfaces A: Physicochemical and Engineering Aspects* **281**, 138-146, doi:http://dx.doi.org/10.1016/j.colsurfa.2006.02.036 (2006).

195. Singh, P. S. *et al.* Probing the structural variations of thin film composite RO membranes obtained by coating polyamide over polysulfone membranes of different pore dimensions. *Journal of Membrane Science* **278**, 19-25, doi:http://dx.doi.org/10.1016/j.memsci.2005.10.039 (2006).

196. Sioutopoulos, D. C., Yiantsios, S. G. & Karabelas, A. J. Relation between fouling characteristics of RO and UF membranes in experiments with colloidal organic and inorganic species. *Journal of Membrane Science* **350**, 62-82, doi:http://dx.doi.org/10.1016/j.memsci.2009.12.012.

197. Skluzacek, J. M., Tejedor, M. I. & Anderson, M. A. NaCl rejection by an inorganic nanofiltration membrane in relation to its central pore potential. *Journal of Membrane Science* **289**, 32-39, doi:http://dx.doi.org/10.1016/j.memsci.2006.11.034 (2007).

198. Song, L. & Singh, G. Influence of various monovalent cations and calcium ion on the colloidal fouling potential. *Journal of Colloid and Interface Science* **289**, 479-487, doi:http://dx.doi.org/10.1016/j.jcis.2005.03.072 (2005).

199. Song, L. F. & Elimelech, M. Theory of Concentration Polarization in Cross-flow Filtration. *J. Chem. Soc.-Faraday Trans.* **91**, 3389-3398, doi:10.1039/ft9959103389 (1995).

200. Song, L., Chen, K. L., Ong, S. L. & Ng, W. J. A new normalization method for determination of colloidal fouling potential in membrane processes. *Journal of Colloid and Interface Science* **271**, 426-433, doi:http://dx.doi.org/10.1016/j.jcis.2003.12.016 (2004).
201. Song, Y., Sun, P., Henry, L. L. & Sun, B. Mechanisms of structure and performance controlled thin film composite membrane formation via interfacial polymerization process. *Journal of Membrane Science* **251**, 67-79, doi:http://dx.doi.org/10.1016/j.memsci.2004.10.042 (2005).

202. Strathmann, H., Giorno, L. & Drioli, E. *An Introduction to Membrane Science and Technology*. (CNR-Servizio Pubblicazioni, 2006)

203. Stroock, A. D. & Whitesides, G. M. Controlling Flows in Microchannels with Patterned Surface Charge and Topography. *Accounts of Chemical Research* **36**, 597-604, doi:10.1021/ar0202870 (2003).

204. Stroock, A. D. *et al.* Chaotic Mixer for Microchannels. *Science* **295**, 647-651, doi:10.1126/science.1066238 (2002).

205. Subramani, A., Kim, S. & Hoek, E. M. V. Pressure, flow, and concentration profiles in open and spacer-filled membrane channels. *Journal of Membrane Science* **277**, 7-17, doi:http://dx.doi.org/10.1016/j.memsci.2005.10.021 (2006).

206. Suki, A., Fane, A. G. & Fell, C. J. D. Flux decline in protein ultrafiltration. *Journal of Membrane Science* **21**, 269-283, doi:http://dx.doi.org/10.1016/S0376-7388(00)80218-5 (1984).

207. Sutzkover, I., Hasson, D. & Semiat, R. Simple technique for measuring the concentration polarization level in a reverse osmosis system. *Desalination* **131**, 117-127, doi:http://dx.doi.org/10.1016/S0011-9164(00)90012-2 (2000).

208. Swaminathan, T., Chaudhuri, M. & Sirkar, K. K. Effect of pH on solvent flux during stirred ultrafiltration of proteins. *Biotechnology and Bioengineering* **23**, 1873-1880, doi:10.1002/bit.260230813 (1981).

209. Tu, K. L., Nghiem, L. D. & Chivas, A. R. Coupling effects of feed solution pH and ionic strength on the rejection of boron by NF/RO membranes. *Chemical Engineering Journal* **168**, 700-706, doi:http://dx.doi.org/10.1016/j.cej.2011.01.101.

210. Ulbricht, M. Advanced functional polymer membranes. *Polymer* **47**, 2217-2262, doi:http://dx.doi.org/10.1016/j.polymer.2006.01.084 (2006).
211. Van den Berg, G. B. & Smolders, C. A. Flux decline in ultrafiltration processes. *Desalination* **77**, 101-133, doi:http://dx.doi.org/10.1016/0011-9164(90)85023-4 (1990).

212. Van den Berg, G. B. & Smolders, C. A. Flux decline in ultrafiltration processes. *Desalination* **77**, 101-133, doi:http://dx.doi.org/10.1016/0011-9164(90)85023-4 (1990).

213. Van Der Bruggen, B., Vandecasteele, C., Van Gestel, T., Doyen, W. & Leysen, R. A review of pressure-driven membrane processes in wastewater treatment and

drinking water production. *Environmental Progress* **22**, 46-56, doi:10.1002/ep.670220116 (2003).

214. Van der Waal, M. J., Stevanovic, S. & Racz, I. G. Mass transfer in corrugated-plate membrane modules. II. Ultrafiltration experiments. *Journal of Membrane Science* **40**, 261-275, doi:http://dx.doi.org/10.1016/0376-7388(89)89009-X (1989).

215. Vogelaar, L. *et al.* Phase Separation Micromolding: A New Generic Approach for Microstructuring Various Materials. *Small* **1**, 645-655, doi:10.1002/smll.200400128 (2005).

216. Vogelaar, L., Barsema, J. N., van Rijn, C. J. M., Nijdam, W. & Wessling, M. Phase Separation Micromolding—PSμM. *Advanced Materials* **15**, 1385-1389, doi:10.1002/adma.200304949 (2003).

217. Vogelaar, L., Lammertink, R. G. H. & Wessling, M. Superhydrophobic Surfaces Having Two-Fold Adjustable Roughness Prepared in a Single Step. *Langmuir* **22**, 3125-3130, doi:10.1021/la052701l (2006).

218. Voros, N. G., Maroulis, Z. B. & Marinos-Kouris, D. Salt and water permeability in reverse osmosis membranes. *Desalination* **104**, 141-154, doi:http://dx.doi.org/10.1016/0011-9164(96)00037-9 (1996).

219. Vrouwenvelder, J. S. & van der Kooij, D. Diagnosis, prediction and prevention of biofouling of NF and RO membranes. *Desalination* **139**, 65-71, doi:10.1016/s0011-9164(01)00295-8 (2001).

220. Wallevik, K. Spontaneous in vivo isomerization of bovine serum albumin as a determinant of its normal catabolism. *The Journal of Clinical Investigation* **57**, 398-407, doi:10.1172/jci108291 (1976).

221. Wandera, D., Wickramasinghe, S. R. & Husson, S. M. Modification and characterization of ultrafiltration membranes for treatment of produced water. *Journal of Membrane Science* **373**, 178-188, doi:http://dx.doi.org/10.1016/j.memsci.2011.03.010.

222. Wang, F. & Tarabara, V. V. Pore blocking mechanisms during early stages of membrane fouling by colloids. *Journal of Colloid and Interface Science* **328**, 464-469, doi:http://dx.doi.org/10.1016/j.jcis.2008.09.028 (2008).

223. Wang, F. & University, M. S. *Combined Fouling of Pressure-driven Membranes Treating Feed Waters of Complex Composition*. (Michigan State University, 2008).

224. Wang, P., Tan, K. L., Kang, E. T. & Neoh, K. G. Synthesis, characterization and anti-fouling properties of poly(ethylene glycol) grafted poly(vinylidene fluoride) copolymer membranes. *Journal of Materials Chemistry* **11**, 783-789, doi:10.1039/b007310p (2001).

225. Wang, Y. N. & Tang, C. T. Protein fouling of nanofiltration, reverse osmosis, and ultrafiltration membranes-The role of hydrodynamic conditions, solution chemistry, and membrane properties. *Journal of Membrane Science* **376**, 275-282 (2011).

226. Wei, X., Wang, Z., Chen, J., Wang, J. & Wang, S. A novel method of surface modification on thin-film-composite reverse osmosis membrane by grafting hydantoin derivative. *Journal of Membrane Science* **346**, 152-162, doi:http://dx.doi.org/10.1016/j.memsci.2009.09.032.

227. Wessling, M., Werner, U. & Hwang, S. T. Pervaporation of aromatic C8-isomers. *Journal of Membrane Science* **57**, 257-270, doi:http://dx.doi.org/10.1016/S0376-7388(00)80682-1 (1991).

228. Wijmans, J. G. & Baker, R. W. The solution-diffusion model: a review. *Journal of Membrane Science* **107**, 1-21, doi:http://dx.doi.org/10.1016/0376-7388(95)00102-I (1995).

229. Wijmans, J. G. The role of permeant molar volume in the solution-diffusion model transport equations. *Journal of Membrane Science* **237**, 39-50, doi:http://dx.doi.org/10.1016/j.memsci.2004.02.028 (2004).

230. Wijmans, J. G. The solution-diffusion model: a review. *Journal of Membrane Science* **107**, 1-21 (1995).

231. Won, Y. J. *et al.* Preparation and Application of Patterned Membranes for Wastewater Treatment. *Environmental Science & Technology* **46**, 11021-11027, doi:10.1021/es3020309.

232. Wu, D., Howell, J. A. & Field, R. W. Critical flux measurement for model colloids. *Journal of Membrane Science* **152**, 89-98, doi:http://dx.doi.org/10.1016/S0376-7388(98)00200-2 (1999).

233. Xia, Y. & Whitesides, G. M. Soft Lithography. Angewandte Chemie International Edition 37, 550-575, doi:10.1002/(sici)1521-3773(19980316)37:5<550::aid-anie550>3.0.co;2-g (1998).

234. Xie, W. *et al.* Polyamide interfacial composite membranes prepared from m-phenylene diamine, trimesoyl chloride and a new disulfonated diamine. *Journal of Membrane Science* **403-404**, 152-161, doi:http://dx.doi.org/10.1016/j.memsci.2012.02.038.

235. Xu, P., Drewes, J. E., Kim, T. U., Bellona, C. & Amy, G. Effect of membrane fouling on transport of organic contaminants in NF/RO membrane applications. *Journal of Membrane Science* **279**, 165-175, doi:10.1016/j.memsci.2005.12.001 (2006).

236. Yan, L., Li, Y. S., Xiang, C. B. & Xianda, S. Effect of nano-sized Al_2O_3-particle addition on PVDF ultrafiltration membrane performance. *Journal of Membrane Science* **276**, 162-167, doi:http://dx.doi.org/10.1016/j.memsci.2005.09.044 (2006).

237. Yang, H.-L., Lin, J. C. T. & Huang, C. Application of nanosilver surface modification to RO membrane and spacer for mitigating biofouling in seawater desalination. *Water Research* **43**, 3777-3786, doi:http://dx.doi.org/10.1016/j.watres.2009.06.002 (2009).

238. Zhang, Z., Dalgleish, D. G. & Goff, H. D. Effect of pH and ionic strength on competitive protein adsorption to air/water interfaces in aqueous foams made with mixed milk proteins. *Colloids and Surfaces B: Biointerfaces* **34**, 113-121, doi:http://dx.doi.org/10.1016/j.colsurfb.2003.11.009 (2004).

239. Zheo, B. & Moore, J. S. Surface-Directed Liquid Flow Inside Microchannels. *Science* **291**, 1023 (2001).

240. Zhou, W. in Nanoimprint Lithography: An Enabling Process for Nanofabrication 111-146 (Springer Berlin Heidelberg).

241. Zhu, X. H. & Elimelech, M. Colloidal fouling of reverse osmosis membranes: Measurements and fouling mechanisms. *Environ. Sci. Technol.* **31**, 3654-3662, doi:10.1021/es970400v (1997).

242. Zydney, A. L. & Colton, C. K. A Cconcentration Polarization Model for the Filtrate Flux in Cross-flow Microfiltration of Particulate Suspensions. *Chemical Engineering Communications* **47**, 1-21, doi:10.1080/00986448608911751 (1986)